SAPIENZA
UNIVERSITÀ DI ROMA

Experimental and numerical analysis of heavy liquid metal systems for Generation IV fast reactors

Facoltà di Ingegneria Civile e Industriale
DIAEE - Dipartimento di Ingegneria Astronautica, Elettrica ed Energetica
Corso di Dottorato in Energia e Ambiente XXXII Ciclo

Candidato:
Pierdomenico Lorusso

Relatori:
Prof. Gianfranco Caruso
Dr. Ing. Fabio Giannetti
Dr. Ing. Mariano Tarantino

A.A. 2018-2019

(Page intentionally left blank)

ABSTRACT

The present work reports the results achieved during the doctoral research activity realized in partnership between DIAEE (Dipartimento di Ingegneria Astronautica, Elettrica ed Energetica) of Sapienza University of Rome and ENEA (Agenzia nazionale per le nuove tecnologie, l'energia e lo sviluppo economico sostenibile). The activities have been carried out within the EU scientific community, since they are part of the R&D activities foreseen in the two HORIZON2020 European Projects SESAME and MYRTE.

After a brief description of the Lead Fast Reactors (LFRs) technologies and the actual status of the related R&D programs worldwide, the description of the Lead Bismuth Eutectic (LBE)-cooled pool-type facility CIRCE is presented. In particular, the work is focalized to the newest test section presently installed on CIRCE and named HERO (Heavy liquid mEtal pRessurized water cOoled tubes). The performed experimental campaigns aimed at characterizing a prototypical steam generator with double-wall bayonet tubes, evaluating its thermal-hydraulic performances in normal operational and transient scenarios.

The experimental activity on CIRCE-HERO has been supported by a numerical pre-test analysis described in the third section of this document. In particular, the RELAP5-3D© model of the HERO secondary loop has been set-up and it has been used to define the start-up procedure of the facility and to achieve feedbacks on the performances of the steam generator.

The core of this document is dedicated to the description and post-test analysis of the two experimental campaigns executed on CIRCE-HERO. The first experimental campaign, consisting of three tests, has been performed in the framework of the HORIZON2020 SESAME EU project, with the objective to support the development of the ALFRED design. The second one, consisting of nine tests, has been executed in the framework of the HORIZON2020 MYRTE EU project, with the purpose to support the development of MYRRHA and acquiring experimental data relevant for MYRRHA primary heat exchanger.

To extend the knowledge and validation of SYS-TH codes when applied for LFRs, a simulation activity has been performed in the Benchmark exercise for SYStem Thermal-Hydraulic (SYS-TH) codes and CFD/SYS-TH codes validation, in the framework of the

H2020 SESAME project. A RELAP5-3D© model of the NACIE-UP facility has been set up and it has been involved to perform a preliminary blind simulation activity and a subsequent post-test analysis on the basis of the experimental results available from the test performed on NACIE-UP.

A final summary, conclusions and future perspectives are given in the final section of the document.

CONTENTS

ABSTRACT **3**

CONTENTS **5**

LIST OF SYMBOLS **9**

LIST OF ABBREVIATIONS **11**

LIST OF FIGURES **15**

LIST OF TABLES **25**

1 INTRODUCTION **27**

1.1 FOCUS ON GENERATION IV HLM FAST REACTORS **28**

1.2 ACTUAL STATUS OF HLM TECHNOLOGIES **34**

1.3 FRAMEWORK OF THE ACTIVITY **41**

1.4 OBJECTIVES OF THE ACTIVITY **41**

2 DESIGN AND OPERATION OF THE CIRCE-HERO FACILITY **45**

2.1 CIRCE EXPERIMENTAL FACILITY **45**

2.2 HERO TEST SECTION **49**

2.2.1 Primary Side 49

2.2.2 Secondary Side 52

2.2.3 HERO SGBT 55

2.2.4 Instrumentation and Data Acquisition & Control System 59

3 PRELIMINARY NUMERICAL ACTIVITIES IN SUPPORT TO THE CIRCE-HERO DESIGN **67**

3.1 DEVELOPMENT OF THE INPUT DECK **67**

3.1.1 Modelling of the hydrodynamic components 67

3.1.2 Modelling of the thermal coupling 68

3.2 THERMAL-HYDRAULIC ANALYSIS OF THE REFERENCE DESIGN **70**

3.2.1 CIRCE-HERO start-up procedure definition 70

3.2.2 Thermal-hydraulic characterization of the HERO SG 75

4 EXPERIMENTAL CAMPAIGN WITHIN H2020 SESAME 83
4.1 HORIZON2020 SESAME EU PROJECT OVERVIEW 83
4.2 CIRCE-HERO EXPERIMENTAL TESTS 84
4.2.1 SCOPE OF THE EXPERIMENTS 84
4.2.2 SE-TEST1 86
4.2.3 SE-TEST2 92
4.2.4 SE-TEST3 98
5 EXPERIMENTAL CAMPAIGN WITHIN H2020 MYRTE 107
5.1 HORIZON2020 MYRTE EU PROJECT OVERVIEW 107
5.2 CIRCE-HERO EXPERIMENTAL TESTS 107
5.2.1 SCOPE OF THE EXPERIMENTS 108
5.2.2 MY-TEST REFERENCE 109
5.2.3 MY-TEST1 116
5.2.4 MY-TEST2 119
5.2.5 MY-TEST3 123
5.2.6 MY-TEST4 127
5.2.7 MY-TEST5 130
5.2.8 MY-TEST6 134
5.2.9 MY-TEST7 137
5.2.10 MY-TEST8 141
6 SYSTEM THERMAL-HYDRAULIC CODE BENCHMARK ACTIVITY 145
6.1 FRAMEWORK OF THE ACTIVITY 145
6.2 SCOPE OF THE ACTIVITY 145
6.3 THE NACIE-UP FACILITY 146
6.4 STH CODE SIMULATIONS AND RESULTS 150
6.4.1 Modelling of the hydrodynamic components 150
6.4.2 Modelling of the thermal coupling 153
6.4.3 Blind Simulations 156
6.4.4 Post-Test Simulations 169
7 FINAL SUMMARY AND CONCLUSIONS 183
7.1 FINAL SUMMARY 183
7.1.1 Set up and pre-test analysis of the experimental facility CIRCE-HERO 184
7.1.2 Experimental campaign on CIRCE-HERO within H2020 SESAME 185

7.1.3 Experimental campaign on CIRCE-HERO within H2020 MYRTE 186
7.1.4 Benchmark numerical activity for RELAP5-3D© validation 187
7.2 CONCLUSIONS AND FUTURE PLANS 188

REFERENCES 191

ANNEX 1 – CIRCE-HERO INSTRUMENTATION LIST 197

ANNEX 2 – PUBLICATIONS 221

(Page intentionally left blank)

LIST OF SYMBOLS

Greek Symbols

β	Thermal dilatation coefficient
ΔP	Pressure difference
ΔT	Temperature difference
ε	Roughness
η	Dynamic viscosity
λ	Thermal conductivity
λ_L	Laminar friction factor
$\lambda_{L,T}$	Transition friction factor
λ_T	Turbulent friction factor
μ	Cinematic viscosity
ϱ	Density
σ	Surface tension
Φ	Shape factor

Latin Symbols

c_p	Isobaric specific heat
d	Diameter
D2O	Heavy water
f	Friction factor
g	Gravity constant
Gr	Grashof number
h	Enthalpy
H2O	Water
He	Helium
k	Thermal conductivity
$\dot{m}$	Mass flow rate
Na	Sodium
Nu	Nusselt number

p	Pitch
P	Pressure
Pb	Lead
Pe	Peclet number
Pr	Prandtl number
Q	Power
r	Electric resistivity
Ra	Rayleigh number
Re	Reynolds number
T	Temperature

LIST OF ABBREVIATIONS

ADS	Accelerator Driven System
AIS	Argon Injection System
ALFRED	Advanced Lead cooled Fast Reactor European Demonstrator
ARS	Argon Recirculation System
BC	Boundary Condition
BT	Bayonet Tube
CFD	Computational Fluid Dynamics
CIRCE	CIRColazione Eutettico (Eutectic CIRCulation)
CLEAR-S	China LEAd-based Reactor
COMPLOT	COMPonent LOop Testing
DACS	Data Acquisition & Control System
DHR	Decay Heat Removal
DIAEE	Dipartimento di Ingegneria Astronautica, Elettrica ed Energetica
DPA	Displacements Per Atom
ENEA	Agenzia nazionale per le nuove tecnologie, l'energia e lo sviluppo economico sostenibile
EU	European Union
FPS	Fuel Pin Simulator
FRETHME	FREtting Tests in Heavy liquid MEtal
GEC	Gas-Enhanced Circulation
GEN IV	GENeration IV
GFR	Gas-cooled Fast Reactor
GIF	Generation IV International Forum
HERO	Heavy liquid mEtal pRessurized water cOoled tubes
HLM	Heavy Liquid Metal
HLMR	Heavy Liquid Metal Reactor
HX	Heat Exchanger
ICE	Integral Circulation Experiment
LBE	Lead-Bismuth Eutectic
LEADER	Lead cooled European Advanced DEmonstration Reactor

LFR	Lead-cooled Fast Reactor
MOX	Mixed Oxide Fuel
MPI	Message Passing Interface
MSR	Molten-Salt Reactor
MYRRHA	Multi-purpose hYbrid Research Reactor for High-tech Applications
MYRTE	MYRRHA Research and Transmutation Endeavour
MY-Test#	MYRTE Test
NACIE-UP	NAtural CIrculation Experiment UPgrade
NC	Natural Circulation
P&ID	Procedure and Instrumentation Diagram
PHX	Primary Heat Exchanger
PLC	Programmable Logic Controller
PLOFA	Protected Loss of Flow Accident
R&D	Research and Development
SESAME	thermal-hydraulics Simulations and Experiments for the Safety Assessment of Metal cooled reactor
SE-Test#	SESAME Test
SFR	Sodium-cooled Fast Reactor
SG	Steam Generator
SGBT	Steam Generator Bayonet Tube
SRS	Servizi di Ricerche e Sviluppo
SS	Steady State
SWCR	Supercritical Water-Cooled Reactor
SYS-TH	SYStem Thermal-Hydraulic
TALL-3D	Thermal-Hydraulic ADS Lead-Bismuth Loop
TC	Thermocouple
TFM	Turbine Flow Meter
THEADES	THErmal-hydraulics and Ads DESign
TMDPVOL	Time Dependent Volume
TMDPJUN	Time Dependent Junction
TS	Test Section
VFM	Venturi Flow Meter

VHTR	Very High Temperature gas Reactor
WP	Work Package

(Page intentionally left blank)

LIST OF FIGURES

Fig. 1-1 – Scheme of THEADES loop (from [5]) 36
Fig. 1-2 – Scheme of TALL-3D experimental facility (from [12]) 37
Fig. 1-3 –Isometric view of the E-SCAPE facility (from [13]) 38
Fig. 1-4 – Isometric view of the COMPLOT facility (from [14]) 38
Fig. 1-5 – Isometrical view of the FRETHME facility (from [15]) 39
Fig. 1-6 – General layout of the CLEAR-S main vessel (from [16]) 40
Fig. 1-7 – View of the KYLIN-II loop (from [17]) 40
Fig. 2-1 – Schematic view of the CIRCE facility 46
Fig. 2-2 – View of the S100 main vessel (a), S200 storage tank (b) and S300 transfer tank (c) 47
Fig. 2-3 – View of the compressor unit for the argon circulation 48
Fig. 2-4 – S100 main vessel and HERO Test Section 50
Fig. 2-5 – External and internal view of the Fuel Pin Simulator, and detail of the spacer grid 51
Fig. 2-6 - View of the fitting volume (left) and drawing of the argon injector (right) 52
Fig. 2-7 – External and internal view of the Separator 52
Fig. 2-8 – Secondary Loop P&ID 54
Fig. 2-9 – View of the secondary loop (left), the SGBT top flange (top, right) and the HEATER component (bottom, right) 55
Fig. 2-10 – Technical drawing of HERO SGBT unit 57
Fig. 2-11 – Bayonet Tube geometry 58
Fig. 2-12 – Top view of the S100 coupling flange 58
Fig. 2-13 – Sketch of the hexagonal geometry (left) and detail of the bayonet tubes (right) 59
Fig. 2-14 – FPS, measurement sections and thermocouples position (TC-FPS-01 – TC-FPS-39) 62
Fig. 2-15 – Instrumentation installed in the S100 pool and in the riser 63
Fig. 2-16 – Distribution of the thermocouples along the LBE side of the steam generator 64
Fig. 2-17 – General Control Panel of the CIRCE-HERO Facility 65
Fig. 3-1 – Secondary loop RELAP5-3D model 69
Fig. 3-2 – Pressure time trend during the start-up 73
Fig. 3-3 – Temperature time trend during the start-up 73

Fig. 3-4 – Steam mass fraction during the start-up....73
Fig. 3-5 – Power removed from the pool during the start-up....74
Fig. 3-6 – Pressure drops along a bayonet tube in nominal conditions....74
Fig. 3-7 – LBE and water temperature trends in nominal conditions....74
Fig. 3-8 – Radial temperature along the double wall thickness in correspondence of the annulus inlet (BT bottom)....75
Fig. 3-9 – Radial temperature along the double wall thickness in correspondence of the annulus outlet (BT top)....75
Fig. 3-10 – Power removed by the SG computed by RELAP5....80
Fig. 3-11 – ΔP along the bayonet tube computed by RELAP5....81
Fig. 3-12 – LBE SG outlet temperature computed by RELAP5....81
Fig. 3-13 – H2O SG outlet temperature computed by RELAP5....81
Fig. 3-14 – Steam Mass Fraction, comparison between RUN #1 and RUN #4....82
Fig. 3-15 – LBE and H2O temperature profiles along the SG during RUN #1....82
Fig. 4-1 – SE-Test1, FPS Power and argon Flow Rate trends....87
Fig. 4-2 – SE-Test1, H2O mass flow rate trends during the PLOFA Test measured by TFMs....88
Fig. 4-3 – SE-Test1, LBE mass flow rate before and after the transient....90
Fig. 4-4 – SE-Test1, LBE temperature trends at the FPS inlet-outlet....90
Fig. 4-5 – SE-Test1, FPS pin clad temperature....91
Fig. 4-6 – SE-Test1, LBE temperature trends at the inlet and outlet sections of the Riser....91
Fig. 4-7 – SE-Test1, LBE temperature trends at the inlet and outlet sections of the SG....91
Fig. 4-8 – SE-Test1, axial temperature profile inside the S100 vessel before and after the transient....92
Fig. 4-9 – SE-Test1, H2O temperature trends at the inlet and outlet sections of the Bayonet Tubes....92
Fig. 4-10 – SE-Test2, FPS Power and argon Flow Rate trends....94
Fig. 4-11 – SE-Test2, H2O mass flow rate trends during the PLOFA Test measured by TFMs....94
Fig. 4-12 – SE-Test2, LBE mass flow rate before and after the transient....96
Fig. 4-13 – SE-Test2, LBE temperature trends at the FPS inlet-outlet....96

Fig. 4-14 – SE-Test2, FPS pin clad temperature....97
Fig. 4-15 – SE-Test2, LBE temperature trends at the inlet and outlet sections of the Riser....97
Fig. 4-16 – SE-Test2, LBE temperature trends at the inlet and outlet sections of the SG....97
Fig. 4-17 – SE-Test2, axial temperature profile inside the S100 vessel before and after the transient....98
Fig. 4-18 – SE-Test2, H2O temperature trends at the inlet and outlet sections of the Bayonet Tubes....98
Fig. 4-19 – SE-Test3, FPS Power and argon Flow Rate trends....100
Fig. 4-20 – SE-Test3, H2O mass flow rate trends during the PLOFA Test measured by TMFs....101
Fig. 4-21 – SE-Test3, LBE mass flow rate before and after the transient....103
Fig. 4-22 – SE-Test3, LBE temperature trends at the FPS inlet-outlet....103
Fig. 4-23 – SE-Test3, FPS pin clad temperature....104
Fig. 4-24 – SE-Test3, LBE temperature trends at the inlet and outlet sections of the Riser....104
Fig. 4-25 – SE-Test3, LBE temperature trends at the inlet and outlet sections of the SG....104
Fig. 4-26 – SE-Test3, axial temperature profile inside the S100 vessel before and after the transient....105
Fig. 4-27 – SE-Test3, H2O temperature trends at the inlet and outlet sections of the Bayonet Tubes....105
Fig. 5-1 – Test Reference Boundary Conditions....111
Fig. 5-2 – LBE Mass Flow Rate measured by VFM during the Test Reference....111
Fig. 5-3 – Inlet and Outlet Temperatures along the FPS during the Test Reference....112
Fig. 5-4 – Inlet and Outlet Temperatures along the Riser during the Test Reference....112
Fig. 5-5 – Inlet and Outlet Temperature along the SGBT Shell Side during the Test Reference....112
Fig. 5-6 – LBE Temperatures along the SG at different levels: inlet section, +4200 mm, +3000 mm, +1500 mm, outlet section during the Test Reference....113
Fig. 5-7 – Axial profile of the temperature inside the S100 vessel during the Test Reference....113
Fig. 5-8 – Temperature measured on supporting rod A during the Test Reference....113
Fig. 5-9 – Temperature measured on supporting rod H during the Test Reference....114

Fig. 5-10 – Temperature measured on supporting rod I during the Test Reference 114
Fig. 5-11 – Water Mass Flow Rate measured by turbine flow meters during the Test Reference 114
Fig. 5-12 – Water Temperatures at the inlet and outlet of the SGBT during the Test Reference 115
Fig. 5-13 – Pressure drops along the bayonet tubes during the Test Reference 115
Fig. 5-14 – Pressure along the secondary loop during the Test Reference 115
Fig. 5-15 – LBE Mass Flow Rate measured by VFM during the MY-Test1 117
Fig. 5-16 – Inlet and Outlet Temperatures along the FPS during the MY-Test1 117
Fig. 5-17 – Inlet and Outlet Temperature along the SGBT Shell Side during the MY-Test1 117
Fig. 5-18 – Axial profile of the temperature inside the S100 vessel during the MY-Test1 118
Fig. 5-19 – Water Mass Flow Rate measured by turbine flow meters during the MY-Test1 118
Fig. 5-20 – Water Temperatures at the inlet and outlet of the SGBT during the MY-Test1 118
Fig. 5-21 – Pressure drops along the bayonet tubes during the MY-Test1 119
Fig. 5-22 – Pressure in 3 different locations in the secondary loop during the MY-Test1 119
Fig. 5-23 – LBE Mass Flow Rate measured by VFM during the MY-Test2 120
Fig. 5-24 – Inlet and Outlet Temperatures along the FPS during the MY-Test2 121
Fig. 5-25 – Inlet and Outlet Temperature along the SGBT Shell Side during the MY-Test2 121
Fig. 5-26 – Axial profile of the temperature inside the S100 vessel during the MY-Test2 121
Fig. 5-27 – Water Mass Flow Rate measured by turbine flow meters during the MY-Test2 122
Fig. 5-28 – Water Temperatures at the inlet and outlet of the SGBT during the MY-Test2 122
Fig. 5-29 – Pressure drops along the bayonet tubes during the MY-Test2 122
Fig. 5-30 – Pressure along the secondary loop during the MY-Test2 123
Fig. 5-31 – LBE Mass Flow Rate measured by VFM during the MY-TEST3 124
Fig. 5-32 – Inlet and Outlet Temperatures along the FPS during the MY-TEST3 124
Fig. 5-33 – Inlet and Outlet Temperature along the SGBT Shell Side during the MY-TEST3 125

Fig. 5-34 – Axial profile of the temperature inside the S100 vessel during the MY-TEST3 125
Fig. 5-35 – Water Mass Flow Rate measured by turbine flow meters during the MY-TEST3 125
Fig. 5-36 – Water Temperatures at the inlet and outlet of the SGBT during the MY-TEST3 126
Fig. 5-37 – Pressure drops along the bayonet tubes during the MY-TEST3 126
Fig. 5-38 – Pressure along the secondary loop during the MY-TEST3 126
Fig. 5-39 – LBE Mass Flow Rate measured by VFM during the MY-Test4 128
Fig. 5-40 – Inlet and Outlet Temperatures along the FPS during the MY-Test4 128
Fig. 5-41 – Inlet and Outlet Temperature along the SGBT Shell Side during the MY-Test4 128
Fig. 5-42 – Axial profile of the temperature inside the S100 vessel during the MY-Test4 129
Fig. 5-43 – Water Mass Flow Rate measured by turbine flow meters during the MY-Test4 129
Fig. 5-44 – Water Temperatures at the inlet and outlet of the SGBT during the MY-Test4 129
Fig. 5-45 – Pressure drops along the bayonet tubes during the MY-Test4 130
Fig. 5-46 – Pressure along the secondary loop during the MY-Test4 130
Fig. 5-47 – LBE Mass Flow Rate measured by VFM during the MY-Test5 131
Fig. 5-48 – Inlet and Outlet Temperatures along the FPS during the MY-Test5 132
Fig. 5-49 – Inlet and Outlet Temperature along the SGBT Shell Side during the MY-Test5 132
Fig. 5-50 – Axial profile of the temperature inside the S100 vessel during the MY-Test5 132
Fig. 5-51 – Water Mass Flow Rate measured by turbine flow meters during the MY-Test5 133
Fig. 5-52 – Water Temperatures at the inlet and outlet of the SGBT during the MY-Test5 133
Fig. 5-53 – Pressure drops along the bayonet tubes during the MY-Test5 133
Fig. 5-54 – Pressure along the secondary loop during the MY-Test5 134
Fig. 5-55 – LBE Mass Flow Rate measured by VFM during the MY-Test6 135

Fig. 5-56 – Inlet and Outlet Temperatures along the FPS during the MY-Test6 135
Fig. 5-57 – Inlet and Outlet Temperature along the SGBT Shell Side during the MY-Test6 135
Fig. 5-58 – Axial profile of the temperature inside the S100 vessel during the MY-Test6 136
Fig. 5-59 – Water Mass Flow Rate measured by turbine flow meters during the MY-Test6 136
Fig. 5-60 – Water Temperatures at the inlet and outlet of the SGBT during the MY-Test6 136
Fig. 5-61 – Pressure drops along the bayonet tubes during the MY-Test6 137
Fig. 5-62 – Pressure along the secondary loop during the MY-Test6 137
Fig. 5-63 – LBE Mass Flow Rate measured by VFM during the MY-Test7 138
Fig. 5-64 – Inlet and Outlet Temperatures along the FPS during the MY-Test7 139
Fig. 5-65 – Inlet and Outlet Temperature along the SGBT Shell Side during the MY-Test7 139
Fig. 5-66 – Axial profile of the temperature inside the S100 vessel during the MY-Test7 139
Fig. 5-67 – Water Mass Flow Rate measured by turbine flow meters during the MY-Test7 140
Fig. 5-68 – Water Temperatures at the inlet and outlet of the SGBT during the MY-Test7 140
Fig. 5-69 – Pressure drops along the bayonet tubes during the MY-Test7 140
Fig. 5-70 – Pressure along the secondary loop during the MY-Test7 141
Fig. 5-71 – LBE Mass Flow Rate measured by VFM during the MY-Test8 142
Fig. 5-72 – Inlet and Outlet Temperatures along the FPS during the MY-Test8 142
Fig. 5-73 – Inlet and Outlet Temperature along the SGBT Shell Side during the MY-Test8 142
Fig. 5-74 – Axial profile of the temperature inside the S100 vessel during the MY-Test8 143
Fig. 5-75 – Water Mass Flow Rate measured by turbine flow meters during the MY-Test8 143
Fig. 5-76 – Water Temperatures at the inlet and outlet of the SGBT during the MY-Test8 143
Fig. 5-77 – Pressure drops along the bayonet tubes during the MY-Test8 144

Fig. 5-78 – Pressure along the secondary loop during the MY-Test8 144
Fig. 6-1 – NACIE-UP P&ID 148
Fig. 6-2 – NACIE-UP facility layout 149
Fig. 6-3 – Fuel Pin Simulator geometry 149
Fig. 6-4 – View of the RELAP5-3D nodalization 151
Fig. 6-5 – Friction factor implemented in R5-3D model 153
Fig. 6-6 – Measurement points of the simulated quantities (from [48]) 158
Fig. 6-7 – Test 1, R5-3D boundary conditions 160
Fig. 6-8 – Test 1, LBE mass flow rate 160
Fig. 6-9 – Test 1, LBE temperature at FPS inlet/outlet and sections A:38 mm, B:300 mm, C:562 mm 160
Fig. 6-10 – Test 1, FPS temperature trend along the active length before and after the transient 161
Fig. 6-11 – Test 1, LBE temperature at the HX inlet and outlet sections 161
Fig. 6-12 – Test 1, H2O temperature at the HX inlet and outlet sections 161
Fig. 6-13 – Test 1, pressure along the primary loop 162
Fig. 6-14 – Test 2, R5-3D boundary conditions 163
Fig. 6-15 – Test 2, LBE mass flow rate 164
Fig. 6-16 – Test 2, LBE temperature at FPS inlet/outlet and sections A:38 mm, B:300 mm, C:562 mm 164
Fig. 6-17 – Test 2, FPS temperature trend along the active length before and after the transient 164
Fig. 6-18 – Test 2, LBE temperature at the HX inlet and outlet sections 165
Fig. 6-19 – Test 2, H2O temperature at the HX inlet and outlet sections 165
Fig. 6-20 – Test 2, pressure along the primary loop 165
Fig. 6-21 – Test 3, R5-3D boundary conditions 167
Fig. 6-22 – Test 3, LBE mass flow rate 167
Fig. 6-23 – Test 3, LBE temperature at FPS inlet/outlet and sections A:38 mm, B:300 mm, C:562 mm 168
Fig. 6-24 – Test 3, FPS temperature trend along the active length before and after the transient 168
Fig. 6-25 – Test 3, LBE temperature at the HX inlet and outlet sections 168

Fig. 6-26 – Test 3, H2O temperature at the HX inlet and outlet sections 169
Fig. 6-27 – Test 3, pressure along the primary loop 169
Fig. 6-28 – Up-dated model of the NACIE-UP loop 172
Fig. 6-29 – Stainless Steel Powder Thermal Conductivity 172
Fig. 6-30 – Power supplied by the Fuel Pin Simulator (left) and the Thermal Flow Meter (right) during the Test 1, experimental vs R5-3D 173
Fig. 6-31 – Argon Mass Flow Rate (left) and HX water inlet temperature (right) during Test 1, experimental vs R5-3D 173
Fig. 6-32 – Test1, LBE Mass Flow Rate, experimental vs R5-3D 174
Fig. 6-33 – Test1, LBE temperatures at FPS inlet-outlet sections, experimental vs R5-3D 175
Fig. 6-34 – Test1, LBE temperatures at HX inlet-outlet sections, experimental vs R5-3D 175
Fig. 6-35 – Test1, H2O temperatures at HX inlet-outlet sections, experimental vs R5-3D 175
Fig. 6-36 – Power supplied by the Fuel Pin Simulator (left) and the Thermal Flow Meter (right) during the Test 2, experimental vs R5-3D 176
Fig. 6-37 – Argon Mass Flow Rate (left) and HX water inlet temperature (right) during Test 2, experimental vs R5-3D 176
Fig. 6-38 – Test 2, LBE Mass Flow Rate, experimental vs R5-3D 177
Fig. 6-39 – Test2, LBE temperatures at FPS inlet-outlet sections, experimental vs R5-3D 178
Fig. 6-40 – Test2, LBE temperatures at HX inlet-outlet sections, experimental vs R5-3D 178
Fig. 6-41 – Test2, H2O temperatures at HX inlet-outlet sections, experimental vs R5-3D 178
Fig. 6-42 – Power supplied by the Fuel Pin Simulator (left) and the Thermal Flow Meter (right) during the Test 3, experimental vs R5-3D 179
Fig. 6-43 – Argon Mass Flow Rate (left) and HX water inlet temperature (right) during Test 3, experimental vs R5-3D 179
Fig. 6-44 – Test 3, LBE Mass Flow Rate, experimental vs R5-3D 180
Fig. 6-45 – Test3, LBE temperatures at FPS inlet-outlet sections, experimental vs R5-3D 181

Fig. 6-46 – Test3, LBE temperatures at HX inlet-outlet sections, experimental vs R5-3D.....181

Fig. 6-47 – Test3, H2O temperatures at HX inlet-outlet sections, experimental vs R5-3D.....181

(Page intentionally left blank)

LIST OF TABLES

Tab. 1-1 – Main characteristics of Generation IV technologies 29

Tab. 1-2 – Main characteristics of GEN IV reactor coolants 29

Tab. 1-3 – Summary of the recommended correlations for thermophysical properties of pure liquid lead 32

Tab. 1-4 – Summary of the recommended correlations for main thermophysical properties of molten LBE 32

Tab. 1-5 – List of the international heavy liquid metal test facilities 35

Tab. 2-1 – CIRCE main parameters 48

Tab. 2-2 – HERO SGBT tubes dimensions 59

Tab. 3-1 – CIRCE-HERO main operating conditions 78

Tab. 3-2 – RELAP5-3D boundary conditions 78

Tab. 3-3 – AISI 316L powder thermal conductivity as a function of the temperature 79

Tab. 3-4 – Secondary loop simulation test matrix 79

Tab. 3-5 – Main results in nominal steady state conditions for CASE A and CASE B 80

Tab. 4-1 – Designed Boundary Conditions for the SGBT unit 85

Tab. 4-2 – Designed Boundary Conditions for the transient 85

Tab. 4-3 – SE-Test1, boundary conditions before and after the transient 87

Tab. 4-4 – SE-Test1, FPS Power decay heat curve during transient 88

Tab. 4-5 – SE-Test2, boundary conditions before and after the transient 93

Tab. 4-6 – SE-Test3, boundary conditions before and after the transient 100

Tab. 4-7 – SE-Test3, FPS Power and argon FLOW RATE trends during the transient 101

Tab. 5-1 – MYRTE Test Matrix 109

Tab. 6-1 – Steel powder AISI 316L+Helium at 5 bar thermal properties 155

Tab. 6-2 – Thermal insulation by mineral wool thermal properties 156

Tab. 6-3 – Designed boundary conditions for NACIE-UP experiments 156

Tab. 6-4 – Parameters for the SYS-TH codes benchmark exercise 157

Tab. 6-5 – Experimental boundary conditions of NACIE-UP tests 170

(Page intentionally left blank)

1 INTRODUCTION

In near future nuclear energy is expected to play an important role in the frame of energy needs in terms of sustainability, safety, proliferation resistance and economy. Moved by a careful policy towards security of supply and climate changes, many countries, including emerging and developing areas, look with a rising interest in nuclear energy for electricity generation and non-electrical purposes. In this scenario, the aim of the Generation IV (GEN IV) reactors is to increase the future growth and benefits deriving from nuclear energy utilization [1][2]. The design of GEN IV plants makes use of the best technologies and systems in order to meet the requested requirements of [3]:

- sustainability: nuclear energy must be generated in a clean way with a manage of nuclear waste in order to protect the public health and the environment, and systems have to ensure performance improvement and more sustainable approach with an effective fuel utilization for worldwide energy production and a minimization of waste;
- economics: the plants and the fuel must have a cost advantage over other energy sources and the level of financial risk must be lower or comparable with other energy projects;
- safety and reliability: the strength of GEN IV systems must be the safety and reliability with a very low chance of a severe accident, especially for reactor core damages, and avoiding the need for offsite emergency response;
- proliferation resistance: physical protection is another important point for nuclear plants. GEN IV systems must assure the least chance of theft of materials useful for military purposes and to provide increased protection against acts of terrorism.

The research programs are promoted by the Generation IV International Forum (GIF), a co-operative international endeavour counting fourteen members worldwide (including EURATOM for the EU). The GIF was set up with the main purpose to support the research and development needed to establish the feasibility and performance capabilities of the next generation nuclear energy systems [4]. In this framework, two EU projects are included: the HORIZON2020 SESAME project, which coordinates a series of thermal-hydraulics Simulations and Experiments for the Safety Assessment of MEtal cooled reactors, in order to support the development of the European liquid metal fast reactors, and the HORIZON2020 MYRTE project, aiming at supporting the development of MYRRHA (Multi-purpose hYbrid Research Reactor for High-tech Applications). These

two projects will be detailed in dedicated sections of this document, since they are the framework of the activities described.

Depending on their respective degree of technical maturity, the first GEN IV systems are expected to be deployed commercially around 2030-2040.

1.1 FOCUS ON GENERATION IV HLM FAST REACTORS

After extensive R&D (Research and Development) activities undertaken since 2000 and an analysis of different solutions, six concepts of reactors have been selected for the organization of the research program:

- ***Gas-cooled fast reactors (GFR)***: helium as coolant and high operating temperatures, resulting in a higher efficiency of electricity production; they also have a self-generating core with fast neutron spectrum and the possible combination with an on-site fuel reprocessing facility for the actinide recycling;
- ***Lead cooled fast reactors (LFR)***: fast neutron spectrum and a closed fuel cycle, operated as a breeder or a burner of actinides from spent fuel using inert matrix fuel. The coolant used could be lead or Lead-bismuth Eutectic (LBE);
- ***Molten salt reactors (MSR)***: molten salts mixture as coolant. Their particularly is the breeding capability in any kind of neutron spectrum from thermal to fast with a considerable reduction of radiotoxic nuclear waste;
- ***Sodium cooled fast reactors (SFR)***: designed in a pool layout or a close loop layout, using liquid sodium as coolant. This choice allows a high power density with low coolant volume fraction. As the LFR, they are characterised by a fast-neutron spectrum and a closed fuel cycle with actinide recycling;
- ***Supercritical water-cooled reactors (SCWR)***: a particular system cooled by water and characterised by high temperature and high pressure above the thermodynamic critical point (374°C, 22.1 MPa). It works with a direct cycle that allows higher thermodynamic efficiency and plant simplifications;
- ***Very high temperature gas reactors (VHTR)***: helium as coolant and graphite as moderator with a thermal neutron spectrum. The operating temperature can be greater than 900°C.

Tab. 1-1 shows the main characteristics of the solutions mentioned above. Each technology involves the use of different types of coolants, each one characterised by particular

properties (see Tab. 1-2), needing different approaches for the technological development of the systems.

Tab. 1-1 – Main characteristics of Generation IV technologies

System	Coolant	Neutron Spectrum	Fuel Cycle
Gas-cooled Fast Reactors (GFR)	Helium	Fast	Closed
Lead-cooled Fast Reactors (LFR)	Lead/LBE	Fast	Closed
Molten-Salt Reactors (MSR)	Fluoride salts	Epithermal	Closed
Sodium-cooled Fast Reactors (SFR)	Sodium	Fast	Closed
Supercritical Water-Cooled Reactor (SWCR)	Water	Thermal/fast	Closed/open
Very High Temperature gas Reactors (VHTR)	Helium	Thermal	Closed

Tab. 1-2 – Main characteristics of GEN IV reactor coolants

Coolant	Atomic Mass [g/mol]	Relative moderating power	Neutron Absorption cross-section (1 MeV) [mbarn]	Neutron scattering cross-sections [barn]	Melting point [°C]	Boiling point [°C]	Chemical reactivity (with air and water)
Pb	207	1	6.001	6.4	327	1737	Inert
LBE	208	0.82	1.492	6.9	125	1670	Inert
Na	23	1.80	0.230	3.2	98	883	Highly reactive
H2O	18	421	0.1056	3.5	0	100	Inert
D2O	20	49	0.0002115	2.6	0	100	Inert
He	2	0.27	0.007953	3.7	-	-269	Inert

The R&D activities have identified the LFRs as one of the most promising technologies to meet the requirements introduced for GEN IV nuclear plants, thanks to the following characteristics:

- very low neutron absorption cross section and poor moderating power, allows to design fast-neutron spectrum with geometries characterized by a high coolant/fuel ratio and fuel bundle with high pitch-to-diameter ratio. The fast neutron spectrum and the breeding ration about 1 make possible an efficient utilization of excess neutrons and reduction of uranium consumptions with a reduction of the high radiotoxic waste thanks to a close fuel cycle.
- the coolant high molten point and the low vapour pressure allows a primary loop operating at atmospheric pressure and low temperatures; moreover, the high shielding capability against gamma radiation offers a great protection to the workers with very low doses. The good thermo-physical properties allow to design cores with a high pitch/diameter ratio with low pressure drops and consequently low power requested for pumping. In terms of passive safety, with an effective configuration it is possible to increase the system capability to remove the decay power in natural circulation regime with a consequent reduction of the active safety systems. The high density can avoid the risk of fuel compaction and subsequent achievement of critical conditions in case of core melting, promoting the dispersion phenomena, moreover, in case of breakage of the steam generator tubes, the high density of coolant reduces the risk of steam inlet inside the core. Finally, in case of loss of flow accident in the primary loop, the leaked lead will solidify in a very short time without significant chemical reactions, avoiding further loss of coolant and protecting the nearby structures and equipment.
- the MOX (Mixed Oxide Fuel) used contains actinides and it makes these systems unattractive for the extraction of weapon-usable materials. After all, the nuclear properties of the coolant can allow the realization of cores with a long life and not useful for the production of weapon-grade plutonium. The physical protection to the public and to the environment is assured by the coolant, which does not react with air and water at low pressure and reduces the need for strong protection against the risk of catastrophic events deriving from natural causes or acts of sabotage, avoiding the chance of significant containment pressurization. Furthermore, the absence of inflammable substances reduces the risk of fire propagation.
- the simple design reduces the building time, the capital cost and the operation and maintenance cost in order to offer a competitive price of the electricity generated.

This is possible thanks to the favourable characteristics of the coolant chosen which allows the realization of low-pressure system with a steam generator integrated in the primary loop with less complexity and dimension of systems. The absence of an intermediate loop makes possible thermal cycles characterized by a very high efficiency.

Among all coolants studied, Lead and LBE, a Lead-Bismuth Eutectic composed by 44.5 wt.% Pb + 55.5 wt.% Bi, developed in order to increase the favourable properties of lead and reduce its drawbacks, have been selected as candidates for GEN IV reactors. The characteristics of these two coolants are hereinafter listed:

- low moderation capability allows the achievement of a harder neutron spectrum, which results in better neutron economy;
- high boiling temperature: it is an important safety feature, essentially eliminating pressurisation and boiling concerns while enhancing the inherent safety of reactor cores.
- higher allowable operating temperatures also improve the efficiency and feasibility of other energy products;
- low melting temperature (especially for LBE) can reduce the risk of uncontrolled local freezing;
- high density promotes the dispersion of molten fuel in case of core failure, avoiding the formation of a secondary critical mass;
- no energetic reaction with air and water makes easier and safer all the operating processes and the procedures in case of an accident; all the causes of fire can be eliminated;
- very good shielding against gamma rays and energetic neutrons reduces to a very low level the dose to workers;
- high solubility of the actinides in the coolant, which could help to minimise the potential for re-criticality events upon core melting;
- excellent thermo-hydraulic properties which allow a good heat transfer in case of both forced circulation and natural circulation, increasing the passive safety and reducing the complexity of components and systems.

The most up-dated properties and the recommended correlations available in the literature for pure lead and LBE are reported in Tab. 1-3 and Tab. 1-4, respectively [5].

Tab. 1-3 – Summary of the recommended correlations for thermophysical properties of pure liquid lead

Property, parameter (at p ~ 0.1 MPa)	SI unit	Correlation	T range [K]	Estimated error ±
Melting temperature	K	$T_{M,0} = 600.6$	n/a	0.1
Latent heat of melting	kJ kg^{-1}	$Q_{M,0} = 23.07$	n/a	0.14
Boiling temperature	K	$T_{B,O} = 2021$	n/a	3
Latent heat of boiling	kJ kg^{-1}	$Q_{B,0} = 858.6$	n/a	1.9
Critical temperature	K	$T_c = 5000$	n/a	200
Critical density	kg m^{-3}	$\varrho_c = 3250$	n/a	100
Critical pressure	MPa	$p_c = 180$	n/a	30
Saturated vapour pressure	Pa	$ps = 1.88 \times 10^{13} \cdot T^{-0.985} \cdot \exp(-23325/T)$ or $p_s = 5.76 \times 10^{9} \cdot \exp(-22131/T)$	601-2021	15% 18%
Surface tension	N m^{-1}	$\sigma = (525.9 - 0.113 \cdot T) \times 10^{-3}$	601-1300	4%
Density	kg m^{-3}	$\varrho = 11441 - 1.2795 \cdot T$	601-1900	1%
Sound velocity	m s^{-1}	$u_s = 1953 - 0.246 \cdot T$	601-2000	2%
Bulk modulus	Pa	$B_s = (43.50 - 1.552 \times 10^{-2} \cdot T + 1.622 \times 10^{-6} \cdot T^2) \times 10^9$	601-1900	5%
Isobaric specific heat	J kg^{-1} K^{-1}	$c_p = 176.2 - 4.923 \times 10^{-2} \cdot T + 1.544 \times 10^{-5} \cdot T^2 - 1.524 \times 10^{6} \cdot T^{-2}$	601-1300	5%
Dynamic viscosity	Pa s	$\eta = 4.55 \times 10^{-4} \cdot \exp(1\,069/T)$	601-1500	5%
Electric resistivity	Ω m	$r = (67.0 + 0.0471 \cdot T) \times 10^{-8}$	601-1300	2%
Thermal conductivity	W m^{-1} K^{-1}	$\lambda = 9.2 + 0.011 \cdot T$	601-1400	(15%)

Tab. 1-4 – Summary of the recommended correlations for main thermophysical properties of molten LBE

Property, parameter (at p ~ 0.1 MPa)	SI unit	Correlation	T range [K]	Estimated error ±
Melting temperature	K	$T_{melt} = 397.7$	--	0.6 K
Latent heat of melting	kJ kg^{-1}	$Q_{melt} = 38.6$	--	0.2 kJ kg^{-1}
Boiling temperature	K	$T_{boil} = 1943$	--	10 K
Latent heat of boiling	kJ kg^{-1}	$Q_{boil} = 854$	--	2 kJ kg^{-1}
Saturated vapour pressure	Pa	$P_s = 11.1 \times 10^9 \_ \exp^{(-22552/T)}$	508-1943	50%
Surface tension	N m^{-1}	$\sigma = (437.1 - 0.066\ T) \times 10^{-3}$	423-1400	5%
Density	kg m^{-3}	$\varrho = 11096 - 1.3236\ T$	403-1300	0.8%
Sound velocity	m s^{-1}	$u_s = 1773 + 0.1049\ T - 2.873 \times 10^{-4}\ T^2$	403-1300	--
Bulk modulus	Pa	$B_s = (35.18 - 1.541 \times 10^{-3}\ T - 9.191 \times 10^{-6}\ T^2)\ 10^9$	430-605	0.05%
Isobaric specific heat	J kg^{-1} K^{-1}	$c_p = 159 - 2.72 \times 10^{-2}\ T + 7.12 \times 10^{-6}\ T^2$	430-605	7% (?)
Dynamic viscosity	Pa s	$\eta = 4.94 \times 10^{-4}\ \exp^{(754.1/T)}$	400-1100	5%
Electric resistivity	Ω m	$r = (86.334 + 0.0511\ T)\ 10^{-8}$	403-1100	6%
Thermal conductivity	W m^{-1} K^{-1}	$\lambda = 3.61 + 1.517 \times 10^{-2}\ T - 1.741 \times 10^{-6}\ T^2$	403-1100	5% (?)

Several research activities and projects related to the lead and LBE technology development are ongoing in EU. In particular, the design of two main systems is actually ongoing: MYRRHA (Multi-purpose hYbrid Research Reactor for High-tech Applications), a subcritical research reactor using LBE as coolant [6] and ALFRED (Advanced Lead Fast Reactor European Demonstrator), developed in the framework of the LEADER (Lead cooled European Advanced DEmonstration Reactor project), designed to test and qualify innovative components and procedures to be used in commercial reactors [7][8]. The extensive R&D efforts undertaken are necessary in order to improve the knowledge and the experience performed in terms of design, operations, maintenance and materials for components. The LFR/ADS (Accelerator Driven System) technological issues concern the following main topics [9]:

- material studies and physical-chemistry coolant characterization – it is necessary to assess the phenomena in which the lead and LBE are involved in LFR/ADS. The contamination of the lead by metal oxide and the corrosion of structural materials is the main issue in these systems. The long term exposure to liquid metal leads to embrittlement and degradation of structures and primary system components as vessel, internals, heat exchangers, fuel cladding;
- irradiation studies – The activities focus on structural materials subject to fast neutron fluxes defining their resistance for thermal stresses and DPA (Displacements Per Atom) and determining whether or not irradiation promotes embrittlement and corrosion attack by Heavy Liquid Metals (HLMs). The main issues on the performance of materials are due to the corrosion on HMLs under irradiation, irradiation embrittlement, as well as neutron irradiation induced effects such as creep and swelling;
- thermal-hydraulic properties – the relevant issues of the HLMs thermal-hydraulics research are related to:
    - HLM pool thermal-hydraulics which identifies as main topics the study of forced convection flow (mixing, stratification, stagnant zones, surface level oscillations), natural convection flow (pressure drops, surface level oscillations), transition to buoyancy-driven flow, fluid-structure interaction and system response to seismic events.
    - Fuel Assembly thermal-hydraulics, with the main scope to define the assembly geometries to achieve optimal conditions for heat transfer between fuel rods and coolant in forced and natural circulation, also demonstrating the capability to maintain the geometrical features, withstanding to irradiation effects, high temperatures, mechanical loads and corrosion. Other

issues needing investigation are: the sub-channel flow distribution, the cladding temperature profile and hot spot, the pressure drops, the vibrations induced by flow, the fluid structure interaction, as a consequence of a hypothetic core damage;

- instrumentation – the suitable instrumentation for LFR/ADS is an important challenge due to the high thermal loads, high temperatures, the corrosive environment, the fast neutron spectrum and the non-transparency of the coolant. The research activities aim to develop instrumentation capable to withstand the operating conditions of the (Heavy Liquid Metal Reactors) HLMRs and to maintain the reliability of the measurements for a long time.

The next section reports the ongoing research activities and experimental facilities aiming at supporting the LFRs technological development.

1.2 ACTUAL STATUS OF HLM TECHNOLOGIES

In the framework of the development of new nuclear technologies, the HLMRs represent one of the most promising concepts, allowing to achieve the requirements introduced for the Generation IV reactors of safety, reliability, sustainability, economic competitiveness and resistance to the proliferation. Since the interest in HLMs is increased, the scientific communities focused the attention on these coolants, undertaking several R&D activities devoted the study of thermal-fluid dynamics, material compatibility and other technological issues related to their use in nuclear applications. For these reasons, a relevant effort has been undertaken by EU to funding a series of R&D projects and several experimental facilities have been designed and realized by laboratories or expert groups participating to the HLM research activities. Such facilities aim at investigating on the key topics of the HLMs, acquiring knowledge related to their use, as well as to characterize and validate the measurement techniques and to provide feedbacks to improve physical models and a database for codes validation.

In particular, hereinafter are reported the most relevant experimental facilities actually involved in the study of Lead-Bismuth Eutectic thermal-hydraulics and related phenomena. A summary is reported in Tab. 1-5 [10].

Tab. 1-5 – List of the international heavy liquid metal test facilities

Association/Country	Name of facility	Type of facility	T max	Flow Rate
KIT, Germany	THEADES	loop	450°C	100 m^3/h
KTH, Sweden	TALL-3D	loop	500°C	5 kg/s
SCK•CEN, Belgium	E-SCAPE	pool	350°C	120 kg/s (FC) 2.4 kg/s (NC)
SCK•CEN, Belgium	COMPLOT	loop	400°C	36 m^3/h
KIT, Germany	FRETHME	----	650°C	----
INEST/FDS	CLEAR-S	pool	500°C	100 m^3/h
INEST/FDS	KYLIN-II	loop	500°C	45 m^3/h
ENEA	CIRCE	pool	500°C	40 kg/s (FC) 6 kg/s (NC)
ENEA	NACIE-UP	loop	500°C	5 kg/s (FC) 1 kg/s (NC)

THEADES (THErmal-hydraulics and Ads DESign), operating at KIT (Germany) [11]: it is a loop-type facility, LBE-cooled, investigating on thermal-hydraulic single-effect investigations of ADS components. The main objectives are:

- cooling capability of ADS beam windows both in window and windowless configuration;
- flow field and surface shape measurements of the HLM in a windowless target configuration
- cooling of single fuel element(s) and fuel rod bundles
- heat transfer characteristics of different heat exchanger types,
- providing a thermal-hydraulic data base for physical model development and code validation for CFD and system analysis code packages.

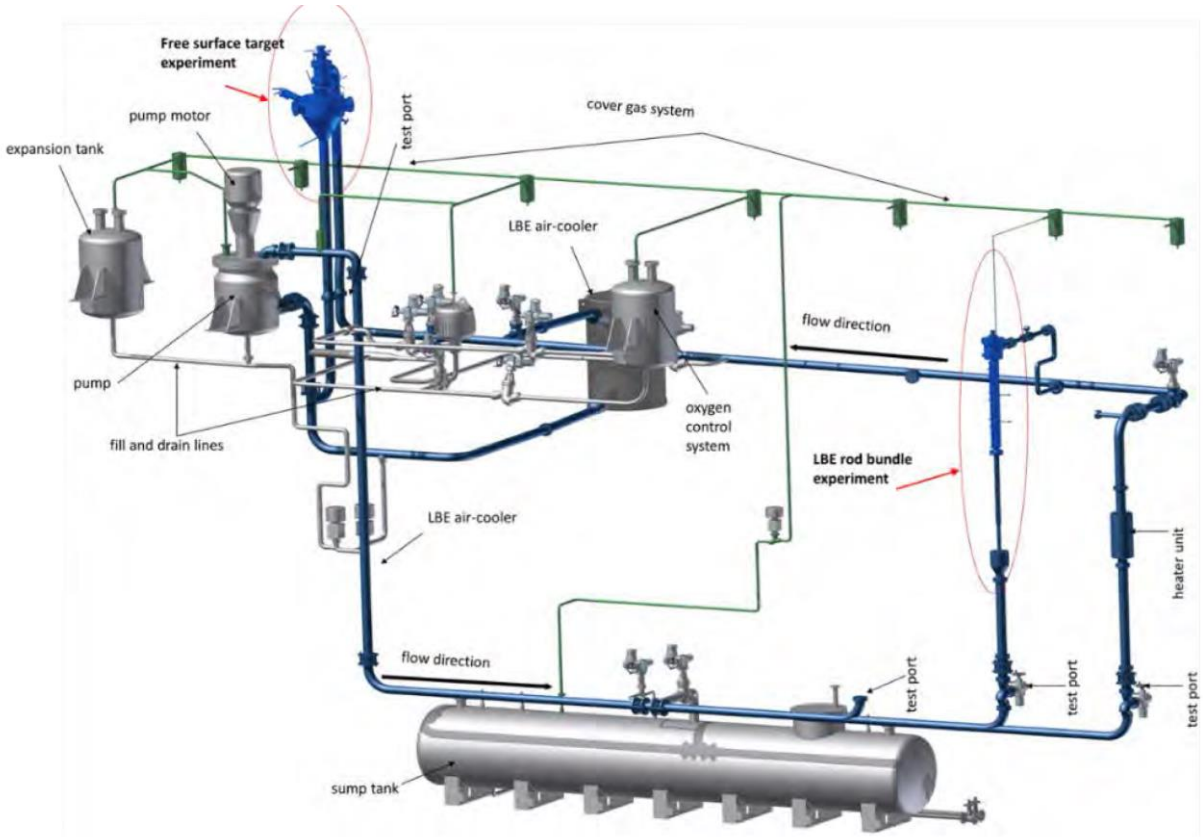

Fig. 1-1 – Scheme of THEADES loop (from [5])

TALL-3D (Thermal-Hydraulic ADS Lead-Bismuth Loop), operating at KTH (Sweden) [12]: 3-leg LBE loop with a small scale pool developed according to the requirements for the experimental data for validation of coupled SYS-TH and CFD codes. The main objectives are [12]:

- to achieve mutual feedback between natural circulation in the loop and complex 3D mixing and stratification phenomena in the pool-type test section;
- a possibility to validate standalone SYStem Thermal-Hydraulics (SYS-TH) and CFD codes for each subsection of the facility;
- to collect experimental data for the set-up of thermal-hydraulics physical models and code validation.

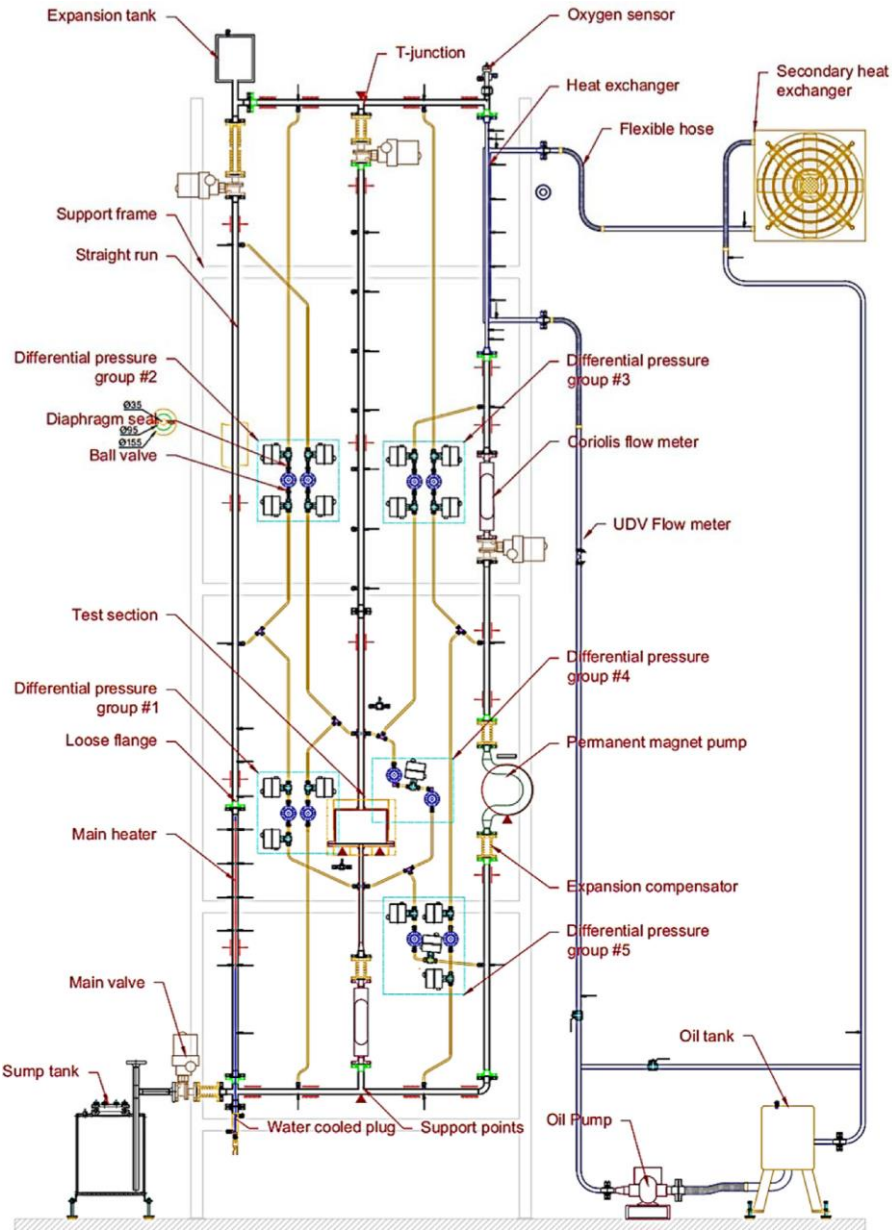

Fig. 1-2 – Scheme of TALL-3D experimental facility (from [12])

E-SCAPE (European Scaled Pool Experiment), operating at SCK•CEN (Belgium) [13]: it is a pool-type reactor with LBE as primary coolant. The facility is a thermal-hydraulic 1/6-scale model of the MYRRHA reactor. The main object of the experiments are:

- investigation on mixing and stratification in liquid-metal pool-type reactors;
- investigation on forced convection, natural convection and the transition;
- tests on integral system behaviour;
- investigation on free surface oscillations;
- to validate the computational methods for their use with LBE.

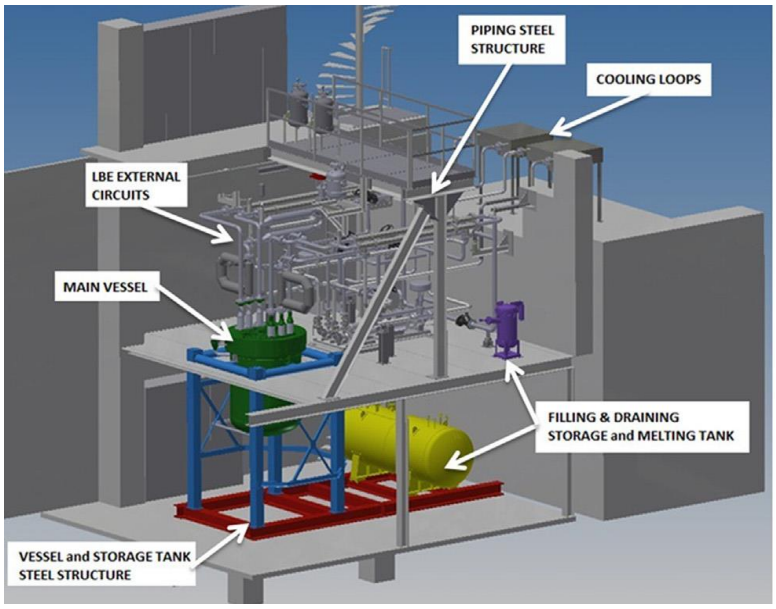

Fig. 1-3 –Isometric view of the E-SCAPE facility (from [13])

COMPLOT (COMPonent LOop Testing), operating at SCK•CEN (Belgium) [14]: an LBE-loop designed to investigate on thermal-hydraulics of MYRRHA components (fuel assembly, spallation target, control rod and safety rod) at full scale. In particular, the loop includes a 1:1 mock-up of the MYRRHA fuel assembly.

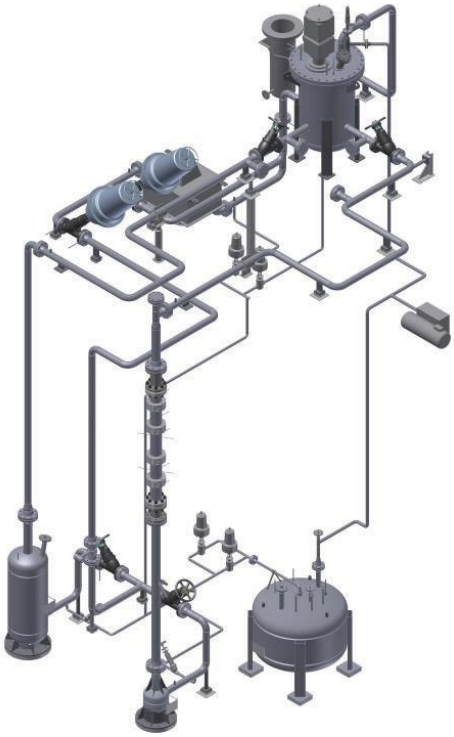

Fig. 1-4 – Isometric view of the COMPLOT facility (from [14])

FRETHME (FREtting Tests in Heavy liquid MEtal), operating at KIT (Germany) [15]: an experimental facility designed to simulate experimentally the fretting corrosion process in heavy liquid metals at reactor relevant conditions. The main objectives are:

- fretting corrosion of cladding materials in stagnant Pb and PbBi;
- effects of frequency, amplitude, temperature, oxygen content, load on fretting corrosion.

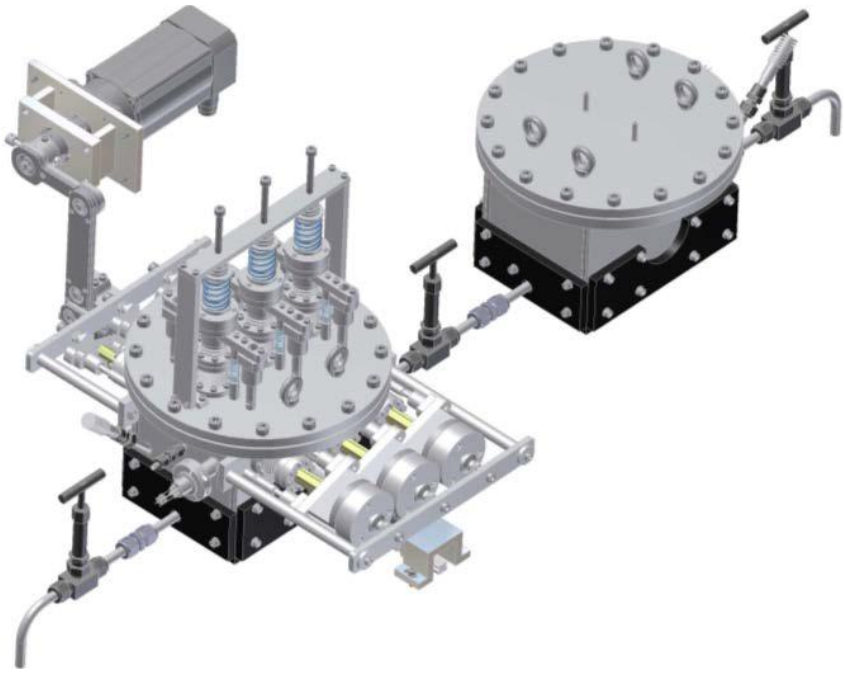

Fig. 1-5 – Isometrical view of the FRETHME facility (from [15])

CLEAR-S (China LEAd-based Reactor), operating at INEST (China) [16]: it is a pool-type integrated test platform designed to carry out a variety of tests for separation or coupling integration of equipment based on the needs of different experiments, which mainly focuses on the following objectives:

- test and validation of the LBE reactor main components (heat exchangers, primary pump, refuelling system, control rod driven system, decay heat removal system, etc.) in a relevant scale, analysing their performances in a pool-type LBE environment for both transients and endurance tests;
- research and validation of key non-nuclear technology (pool-type reactor coolant process technology, pool-type LBE environment measuring technology, integration and control technology, verification and validation of numerical tools)
- obtain the experiment data to support the construction and operation license of CLEAR-I.

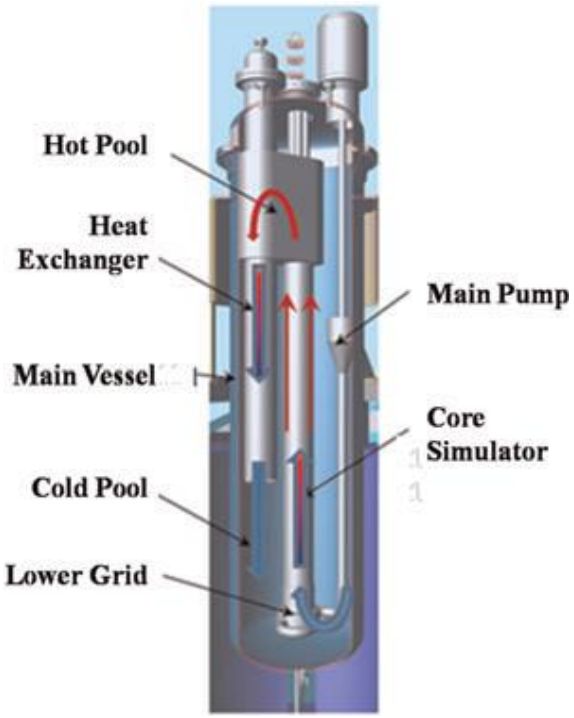

Fig. 1-6 – General layout of the CLEAR-S main vessel (from [16])

KYLIN-II, operating at INEST (China) [17]: it is a large multi-functional LBE-cooled loop-type facility. The KYLIN-II forced circulation loop is aimed to perform hydraulic components test related to reactors cooled by HLMs, as well as structural materials corrosion experiment, fuel assembly flow and heat transfer investigation, forced and natural circulation experiment, components prototype proof test, and heat exchanger tube rupture accident investigation.

Fig. 1-7 – View of the KYLIN-II loop (from [17])

CIRCE (CIRColazione Eutettico), operating at ENEA Brasimone R.C. (Italy): a pool-type facility hosting dedicated test sections for integral effect tests. A detailed description of the facility is provided in this document in Section 2.

NACIE-UP (NAtural CIrculation Experiment), operating at ENEA Brasimone R.C. (Italy): a loop-type facility dedicated to investigate flow behaviour in all flow regimes and specifically the transition from forced to natural circulation regime due to a protected loss of flow accident in different scales of HLM pools and to experimental data for the validation and benchmarking of numerical codes. A detailed description of the facility is provided in this document in Section 6.2.

1.3 FRAMEWORK OF THE ACTIVITY

This research activity has been realized in partnership between DIAEE (Dipartimento di Ingegneria Astronautica, Elettrica ed Energetica) of Sapienza University of Rome and ENEA (Agenzia nazionale per le nuove tecnologie, l'energia e lo sviluppo economico sostenibile), and it has been co-financed by ENEA and SRS (Servizi di Ricerche e Sviluppo). The activities are strictly connected to the EU scientific community, since DIAEE and ENEA are partners of the two HORIZON2020 European Projects SESAME and MYRTE.

1.4 OBJECTIVES OF THE ACTIVITY

The main goal of this doctoral research is to support the development of HLMRs technologies by means of experimental and numerical activities performed on dedicated prototypical experimental facilities reproducing the main thermal-hydraulic aspects of nuclear plants.

Thanks to the collaboration with ENEA, two experimental campaigns have been set-up and performed, involving CIRCE (CIRColazione Eutettico), the largest pool-type facility worldwide in operation, cooled by LBE. The experiments allowed to achieve important feedback on the HLM thermal-hydraulics, reproducing in relevant scale the operative conditions of LFRs, acquiring engineering and safety feedbacks for designer and high quality data for code validation/model development. Furthermore, a numerical benchmark activity has been performed on the LBE-cooled NACIE-UP (NAtural CIrculation Experiment- UPgraded) experimental facility, developed and built in the

ENEA Brasimone R.C., with the objective to validate the code RELAP5-3D© for the assessment of the thermal-hydraulic behaviour of the heavy liquid metals, in order to apply it for the simulation of the next GEN IV reactors.

At the present, the following activities have been carried out and the related objectives have been achieved during the doctoral activity:

- Set-up and execution of an experimental campaign on the pool-type LBE-cooled CIRCE facility at ENEA Brasimone R.C. in the framework of HORIZON2020 SESAME European project, in support of the development of the ALFRED steam generator:
  - design and set-up of the experimental facility (i.e. systems, components, instrumentation, data and control acquisition systems).
  - execution of three experimental tests consisting of transients reproducing Protected Loss Of Flow Accident (PLOFA) scenarios.
  - data collected and delivered within the project to improve the knowledge and the experience in terms of design and operations and for code validation/model development.
- Set-up and execution of an experimental campaign on the CIRCE facility at ENEA Brasimone R.C. in the framework of HORIZON2020 MYRTE European project, in support of the development of the primary heat exchanger of MYRRHA:
  - set up of the experimental devices;
  - preliminary numerical analysis by RELAP5-3D© v. 4.3.4 code for the definition of the test conditions;
  - execution of nine experimental tests consisting of steady states in relevant condition for the MYRRHA primary heat exchanger;
  - data collected and delivered to the project members;
- Participation at Benchmark numerical activity on NACIE-UP HLM experimental facility in the framework of HORIZON2020 SESAME European project:
  - set-up of a thermal-hydraulic model of the LBE-cooled loop type facility NACIE-UP by RELAP5-3D© v. 4.3.4 code;
  - blind Simulation of the tests foreseen in the experimental campaign, reproducing steady-state, transient and accidental scenarios;
  - post-test calculation and comparison with the experimental data;
  - assessment of the RELAP5-3D© capabilities to reproduce the tests and related phenomena;

- thermal-hydraulic analysis of wire wrapped rod bundle and test of the available correlations;
- benchmark activity with comparison of the results among different SYS-TH codes used by the participants.

On the basis of the activities performed, the present work is structured as follows.

The first section provides the main information of the work, presenting a general overview of the LFRs development, as well as the ongoing projects and the facility actually involved in the R&D programs. Furthermore, the framework of the doctoral activity is presented and the objectives are explained.

The second section is dedicated to the description of the LBE-cooled pool-type facility CIRCE. In particular, a detailed description of the new test section named HERO (Heavy liquid mEtal pRessurized water cOoled tubes), installed in the CIRCE main vessel, is provided. The test section aims to test a new component consisting of a steam generator with double-wall bayonet tubes, evaluating its thermal-hydraulic performances in normal operational and transient scenarios. For this purpose, the experimental set-up has been prepared and the test conditions have been defined.

The third section is dedicated to the preliminary numerical activities in support of the CIRCE-HERO design. In particular, the RELAP5-3D© model of the HERO secondary loop has been set-up and it has been used to perform a pre-test analysis to define the start-up procedure of the facility and to achieve feedbacks on the performances of the steam generator.

The fourth and fifth sections are the core of the activity, since they describe the two experimental campaign executed on CIRCE-HERO. An experimental campaign, consisting of three tests, has been performed in the framework of the HORIZON2020 SESAME EU project, with the objective to support the development of the ALFRED design. A second experimental campaign, consisting of nine tests, has been executed in the framework of the HORIZON2020 MYRTE EU project, with the purpose to provide support to the development of MYRRHA and acquiring experimental data relevant for MYRRHA primary heat exchanger.

The last section describes the simulation activity performed in the Benchmark exercise for SYS-TH codes and CFD/SYS-TH codes validation, in the framework of the H2020 SESAME project. A RELAP5-3D© model of the NACIE-UP facility has been set up and it has been involved to perform a preliminary blind simulation activity and a subsequent post-test analysis on the basis of the experimental results available from the test performed on NACIE-UP.

Conclusions and future perspectives are given in the last section. An Appendix at the end of the document has been introduced, reporting the instrumentation list of the CIRCE-HERO facility. A second Appendix reports the Journal papers and Conference papers published, as well as the technical documents produced during the research activity.

2 DESIGN AND OPERATION OF THE CIRCE-HERO FACILITY

This section provides a detailed description of the geometries and materials of the components of the CIRCE facility and the HERO (Heavy liquid mEtal pRessurized water cOoled tubes) Test Section (TS) realized and implemented for the experimental campaigns described in this work.

2.1 CIRCE EXPERIMENTAL FACILITY

CIRCE (CIRcolazione Eutettico) is an integral effect pool-type facility using LBE as primary coolant, designed and realized at the ENEA Brasimone Research Centre [18][19]. A 3D view of the facility is reported in Fig. 2-1. It is mainly composed of:

- ***S100 main vessel*** (Fig. 2-2(a)), having an inner diameter of 1170 mm, a thickness of 15 mm, and height of about 8500 mm. It is partially filled (up to 500 mm from the top flange) with about 70 tons of LBE and argon as cover gas maintained at about 0.2 barg. The S100 main vessel is coated by rock wool to minimize the thermal losses in the environment and it is equipped with electrical heating cables, installed on its bottom and lateral surfaces. This heating system allows operating in a temperature range of 250÷300°C. The cover gas of the main vessel is also equipped by a self-controlled discharge system and a passive pressure safety system (rupture disks), in order to prevent accidental overpressure. The main vessel has been designed to host the test sections realized for the execution of the experimental campaigns;

- ***S200 storage tank*** (Fig. 2-2(b)), in which the LBE is stored during the periods of maintenance and refurbishment of the facility. The tank is coated by rock wool to minimize the thermal losses and it is equipped by heating cables that maintain the temperature of the LBE in range of 250°C-300°C.

- ***S300 transfer tank*** (Fig. 2-2(c)), used during the filling and draining phases of the main vessel. The tank is used as a lung during the transfer of the LBE from the storage tank to the S100 main vessel and vice-versa. The transfer tank is coated by rock wool and it is equipped by heating cable, as well as the piping and valves installed along the draining line.

- ***Gas circulation system***, used for the for gas enhanced-circulation of the LBE. It is composed by two sub-systems: the Argon Recirculation System (ARS) and the

Argon Injection System (AIS). The ARS is equipped by a set of 5 compressors connected in parallel (Fig. 2-3) and an argon storage tank, acting as gas lung and directly connected to external gas tanks used for argon re-integration. The AIS is connected to the ARS upstream of the set of compressors. The compressors are alternative type, oil-free, using water as cooling fluid and suitable for no-stop service.

The main parameters of CIRCE are listed in Tab. 2-1.

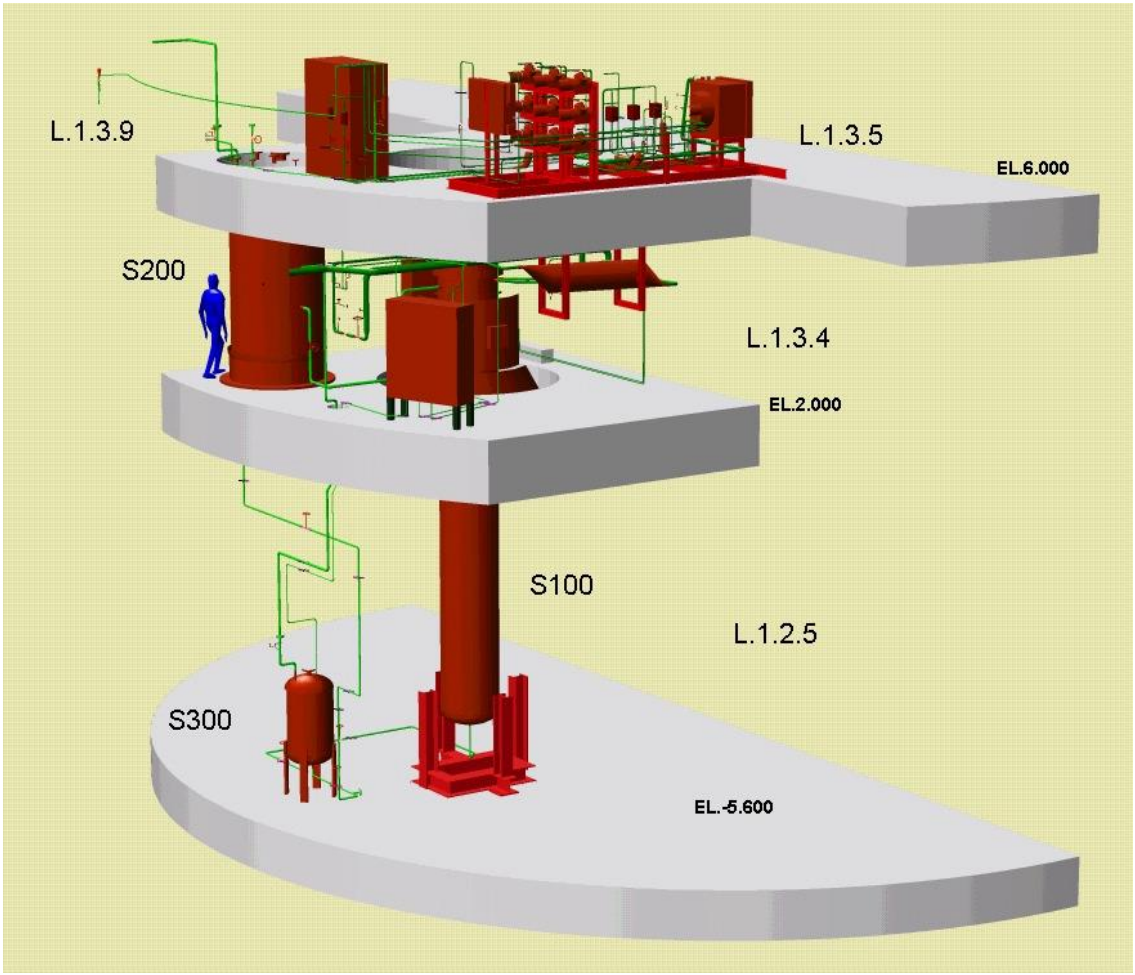

Fig. 2-1 – Schematic view of the CIRCE facility

(a)

(b)

(c)

Fig. 2-2 – View of the S100 main vessel (a), S200 storage tank (b) and S300 transfer tank (c)

Fig. 2-3 – View of the compressor unit for the argon circulation

Tab. 2-1 – CIRCE main parameters

CIRCE Parameters	**Value**
Outside Diameter [mm]	1200
Wall Thickness [mm]	15
Material	AISI316L
Max LBE Inventory [kg]	90000
Electrical Heating [kW]	47
Temperature Range [°C]	200 to 500
Operating Pressure [kPa]	15 (gauge)
Design Pressure [kPa]	450 (gauge)
Argon Flow Rate [Nl/s]	15
Argon Injection Pressure [kPa]	600 (gauge)

2.2 HERO TEST SECTION

2.2.1 Primary Side

The HERO (Heavy liquid mEtal pRessurized water cOoled tubes) TS [20][21] is installed inside CIRCE from the top of the main vessel, through a coupling flange. This new TS has been obtained from the previous one named ICE (Integral Circulation Experiment) [22], replacing the heat exchanger designed for the previous experimental campaigns with a new one, SGBT type, composed by 7 bayonet tubes with geometry and working conditions relevant for LFRs. This new solution improves the plant safety, reducing the possibility of water-lead/LBE interaction thanks to a double physical separation between them, and allowing an easier control of eventual leakages from the coolant by pressurizing the separation region with inert gas. All the other components are the same as the pre-existing TS:

- ***Fuel Pin Simulator*** (FPS, in red in Fig. 2-4), consisting of an electrical pin bundle of 37 pins, for a nominal thermal power of 1 MW (~27 kW for each pin). The pins are arranged in a wrapped hexagonal lattice with a pitch to diameter ratio equal to 1.8. The component is designed to provide a primary coolant temperature gradient of 100°C/m with LBE average speed of 1 m/s and pin power density of 500 W/cm^3. Each pin is characterized by an outer diameter of 8.2 mm and a total length of 1885 mm. The heat source is located in the central part and it is 1000 mm long. The remaining zones upstream and downstream the active length act as mixing zones. The relative position between the pins and the wrapper is fixed by three spacer grids placed along the axis of the component, at the upper, middle and lower section of the pin bundle. The LBE exit is realized by 6 holes in the upper part of the hexagonal shell. The FPS hexagonal wrapper is included in a cylindrical shroud, where penetrations for the instrumentation connections are placed. The gap between the inner hexagonal wrapper and the outer cylindrical shroud, is filled with stagnant LBE;
- ***Fitting Volume*** (green in Fig. 2-4) which collects the hot LBE rising from the FPS; achieving the hydraulic connection with the riser. In the upper part, the mechanical connection with the dead volume (hosting the electrical cables of the pin bundle) is realized by means of a coupling flange (see Fig. 2-6, left). On the bottom surface of the main chamber, a penetration is achieved to allow the positioning of the argon injector (depicted in Fig. 2-6, right). Additionally, a penetration for pressure measurement system is obtained on the lateral surface of the main chamber, 150 mm above the bottom surface;

- ***Riser*** (yellow in Fig. 2-4), in which the LBE flows upward up to the separator. The riser is a double wall pipe 3810 mm long. At the inlet section of the riser is positioned the argon injector to perform Gas-Enhanced Circulation (GEC) of the primary coolant. The riser is equipped by an axial bellow to compensate the dilatations and contractions of the component due to the temperature and a double wall air-filled pipe to prevent the heat losses from the riser to the pool;
- ***Separator*** (gold in Fig. 2-4), located on the top of the TS, providing a hot plenum for the primary coolant and allowing the hydraulic connection between the riser and the shell side of the steam generator Fig. 2-7. The component also acts as a separation region between the LBE and the argon injected. The separation occurs since the hot LBE is driven downward, towards the steam generator inlet, while the argon flows upward into the gas plenum through the free surface;

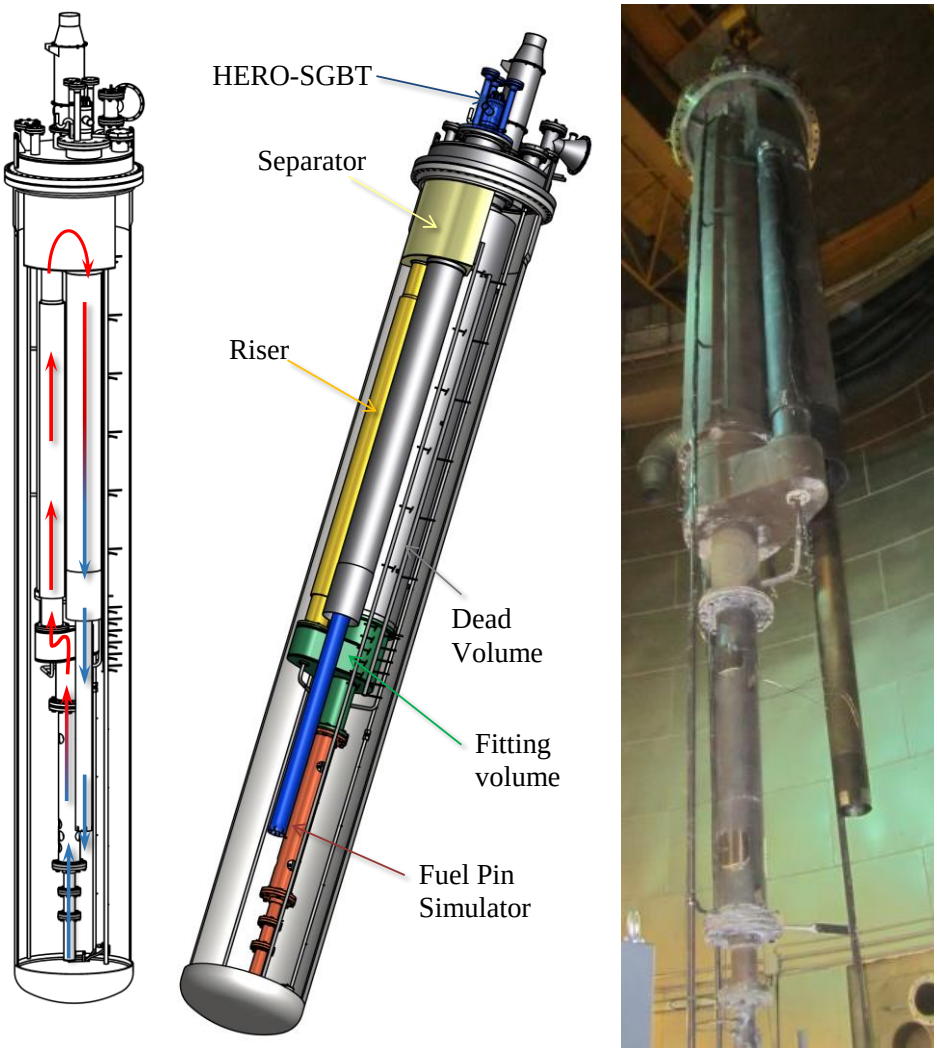

Fig. 2-4 – S100 main vessel and HERO Test Section

- ***Steam Generator Bayonet Tube*** (SGBT, in blue in Fig. 2-4) acting as a primary heat sink during the normal operative conditions and as DHR (Decay Heat Removal) system during the transients. Details of this component are given in the dedicated section 2.2.3;
- ***Dead Volume***, located above the fitting volume, which encloses and maintains insulated the power supply rods feeding the Fuel Pin Simulator.

The main flow path of the coolant inside the pool is reported in Fig. 2-4. The LBE flows upwards trough the FPS, it passes the Fitting Volume and it enters into the Riser. At this position, argon could be injected for performing GEC (gas lift). Then, LBE enters into the Separator, in which the free level reaches about the middle height of the wall. From this small pool, the LBE comes in the SGBT (blue) and starts to flow downward, shell side. Then, LBE completes its loop into the pool bottom.

Fig. 2-5 – External and internal view of the Fuel Pin Simulator, and detail of the spacer grid

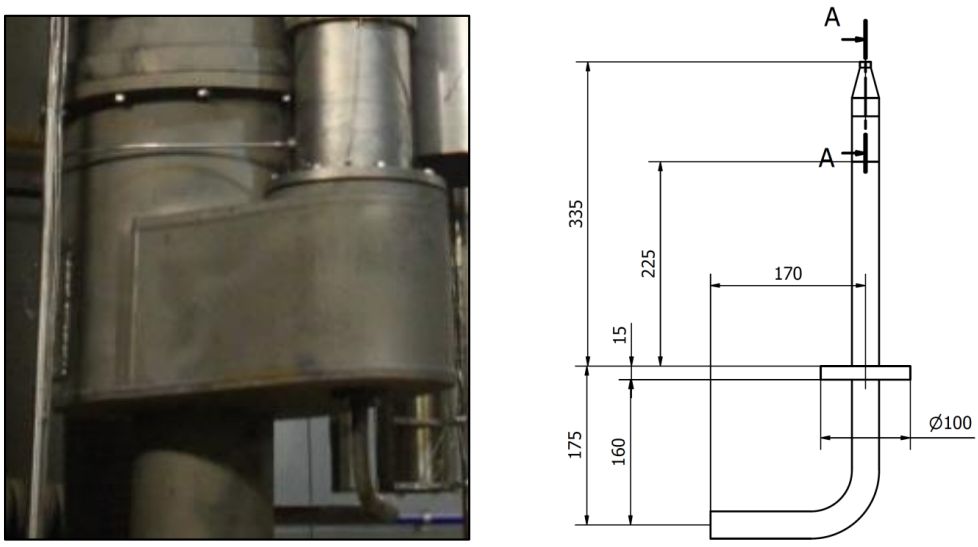

Fig. 2-6 - View of the fitting volume (left) and drawing of the argon injector (right)

Fig. 2-7 – External and internal view of the Separator

2.2.2 Secondary Side

A once-through secondary loop has been realized to supply liquid water at the HERO SGBT unit [18]. At the nominal working conditions the seven Bayonet Tubes (BTs) of the SG are fed by an overall sub-cooled water mass flow rate of about 0.33 kg/s at 335°C and ~172 bar. The SGBT output is computed to be (on the basis of RELAP5 calculations [18]) single-phase superheated steam flow, at about 400°C and ~172 bar. The mentioned boundary conditions are guaranteed to be reached and maintained steadily before tests take place and successively modified coherently with planned transient test matrix. For these purposes, the secondary loop for the HERO SGBT unit has been designed and realized, and the related instrumentation has been installed. With reference to the

Procedure and Instrumentation Diagram (P&ID) presented in Fig. 2-8 and Fig. 2-9, the main components are hereafter described:

- a filter demineralizer (DEMI in Fig. 2-8), providing clean water at ambient temperature and low pressure;
- a 3 pistons volumetric pump regulated by a bypass valve and inverter and equipped with a 40 bar accumulator and a check valve;
- a helical heating system (HEATER in Fig. 2-8 and Fig. 2-9) for water pre-heating up to ~335°C. An electrical potential difference of about 100 V is applied to the electrical connections by the power supply, providing up to about 500 kW;
- 1'' (Class 2500) valves V1 (on/off) and V2 (regulation valve), downstream the HEATER, opened alternatively bring water toward the SGBT and bypass line (both ¾'' tube BWG16), respectively;
- a safety valve and a filter, located downstream the V1;
- a manifold, which distributes water to each one of the seven BTs, by seven lines of ½'' tube, on which turbine flow meters, pressure transmitters and thermocouples (TFMs in azure, PCs in yellow and TCs in green, respectively, are shown in Fig. 2-8) are installed.
- Seven orifices with O.D. 3 mm are positioned along the seven ½'' tube (one orifice for each tube), between the manifold and the SGBT inlet, in order to achieve a uniform distribution of the feedwater among the bayonet tubes.
- a 2 ½" discharge line, thanks to which the steam produced in the HERO TS outflows in the environment; the pressure along the loop is maintained at the operating pressure through the regulation of valve V3;
- a ¾'' bypass line used for the start-up phases, equipped with the regulation of valve V2;
- a helium line, for pressurizing the AISI316L stainless steel powder gap of bayonet tubes at ~8 bar.

Fig. 2-8 also highlights the dimensions of the piping, valves activation systems, flow meters, pressure transmitters and thermocouples positions, besides the argon supply system for performing the gas lift. Three main valves V1, V2 and V3, pneumatically actuated, allow the whole range of needed regulations for actuating the initial heating

phase of the feed-water and reaching the selected initial and boundary conditions of the tests.

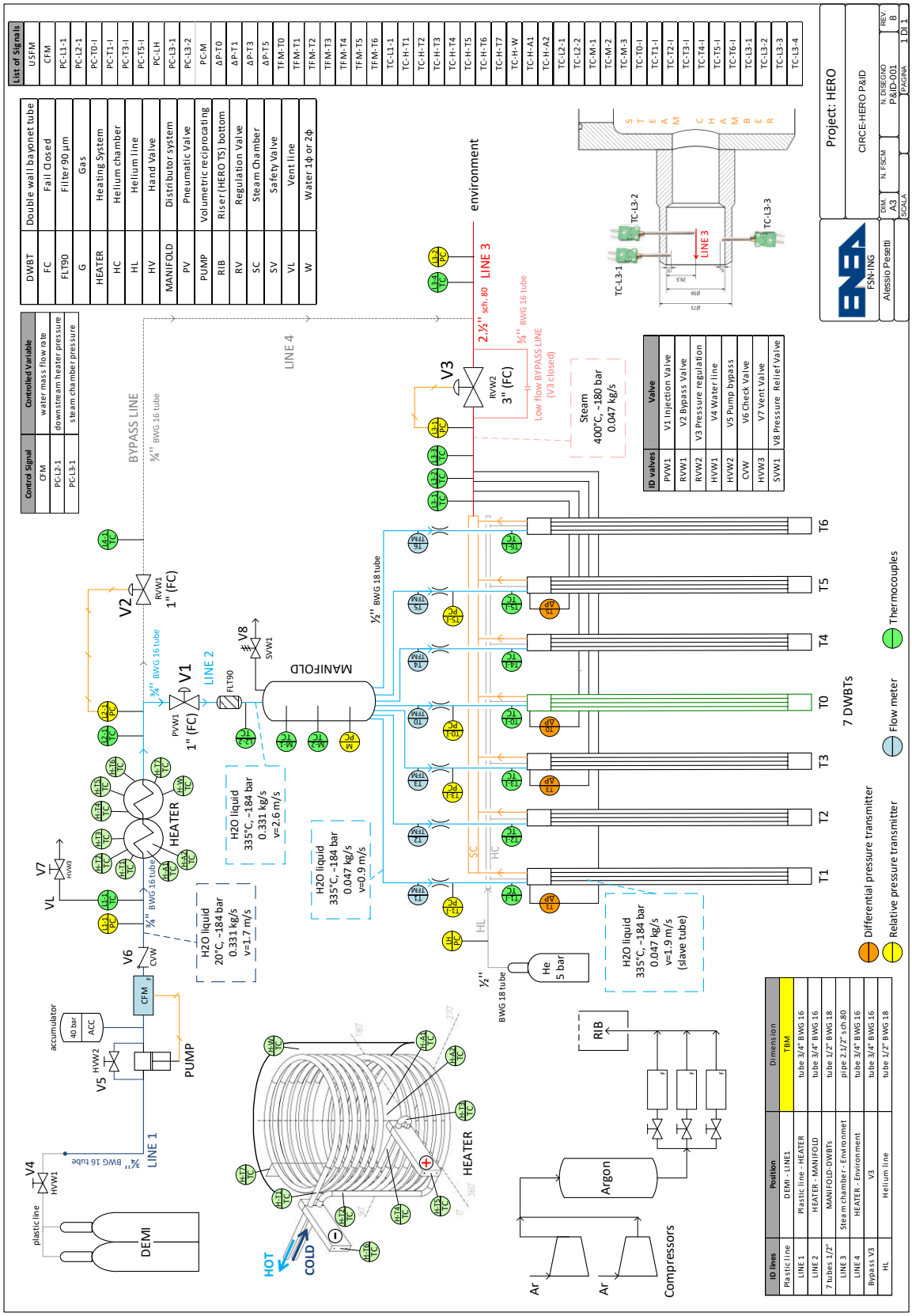

Fig. 2-8 – Secondary Loop P&ID

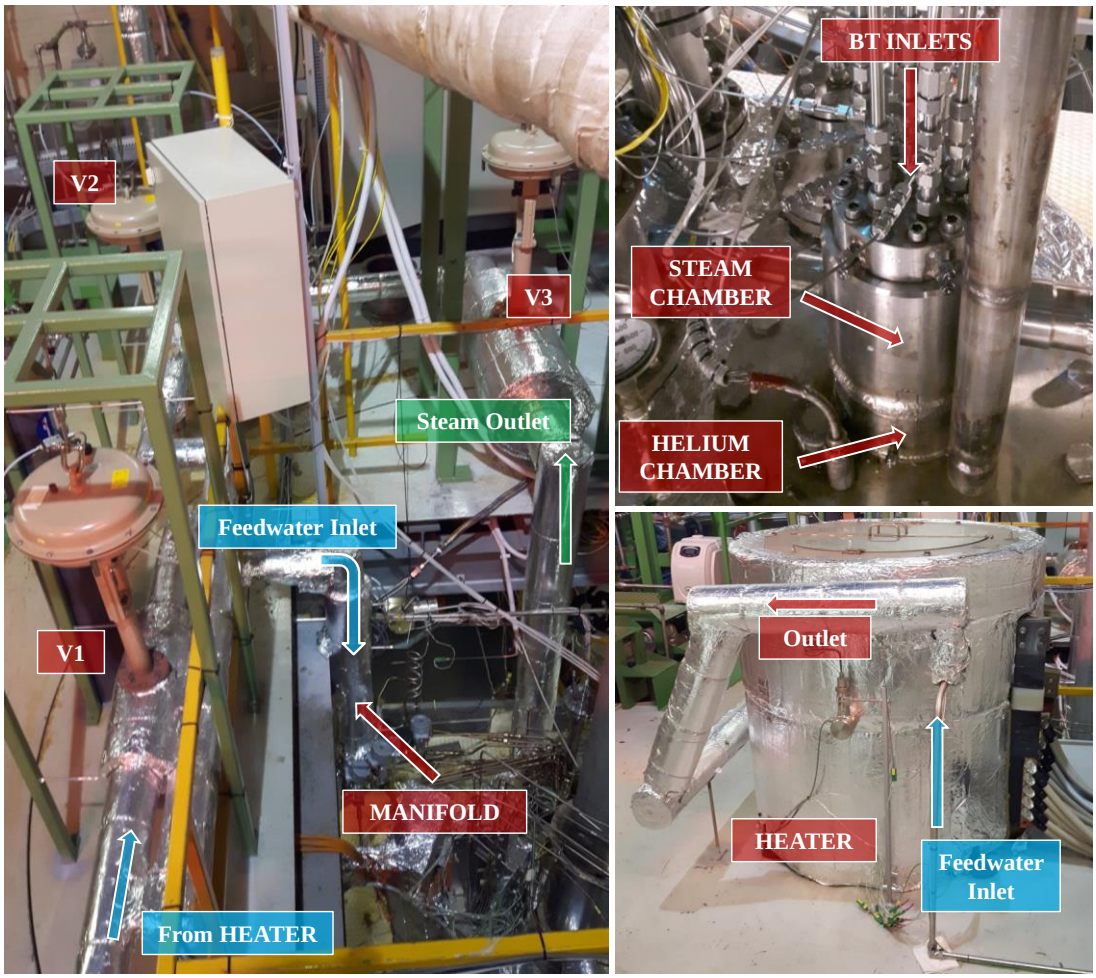

Fig. 2-9 – View of the secondary loop (left), the SGBT top flange (top, right) and the HEATER component (bottom, right)

2.2.3 HERO SGBT

The technical draw of HERO SGBT unit is depicted in Fig. 2-10, which also shows the bayonet tube bundle extracted from the hexagonal shell. A conceptual sketch of the HERO bayonet tube is reported in Fig. 2-11. The SGBT is composed of:

- a top flange with seven holes to accommodate the bayonet tubes and one hole for the instrumentation. The flange connects the SG bayonet tube unit to the CIRCE main vessel on the S100 top flange (Fig. 2-12). It sustains the helium chamber, the steam chamber, the bayonet tubes and the hexagonal shroud;
- the helium chamber, welded above the top flange and located outside CIRCE S100. It is constituted by an AISI-304 tube 6" sch.40 with an integral roof. The helium chamber has appropriate holes to accommodate the bayonet tubes. These have been fixed to the holes by welding to guarantee no helium leakages up to 10 bar;

- the steam chamber, located on the top of the helium chamber; it collects the superheated steam and it contains the feed-water tubes;
- the tube bundle, composed of 7 bayonet tubes with a main length of about 7360 mm and the active length equal to 6000 mm (see Fig. 2-10), arranged in a hexagonal shell (Fig. 2-13, left) with a triangular pitch. Each bayonet tube is composed of four coaxial tubes, as represented in Fig. 2-13 (right): the feedwater enters in the slave tube from the top of the SGBT unit, flowing downward and then rising through the annular riser between the first and second tube, where the steam is produced. The gap between slave and first tube is filled by air (slight vacuum) as insulator in order to avoid steam condensation. The gap between second and third tube is filled with AISI316L powder and slightly pressurized by helium at ~8 bar to detect any leakages, and maintaining a good heat exchange capability, thanks to the metallic powder. The dimensions of the tubes are reported in Tab. 2-2. The ends of the bayonet tubes are closed with a welded steel cap. The bayonet tubes are kept in position by means of five hexagonal spacer grids.

The LBE inlet inside the SG is realized by six holes on the hexagonal shroud (Fig. 2-7, right) positioned 300 mm from the separator bottom. The holes are 180mm x 40mm, realized in the wrap at the top of the active length and designed to be placed inside the separator being totally submerged by the LBE. The hexagonal shell is then contained in a cylindrical shroud (in blue in Fig. 2-4). It is positioned concentric to the hexagonal wrap and it is sealed at the bottom and at the top in order to provide a meatus which is filled by air to avoid heat exchange between the pool and the SGBT unit. The external shroud includes a thermal compensator to accommodate the differential elongation between the shroud and the hexagonal wrap.

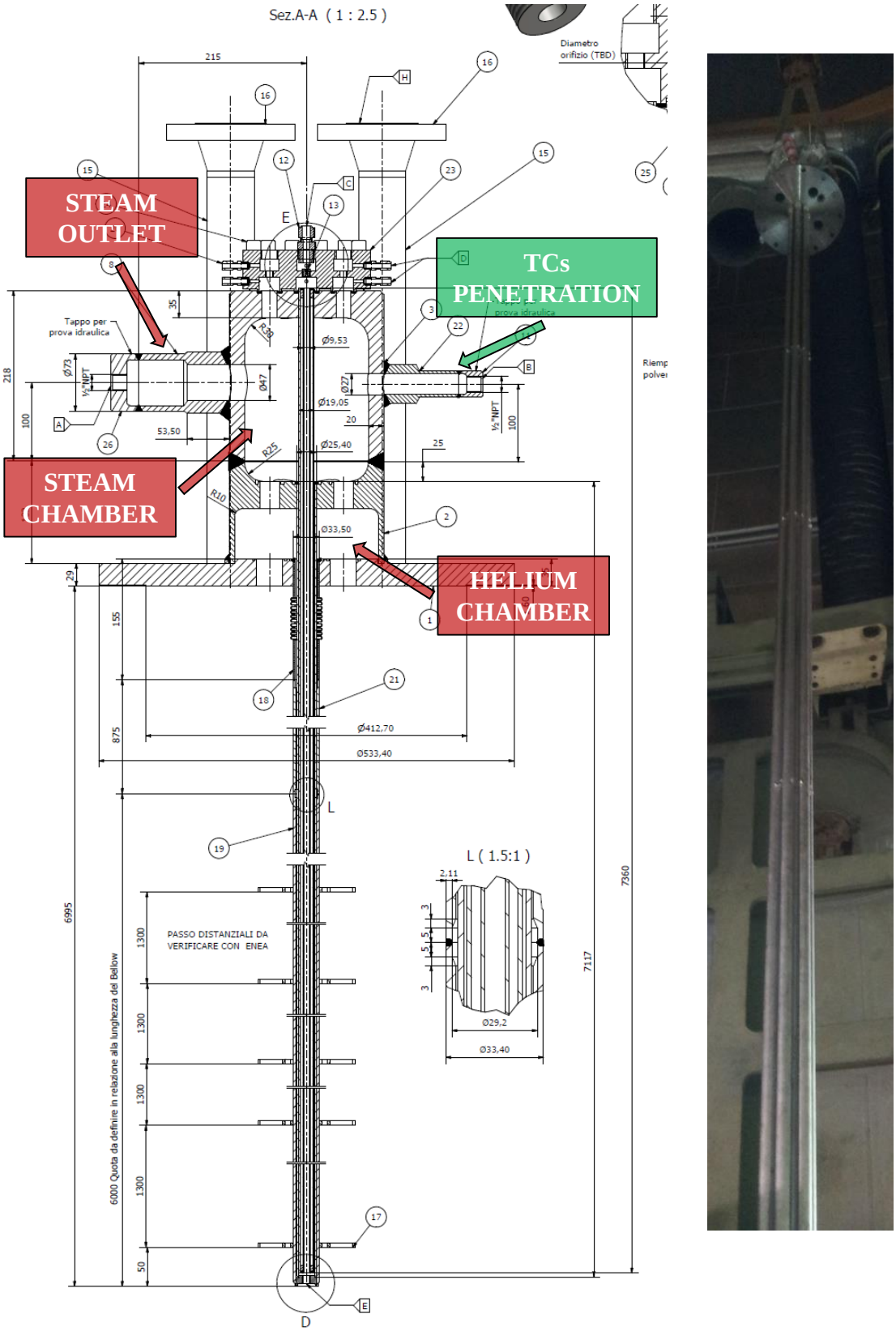

Fig. 2-10 – Technical drawing of HERO SGBT unit

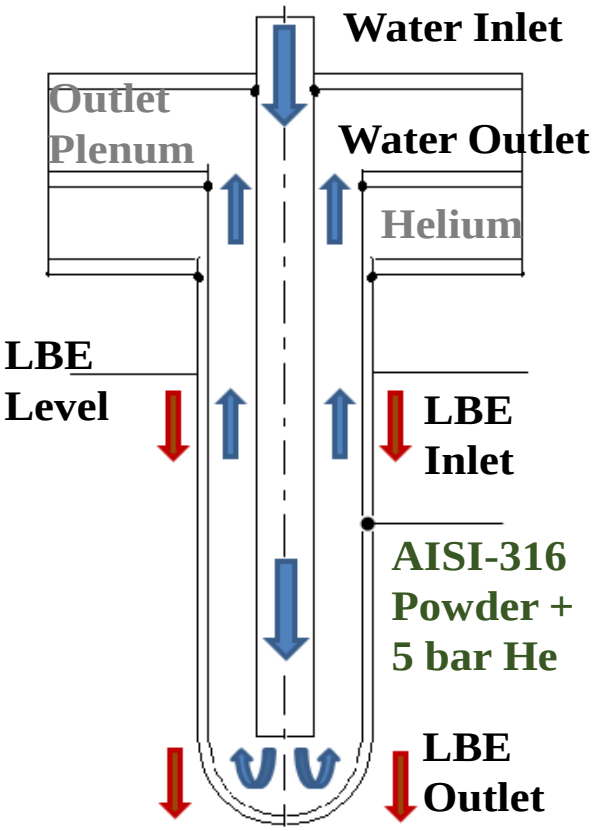

Fig. 2-11 – Bayonet Tube geometry

Fig. 2-12 – Top view of the S100 coupling flange

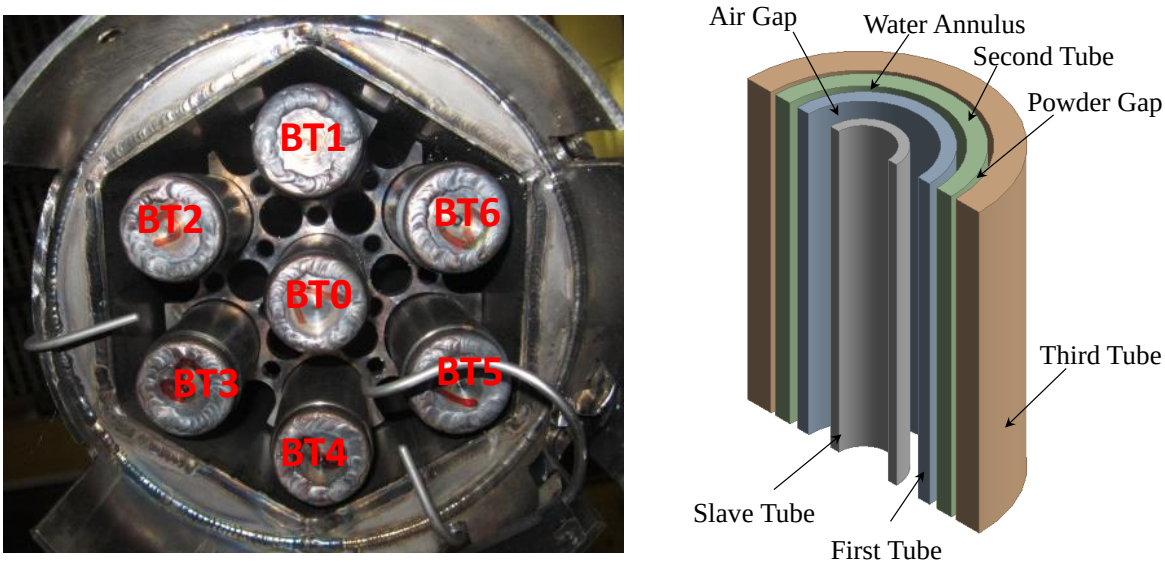

Fig. 2-13 – Sketch of the hexagonal geometry (left) and detail of the bayonet tubes (right)

Tab. 2-2 – HERO SGBT tubes dimensions

Label	Outer diameter (mm)	Thickness (mm)	Material
Slave tube	9.53	1.22	AISI 304
First tube	19.05	1.65	AISI 304
Second tube	25.40	2.11	AISI 304
Third tube	33.40	3.38	AISI 304

2.2.4 Instrumentation and Data Acquisition & Control System

HERO test section is highly instrumented for achieving well defined initial and boundary conditions relevant for nuclear systems (e.g. ALFRED and MYRRHA reactors) and characterizing both pool/LBE and heat exchanger/water side during stationary and transient scenarios. An overall number of about 240 thermocouples, 10 bubble tubes, 1 Venturi Flow Meter (VFM), 2 LBE level sensors and 1 LBE laser level transmitter are implemented and acquired at 1 Hz.

In the primary loop, the instrumentation installed in HERO TS is composed of an overall number of about 170 thermocouples, 10 bubble tubes, 1 Venturi flow meter and 3 LBE level meters. Two pressure transmitters are set in S100 cover gas. Moreover, an argon flow meter measures the normal litres per second injected in the riser, for gas lift occurrence.

A total of 39 TCs set in the FPS and positioned as reported in Fig. 2-14, 3 TCs at the inlet and 3 TCs at the outlet section of the riser (see Fig. 2-15).

One of the main tasks of the experimental campaign is to investigate three-dimensional phenomena inside a heavy liquid metal pool, such as thermal stratification. For this purpose, a detailed temperature measuring system has been adopted inside the pool, as shown in Fig. 2-15. A total of 119 TCs are distributed in the pool on dedicated rods at different levels, for mixing and stratification feedback, maintained in the same position of ICE test section [21]. Three TCs have been addicted and positioned accordingly with the expected thermal stratification level, predicted with a pre-test analysis realized by the SYS-TH code RELAP5-3D© [23], obtained improving the pre-existing numerical model of the ICE TS [24]. Regarding the 10 bubble tubes [25], six of them are connected to 3 differential pressure transmitters for measuring ΔP:

- in the Venturi flow meter (inlet and throat section);
- between LBE free level in the pool and separator;
- across the lower spacer grid of the FPS.

Remaining 4 bubble tubes are acquired by 4 absolute pressure transmitters, for measuring time trends inside the fitting volume, along the riser (inlet and outlet section) and in the pool cover gas.

The LBE temperature is measured along the SG shell side at four different levels (+1500, +3000, +4200 and +6000 mm, assuming 0.0 m the SG outlet section), as reported in Fig. 2-16. In particular, the thermocouples are positioned as follows:

- 12 TCs located on three azimuthal positions of central BT;
- 6 TCs on the outer surface of two outer BTs at +1500 mm, +3000 mm, +4200 mm;
- 12 TCs at the centre of one central and three outer sub-channels at +1500 mm, +3000 mm, +4200 mm;
- 3 TCs at the SG outlet section (+0 mm);
- 3 TCs are set at the middle height of LBE inlet windows, about 150 mm from the separator bottom.

The instrumentation installed in the secondary loop is reported in Fig. 2-8. It is composed of 30 K-type TCs (in green), 9 relative and 4 differential pressure transmitters (in yellow and orange, respectively), one Coriolis and 7 mini turbine flow meters TFMs (in azure), installed in order to highlight possible unbalanced flow. Water temperature and pressure are monitored at HEATER, MANIFOLD and BTs inlet and outlet as well as downstream

V3. Differential pressure measurements across 4 BTs will characterize single and two-phases pressure losses. Three thermocouples set at the steam chamber exit aim to detect possible condensation and radial stratification. An overall number of 12 TCs, having a diameter of 0.5 mm, are positioned in the annular gap of the bayonet tubes:

- 5 TCs located in the central tube, named as T0, 5 set at different levels (+500 mm, +1500 mm, +3000 mm, +4200 mm, +6000 mm, assuming as 0 mm the bottom part of the bayonet tube) aiming at characterizing water vaporization;
- 7 TCs at the exit of each bayonet tube gap.

The complete list on the instrumentation installed in the primary and secondary systems is reported in ANNEX 1.

The Data Acquisition & Control System (DACS) is realized with a PC acting as a control unit, connected to the Programmable Logic Controller (PLC) through the Message Passing Interface (MPI) network. The DACS consists of two sub-systems:

- ***Plant Management Subsystem (CONTROL)***, which controls and manages the servo-mechanisms, detecting the critical states of the system and acting the related protection systems in order to keep the plant safety at the required working conditions. Furthermore, it manages automatically the plant operative parameters (i.e. temperature, flow rate, pressure);
- ***User Interface Subsystem (SCADA),*** which provides to the CONTROL the set-points and the input commands, ensuring the interface human-machine. The SCADA provides the graphic interface on the PC of the plant user, allowing the control of the operative conditions of the systems and reporting all the alarms coming from the plant. Furthermore, the SCADA records all the operative parameters during the plant operation, in order to generate an historical database of the tests performed.

The control panel is composed of 15 sheets, each one dedicated to the control of a specific system of the plant. As an example, Fig. 2-17 reports the sheet named "HERO Test Section", which controls the main operative parameters of the facility.

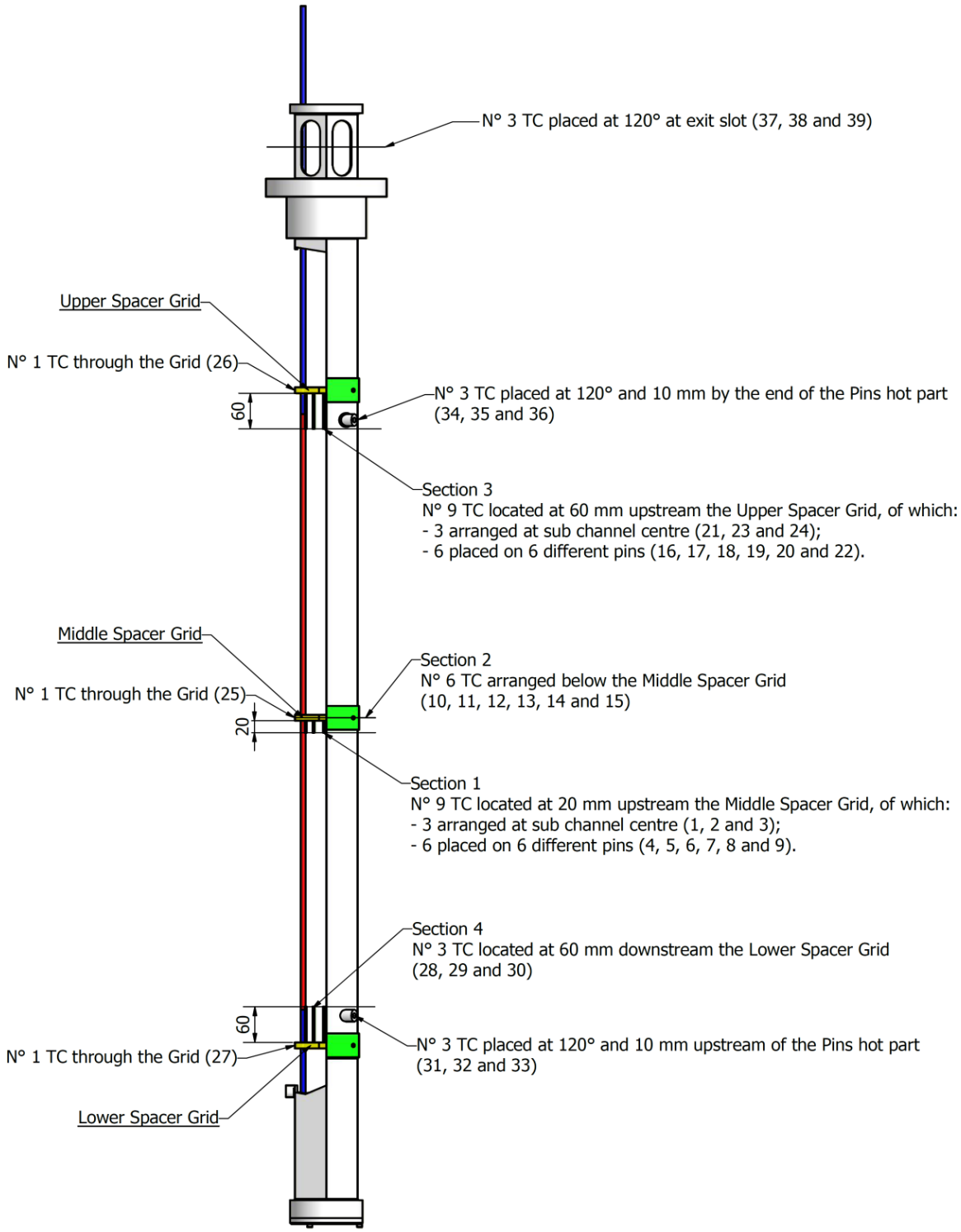

Fig. 2-14 – FPS, measurement sections and thermocouples position (TC-FPS-01 – TC-FPS-39)

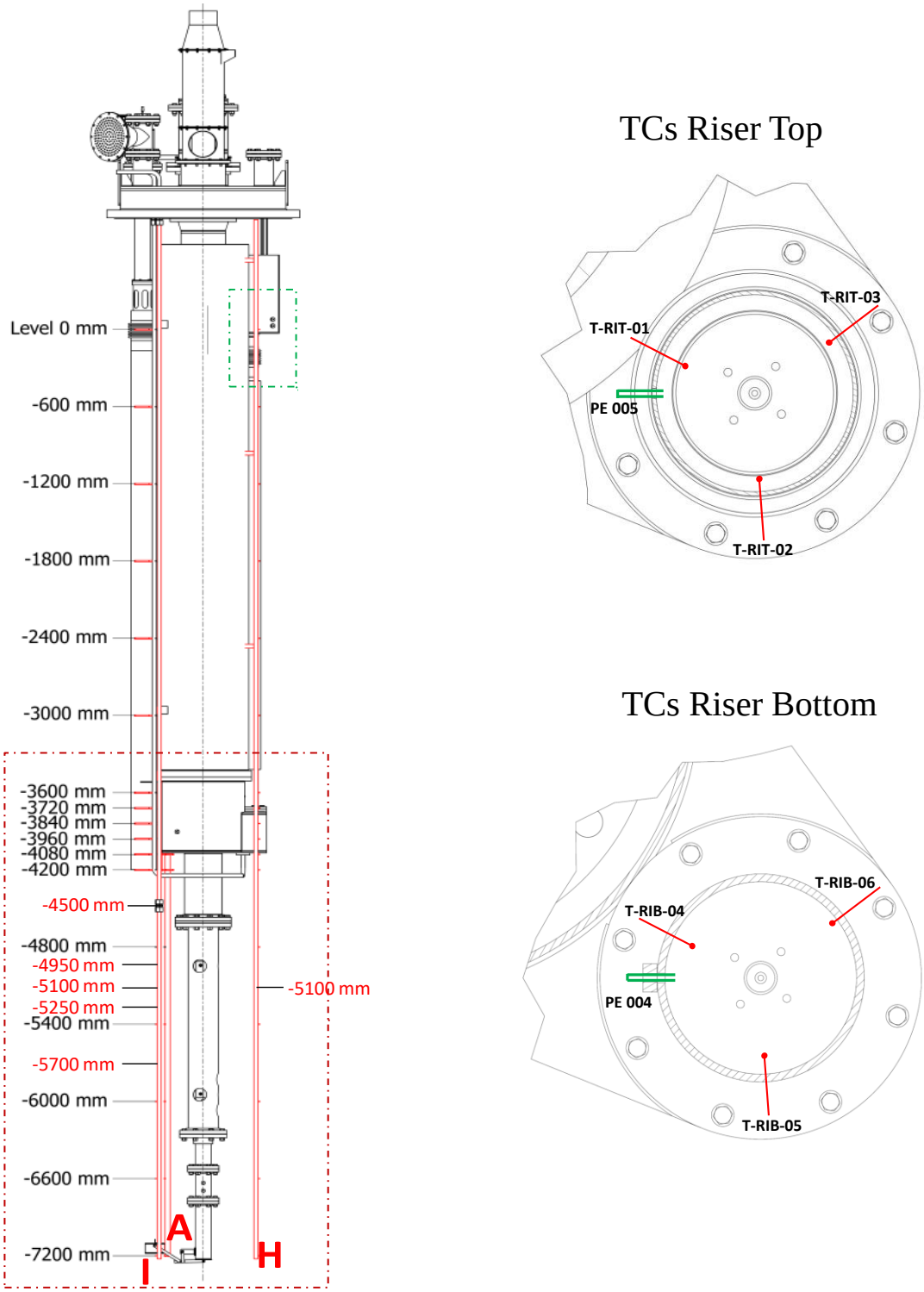

Fig. 2-15 – Instrumentation installed in the S100 pool and in the riser

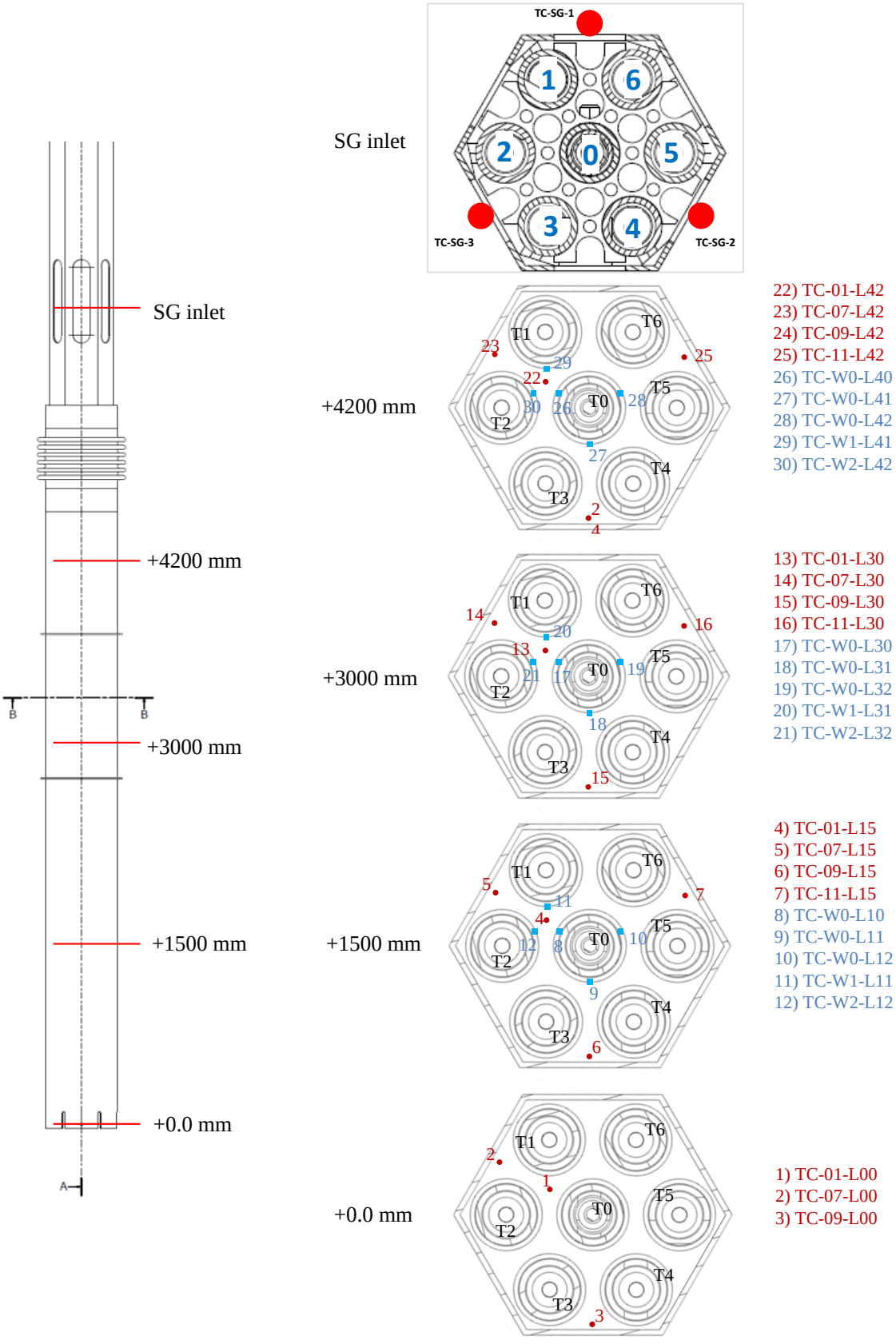

Fig. 2-16 – Distribution of the thermocouples along the LBE side of the steam generator

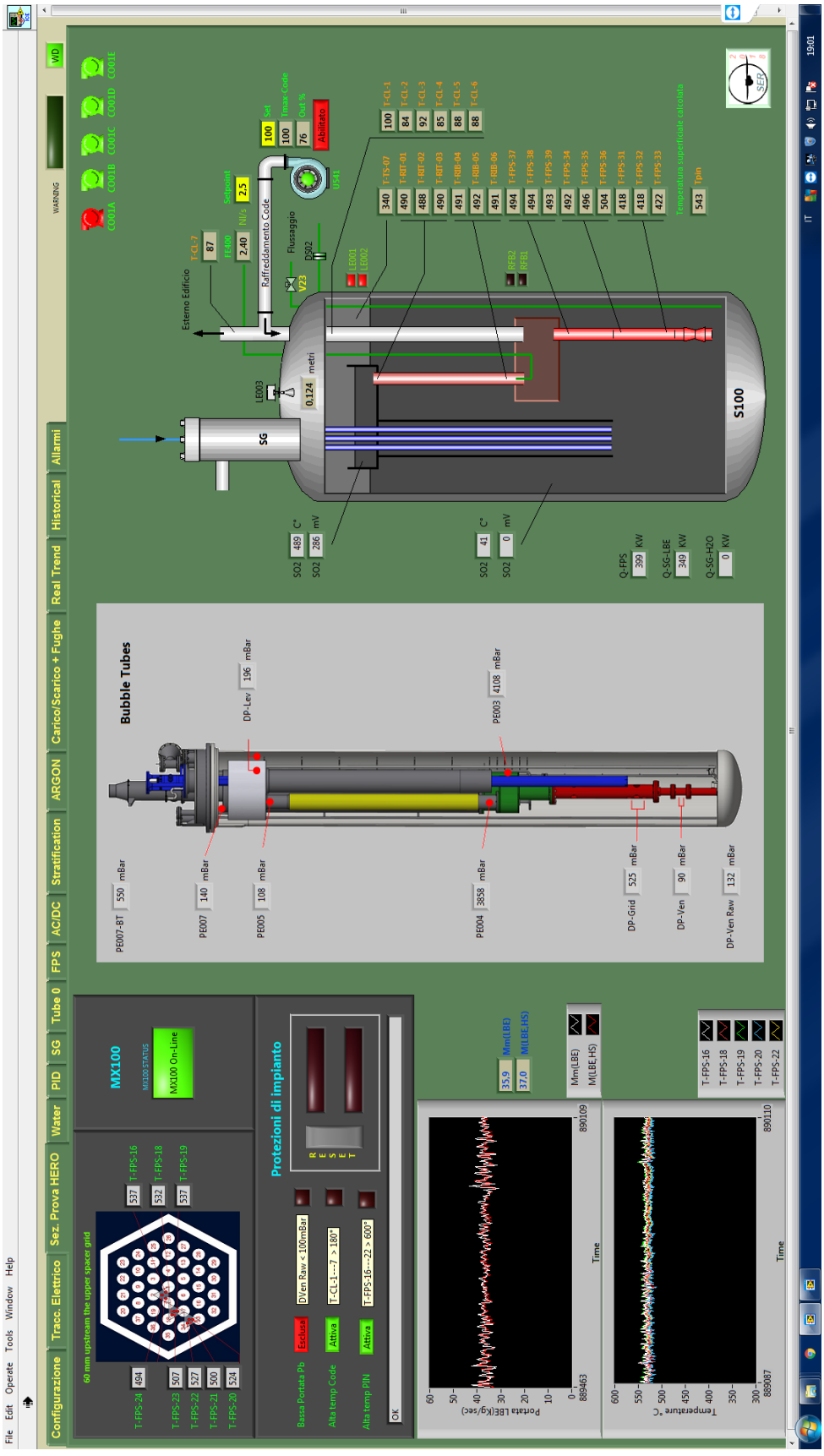

Fig. 2-17 – General Control Panel of the CIRCE-HERO Facility

(Page intentionally left blank)

3 PRELIMINARY NUMERICAL ACTIVITIES IN SUPPORT TO THE CIRCE-HERO DESIGN

3.1 DEVELOPMENT OF THE INPUT DECK

A numerical model of the steam generator along with the secondary system has been realized [26] using the SYS-TH code RELAP5-3D© v. 4.3.4, aiming at supporting the design and the realization of the secondary circuit and achieving information on the HERO SGBT performances. The nodalization consists of a one-dimensional model with several pipes and junctions connected each other in such a way to build an accurate simulation of the different parts of the loop. The entire system is composed of 1034 hydrodynamic volumes, 1039 junctions, 437 heat structures and 5081 heat transfer nodes.

3.1.1 Modelling of the hydrodynamic components

Fig. 3-1 shows a schematic view of the entire nodalization. The components are listed below.

- **Water distribution and SGBT inlet section**
  - Pipe 214 simulates the Manifold;
  - Branch 218 simulates the distribution zone of the manifold with the seven connections to the SGBT tubes;
  - Pipes from 219 to 225 simulate the piping connections between the manifold and the SGBT tubes;
  - Pipes from 301 to 309 simulate the helical heater for water pre-heating;
  - Pipe 216 represents the bypass line;
  - Valves 215 (V2) and 211 (V1) manage the passage in the bypass line and through the SGBT respectively.

- **Steam Generator Bayonet Tube**
  - 7 bayonet tube bundle modelled tube by tube;
  - The 7 downcomers have been modelled with 7 pipe components;
  - The 7 annular regions have been modelled with 7 annulus components.

- **Discharge Section**
  - Branch 150 simulates the steam chamber for the steam collection from the 7 tubes;
  - Pipes 153, 163, 165, 167 simulate the discharge pipeline;
  - Valve 166 (V3) regulates the pressure along the circuit.

The Time Dependent Volume (TMDPVOL) 201 sets the water inlet conditions at the inlet section of the helical heater and Time Dependent Junction (TMDPJUN) 202 works instead of the pump setting the water mass flow rate, while TMDPVOL 171 defines the environment conditions of the air for the steam discharge at 10°C and atmospheric pressure. The LBE shell side of SGBT has been simulated with an equivalent channel (PIPE 403); the TMDPVOL 401 sets the LBE inlet temperature and TMDPJUN 402 fixes the LBE mass flow rate, while the TMDPVOL 405 represents the LBE outlet. The LBE side is simulated with such simplification since the numerical analysis is focused on the secondary loop of the facility. The boundary conditions for the LBE assumed in the TMDPVOL 401 and TMDPJUN 402 are obtained from an analytical calculation, assuming the designed working conditions reported in [18].

The division in volumes of the loop has been carried out in order to consider the correct position of the thermocouples located along the loop and the bulk thermocouples in the HERO SGBT active length.

3.1.2 Modelling of the thermal coupling

Concerning the heat structures, a thermal coupling has been simulated:

- downcomer assumed insulated respect to the annulus;
- thermal connection simulated between the double wall of the annulus of each bayonet tube and the equivalent LBE channel;
- manifold and other pipelines assumed insulated;
- power source introduced to simulate the water warm-up inside the helical heater, realizing a heating source set uniform along the pipe thickness and uniformly distributed along the pipe length.

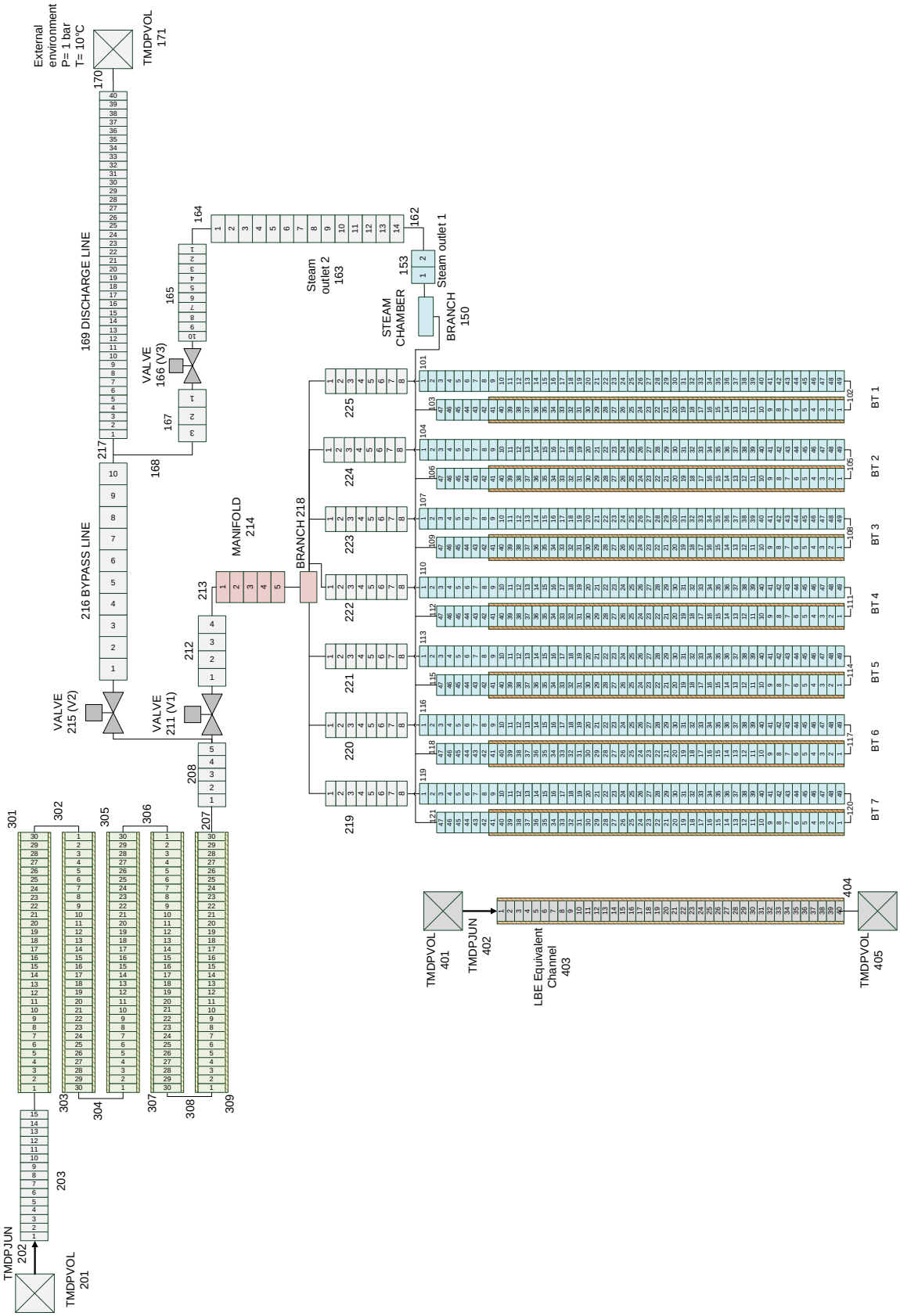

Fig. 3-1 – Secondary loop RELAP5-3D model

3.2 THERMAL-HYDRAULIC ANALYSIS OF THE REFERENCE DESIGN

A preliminary thermal-hydraulic analysis of the HERO SG along with the secondary loop has been carried out using RELAP5-3D© Ver. 4.3.4 code. An analysis of the secondary loop has been performed in order to test the loop layout and to characterize the main components from a thermal-hydraulic point of view, defining the start-up procedures for the achievement of the working conditions for the high-pressure tests. A thermal-hydraulic characterization of the HERO steam generator (~172 bar) has been performed, evaluating the system behaviour during the nominal operating conditions. A sensitivity analysis has been realized considering different LBE mass flow rates and two sets of values for the AISI316L powder thermal conductivity in order to evaluate the influence of such parameters on the overall performances of the component.

3.2.1 CIRCE-HERO start-up procedure definition

A preliminary test of the secondary loop has been carried out to define the steps needed to lead the system from the initial conditions of zero power and no mass flow rate until the nominal working conditions with the generation of superheated steam at 172 bar at the SGBT outlet, supplying a nominal water mass flow rate $\dot{m}_{nom}$ of 0.33 kg/s. During the start-up phases, the control parameters (water mass flow rate, pressure, heater thermal power) are managed in such a way to reach the nominal condition with a profile as smooth as possible, avoiding excessive peaks of pressure or temperature during the transients. The points monitored during the simulations are:

- the heater outlet;
- the inlet/outlet of the bayonet tubes;
- the points upstream the valves V1 and V2 and the point upstream the valve V3.

The magnitudes monitored are: the water temperature and pressure, the steam mass fraction, the power removed by the heat exchanger from the pool and the radial temperature profile along the bayonet tubes. In the following, each step is presented, while the pressure time trend and temperature time trend are reported in Fig. 3-2 and Fig. 3-3.

Step 1: at the beginning of the test, the feedwater line and the heat exchanger are empty and at atmospheric pressure, the water mass flow rate is zero and the heater is switched off. The main pipeline is closed by the valve V1 and the heat exchanger is bypassed and

closed upstream and downstream by valves V1 and V3, while the valve V2 opens the bypass line. The LBE equivalent channel is maintained at the constant temperature of 400°C with TMDPVOL 401 and the nominal mass flow rate is set 44.6 kg/s with TMDPJUN 402.

In this configuration, a water mass flow rate $\dot{m}$ = 1/10 of $\dot{m}_{nom}$ (0.033 kg/s) is injected in the feedwater line at the conditions of 10°C and 1 bar. As the entire line is completely filled by water (the heat exchanger is insulated and remains empty), the heater is switched on, supplying a thermal power of ~90 kW needed for the vaporization of the water. It can be noticed (Fig. 3-2) a pressure peak due to the water vaporization along the spiral heater which leads the pressure up to ~20 bar, and a consequent fast decrease when the steam produced reaches the discharge. In order to maintain the pressure peak under a reasonable value, the power ramp for the vaporization has been lengthened for 20 minutes and the water mass flow rate injected has been maintained low. A further reduction of the mass flow rate or an increase of the time for the power ramp will contribute to reduce the pressure peak.

Step2: the power is increased up to a value of ~290 kW needed for the vaporization of 1/3 of the nominal mass flow rate. After few seconds from the beginning of the power transition, the water mass flow rate is increased passing from 1/10 to 1/3 of $\dot{m}_{nom}$.

Step 3: the power of the heater is increased up to the value needed for the generation of superheated steam at 270°C at 40 bar, passing from ~290 kW to ~315 kW. After few seconds from this power transition, the valve V2 on the bypass line is regulated in order to pressurize the loop up to 40 bar. At the end of this step, the secondary side produces superheated steam at 270°C and 40 bar. When the steady-state conditions are achieved, the system is ready to open the main pipeline and to supply the HERO SGBT unit with the superheated steam. The steam injected at ~270°C assures a low heat transfer coefficient, a very low fraction of thermal power removed from the LBE pool and a small difference in temperature between the second tube, the AISI-316L powder gap and the third tube of the bayonet tubes. The valves V1 and V3 are opened allowing the passage of the steam in the main pipeline and through the bayonet tubes; after few seconds the valve V2 is closed avoiding the passage of the steam through the bypass. At the same time, the valve V3 is regulated in order to pressurize the entire main pipeline at 40 bar. After this transition, the system is capable to produce superheated steam at 40 bar. In these conditions, the power removed by the LBE pool is very low, as reported in Fig. 3-5.

Step 4: the valve V3 is regulated in order to pressurize the loop from 40 bar to 100 bar, leaving unchanged the heater thermal power and the water mass flow rate. In such a way, the steam produced in the heater comes out with a higher temperature (~340°C) and, consequently the power removed by the SGBT from the pool is lower. After the pressurization, the water mass flow rate is increased from 1/3 to 1/2 of $\dot{m}_{nom}$, while the heater power is increased up to 335 kW. In these conditions, the heater produces a mixture of liquid water/steam with a steam mass fraction of ~0.45 (Fig. 3-4)

Step 5: after few seconds from the end of the water mass flow rate transition, the pipeline is pressurized from 100 bar to 140, and then to 150, 160 up to 172 bar. The other parameters remain constant.

Step 6: growth in several steps of water mass flow rate and pre-heating thermal power up to the working conditions of 0.33 kg/s and 495 kW respectively, obtaining a water inlet temperature in the SGBT unit of ~335°C. At last, the temperature is increased in the LBE pool from 400°C to 480°C. When stationary conditions are reached, the power removed from the LBE pool is about 420 kW (see Fig. 3-5).

In Fig. 3-6 the pressure drop along the bayonet tubes is reported. The pressure remains almost constant along the downcomer and then decreases along the annular region, with a total pressure drop of 2.8 bar. Fig. 3-7 reports the temperature trends for the LBE and the water. The temperature of the LBE in nominal conditions is maintained at 480°C, then it decreases passing through the shell side of the SGBT unit achieving an outlet temperature of ~410°C, for a ΔT of ~70°C. The water temperature firstly reaches the saturation temperature of ~354.5°C (T_{sat} at 172 bar) and then, after the plateau corresponding to the water vaporization, the temperature of the steam increases up to ~390°C.
Finally, in Fig. 3-8 and Fig. 3-9 the radial temperature profiles along the double wall thickness of the bayonet tube is reported. Two different points have been monitored, the annulus inlet (bottom part of the BT) and the annulus outlet (top part of the BT), considering different moments during the transients. As can be seen, during the start-up phases the radial difference in temperature in the double-wall is very small, thanks to the high temperature steam crossing the bayonet tubes which maintains low the heat transfer. The higher difference in temperature is achieved when nominal conditions are reached (red line for t = 150 min) with a final ΔT of ~50°C.

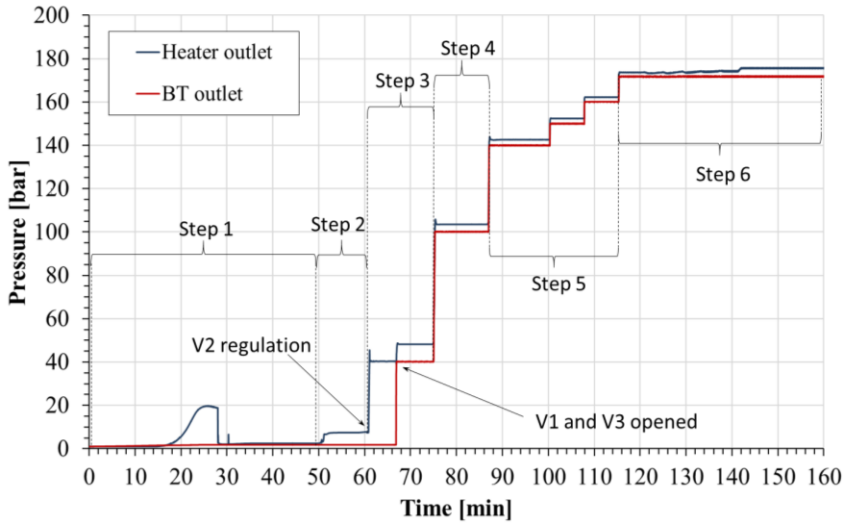

Fig. 3-2 – Pressure time trend during the start-up

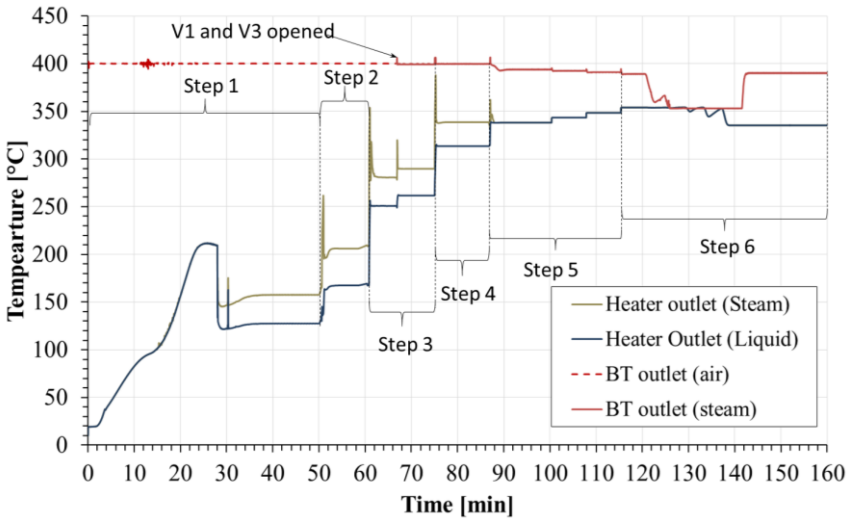

Fig. 3-3 – Temperature time trend during the start-up

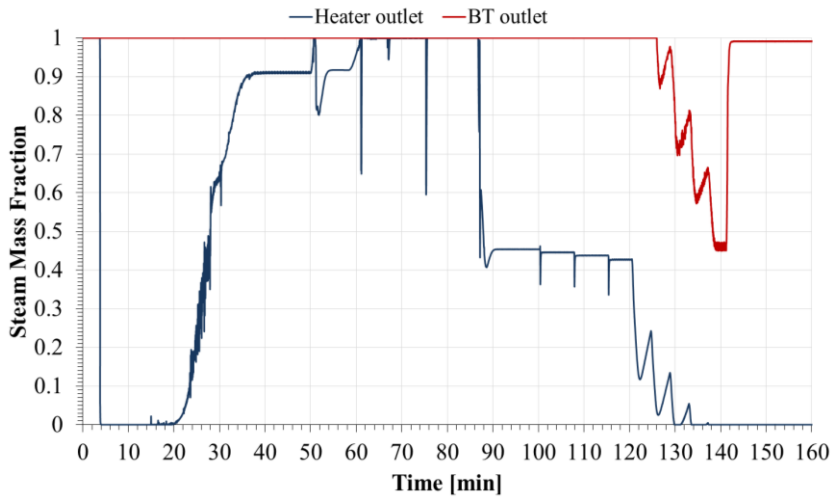

Fig. 3-4 – Steam mass fraction during the start-up

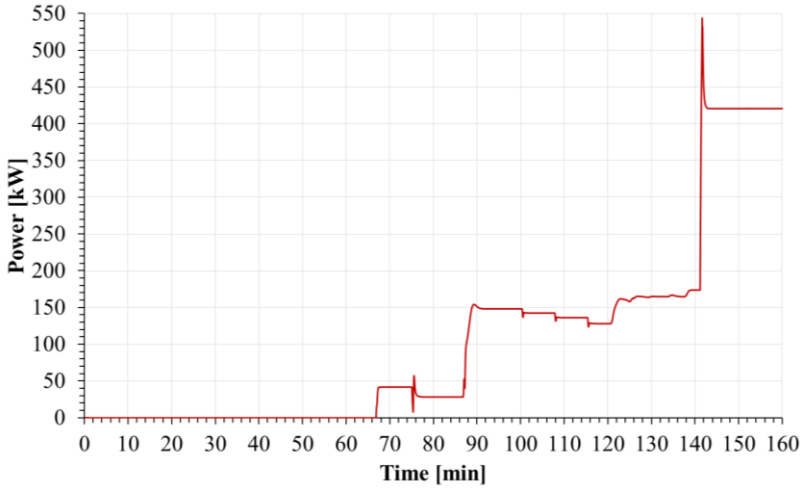

Fig. 3-5 – Power removed from the pool during the start-up

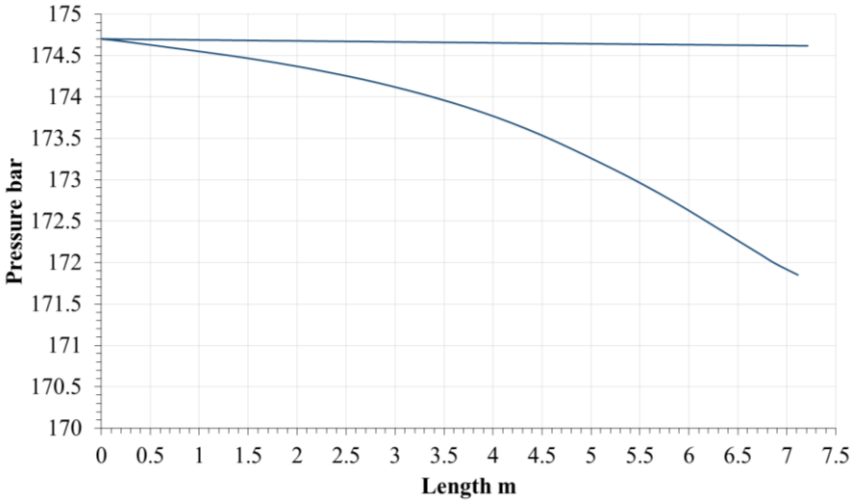

Fig. 3-6 – Pressure drops along a bayonet tube in nominal conditions

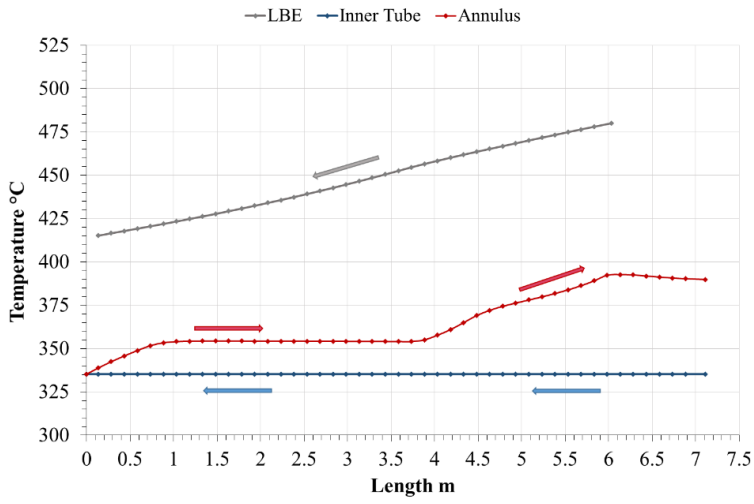

Fig. 3-7 – LBE and water temperature trends in nominal conditions

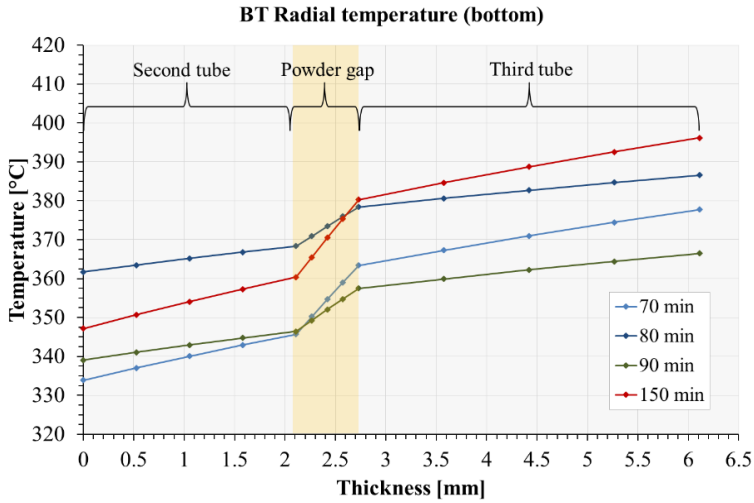

Fig. 3-8 – Radial temperature along the double wall thickness in correspondence of the annulus inlet (BT bottom)

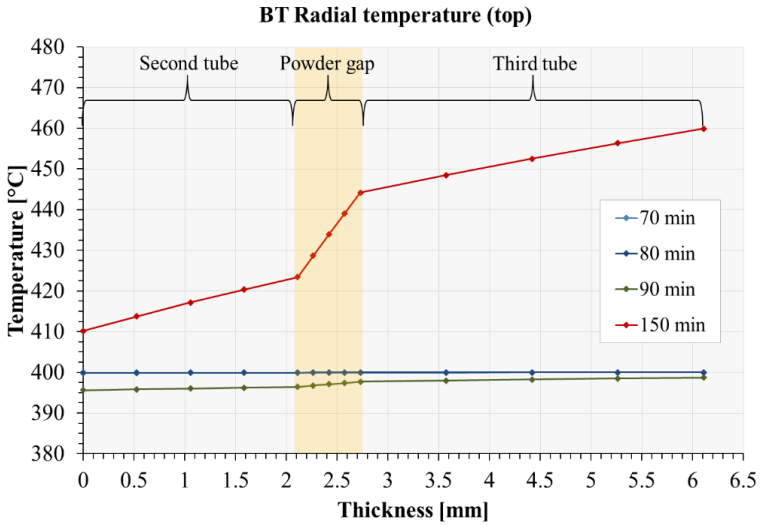

Fig. 3-9 – Radial temperature along the double wall thickness in correspondence of the annulus outlet (BT top)

3.2.2 Thermal-hydraulic characterization of the HERO SG

The HERO SGBT unit, along with the entire secondary loop, has been analysed from a thermal-hydraulic point of view by the model reported in Fig. 3-1. Starting from the nominal initial conditions defined both for primary and secondary side in Tab. 3-1, the Steady State (SS) has been reached and used as a starting point to carry out several simulations of transient. The transients considered involve variations in terms of water mass flow rate and LBE mass flow rate, while the LBE and water inlet temperatures are maintained constant. Assuming a LBE inlet temperature of 480°C, a difference in temperature of 80°C and a power supplied by the FPS to the LBE of 450 kW, it is possible

to obtain, from the thermal balance equation, the LBE mass flow rate needed in nominal working conditions:

$$Q_{FPS} = \dot{m}_{LBE} c_{p,LBE} \Delta T_{LBE}$$

where Q is the thermal power expressed in W, ΔT is the temperature difference, ṁ is the mass flow rate and cp is the LBE isobaric specific heat (J/kgK) evaluated by the following correlation [5]:

$$c_{p,LBE} = 160 - 0.024 * T$$

where the temperature is expressed in Kelvin. Assuming an average LBE temperature of 440°C, a value of 142.9 J/(kgK) is obtained. With these conditions, the LBE mass flow rate needed for the achievement of the operating steady state is ~39.4 kg/s.

Three tests have been considered to characterize the thermal-hydraulic behaviour of the HERO SG, assuming as initial conditions for both LBE and water the values reported in Tab. 3-1 and changing the LBE mass flow rate of +/-5% on the nominal value of 39.4 kg/s. The nominal boundary conditions for the tests are reported in Tab. 3-2. For each run, two transients, with a consequent related steady-state, have been considered, in which the water mass flow rate and the LBE mass flow rate are reduced respectively to 75% and 50% of the nominal values.

In addition, during the pre-test activity, a sensitivity analysis has been carried out in order to evaluate the influence of the AISI 316L thermal conductivity on the thermal-hydraulic performances of the steam generator. The steel powder thermal conductivity is a function of the temperature and it is influenced by different factors, i.e. the grain size and growth, powder compaction, thermal cycling. For this purpose, two cases for each test have been simulated, assuming two different sets of values for the thermal conductivity of the AISI316L powder (reported in Tab. 3-3):

- CASE A: based on TxP tests after powder thermal cycling under He at 4 bar [27];
- CASE B: based on experimental data of NACIE Heat Exchanger [28].

The complete test matrix simulated during the pre-test activity is reported in Tab. 3-4. From the table, it is possible to notice a relevant discrepancy between the two sets of data.

As anticipated above, these differences are due to different factors, i.e. grain size and growth, powder compaction and thermal cycling, as well as to the different test conditions, in particular the temperature, from which the data have been obtained. A further contribution to the discrepancy is also given by the uncertainty related to the experimental measurements.

The main results for the nominal steady state conditions are reported in Tab. 3-5 for both CASE A and CASE B. It can be seen how the different thermal conductivity influences the performances of the steam generator. In particular, the lower thermal conductivity causes a reduction of the power removed, as reported in Fig. 3-10, which shows a difference of about 25/30 kW among the tests of CASE A and CASE B, during steady-state 1. This difference is reduced during SS2 and it is minimum in SS3. The higher value reached is ~440 kW, achieved in RUN #3 during SS1, then the power decreases during the transients accordingly with the LBE and water mass flow rate reduction.

The pressure drops along the annular region of the bayonet tubes (Fig. 3-11) are between 2.4 and 2.6 bar during SS1 in CASE A, with a reduction up to ~1 bar when the water mass flow rate is set to 50% of the nominal value. CASE B is characterized by a pressure drop of about 2.3 bar during SS1, slightly lower respect to CASE A, while in the other steady states the values are similar to the first case. The reduction of the ΔP among the steady states and between the two cases is due to the lower steam mass fraction produced.

The LBE and water outlet temperatures are reported in Fig. 3-12 and Fig. 3-13, respectively. In CASE A, the LBE temperature at the SG outlet is about 405°C in SS1, of RUN #1, then it decreases to 396°C in SS2 and to 388°C in SS3, accordingly with the reduction of the LBE mass flow rate. The values reached in the other two tests of CASE A, RUN #2 and RUN #3, are close to the ones of RUN #1 with a slight difference of about +3°C for RUN #2 and -3°C for RUN#3. The temperature of the steam produced by the SG is subjected to an increase due to the water flow rate reduction, passing from 392°C in SS1, to 420°C in SS2, up to 456°C in SS3, in RUN #1. The temperatures achieved in RUN #2 are slightly lower than RUN #1, while in RUN #3 they are slightly higher. A similar situation can be found in the tests of CASE B (RUN #4, RUN #5 and RUN #6), which are characterized by an overall LBE temperature slightly higher and H2O temperature slightly lower than the CASE A due to the lower powder thermal conductivity assumed.
Fig. 3-14 reports the steam mass fraction produced along the active length of the bayonet tubes for RUN #1 and RUN #4, which are characterized by the same conditions. The

comparison shows as the different thermal conductivity assumed in the two tests affects the performances of the SG, reducing the steam production in RUN #4.

The LBE and water temperature trends along the steam generator length are shown in Fig. 3-15 for RUN #1. It can be noticed how the steam outlet temperature increases (from ~390°C to ~460°C), while the LBE outlet temperature decreases from ~405°C to ~390°C, accordingly with the LBE and water mass flow rate reduction from 100% to 75% and 50%.

In summary, the simulations show a LBE temperature difference of about 75°C and a power removed of ~420 kW for the case with higher thermal conductivity and nominal LBE mass flow rate (RUN #1), while a LBE temperature difference of ~71°C and a power removed by HERO of ~400 kW for case with the lower thermal conductivity (RUN #4), showing that the powder thermal conductivity is a relevant parameter which influences directly the overall performances of the steam generator.

Tab. 3-1 – CIRCE-HERO main operating conditions

Description	Unit	Nominal Value
FPS Power	kW	450
Pool Initial Temp.	°C	400
ΔT across the FPS	°C	80
Feed-water pressure	bar	172
Feed-water inlet Temp.	°C	335
Feed-water mass flow rate	kg/s	0.33
Heat Losses	kW	15

Tab. 3-2 – RELAP5-3D boundary conditions

Description	Unit	RUN #1	RUN #2	RUN #3
LBE Inlet temperature	°C	480.0	480.0	480.0
LBE Mass Flow Rate	kg/s	39.4	37.4	41.3
LBE Mass Flow Rate Variation	-	0%	-5%	+5%
Water Inlet temperature	°C	335.0	335.0	335.0
Water Outlet Pressure	bar	172.0	172.0	172.0
Feed-Water Mass Flow Rate	kg/s	0.33	0.33	0.33

Tab. 3-3 – AISI 316L powder thermal conductivity as a function of the temperature

Temperature (°C)	Thermal Conductivity (W/mK)	
	CASE A	CASE B
0	3.254	1.312
200	3.291	1.680
300	3.319	2.010
400	3.411	2.434
600	3.438	3.600
750	3.502	4.732

Tab. 3-4 – Secondary loop simulation test matrix

Parameter	Unit	CASE A			CASE B		
Test #	-	RUN #1	RUN #2	RUN #3	RUN #4	RUN #5	RUN #6
LBE inlet temperature	°C	480	480	480	480	480	480
HERO outlet Pressure	bar	172	172	172	172	172	172
Water SGBT Tin	°C	335	335	335	335	335	335
LBE mfr SS1	kg/s	39.4 (100%)	37.4 (100%)	41.3 (100%)	39.4 (100%)	37.4 (100%)	41.3 (100%)
LBE mfr SS2	kg/s	2.95 (75%)	28.0 (75%)	31.0 (75%)	2.95 (75%)	28.0 (75%)	31.0 (75%)
LBE mfr SS3	kg/s	19.7 (50%)	18.7 (50%)	20.6 (50%)	19.7 (50%)	18.7 (50%)	20.6 (50%)
Water mfr SS1	kg/s	0.33 (100%)	0.33 (100%)	0.33 (100%)	0.33 (100%)	0.33 (100%)	0.33 (100%)
Water mfr SS2	kg/s	0.25 (75%)	0.25 (75%)	0.25 (75%)	0.25 (75%)	0.25 (75%)	0.25 (75%)
Water mfr SS3	kg/s	0.17 (50%)	0.17 (50%)	0.17 (50%)	0.17 (50%)	0.17 (50%)	0.17 (50%)

Tab. 3-5 – Main results in nominal steady state conditions for CASE A and CASE B

Case	Parameter	Unit	RUN #1	RUN #2	RUN #3
CASE A	LBE Outlet Temperature	°C	404.7	402.1	407.1
	LBE ΔT	°C	75.3	77.8	72.9
	Steam Outlet Temperature	°C	392.1	388.3	395.8
	Power Removed	kW	424	416	431
	Annulus ΔP	bar	2.51	2.45	2.57
CASE B	LBE Outlet Temperature	°C	408.5	406.1	410.6
	LBE ΔT	°C	71.6	73.8	69.3
	Steam Outlet Temperature	°C	382.4	379.4	385.4
	Power Removed	kW	403	394	410
	Annulus ΔP	bar	2.34	2.25	2.39

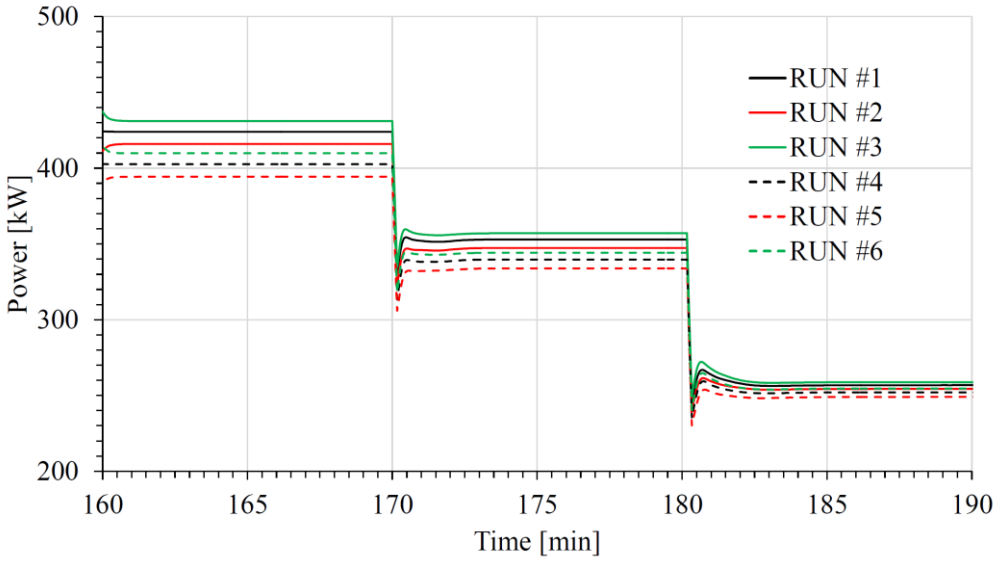

Fig. 3-10 – Power removed by the SG computed by RELAP5

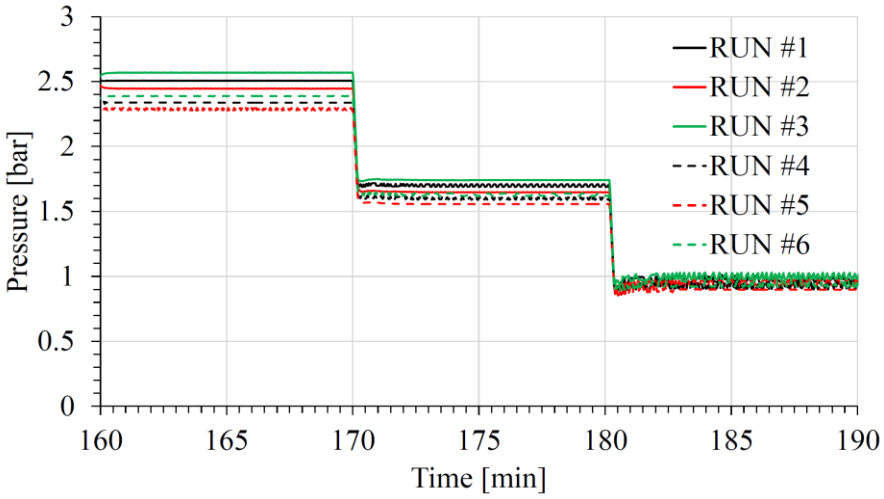

Fig. 3-11 – ΔP along the bayonet tube computed by RELAP5

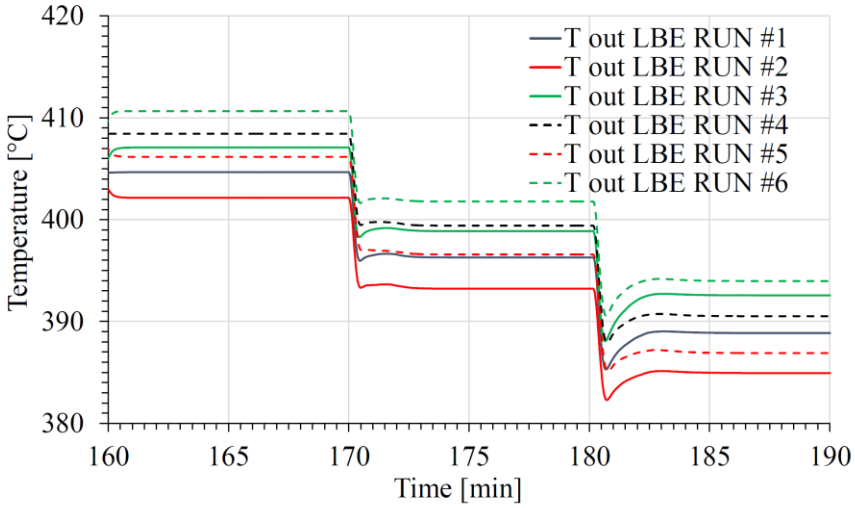

Fig. 3-12 – LBE SG outlet temperature computed by RELAP5

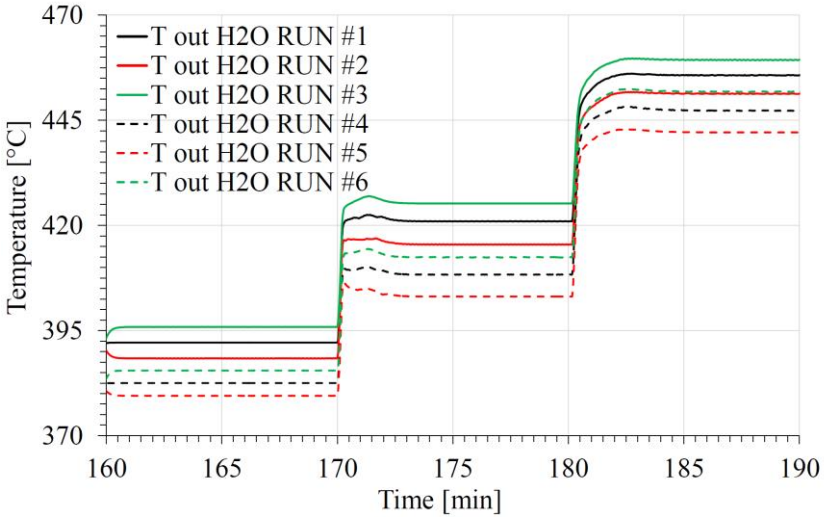

Fig. 3-13 – H2O SG outlet temperature computed by RELAP5

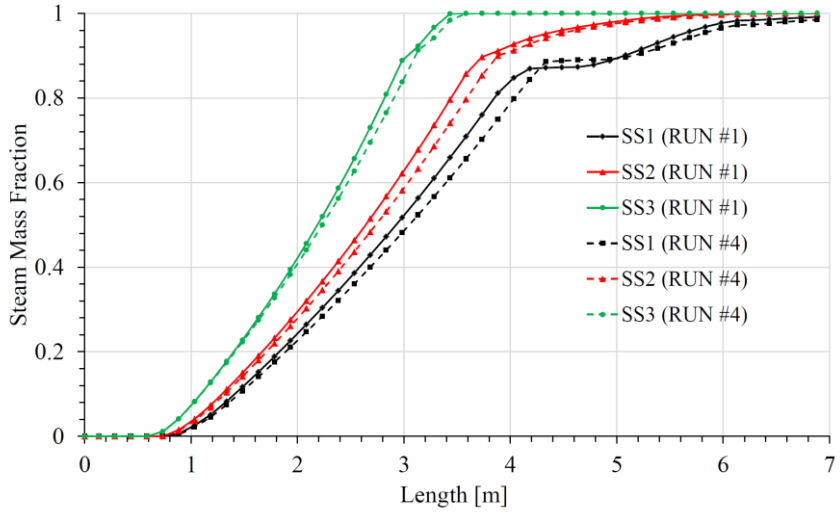

Fig. 3-14 – Steam Mass Fraction, comparison between RUN #1 and RUN #4

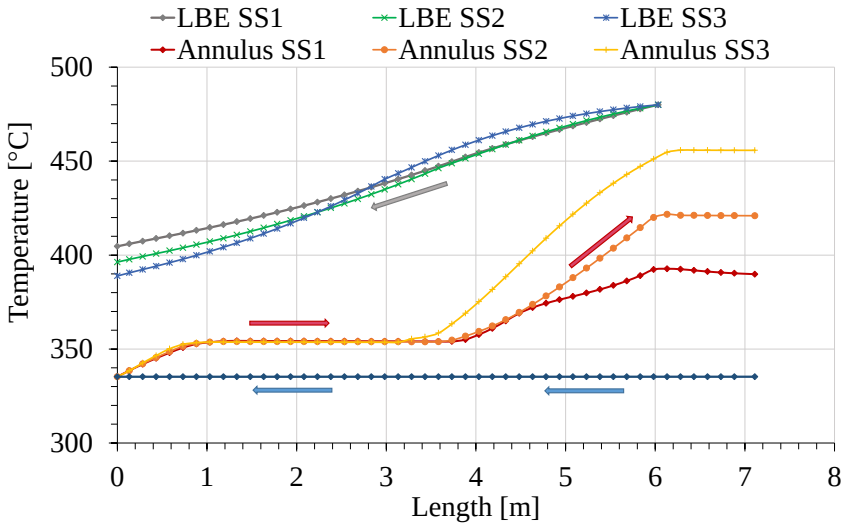

Fig. 3-15 – LBE and H2O temperature profiles along the SG during RUN #1

4 EXPERIMENTAL CAMPAIGN WITHIN H2020 SESAME

4.1 HORIZON2020 SESAME EU PROJECT OVERVIEW

The HORIZON2020 EU project SESAME [29] (thermal-hydraulics Simulations and Experiments for the Safety Assessment of MEtal cooled reactor) supports the development of the most relevant European liquid metal cooled reactors (ASTRID, ALFRED, MYRRHA, SEALER). The project focuses on pre-normative, fundamental, safety-related, challenges for these reactors with the following objectives:

- development and validation of advanced numerical approaches for the design and safety evaluation of advanced reactors;
- achievement of a new or extended validation base by the creation of new reference data;
- establishment of best practice guidelines, Verification & Validation methodologies, and uncertainty quantification methods for liquid metal fast reactor thermal hydraulics.

The SESAME project aims at improving the safety of GEN IV HLMRs, by making available new safety-related experimental results and improved numerical approaches. The experimental data collected aim at improving the knowledge and the experience in terms of design and operations, providing a database for code validation and model development. The results obtained will support the safety policy of the EU members, creating the basis for the further development of the European experimental facilities and numerical tools.

The consortium comprises a total of 25 partners, with a long-standing experience in the field of nuclear technology and nuclear thermal-hydraulics and most of them have already been successfully involved in similar projects.

An important purpose of SESAME is the sharing and dissemination of the knowledge achieved, with the research and scientific community, industry, universities, international and European projects and initiatives, as well as the general public.

4.2 CIRCE-HERO EXPERIMENTAL TESTS

In the framework of the Work Package 4 (WP4) of HORIZON2020 SESAME European project [29], an experimental campaign has been designed and performed on the large LBE pool integral effect CIRCE facility at ENEA Brasimone R.C., implementing the HERO TS. The activity aims at supporting the development of the ALFRED design [30]. The secondary loop for the HERO SGBT unit has been designed and realized, and both the primary and secondary systems have been instrumented.

Three tests have been designed and carried out [31][32], consisting of a Protected Loss of Flow Accident (PLOFA) occurring with the facility operated in nominal steady-state conditions for both primary side (LBE) and secondary side (high pressure water). In steady-state conditions, the LBE mass flow rate is promoted by the injection of argon simulating the behavior of the primary pump, while the thermal power is supplied with the FPS. The transient is obtained reducing the FPS power according to a characteristic heat decay curve, while the loss of the primary pump is simulated by the reduction of the gas injection. The loss of the heat sink is simulated managing the HERO feedwater in the secondary loop.

This section presents the experimental data achieved, in particular in terms of mass flow rates and temperature for both the primary and secondary systems, providing relevant information about the system behavior when subjected to accidental scenarios.

4.2.1 SCOPE OF THE EXPERIMENTS

The tests consist of PLOFA scenarios, occurred during the normal operation of the facility. The nominal working conditions, for both primary and secondary loop, have been maintained constant for a relevant time lapse. After that, PLOFAs have been performed, managing the FPS power supplied, the argon injection and the water mass flow rate to the HERO steam generator. After the transient, the system continues the operation with the primary loop working in Natural Circulation (NC) regime and the HERO SG acting as a DHR system.

The designed nominal working conditions in the SGBT unit assumed before the transition are reported in Tab. 4-1. Each test is marked by the initials SE-Test, meaning SESAME-Test, followed by the test number. The LBE SG inlet temperature is kept constant at 480°C, with an LBE mass flow rate set to ~39 kg/s, in GEC regime. In the secondary loop, the

operating pressure of 172 bar is maintained constant at the BTs through the regulation of valve V3 (see Fig. 2-8) with a water inlet temperature of ~335°C, while the pump provides a total water mass flow rate of ~0.33 kg/s.

The transient conditions are reported in Tab. 4-2. All three tests are characterized by a FPS power transient with a power reduction fixed accordingly to a characteristic heat decay curve. In SE-Test1 and SE-Test2, the argon flow rate is reduced with a linear ramp from 100% to 0% in a time-lapse of 10 s, while in SE-Test3 the argon flow rate follows a particular curve that simulates the effect of the pump flywheel. Concerning the secondary loop, the water mass flow rate is reduced from 100% to 30% in 2 s in SE-Test1 and SE-Test3, simulating the activation of the DHR, while in SE-Test2 the water mass flow rate passes from 100% to 0%, simulating the total loss of the heat sink.

Tab. 4-1 – Designed Boundary Conditions for the SGBT unit

Parameter	Unit	SE-Test1	SE-Test2	SE-Test3
LBE SG inlet temperature	°C	480	480	480
LBE mass flow rate	kg/s	39	39	39
H2O SG inlet temperature	°C	335	335	335
H2O mass flow rate	kg/s	0.33	0.33	0.33
H2O pressure	bar	172	172	172

Tab. 4-2 – Designed Boundary Conditions for the transient

Parameter	SE-Test1	SE-Test2	SE-Test3
FPS Power	Characteristic decay heat curve	Characteristic decay heat curve	Characteristic decay heat curve
Argon Flow Rate	From 100% to 0% in 10 s	From 100% to 0% in 10 s	Curve simulating pump flywheel
H2O Mass Flow Rate	From 100% to 30% in 2 s	From 100% to 0% in 2 s	From 100% to 30% in 2 s

4.2.2 SE-TEST1

The boundary conditions assumed before and after the transient are summarized in Tab. 4-3. At the beginning of the test, the power supplied by the FPS is about 352 kW (see Tab. 4-3 and Fig. 4-1), to compensate the power removed by the HERO SGBT and the heat losses to the environment. The LBE mass flow rate achieved before the transition is about 35 kg/s, maintained in GEC regime with an argon flow rate of 2.75 Nl/s (Tab. 4-3 and Fig. 4-1) injected in the riser. In the secondary loop, the water mass flow rate is supplied by the volumetric pump, which maintains a constant value of mass flow rate of about 0.274 kg/s. This value has been obtained applying the thermal balance equation on the heater component:

$$\dot{m}_{H2O} = \frac{\dot{Q}_{H2O}}{hout - hin}$$

where:

- Q_{H2O} is the electrical heat supplied to the water by the heater before the transient, corresponding to 412 kW;
- h_{out}-h_{in} is the water enthalpy at the inlet and outlet of the heater, corresponding to 74 kJ/(kg*K) (P_{H2O} = 177 bar, T_{H2O} = 13.6°C) and 1577 kJ/(kg*K) (P_{H2O} = 174 bar, T_{H2O} = 339.4°C) respectively;

achieving the value reported above of 0.274 kg/s.

The water temperature at the inlet section of the BTs is maintained at about 336°C, managing the power of the heater component. The pressure of the helium line in the AISI316L powder gap has been maintained at 8.0 bar.

The transient has been obtained reducing the FPS power according to a characteristic heat decay curve shown in Fig. 4-1, while the loss of the primary pump is simulated by the reduction of the argon flow rate injection (FE400) from 2.75 Nl/s to 0 with a linear trend (Fig. 4-1). The loss of the heat sink is simulated reducing the HERO feedwater in the secondary loop to 30% of the value before the transient in time ramp of 2 s, evaluating the SG behavior as DHR system. The beginning of the transient for the FPS power, argon flow rate and water mass flow rate occurs at the same time. The FPS power curve is detailed in Tab. 4-4.

Fig. 4-2 reports the water flow rate measured by the mini-turbine flow meters, in particular by TFM-T4, installed upstream the tube T4, TFM-T5 installed upstream the tube T5 and TFM-T6 installed upstream the tube T6. From the data measured, assuming a water density of ~640 kg/m^3 and a uniform distribution of the water flow among the seven tubes (verified during the commissioning tests), it is possible to obtain the water mass flow rate equal to 0.245 kg/s before the transient, slightly lower than the value obtained from the thermal balance. After the transient, the measured mass flow rate reaches the value of 0.095 kg/s, assuming a uniform distribution among the seven tubes, slightly higher to the value calculated with the power balance on the heater, equal to ~0.080 kg/s. The loss of signals of TFM-T5 and TFM-T6 is due to the low flow rate achieved after the transient, which is close to the lower limit of the measurement range of the instruments.

Tab. 4-3 – SE-Test1, boundary conditions before and after the transient

Parameter	Unit	Value (Before Transient)	Value (After Transient)
FPS Power	[kW]	352	20
Argon Flow Rate	[Nl/s]	2.75	0
H2O mass flow rate	[kg/s]	0.294	0.095
H2O T inlet SG	[°C]	~336	~336

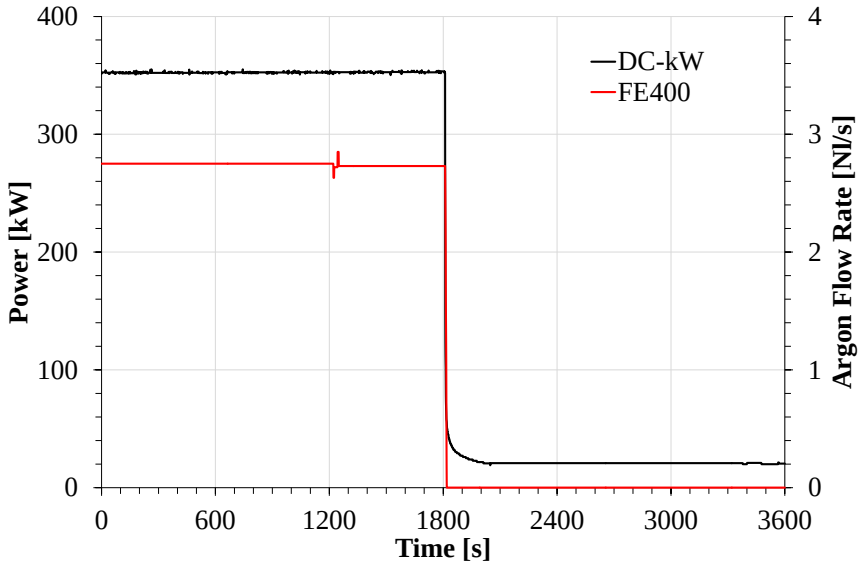

Fig. 4-1 – SE-Test1, FPS Power and argon Flow Rate trends

Tab. 4-4 – SE-Test1, FPS Power decay heat curve during transient

FPS POWER			
Time [s]	*Value*	*Time [s]*	*Value*
0	100%	22.5	10%
1	25%	30	9%
2	22%	50	8%
3.5	19%	60	7%
5	17%	90	6%
7.5	15%	180	6%
10	14%	240	5%
15	12%	300	5%

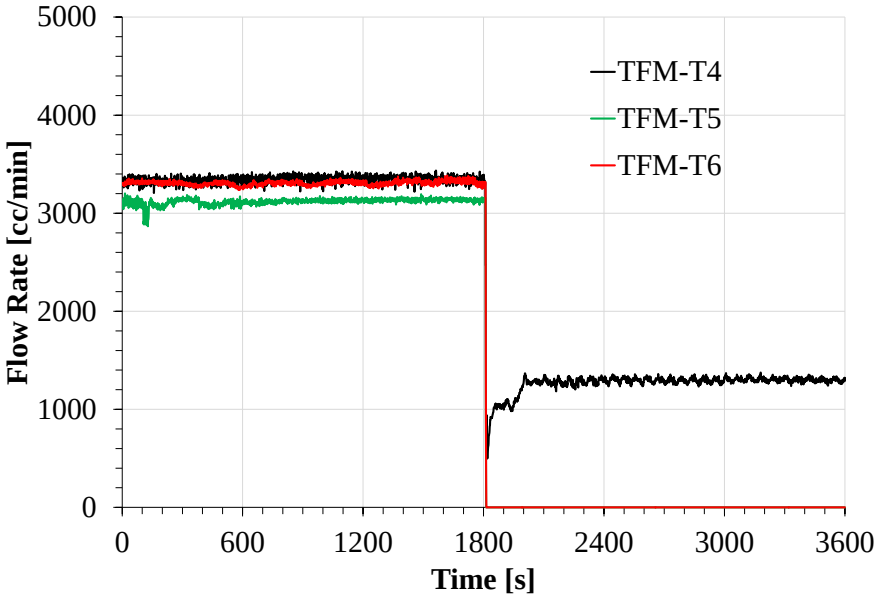

Fig. 4-2 – SE-Test1, H2O mass flow rate trends during the PLOFA Test measured by TFMs

The LBE mass flow rate is reported in Fig. 4-3. Before the transient, the mass flow rate shows a slight decreasing trend with oscillations. This behavior can be addressed to the prototypical argon injection system adopted during the gas-enhanced circulation. Further analysis on this phenomenon will be carried out during the next refurbishment of the facility. The same consideration can be made for the LBE mass flow rate trends of the next two tests. The value of ~35 kg/s, achieved before the transient, is subjected to a fast decrease due to the reduction of the argon flow rate, reaching a minimum of 2 kg/s immediately after the gas transition and assuming the final value in NC of about 6 kg/s.

Fig. 4-4 and Fig. 4-5 report the temperature inside the FPS for the coolant and the pin clad, respectively. The LBE temperatures at the FPS outlet decreases significantly due to the power decrease, reaching a maximum of ~495°C before the transient and then a minimum of ~460°C immediately after, from which it starts to decrease slowly, when NC of the LBE is established. The temperatures at the FPS inlet section remain almost the same during the test at ~420°C, with a low decrease after the transient. The pin clad temperature (Fig. 4-5) decreases from ~530°C before the transient, to ~450°C, passing through a minimum of 445°C and a subsequent maximum peak of 486°C, corresponding to the minimum of LBE mass flow rate.

The temperatures in the riser are shown in Fig. 4-6. Before the transient, the temperature at the inlet of the riser is about 495°C. Arising from the bottom part of the riser up to the separator, the LBE temperature is subjected to a low decrease of about 6°C due to the heat losses along the tube. Immediately after the transition, it rapidly decreases to ~470°C and then it continues to decrease with a smoother ramp. However, the LBE in the top part of the riser and inside the separator does not suffer immediately the effects of the transient, due to the sudden reduction of the LBE mass flow rate, and its temperature decreases slowly. This results in an inversion of the temperatures in the rising leg, in which the LBE on the top remains hotter than the coolant flowing up from the FPS.

The LBE temperatures in the HERO SGBT are reported in Fig. 4-7. Before the transient, at the inlet section, the temperature is about 480°C, while after the cooling it is about 406°C. When the transient occurs, the inlet and outlet LBE temperatures start to decrease slowly, without abrupt changes. It can be noticed that the temperature measured at the inlet by TC-SG-01 suffers of an instability in GEC respect to the other two TCs, because of its position in the separator. In fact, this TC is directly exposed to the rising LBE, mixed to the argon injected at the bottom of the riser and this turbulence affects the measure acquired.

Fig. 4-8 shows the temperatures measured by the 119 TCs placed in the LBE pool, as a function of their vertical position on the supporting bars (A-I), before and after the transient. The stratification in the pool occurs between the positions at 5000 mm and 6000 mm, assuming 0 mm the bottom part of the separator. Before the transient, the maximum temperature reached is ~475°C, in the upper part of the pool, while the lower value is ~422°C in the lower part of the pool; after the transient, the temperature profile is shifted to lower values, with a maximum and minimum temperature reached of 465°C and 407°C

respectively. It can be noticed from Fig. 4-8 that the thermal stratification in the LBE pool occurs in the vertical direction only, with uniformity along the horizontal planes.

Concerning the secondary loop, the water temperatures are reported in Fig. 4-9. At the BTs inlet section, the temperature is maintained constant at ~336°C for the entire test, excepting for few seconds of oscillations, when the transient occurred, due to the re-balancing of the heater power, when the water mass flow rate is reduced. At the BTs outlet, instead, the steam temperature is subjected to a sudden variation, passing from an average value of ~390°C before the transient to a maximum value of ~450°C immediately after, due to the reduction of the water mass flow rate. From this value, the temperature starts to decrease slowly, because of the lower thermal field in the primary system (SG shell side).

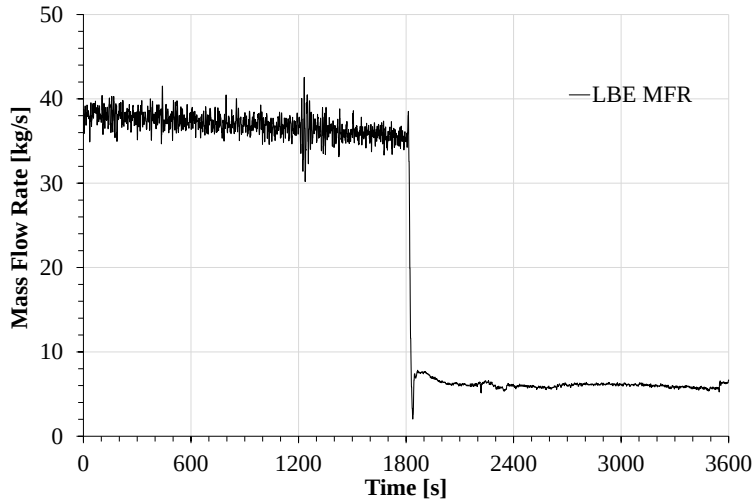

Fig. 4-3 – SE-Test1, LBE mass flow rate before and after the transient

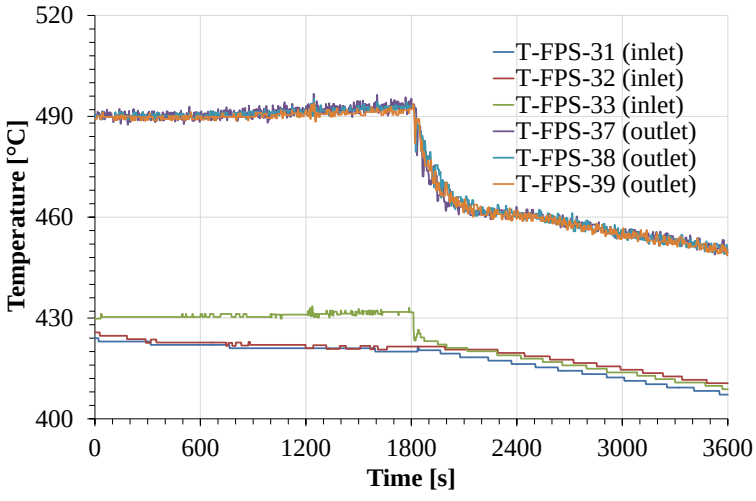

Fig. 4-4 – SE-Test1, LBE temperature trends at the FPS inlet-outlet

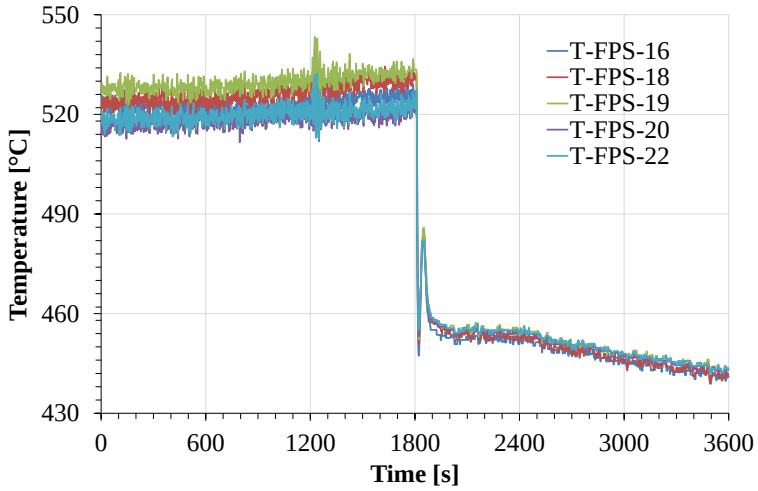

Fig. 4-5 – SE-Test1, FPS pin clad temperature

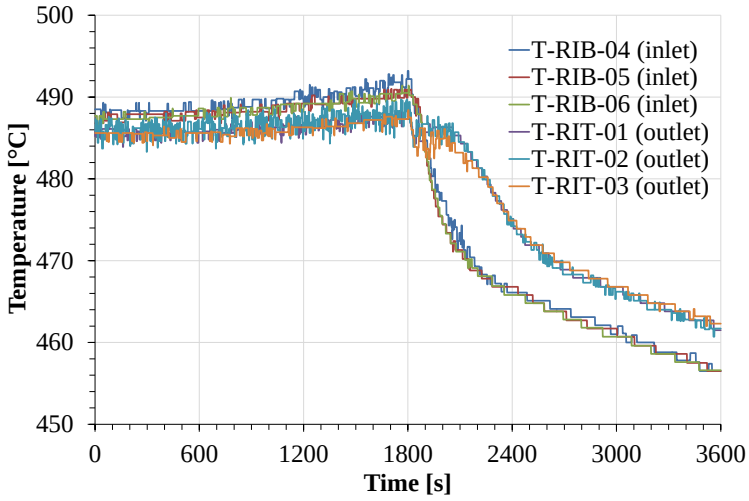

Fig. 4-6 – SE-Test1, LBE temperature trends at the inlet and outlet sections of the Riser

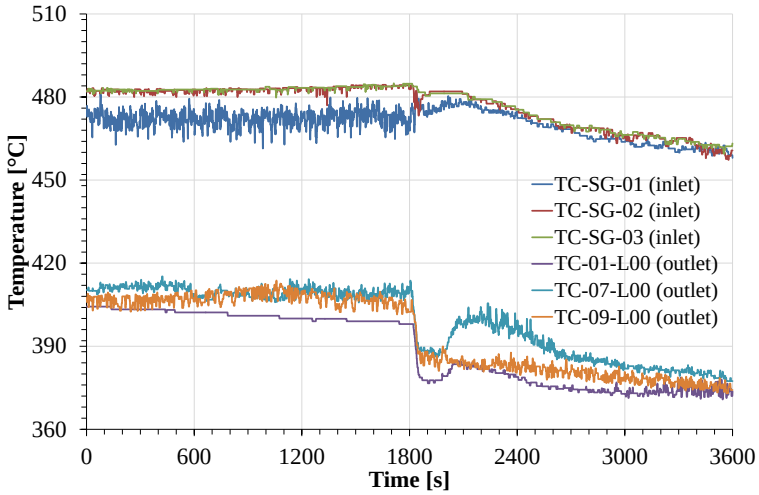

Fig. 4-7 – SE-Test1, LBE temperature trends at the inlet and outlet sections of the SG

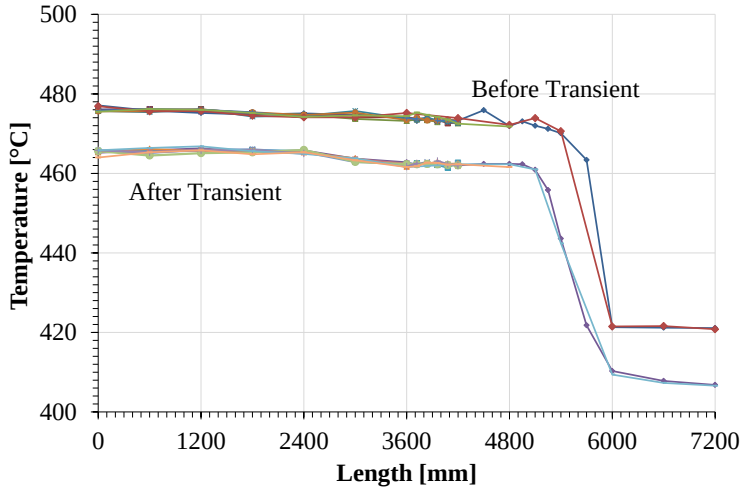

Fig. 4-8 – SE-Test1, axial temperature profile inside the S100 vessel before and after the transient

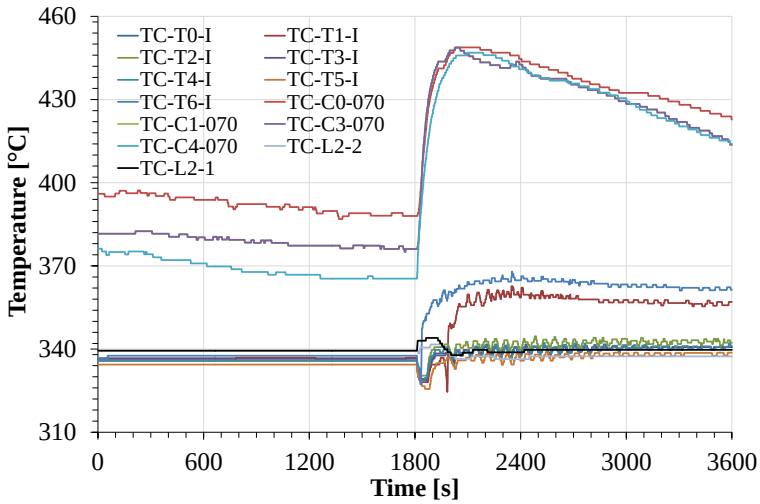

Fig. 4-9 – SE-Test1, H2O temperature trends at the inlet and outlet sections of the Bayonet Tubes

4.2.3 SE-TEST2

The SE-Test2 is similar to the SE-Test1, with the difference in the management of the water injection, which is reduced to zero during the PLOFA transient, simulating the full loss of the heat sink. The boundary conditions assumed before and after the transient are summarized in Tab. 4-5.

Before the transient, the power supplied by the FPS is about 379 kW (Tab. 4-5 and Fig. 4-10), while the LBE mass flow rate reaches an average value of 36 kg/s, thanks to an argon injection in the riser with a flow rate of 3.35 Nl/s. In the secondary side, the water mass flow rate is set constant at 0.270 kg/s. As for SE-Test1, this value has been calculated by

applying the thermal balance equation on the heater component, with the following assumptions:

- electrical heat supplied to the water by the heater before the transient 400 kW;
- water enthalpy at the inlet of the heater corresponding to 88 kJ/(kg*K) (P_{H2O} = 176 bar, T_{H2O} = 17°C);
- water enthalpy at the outlet of the heater, corresponding to 1580 kJ/(kg*K) (P_{H2O} = 175 bar, T_{H2O} = 340°C).

The water temperature at the inlet section of the BTs is maintained at about 335°C, managing the power of the heater component.

The transient has been obtained reducing the FPS power according to a characteristic heat decay curve already presented in Tab. 4-4 and in the following in Fig. 4-10, while the loss of the primary pump is simulated by the reduction of the argon flow rate injection from 2.75 Nl/s to 0 Nl/s with a linear trend. The full loss of the heat sink is realized reducing the HERO feedwater from 100% to 0% in 2 s. The beginning of the transient for the FPS power, argon flow rate and water mass flow rate occurs at the same time. The FPS power curve is detailed in Tab. 4-4, already presented in the previous paragraph.

The water flow rate measured by the mini-turbine flow meters is reported in Fig. 4-11. The measure has been acquired by all the flow meters, except for TFM-T1 and TFM-T2. From the data measured, assuming a uniform distribution of the water flow among the seven tubes, it is possible to obtain the water mass flow rate equal to 0.253 kg/s (water density assumed of ~640 kg/m^3) before the transient. This value is slightly lower respect to the previous one of 0.270 kg/s calculated by the thermal balance equation on the heater.

Tab. 4-5 – SE-Test2, boundary conditions before and after the transient

Parameter	**Unit**	**Value (Before Transient)**	**Value (After Transient)**
FPS Power	[kW]	379	22
Argon Flow Rate	[Nl/s]	3.35	0
H2O mass flow rate	[kg/s]	0.294	0
H2O T inlet SG	[°C]	~335	----

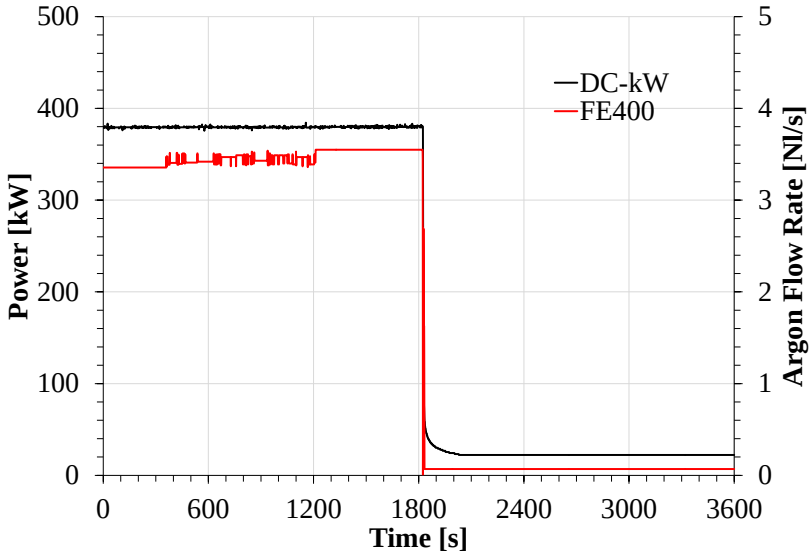

Fig. 4-10 – SE-Test2, FPS Power and argon Flow Rate trends

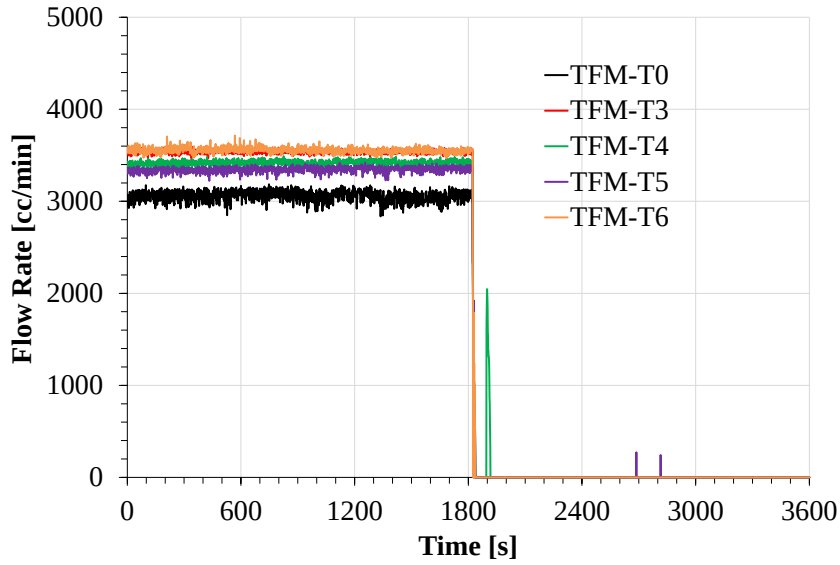

Fig. 4-11 – SE-Test2, H2O mass flow rate trends during the PLOFA Test measured by TFMs

The following graphs present the experimental data achieved in the primary side in terms of mass flow rates and temperatures. The LBE mass flow rate is reported in Fig. 4-12, which shows that the value achieved before the transient is ~36 kg/s. When the transient occurs, the LBE flow rate is subjected to a sudden decrease due to the reduction of the argon flow rate, reaching a minimum of ~4 kg/s immediately after the gas transition, then a maximum peak of 8 kg/s and finally assuming the value of about 4 kg/s in NC.

Fig. 4-13 and Fig. 4-14 report the temperature inside the FPS for the coolant and the pin clad, respectively. During the power reduction, the LBE temperatures at the FPS outlet

decreases rapidly, reaching a maximum of ~495°C before the transient and then a minimum of ~470°C immediately after, from which it reaches a constant value of ~475°C. The temperatures at the FPS inlet section remain almost constant during the test at ~415°C. A particular trend can be noticed for the thermocouple T-FPS-32 at the FPS inlet, which measures an increase of the temperature after the transient. This can be due to the low mass flow rate achieved in NC, which can lead to a stagnation point near the thermocouple. The pin clad temperature (Fig. 4-14) decreases from ~535°C before the transient to a minimum of 445°C immediately after, a subsequent peak of ~480°C and a new minimum of ~460°C. From this last value, the temperature increases due to the small power supplied by the FPS, reaching slowly a maximum of 500°C, from which it starts to decrease due to the heat losses which exceed the power supplied.

The temperatures in the riser are shown in Fig. 4-15. Before the transient, the temperature at the inlet of the riser is about 495°C. Arising from the bottom part of the riser up to the separator, the LBE temperature is subjected to a low decrease of about 6°C due to the heat losses along the tube. During the transient, the riser LBE inlet temperature decreases rapidly at ~470°C due to the cold LBE arising from the FPS. The LBE in the top part of the riser and inside the separator does not suffer immediately the effects of the transient, due to the sudden reduction of the LBE mass flow rate, which delays the ascent of the coolant, and its temperature decreases slowly. As occurred in SE-Test1, there is an inversion of the temperatures in the rising leg, in which the LBE on the top remains hotter than the coolant flowing up from the FPS.

The LBE temperatures in the HERO SGBT are reported in Fig. 4-16. Before the transient, at the inlet section, the temperature is about 480°C, while after the cooling it is about 410°C. When the transient occurs, the complete loss of the heat sink leads to an increase of the temperatures along the SG shell side, with the LBE temperature at the outlet section which reaches in few minutes the same value of the SG inlet section. Also for this test, it can be noticed that the temperature measured at the inlet by TC-SG-01 suffers of an instability in GEC respect to the other two TCs, because of its position in the separator, as already explained in the previous paragraph.

Fig. 4-17 shows the temperatures in the LBE pool, measured by the 119 TCs, before and after the transient. The stratification in the pool occurs between the positions at 5000 mm and 6000 mm (assuming 0 mm the bottom part of the separator). Before the transient, the maximum temperature reached is ~475°C, in the upper part of the pool, while the lower

value is ~418°C in the lower part of the pool; after the transient, the temperature profile assumes values slightly lower than the previous ones, with a maximum and minimum temperature reached of 465°C and 418°C respectively. The temperature decrease in the pool achieved in this test is due only to the heat losses through the vessel, since the steam generator has been disabled after the transient. Also in this case, the thermal stratification in the LBE pool occurs in the vertical direction only, with uniformity along the horizontal planes.

Concerning the secondary loop, the water temperatures are reported in Fig. 4-18, showing a constant temperature of ~335°C at the BTs inlet and an average outlet temperature of 380°C.

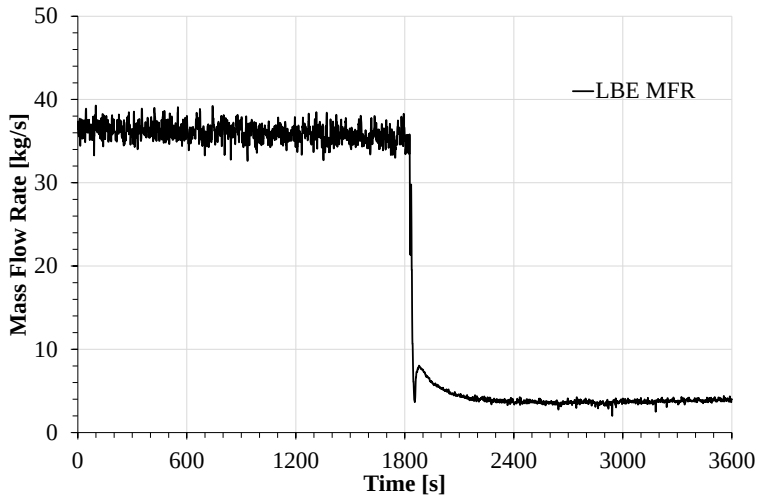

Fig. 4-12 – SE-Test2, LBE mass flow rate before and after the transient

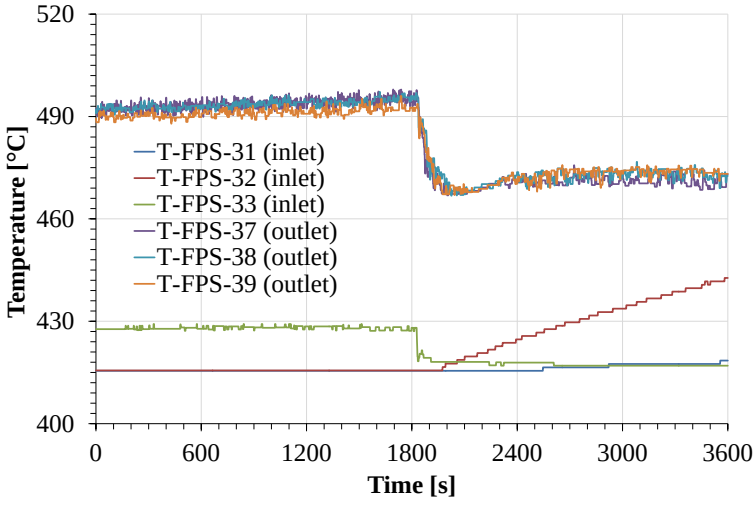

Fig. 4-13 – SE-Test2, LBE temperature trends at the FPS inlet-outlet

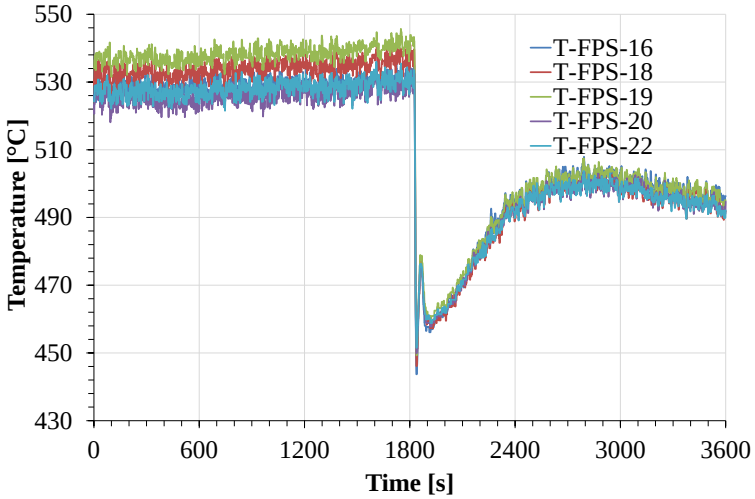

Fig. 4-14 – SE-Test2, FPS pin clad temperature

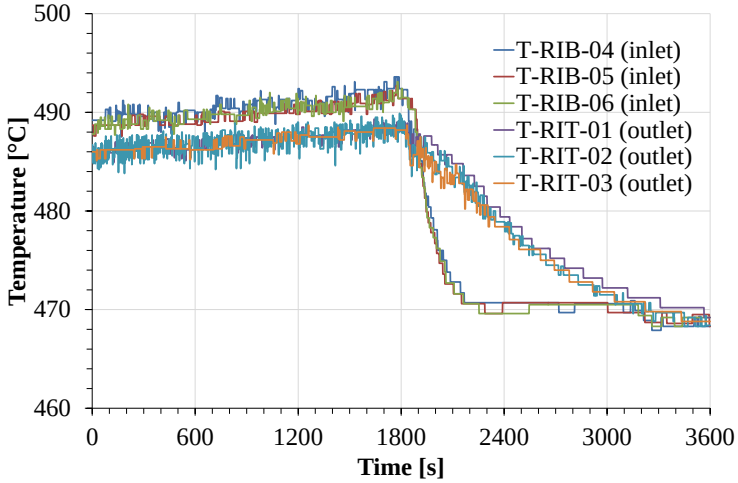

Fig. 4-15 – SE-Test2, LBE temperature trends at the inlet and outlet sections of the Riser

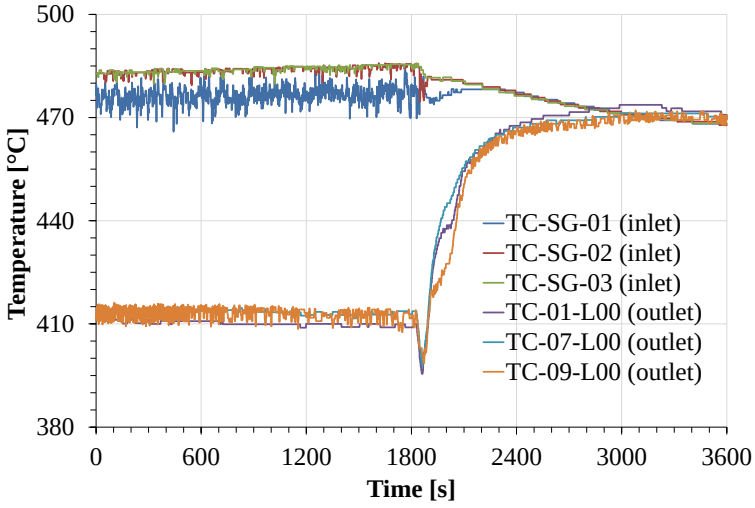

Fig. 4-16 – SE-Test2, LBE temperature trends at the inlet and outlet sections of the SG

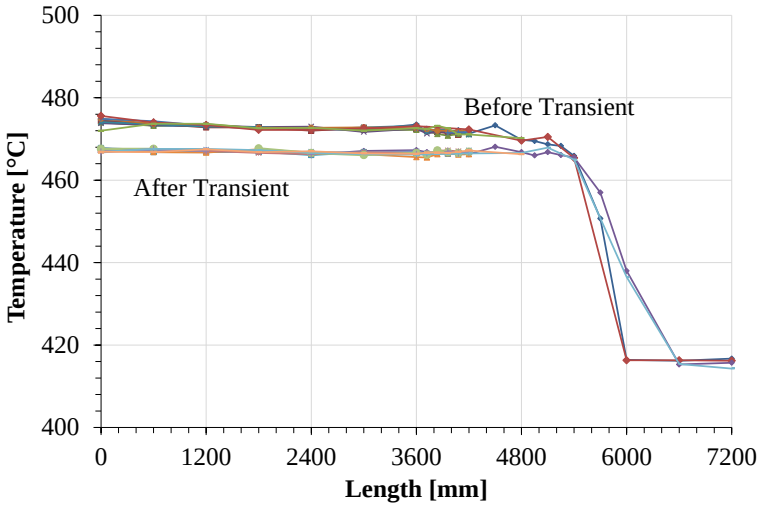

Fig. 4-17 – SE-Test2, axial temperature profile inside the S100 vessel before and after the transient

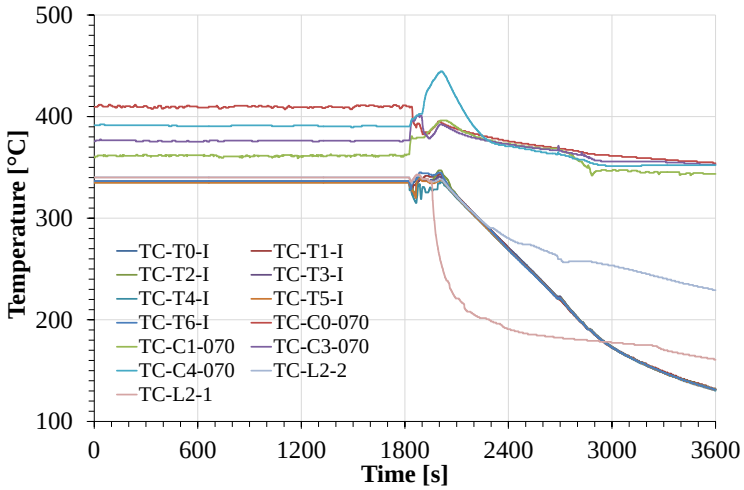

Fig. 4-18 – SE-Test2, H2O temperature trends at the inlet and outlet sections of the Bayonet Tubes

4.2.4 SE-TEST3

The third test reproduces the last PLOFA transient and it has been assumed as a reference test for a benchmark numerical activity foreseen within the SESAME project [33]. As reported for SE-Test1 and SE-Test2, the boundary conditions assumed before and after the transient are summarized in Tab. 4-6. At the beginning of the test, the power supplied by the FPS is about 356 kW (see Tab. 4-6 and Fig. 4-19), to compensate the power removed by the HERO SGBT and the heat losses to the environment; the LBE mass flow rate achieved before the transition is about 34 kg/s, maintained in GEC regime with an argon flow rate of 2.73 Nl/s (Tab. 4-6 and Fig. 4-19) injected in the riser. In the secondary loop, the water mass flow rate is supplied by the volumetric pump, which maintains a constant value of

mass flow rate of about 0.294 kg/s, calculated with the thermal balance equation on the heater component, with the following assumptions:

- electrical heat supplied to the water by the heater before the transient 440 kW;
- water enthalpy at the inlet of the heater corresponding to 78 kJ/(kg*K) (P_{H2O} = 177 bar, T_{H2O} = 14.5°C);
- water enthalpy at the outlet of the heater, corresponding to 1577 kJ/(kg*K) (P_{H2O} = 175 bar, T_{H2O} = 339.5°C).

The water temperature at the inlet section of the BTs is maintained at about 336°C.

The transient has been obtained reducing the FPS power according to a characteristic heat decay curve shown in Fig. 4-19, while the loss of the primary pump is simulated by the reduction of the argon flow rate injection from 2.75 Nl/s to 0 with a curve reproducing the pump flywheel (Fig. 4-19). The loss of the heat sink is simulated reducing the HERO feedwater in the secondary loop to 30% of the value before the transient in time ramp of 2 s, evaluating the SG behavior as DHR system. The beginning of the transient for the FPS power, argon flow rate and water mass flow rate occurs at the same time. The FPS and argon flow rate curves are detailed in Tab. 4-7.

Fig. 4-20 reports the water flow rate measured by the mini-turbine flow meters, in particular by TFM-T0, installed upstream the central tube T0, and TFM-T4, installed upstream the tube T4. From the data measured, assuming a water density of ~640 kg/m3 and an uniform distribution of the water flow among the seven tubes, it is possible to obtain the water mass flow rate equal to 0.26 kg/s before the transient (slightly lower than the value calculated with the thermal balance) and 0.078 kg/s after the transient, close to the value calculated with the power balance on the heater, equal to 0.079 kg/s.

The LBE mass flow rate is reported in Fig. 4-21: the value of ~34 kg/s, achieved before the transient, is subjected to a fast decrease due to the reduction of the argon flow rate, reaching the final value in NC of about 6 kg/s.

Tab. 4-6 – SE-Test3, boundary conditions before and after the transient

BEFORE TRANSIENT		
Parameter	**Unit**	**Value**
FPS Power	[kW]	356
Argon flow rate	[Nl/s]	2.75
Water mass flow rate	[kg/s]	0.294
Water T inlet SG	[°C]	~336
AFTER TRANSIENT		
Parameter	**Unit**	**Value**
FPS Power	[kW]	20
Argon flow rate	[Nl/s]	0
Water mass flow rate	[kg/s]	0.078
Water T inlet SG	[°C]	~336

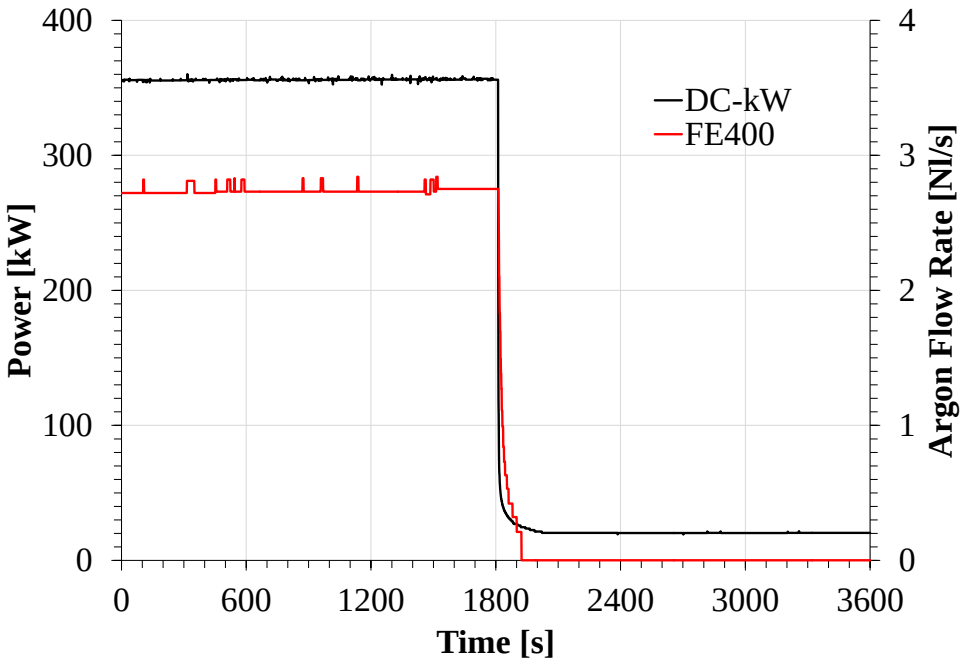

Fig. 4-19 – SE-Test3, FPS Power and argon Flow Rate trends

Tab. 4-7 – SE-Test3, FPS Power and argon FLOW RATE trends during the transient

FPS POWER	
Time [s]	**Value**
0	100%
1	25%
2	22%
3.5	19%
5	17%
7.5	15%
10	14%
15	12%
22.5	10%
30	9%
50	8%
60	7%
90	6%
180	6%
240	5%

ARGON FLOW RATE	
Time [s]	**Value**
0	100%
1	90%
2	83%
3	77%
4	71%
5	67%
10	50%
20	33%
30	25%
50	17%
100	9%
150	5%
200	2%
300	0%

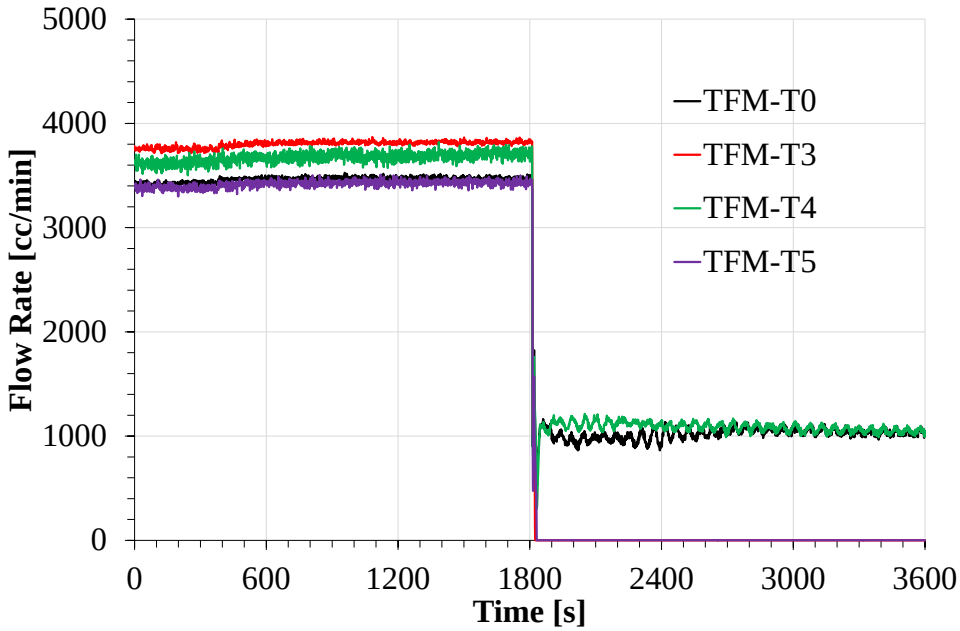

Fig. 4-20 – SE-Test3, H2O mass flow rate trends during the PLOFA Test measured by TMFs

Fig. 4-22, Fig. 4-23, Fig. 4-24 and Fig. 4-25 report the temperatures in the primary system, in the FPS, Riser and SG respectively. The LBE temperatures at the FPS outlet decreases significantly due to the power decrease, passing from 496°C to the minimum value (446°C)

immediately after the transient, and then reaching a maximum of 465°C, from which it starts to decrease slowly, when NC of the LBE is established. The temperatures at the FPS inlet section remain almost the same during the test at ~420°C, with a low decrease after the transient. The pin clad temperature (Fig. 4-23) decreases from ~530°C, before the transient, to 460°C, passing through a minimum of 435°C and a subsequent maximum peak of 470°C, corresponding to the minimum of LBE mass flow rate.

The temperatures in the riser are shown in Fig. 4-24. Before the transient, the temperature at the inlet of the riser is about 495°C. Arising from the bottom part of the riser up to the separator, the LBE temperature decreases of about 5°C. During the transient, the significant reduction of the FPS power leads to a low LBE inlet temperature in the riser, which rapidly decreases to ~470°C; however, the LBE in the top part of the riser and inside the separator does not suffer immediately the effects of the transient, due to the sudden reduction of the LBE mass flow rate, and its temperature decreases slowly. As occurred in SE-Test1 and SE-Test2, the LBE on the riser top part remains hotter than the coolant flowing up from the FPS.

The LBE temperatures in the HERO SGBT are reported in Fig. 4-25. Before the transient, at the inlet section, the temperature is about 480°C, while after the cooling it is about 408°C. When the transient occurs, the inlet and outlet LBE temperatures start to decrease slowly, without abrupt changes. Also for this test, it can be noticed an instability in the temperature measured at the SG inlet by TC-SG-0, due to the reasons already explained in the previous paragraphs.

Fig. 4-26 shows the temperatures measured by the 119 TCs placed in the LBE pool, as a function of their vertical position on the supporting bars (A-I), before and after the transient. The stratification in the pool occurs between the positions at 5000 mm and 6000 mm, assuming 0 mm the bottom part of the separator. Before the transient, the maximum temperature reached is ~478°C, in the upper part of the pool, while the lower value is ~420°C in the lower part of the pool; after the transient, the temperature profile is shifted to lower values, with a maximum and minimum temperature reached of 468°C and 406°C respectively. It can be noticed from Fig. 4-26 that the thermal stratification in the LBE pool occurs in the vertical direction only, with uniformity along the horizontal planes.

Concerning the secondary loop, the water temperatures are reported in Fig. 4-27. At the BTs inlet section, the temperature is maintained constant at ~336°C for the entire test,

excepting for few seconds, at the beginning of the transient, due to the re-balancing of the heater power, when the water mass flow rate is reduced. At the BTs outlet, instead, the steam temperature is subjected to a sudden variation, passing from ~360°C before the transient to a maximum value of ~450°C immediately after, due to the reduction of the water mass flow rate. From this value, the temperature starts to decrease slowly, because of the lower thermal field along the SG shell side, with the consequent reduction of power removed.

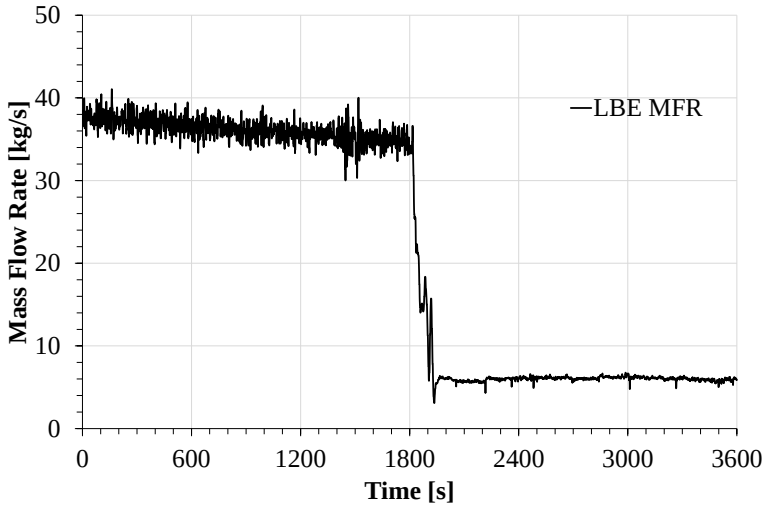

Fig. 4-21 – SE-Test3, LBE mass flow rate before and after the transient

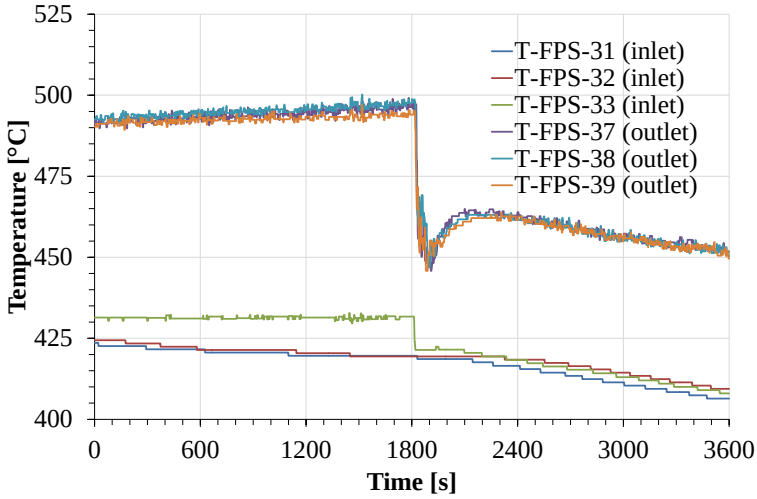

Fig. 4-22 – SE-Test3, LBE temperature trends at the FPS inlet-outlet

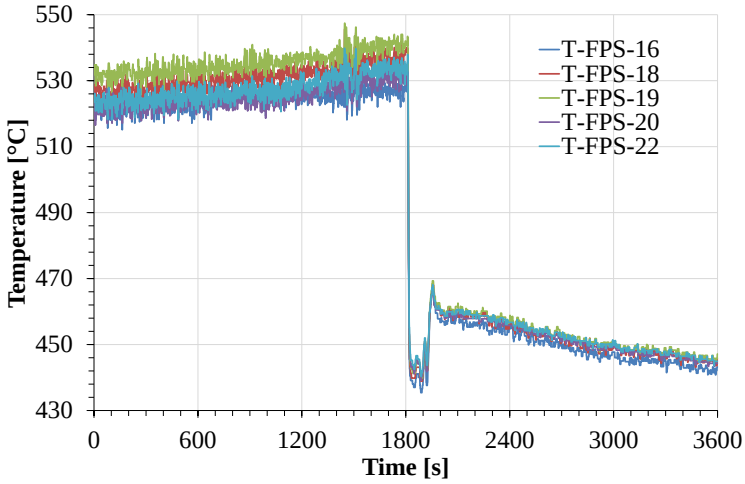

Fig. 4-23 – SE-Test3, FPS pin clad temperature

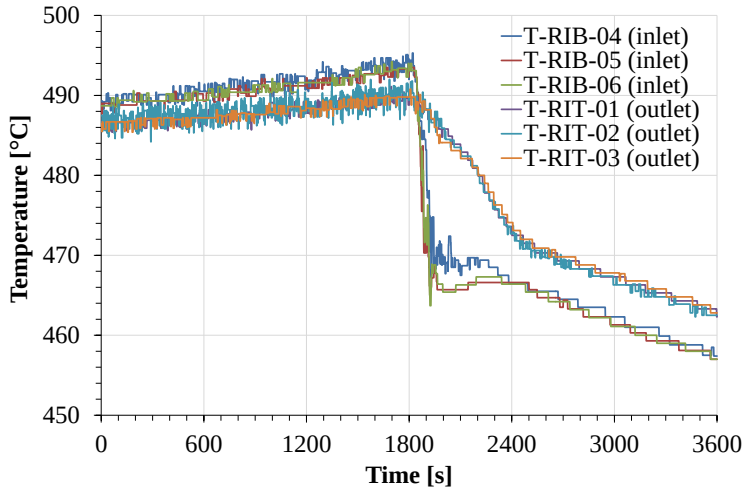

Fig. 4-24 – SE-Test3, LBE temperature trends at the inlet and outlet sections of the Riser

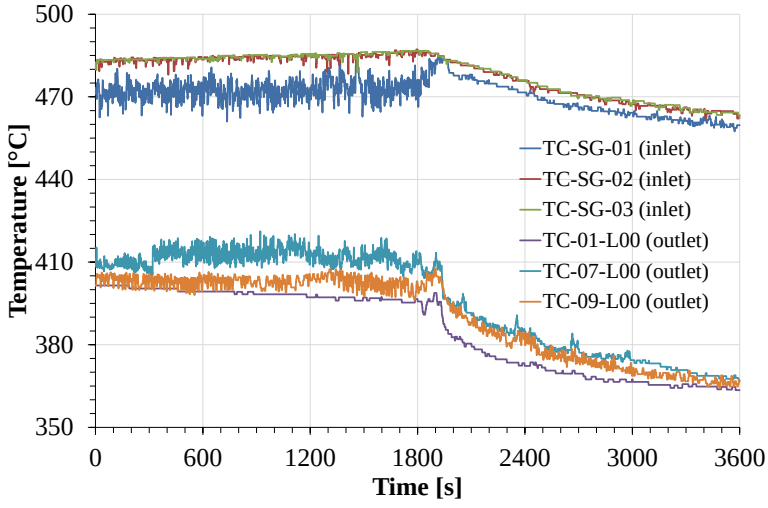

Fig. 4-25 – SE-Test3, LBE temperature trends at the inlet and outlet sections of the SG

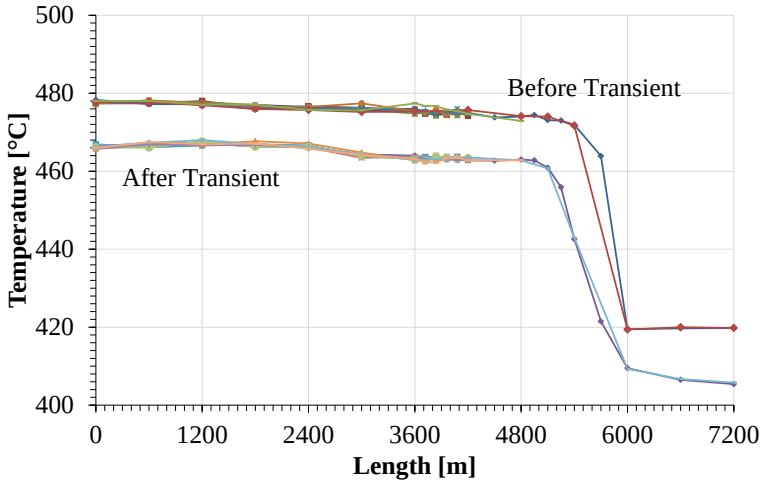

Fig. 4-26 – SE-Test3, axial temperature profile inside the S100 vessel before and after the transient

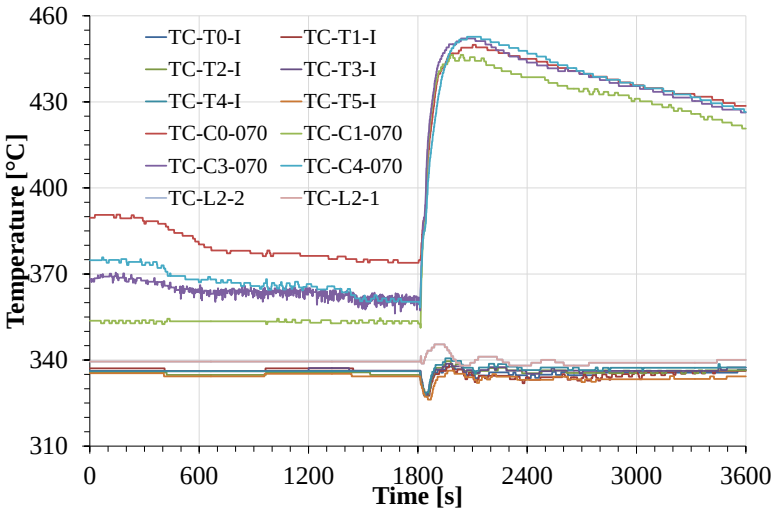

Fig. 4-27 – SE-Test3, H2O temperature trends at the inlet and outlet sections of the Bayonet Tubes

(Page intentionally left blank)

5 EXPERIMENTAL CAMPAIGN WITHIN H2020 MYRTE

5.1 HORIZON2020 MYRTE EU PROJECT OVERVIEW

The main purpose of the H2020 MYRTE EU Project [34] is the research in support of the development of the MYRRHA [6][35] research facility. The project is managed by the SCK•CEN and it aims at demonstrating the technological feasibility of high-level nuclear waste transmutation at industrial scale through the realization of a LBE-cooled nuclear fast reactor coupled with an ADS. The research activity is supported by numerical and experimental studies, coordinated in the framework of the MYRTE project. The main objectives are addressed to specific work packages, divided as follows [34]:

- a first WP is dedicated to the aims at the realization of the injector part of the MYRRHA accelerator to demonstrate the feasibility and the required reliability of this non-semi-conducting part of the accelerator;
- a WP coordinated the R&D concerning the technical issues in HLMs thermal hydraulics, pool thermal-hydraulics and thermal hydraulics of the fuel assembly by numerical simulations and experimental validation;
- a dedicated WP is focused on the chemistry of HLMs, in particular LBE, studying the evaporation from LBE, capture and deposition of Po and fission products, as part of the safety analysis;
- a WP dedicated to experimental reactor physics;
- a last WP dedicated to the studies on Americium bearing oxide fuel, to demonstrate the capability of developing minor actinide fuel for transmutation.

The MYRTE consortium involves 27 European organizations including universities, research institutes and industrial corporations. Most MYRTE Consortium members have been involved previously in major projects concerning the development of Generation IV LFR and ADS technology.

5.2 CIRCE-HERO EXPERIMENTAL TESTS

In the framework of the WP3 of the HORIZON2020 MYRTE European project [34], a dedicated experimental activity has been performed on CIRCE facility in HERO configuration at the ENEA Brasimone R.C., providing support to the development of MYRRHA [35] and acquiring thermo-dynamic feedbacks and experimental data relevant

for MYRRHA Primary Heat eXchanger (PHX). In the following, a test matrix consisting of 9 tests is presented and the results of the experimental campaign are described [36][37].

During the experimental activity, the LBE pool-type facility CIRCE, implementing the HERO TS, has been involved in a low pressure secondary side (~16 bar) experimental campaign. On the basis of the final layout of the secondary circuit, already presented in Section 2.2.2, a numerical model has been developed with the SYS-TH code RELAP5-3D© in order to carry out a pre-test analysis for the setup of the low pressure tests experimental campaign. The preliminary numerical results obtained have been used to define the tests to be included in the experimental test matrix. The tests are characterized by an operating pressure of ~16 bar, maintained constant at the inlet of the annular region of each bayonet tube and a water inlet temperature of ~198°C in order to assure few degrees of sub-cooling at the HERO inlet.

5.2.1 SCOPE OF THE EXPERIMENTS

The experiments consist of steady-state tests, in operative conditions suitable for the MYRRHA heat exchanger. The boundary conditions of the tests have been defined by performing a preliminary simulation activity by the SYS-TH code RELAP5-3D© Ver. 4.3.4, using the model already described in Section 3. The preliminary numerical results obtained from the simulations have been used to choose the tests to be included in the experimental test matrix [38]. The tests presented are characterized by an operating pressure of 16 bar maintained constant at the inlet of the annular region of each bayonet tube through the regulation of valve V3 (see Fig. 2-8) and a water inlet temperature of ~198°C in order to assure few degrees of sub-cooling. The water pre-heating is realized managing the heater component (see Fig. 2-8).

A test reference has been set, assuming on the primary side, the LBE mass flow rate of 30 kg/s and the LBE inlet temperature in the shell side of the steam generator maintained at 235°C, while in the secondary loop the water mass flow rate is assumed constant at ~0.17 kg/s, corresponding to the 50% of the HERO nominal water mass flow rate (0.33 kg/s), in order to keep low pressure drops along the bayonet tubes. Starting from the conditions of the test reference, a sensitivity has been carried out changing one parameter at a time as shown in Tab. 5-1: a difference of +/-30% has been assumed for the LBE mass flow rate (Tests #3 and #4) and for the water mass flow rate (Tests #7 and #8), while a difference of +/-20°C has been assumed for the LBE temperature (Tests #1 and #2) and for the water

temperature (Tests #5 and #6). It can be noticed that for Test #5 the water inlet pressure has been set to 23 bar instead of 16 bar because of the higher temperature assumed for water (at 23 bar T_{sat}=219.56°C).

The conditions assumed for the tests are reported in Tab. 5-1. During the experiments, each test has been performed after that 1 h of steady-state was reached with the conditions of the Test Reference, in order to assure in such a way the repeatability of the tests. Each test is marked by the initials MY-Test, meaning MYRTE-Test, followed by the test number.

Tab. 5-1 – MYRTE Test Matrix

Parameter	**Unit**	**MY-TestRef.**	**MY-Test1**	**MY-Test2**	**MY-Test3**	**MY-Test4**	**MY-Test5**	**MY-Test 6**	**MY-Test 7**	**MY-Test 8**
TLBE inlet SG	°C	235	255 (+20°C)	215 (-20°C)	235	235	235	235	235	235
LBE mass flow rate	kg/s	30	30	30	39 (+30%)	21 (-30%)	30	30	30	30
T H2O inlet SG	°C	198.0	198.0	198.0	198.0	198.0	218.0 (+20°C)	178.0 (-20°C)	198.0	198.0
H2O mass flow rate	kg/s	0.17	0.17	0.17	0.17	0.17	0.17	0.17	0.21 (+30%)	0.12 (-30%)
P H2O outlet SG	bar	~16	~16	~16	~16	~16	~23	~16	~16	~16

5.2.2 MY-TEST REFERENCE

The first test (MY-TestRef) has been considered as Test Reference, and was ended after 1 h of steady-state. The argon gas lift has been set at 1 Nl/s (see Fig. 5-1) in order to reach the designed LBE mass flow rate of 30 kg/s (see Fig. 5-2). The power of the FPS has been set to 90 kW (see Fig. 5-1), achieving a LBE inlet temperature in the HERO SGBT of about 239°C.

In the secondary loop, the water temperature at the heater outlet has been set at 204°C, in order to achieve a water temperature at the SGBT inlet of ~200°C. The pump has been set in order to achieve a water mass flow rate of ~160 g/s, while the V3 has been regulated to maintain a SG inlet pressure of ~16.5 bar. The pressure of the helium line in the AISI316L powder gap has been maintained at 8.2 bar.

As shown in Fig. 5-3, the temperature at the FPS inlet is ~222°C, while the outlet temperature is ~240°C, with a ΔT along the active length of about 18°C. Arising from the bottom part of the riser up to the separator, the LBE temperature remains almost constant, as shown in Fig. 5-4. The LBE temperatures in the HERO SGBT are reported in Fig. 5-5 and Fig. 5-6: at the inlet section the temperature is about 237°C, while after the cooling it is about 222°C. It can be noticed that the temperature measured at the inlet by TC-SG-01 suffers an instability respect to the other two TCs, because of its position in the separator. In fact, this TC is directly exposed to the rising LBE, mixed to the argon injected at the bottom of the riser and this turbulence affects the measure acquired.

In these conditions it is possible to evaluate the power removed by HERO, assuming an average cp for the LBE of 146 kJ/(kg*K), the average LBE mass flow rate of 30 kg/s and the average ΔT of 17.3°C, obtaining from the thermal balance equation the average value of ~77 kW.

Fig. 5-7 shows the temperatures measured by the 119 TCs placed in the LBE pool as a function of their vertical position on the supporting bars (A-I), after 1 h of steady-state in the designed conditions (end of the test). The stratification in the pool occurs between the positions at 5000 mm and 6000 mm (assuming 0 mm the bottom part of the separator), with a maximum temperature reached of ~235°C, in the upper part of the pool, while the lower value is ~221°C in the lower part of the pool. It can be noticed from Fig. 5-7 that the thermal stratification in the LBE pool occurs in the vertical direction only, with uniformity along the horizontal planes. Fig. 5-8, Fig. 5-9 and Fig. 5-10 report the temperature trends in the LBE pool during 1 h of steady-state for the TCs in rods A, H and I respectively.

Concerning the secondary loop, Fig. 5-11 reports the water flow rate measured by the seven turbine flow meters placed at the inlet of each one of the seven bayonet tubes. The flow rate is equally distributed among the tubes, except for the tube 6, in which the value measured by the TFM-T6 is ~50% lower than the other flow rates measured. This unbalanced distribution in tube 6 has been investigated replacing the TFM-T6 with TFM-

T5, obtaining the same discrepancy in the measure of the flow rate and concluding that it is not related to an error in the instrumentation, but it is due to the geometry of the BT itself (e.g. tolerances of manufacturing).

Fig. 5-12 and Fig. 5-13 show the BT inlet and outlet water temperatures, equal to ~202°C due to the saturation conditions) and the BT pressure drops reached of about 0.8 bar. The low water outlet temperature of TC-T1-I reported in Fig. 5-12 is due to a malfunction of its acquisition channel of the DACS and it is not related to the instrument. Finally, Fig. 5-14 reports the pressure trend along the secondary loop measured upstream the heater (PC-L1-1), downstream the heater (PC-L2-1) and upstream the V3 (PC-L3-1).

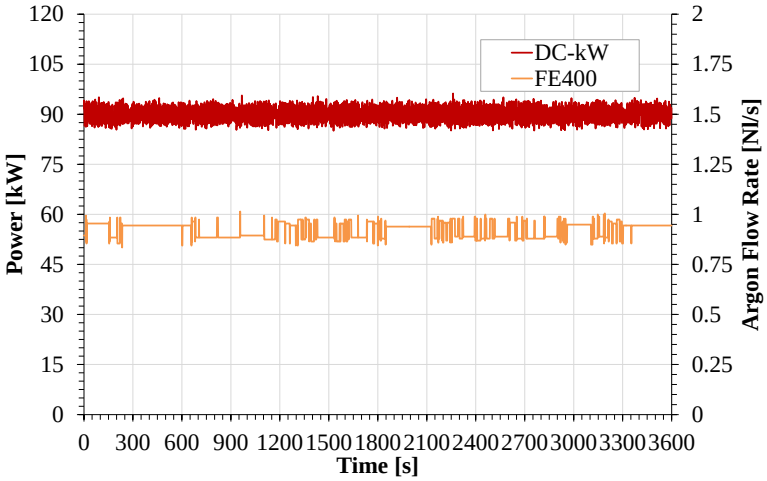

Fig. 5-1 – Test Reference Boundary Conditions

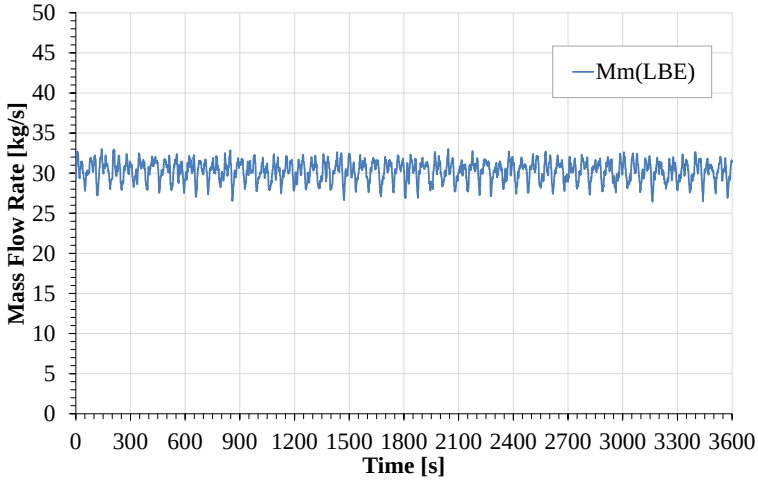

Fig. 5-2 – LBE Mass Flow Rate measured by VFM during the Test Reference

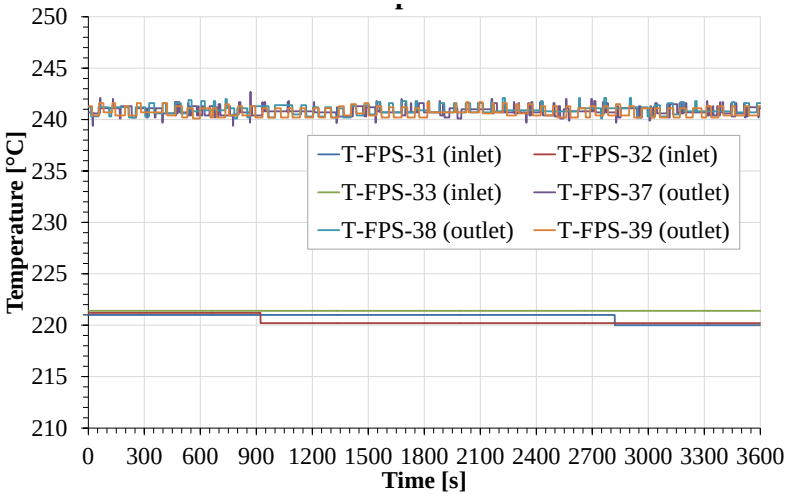

Fig. 5-3 – Inlet and Outlet Temperatures along the FPS during the Test Reference

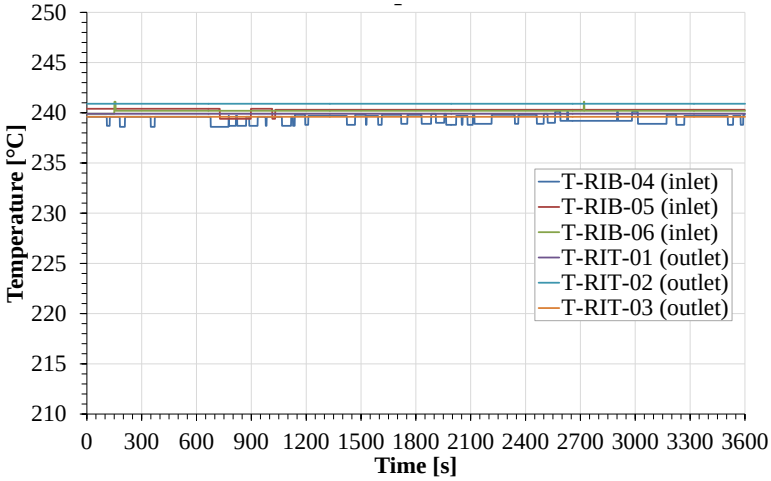

Fig. 5-4 – Inlet and Outlet Temperatures along the Riser during the Test Reference

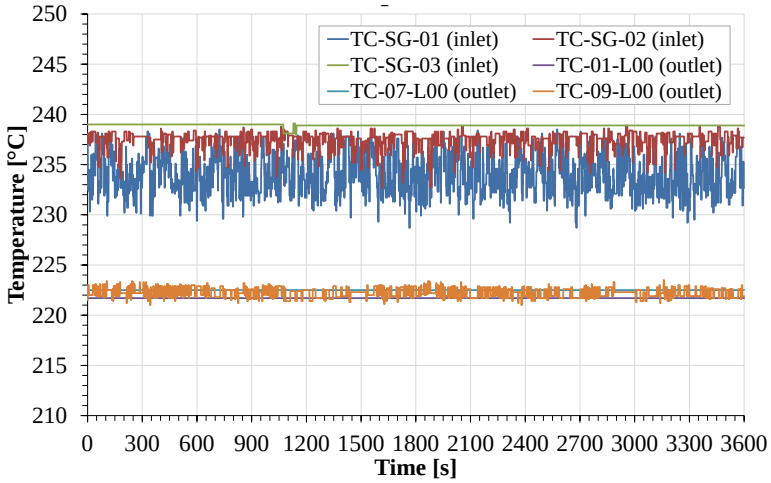

Fig. 5-5 – Inlet and Outlet Temperature along the SGBT Shell Side during the Test Reference

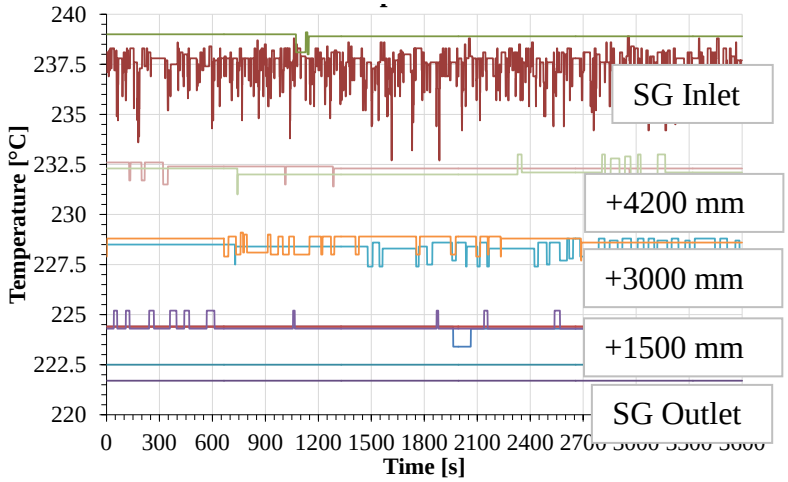

Fig. 5-6 – LBE Temperatures along the SG at different levels: inlet section, +4200 mm, +3000 mm, +1500 mm, outlet section during the Test Reference

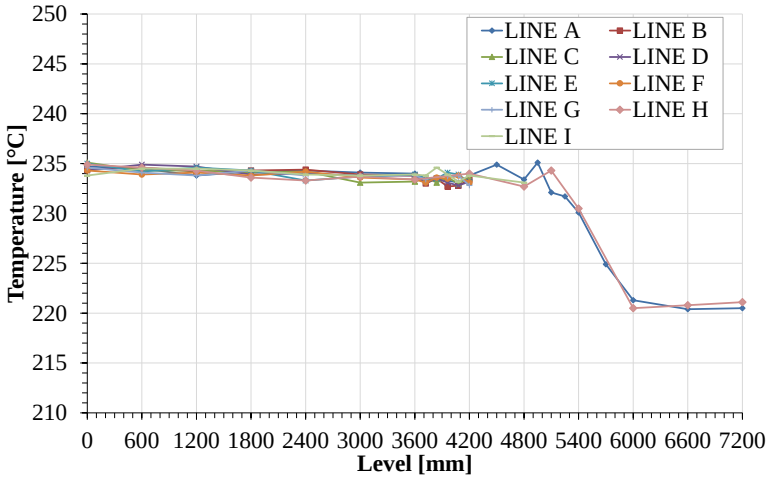

Fig. 5-7 – Axial profile of the temperature inside the S100 vessel during the Test Reference

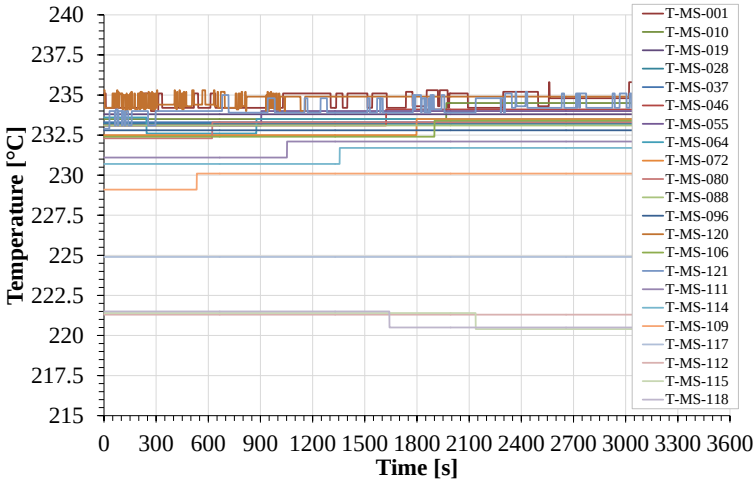

Fig. 5-8 – Temperature measured on supporting rod A during the Test Reference

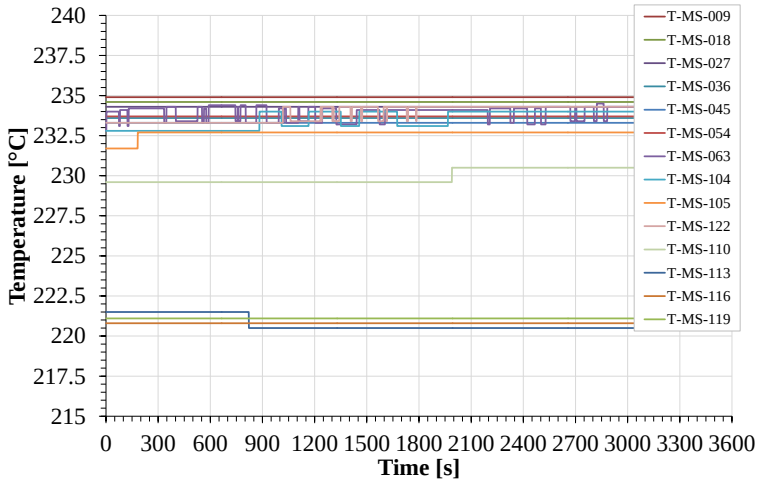

Fig. 5-9 – Temperature measured on supporting rod H during the Test Reference

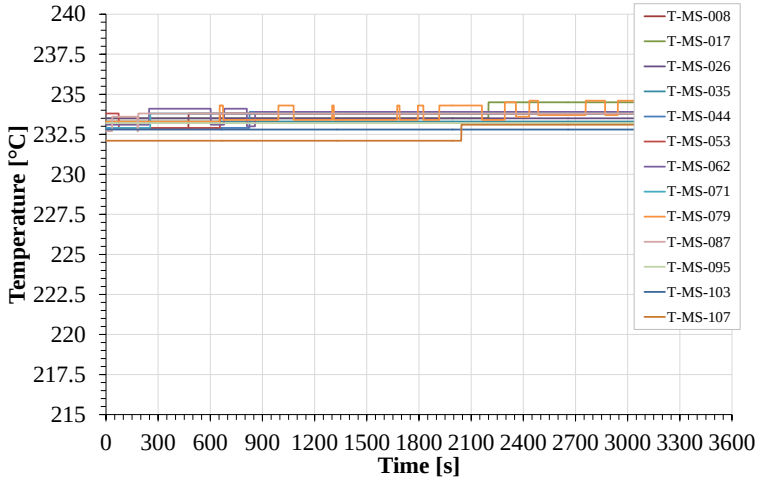

Fig. 5-10 – Temperature measured on supporting rod I during the Test Reference

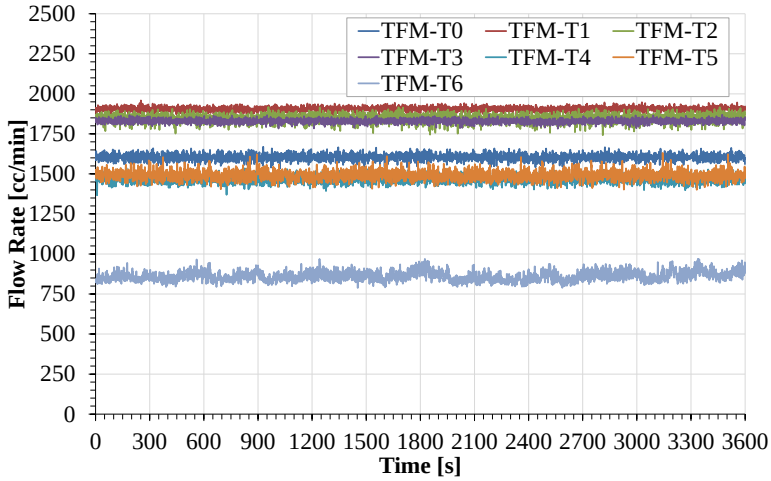

Fig. 5-11 – Water Mass Flow Rate measured by turbine flow meters during the Test Reference

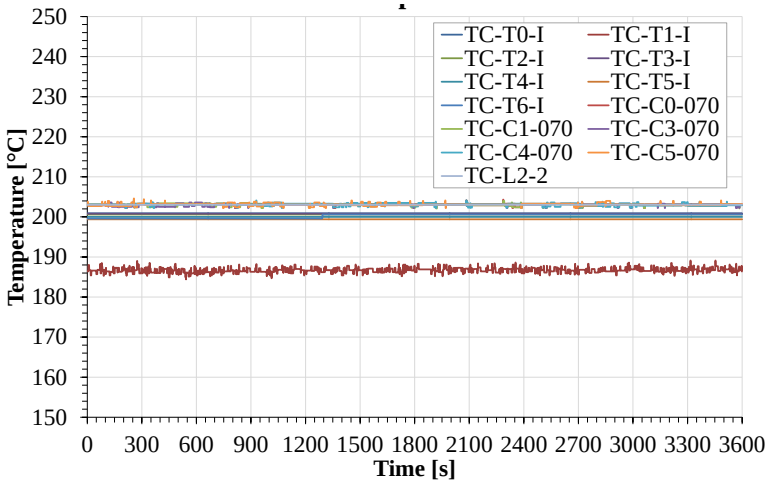

Fig. 5-12 – Water Temperatures at the inlet and outlet of the SGBT during the Test Reference

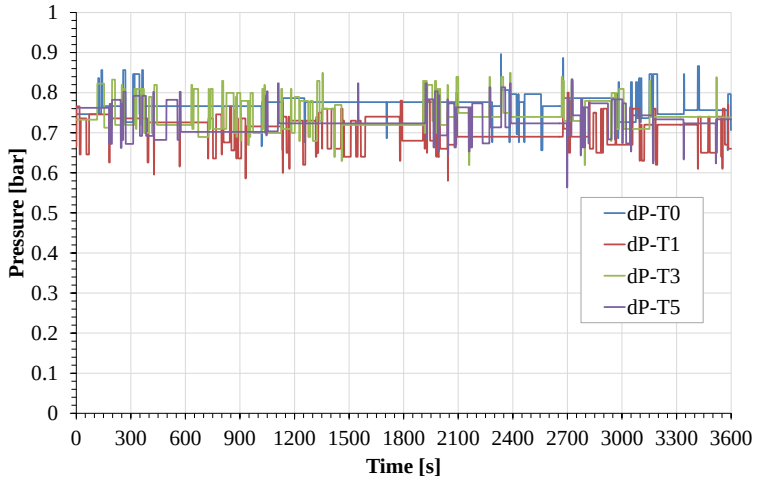

Fig. 5-13 – Pressure drops along the bayonet tubes during the Test Reference

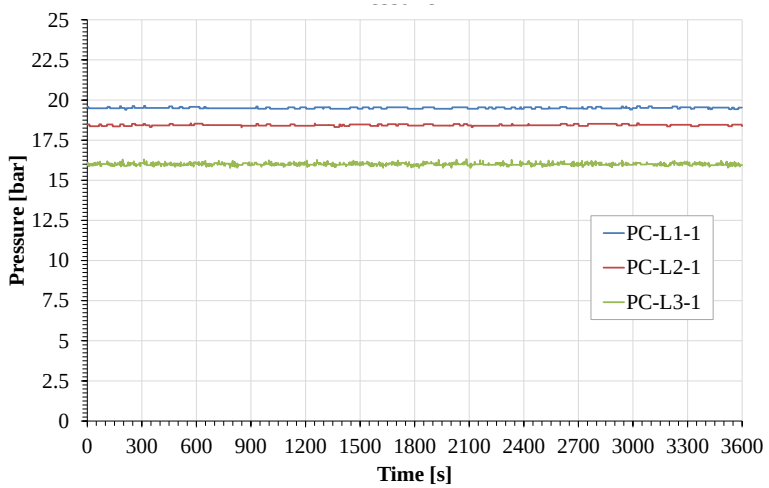

Fig. 5-14 – Pressure along the secondary loop during the Test Reference

5.2.3 MY-TEST1

The MY-Test1 is characterized by a LBE SG inlet temperature of 255°C, with +20°C respect to the Test Reference, while the other parameters are maintained the same. The argon gas lift has been set at 1 Nl/s, reaching the LBE mass flow rate of ~30 kg/s (see Fig. 5-15) and the power of the FPS has been set at ~140 kW in order to maintain a LBE SG inlet temperature of about 239°C.

In the secondary loop, the water flow rate has been maintained at ~160 g/s, the water temperature at the heater outlet has been set at 202°C, achieving a SG water inlet temperature of about 198°C, and the SG inlet pressure at~16.5 bar. The pressure of the helium line in the AISI316L powder gap has been maintained at 8.0 bar. The test was ended after 1 h of steady-state.

Fig. 5-16, Fig. 5-17 and Fig. 5-18 show the temperature trends in the primary loop along the FPS, the SG and inside the pool respectively. In particular, the LBE temperature achieved at the outlet section of the FPS in this test is about 263°C, while the LBE temperature at the SG inlet is ~258°C, with a temperature decrease along the fitting volume and riser of about 5°C. The power removed by HERO, applying the thermal balance equation, is about 125 kW, with a LBE temperature at the outlet section of ~232°C. The stratification in the pool (see Fig. 5-18) occurs between 5000 mm and 6000 mm with a temperature range higher than the Test Reference and comprised between ~255°C and ~231°C.

The parameters monitored in the secondary loop are reported in Fig. 5-19, Fig. 5-20 and Fig. 5-21. Fig. 5-19 shows the water flow rate in the seven BTs, in which it is possible to notice the low flow rate passing in Tube 6 (already discussed in the previous paragraph), while Fig. 5-20 reports the BTs inlet and outlet temperatures. The pressure drops (see Fig. 5-21) in the BTs are about 1.4 bar, higher than the 0.8 bar of Test Reference, due to the higher steam mass fraction produced. The pressure along the loop is reported in Fig. 5-22.

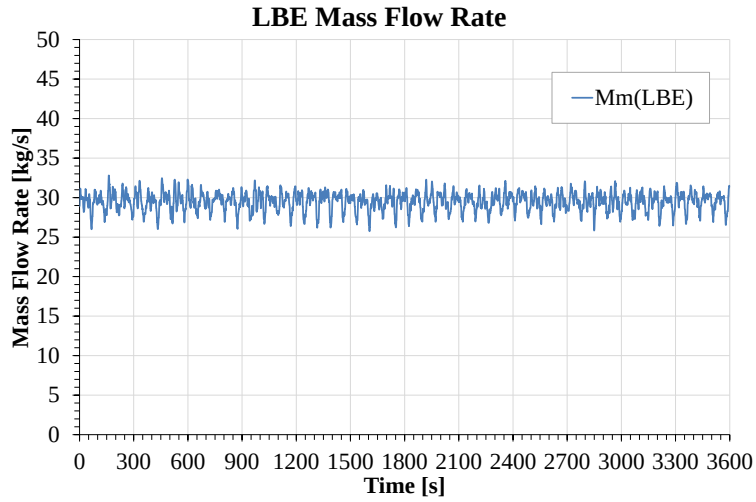

Fig. 5-15 – LBE Mass Flow Rate measured by VFM during the MY-Test1

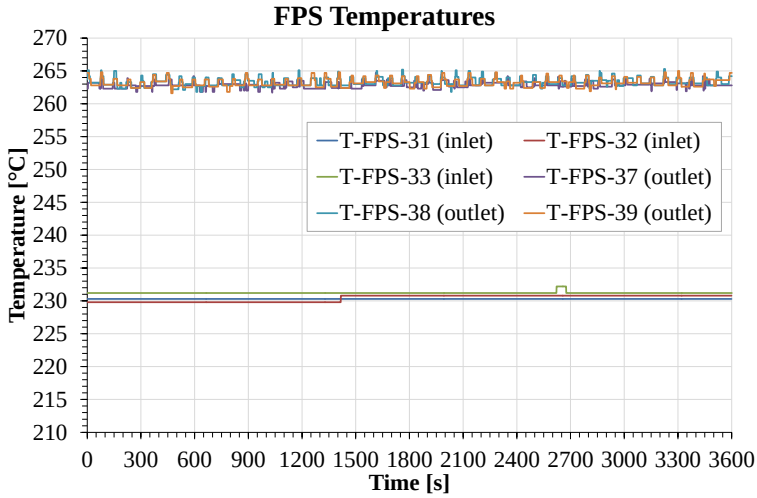

Fig. 5-16 – Inlet and Outlet Temperatures along the FPS during the MY-Test1

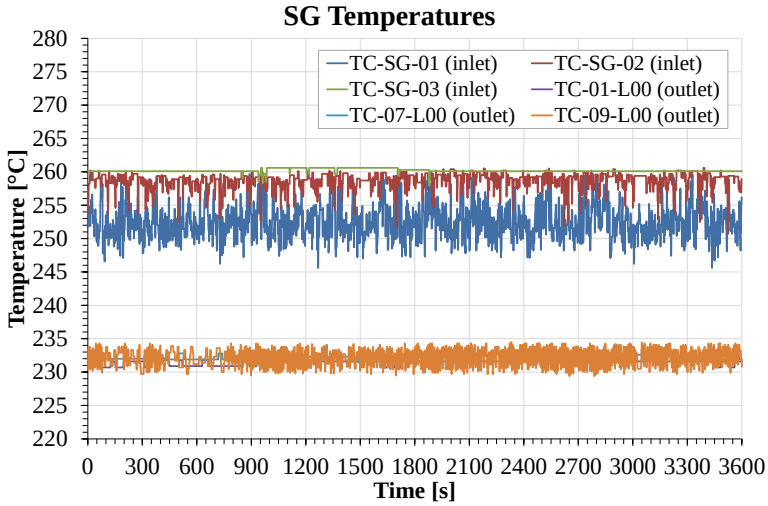

Fig. 5-17 – Inlet and Outlet Temperature along the SGBT Shell Side during the MY-Test1

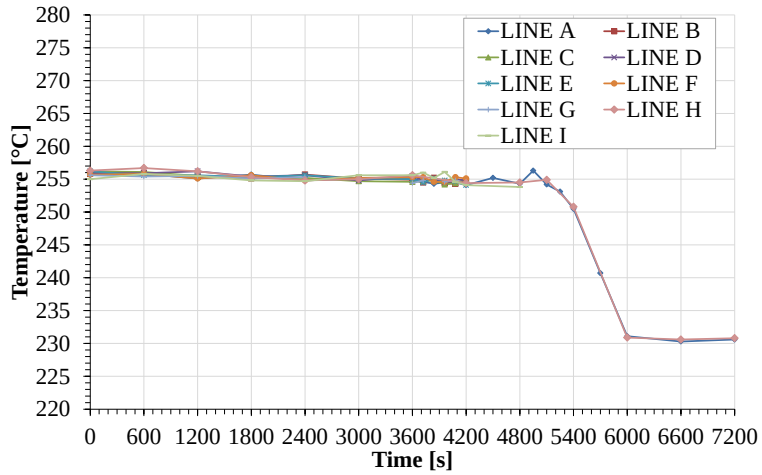

Fig. 5-18 – Axial profile of the temperature inside the S100 vessel during the MY-Test1

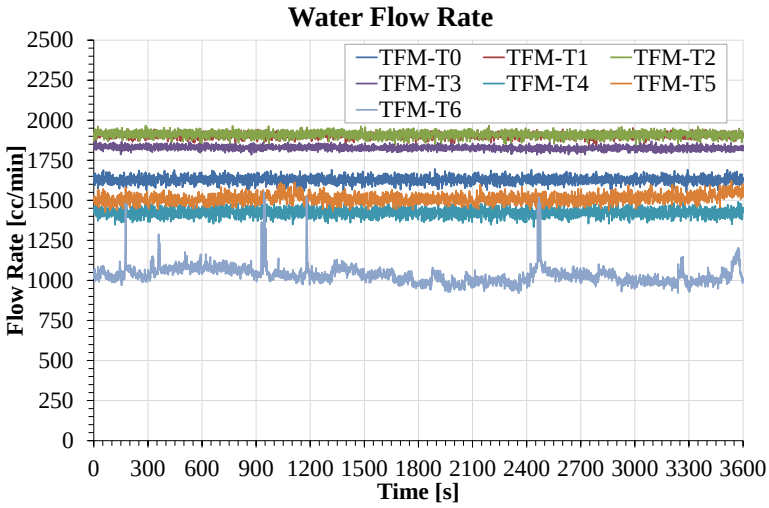

Fig. 5-19 – Water Mass Flow Rate measured by turbine flow meters during the MY-Test1

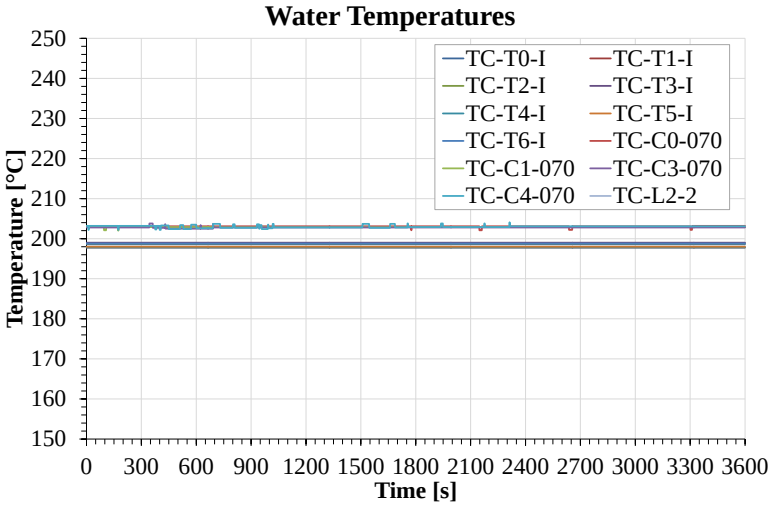

Fig. 5-20 – Water Temperatures at the inlet and outlet of the SGBT during the MY-Test1

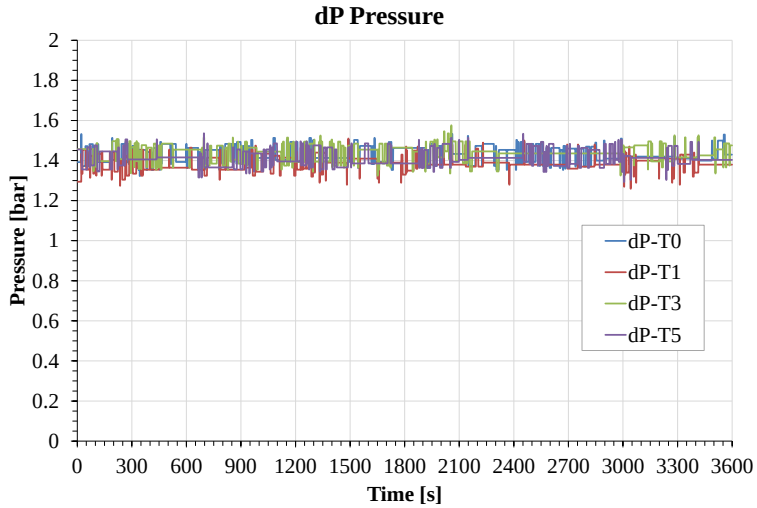

Fig. 5-21 – Pressure drops along the bayonet tubes during the MY-Test1

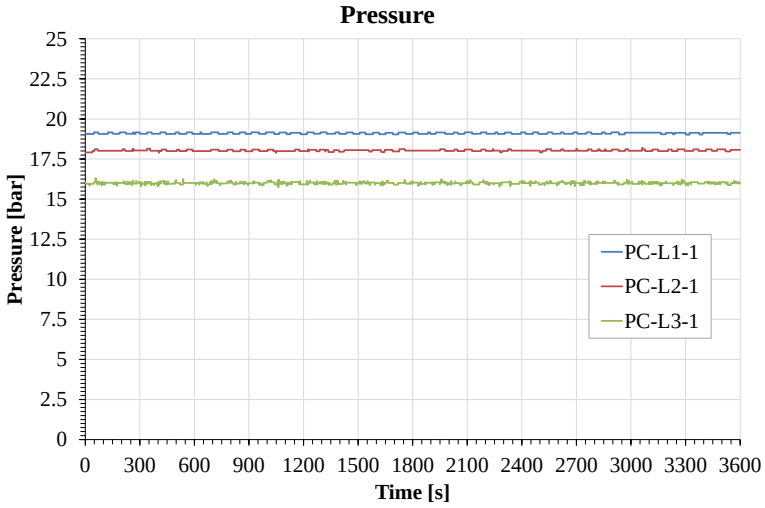

Fig. 5-22 – Pressure in 3 different locations in the secondary loop during the MY-Test1

5.2.4 MY-TEST2

In the MY-Test2, the LBE SG inlet temperature is reduced from 235°C to 215°C (-20°C respect to the Test Reference), while the other parameters are maintained the same of TestRef. The argon gas lift has been set at 1 Nl/s, achieving an LBE mass flow rate of ~29 kg/s (see Fig. 5-23) while the power of the FPS has been set at 27 kW in order to maintain a LBE SG inlet temperature of ~215°C.

In the secondary loop, the water mass flow rate has been maintained at ~160 g/s, the water temperature at the heater outlet has been set at 202°C, achieving a SG water inlet temperature of about 198°C, and the SG inlet pressure at~16.5 bar. The pressure of the

helium line in the AISI316L powder gap has been maintained at 8.0 bar. The test was ended after 1 h of steady-state.

The temperatures in the primary loop are reported in Fig. 5-24, Fig. 5-25 and Fig. 5-26. The LBE temperature at the FPS inlet is 207°C, while the outlet temperature is about 214°C, achieving a ΔT along the active length of ~7°C. A similar thermal field is obtained in the LBE side of the SG (see Fig. 5-25), with an inlet and outlet temperature of 213°C and 209°C respectively. The power removed by HERO in these conditions is very low, about 20 kW, due to the low LBE temperature at the SG inlet. Consequently to the restricted temperature field of the test, also the axial thermal stratification in the pool is less pronounced, passing from a temperature of 210°C to 207°C between 5000 mm and 6000 mm (see Fig. 5-26).

Fig. 5-27, Fig. 5-28, Fig. 5-29 and Fig. 5-30 show the main parameters monitored in the secondary loop. The water flow rate in the seven BTs is reported in Fig. 5-27, in which it is possible to notice the lower flow rate passing in Tube 6, while Fig. 5-28 reports the BTs inlet and outlet temperatures of ~198°C and ~202°C respectively. The pressure drops (see Fig. 5-29) along the BTs in this test are very low, about 0.1 bar, due to the low power removed and thus the small steam mass fraction produced. The pressure along the loop is reported in Fig. 5-30.

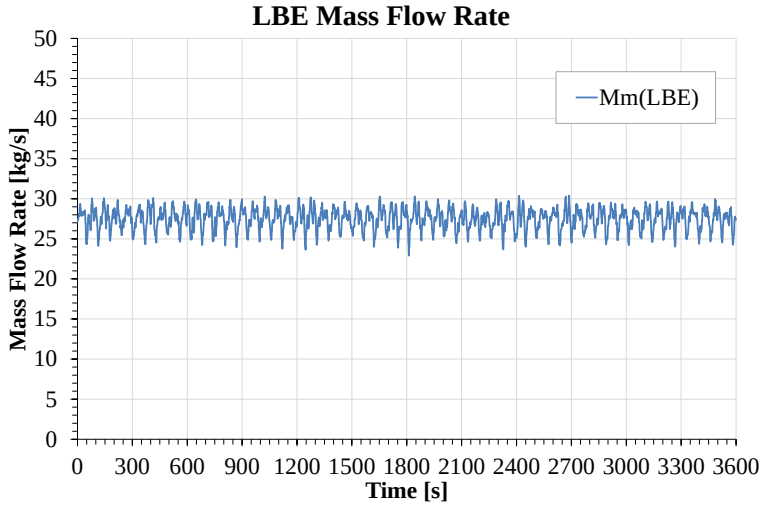

Fig. 5-23 – LBE Mass Flow Rate measured by VFM during the MY-Test2

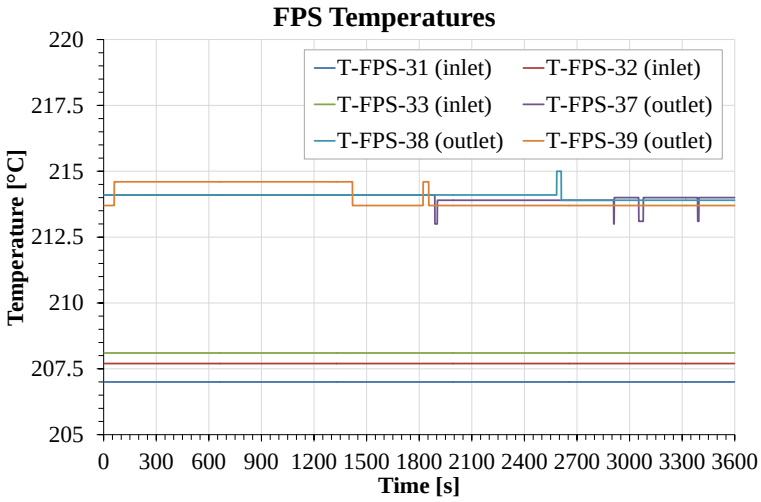

Fig. 5-24 – Inlet and Outlet Temperatures along the FPS during the MY-Test2

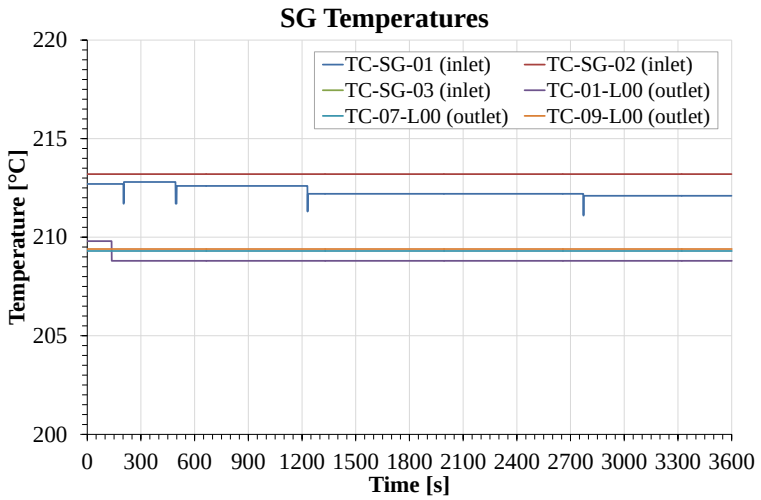

Fig. 5-25 – Inlet and Outlet Temperature along the SGBT Shell Side during the MY-Test2

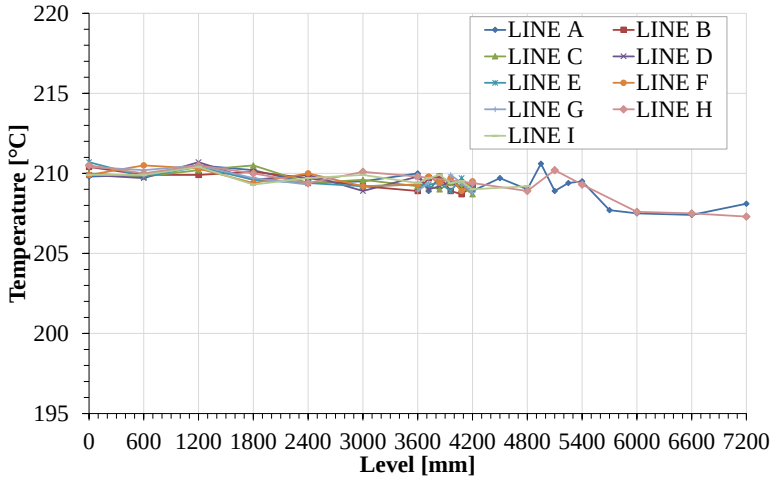

Fig. 5-26 – Axial profile of the temperature inside the S100 vessel during the MY-Test2

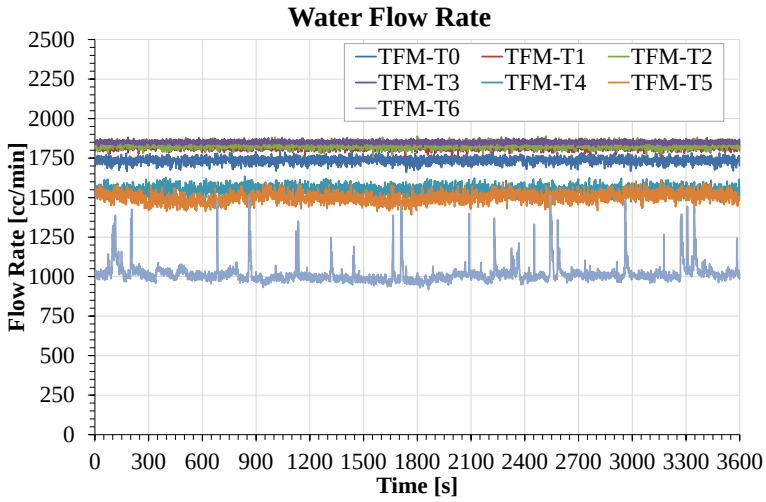

Fig. 5-27 – Water Mass Flow Rate measured by turbine flow meters during the MY-Test2

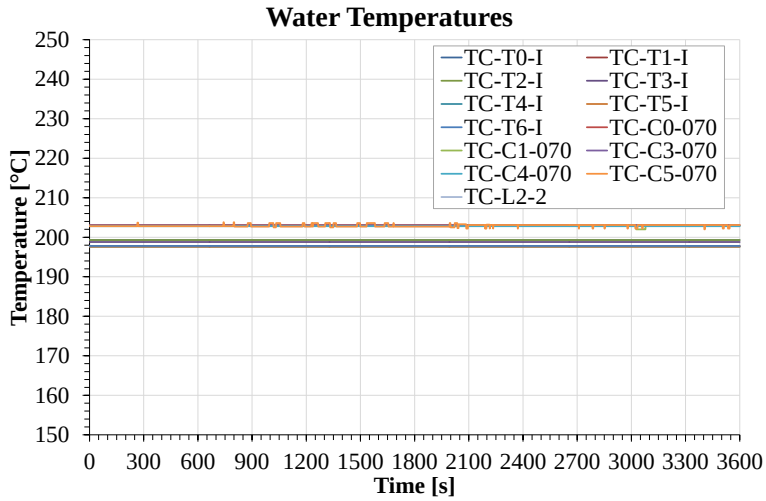

Fig. 5-28 – Water Temperatures at the inlet and outlet of the SGBT during the MY-Test2

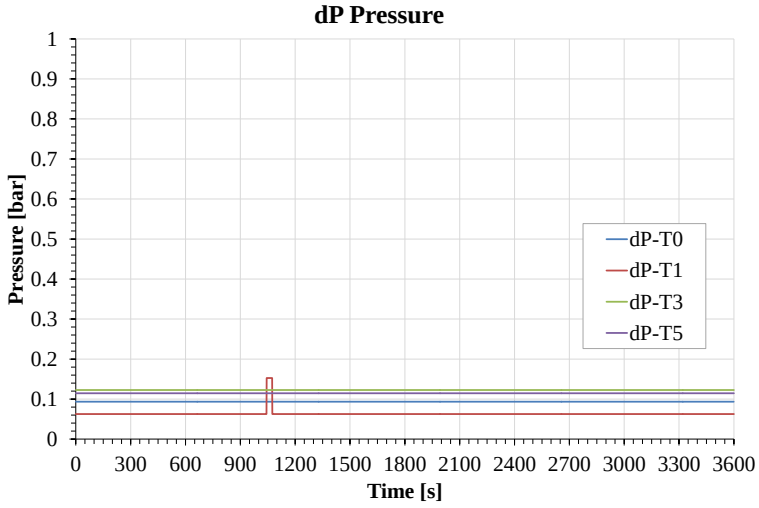

Fig. 5-29 – Pressure drops along the bayonet tubes during the MY-Test2

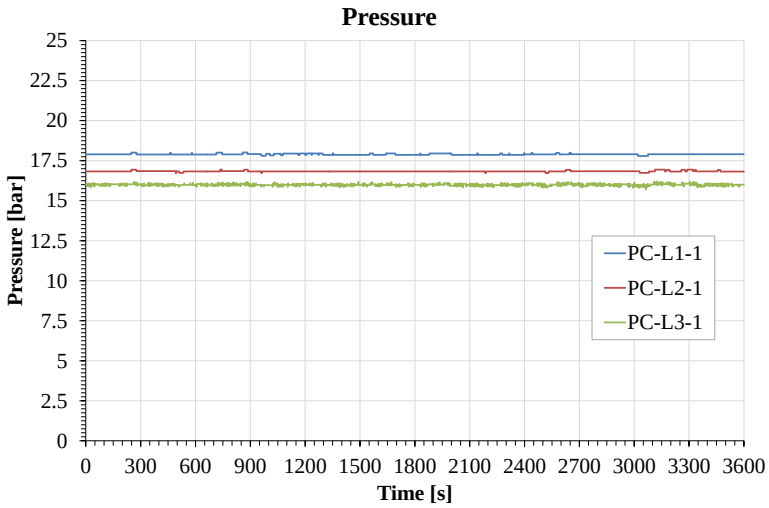

Fig. 5-30 – Pressure along the secondary loop during the MY-Test2

5.2.5 MY-TEST3

In the MY-Test3 the argon injection is managed in order to increase the LBE mass flow rate from 30 kg/s of the Test Reference to ~39 kg/s (see Fig. 5-31). This last value of LBE mass flow rate has been obtained setting the argon flow rate injected at 3 Nl/s. The other parameters (FPS power and water conditions) are set as the Test Reference. The pressure of the helium line in the AISI316L powder gap has been maintained at 7.0 bar. The test was ended after 1 h of steady-state.

Fig. 5-32 reports the inlet and outlet temperature in the FPS. It can be noticed that the ΔT in this case is lower than the Test Reference, due to the higher LBE mass flow rate. The inlet and outlet temperatures are ~222°C and ~237°C respectively, with a ΔT of about 15°C. The same situation can be seen in the LBE side of the SG (see Fig. 5-33), where the inlet and outlet temperatures are ~235°C and 222°C respectively. The result of this condition can be found in a slightly higher average temperature respect to the Test Reference in the lower part of the pool (between 6000 mm and 7200 mm), as reported in Fig. 5-34, which shows the axial thermal stratification. The power removed by HERO during the test is about 70 kW.

Concerning the secondary loop, the water flow rate in the seven BTs is reported in Fig. 5-35, which shows also for this test a lower flow rate in Tube 6. The temperature at the inlet section of the BTs is maintained constant by the heater at about 198°C, while the outlet temperature is ~202°C (Fig. 5-36, corresponding to the T_{sat} at 16 bar.

Finally, the pressure drops along the BTs (see Fig. 5-37) are about 0.75 bar, very similar to the pressure drops of the Test Reference, such as the pressure along the entire water loop (see Fig. 5-38).

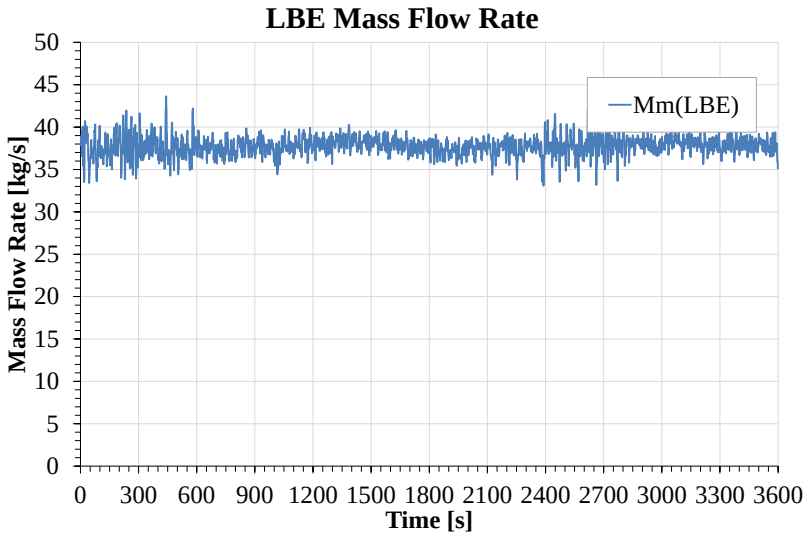

Fig. 5-31 – LBE Mass Flow Rate measured by VFM during the MY-TEST3

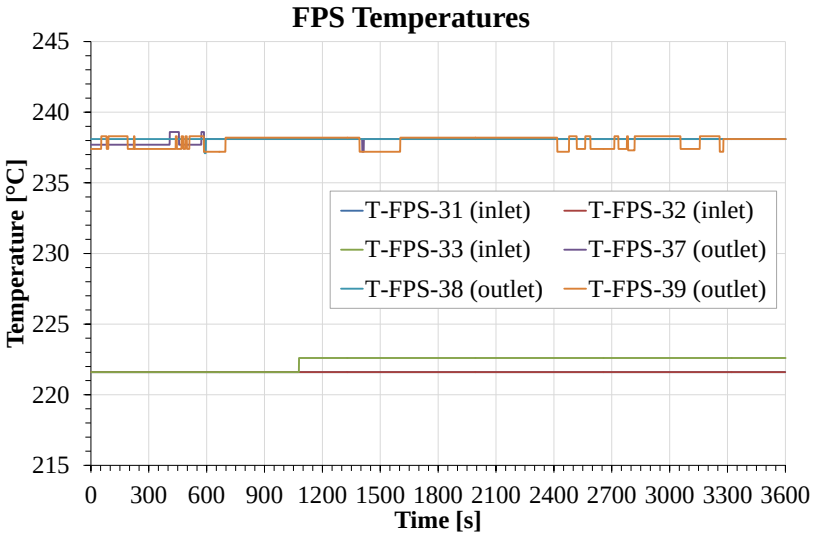

Fig. 5-32 – Inlet and Outlet Temperatures along the FPS during the MY-TEST3

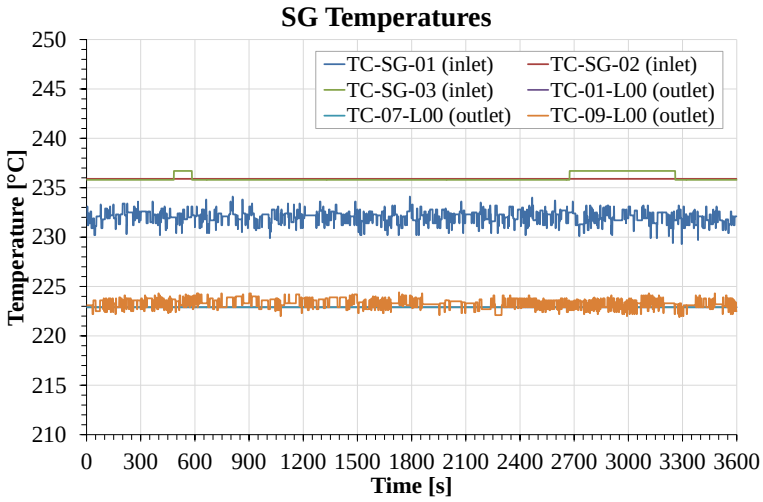

Fig. 5-33 – Inlet and Outlet Temperature along the SGBT Shell Side during the MY-TEST3

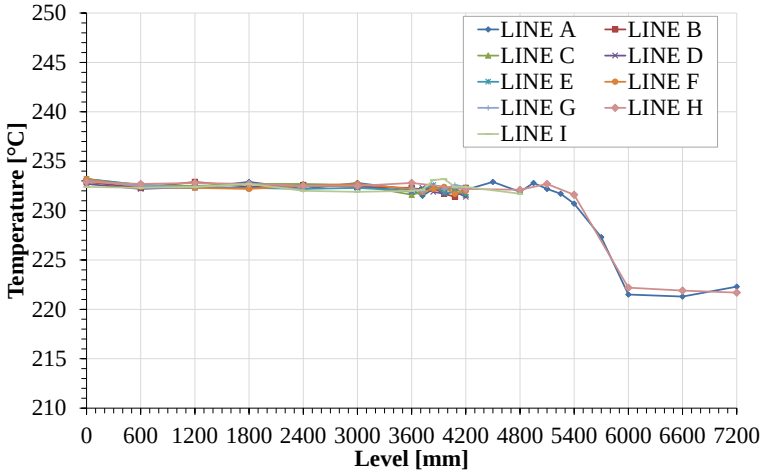

Fig. 5-34 – Axial profile of the temperature inside the S100 vessel during the MY-TEST3

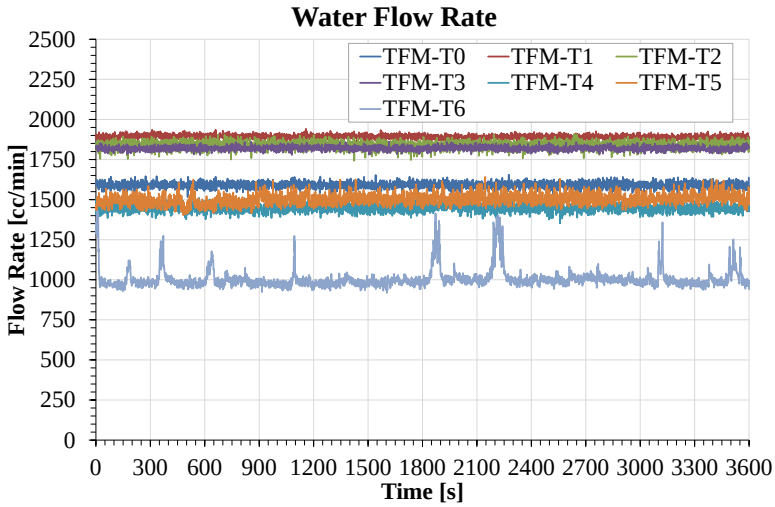

Fig. 5-35 – Water Mass Flow Rate measured by turbine flow meters during the MY-TEST3

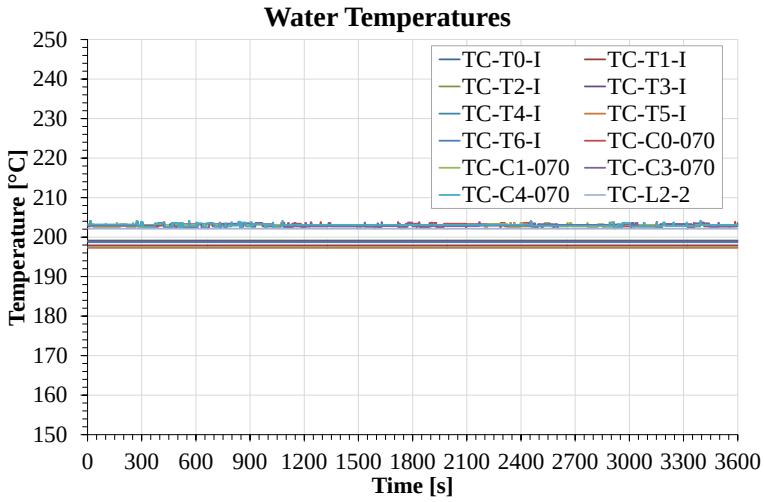

Fig. 5-36 – Water Temperatures at the inlet and outlet of the SGBT during the MY-TEST3

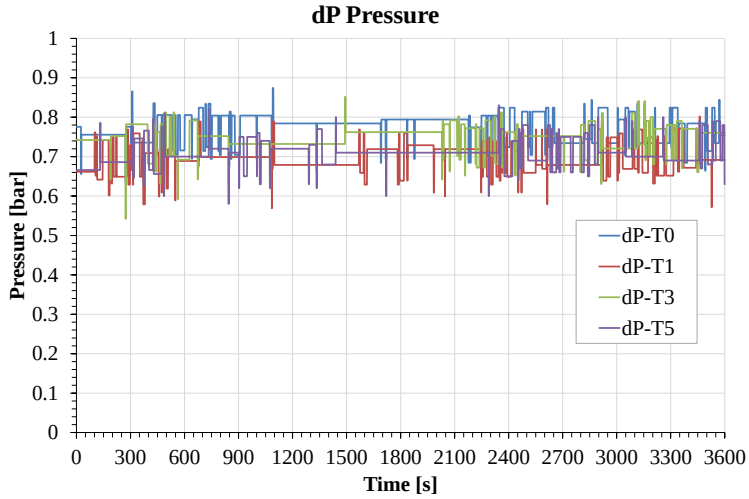

Fig. 5-37 – Pressure drops along the bayonet tubes during the MY-TEST3

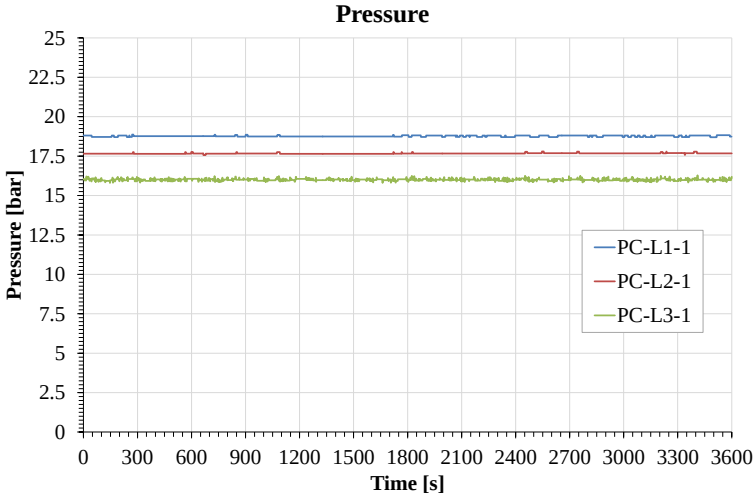

Fig. 5-38 – Pressure along the secondary loop during the MY-TEST3

5.2.6 MY-TEST4

The MY-Test4 is characterized by a low argon flow rate injected (set at 0.5 Nl/s) in order to reduce the LBE mass flow rate from 30 kg/s of the Test Reference to ~20 kg/s (see Fig. 5-39). The other parameters are maintained the same as TestRef. The power of the FPS has been set at 90 kW, obtaining a LBE inlet temperature in the SG of about 244°C, with few degrees exceeding the target value of 235°C foreseen in the test specifications.

In the secondary loop, the water mass flow rate has been maintained at ~160 g/s, the water temperature at the heater outlet has been set at 202°C, achieving a SG water inlet temperature of about 198°C, and the SG inlet pressure at~16.3 bar. The pressure of the helium line in the AISI316L powder gap has been maintained at 8.0 bar. The test was ended after 50 minutes of steady-state.

Fig. 5-40, Fig. 5-41 and Fig. 5-42 show the temperatures in the primary loop at the inlet and outlet sections of the FPS, the SG and inside the pool, respectively. In particular, the LBE temperature achieved at the outlet section of the FPS in this test is close to 248°C, while the LBE temperature at the SG inlet is ~244°C, with a temperature decrease along the fitting volume and riser of about 4°C. The power removed by HERO during this test, applying the thermal balance equation, is about 75 kW, with a LBE temperature at the outlet section of ~219°C. The axial thermal stratification in the pool (see Fig. 5-42) occurs between 5000 mm and 6000 mm with a temperature range comprised between ~239°C and ~218°C.

Fig. 5-43, Fig. 5-44, Fig. 5-45 and Fig. 5-46 show the parameters monitored in the secondary loop. From Fig. 5-43 is possible to see that also in this test a uniform distribution of the water flow rate among seven tubes from Tube 0 to Tube 5, while the flow rate passing in Tube 6 is lower of about 50% respect to the other 6 tubes. Fig. 5-44 reports the BTs inlet and outlet temperatures of ~198°C and ~202°C respectively, showing the saturation conditions at the BTs outlet. The pressure drops (see Fig. 5-45) along the BTs are about 0.65 bar, slightly lower than the Test Reference. The pressure along the loop is reported in Fig. 5-46.

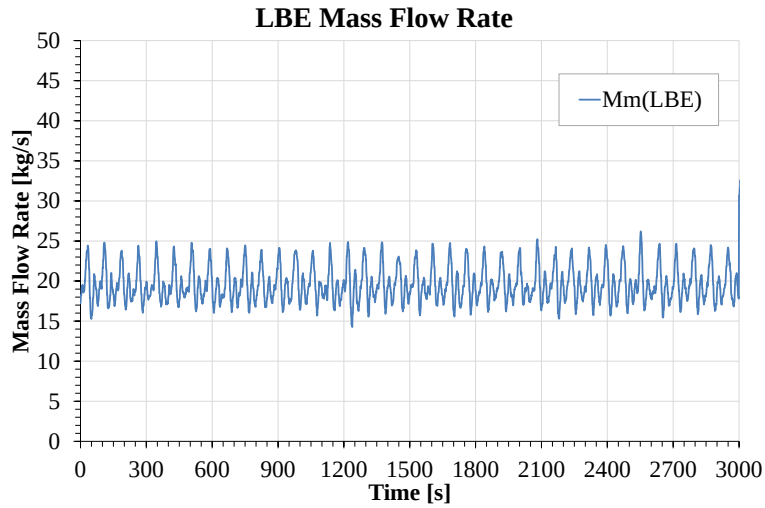

Fig. 5-39 – LBE Mass Flow Rate measured by VFM during the MY-Test4

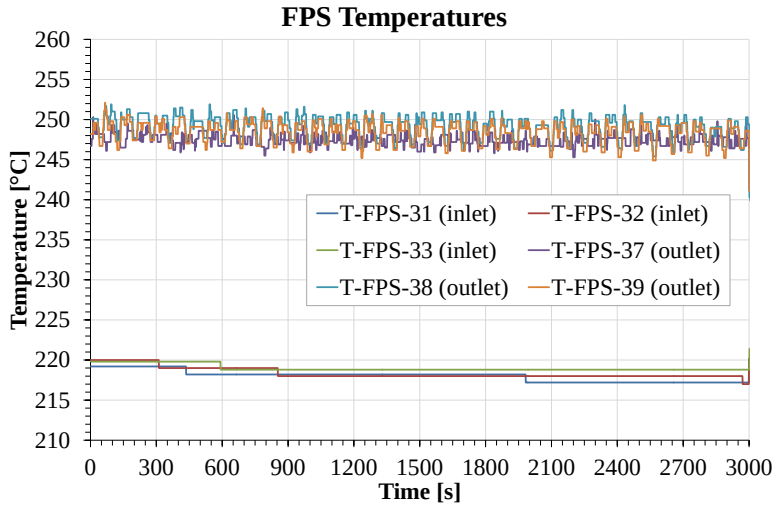

Fig. 5-40 – Inlet and Outlet Temperatures along the FPS during the MY-Test4

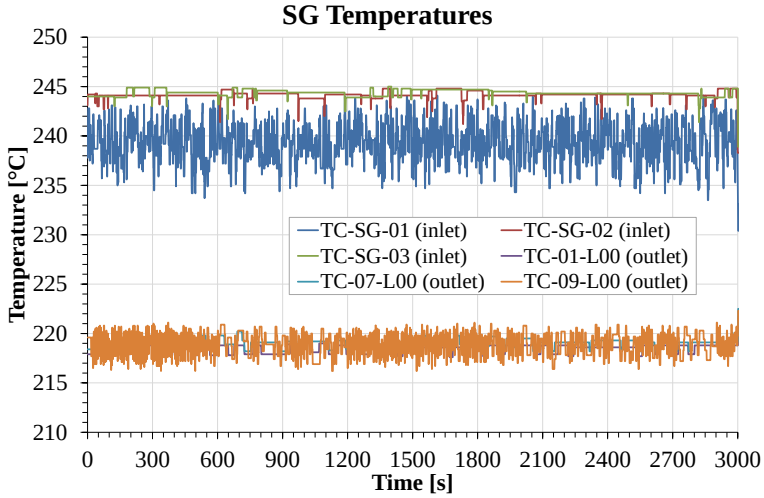

Fig. 5-41 – Inlet and Outlet Temperature along the SGBT Shell Side during the MY-Test4

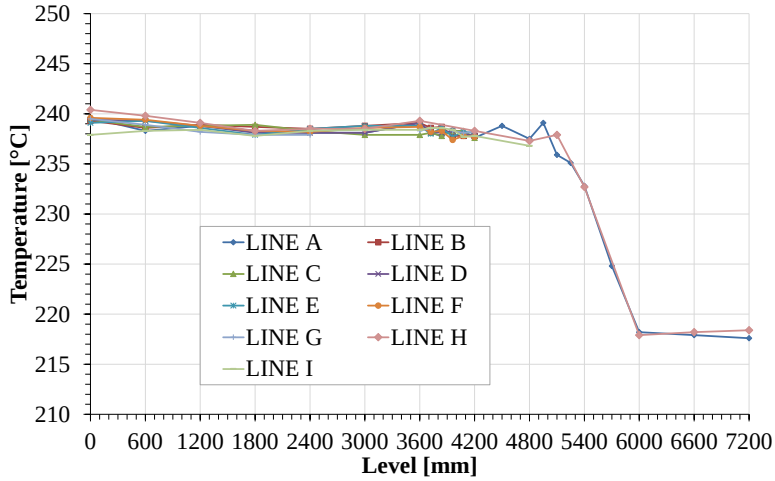

Fig. 5-42 – Axial profile of the temperature inside the S100 vessel during the MY-Test4

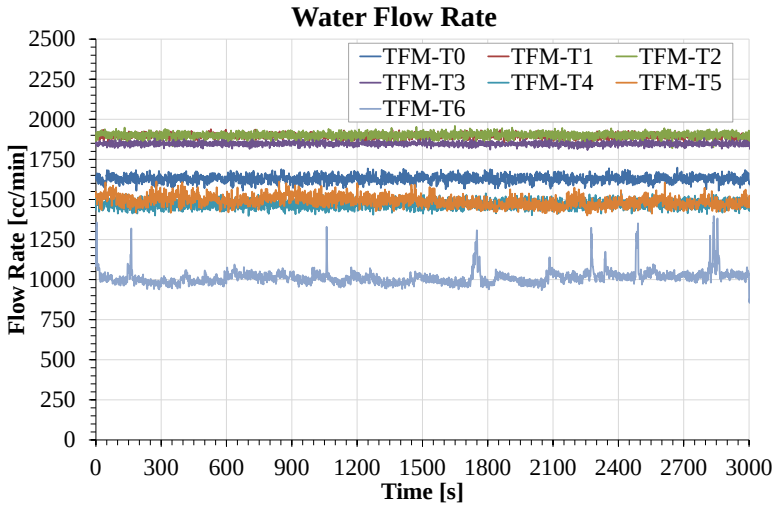

Fig. 5-43 – Water Mass Flow Rate measured by turbine flow meters during the MY-Test4

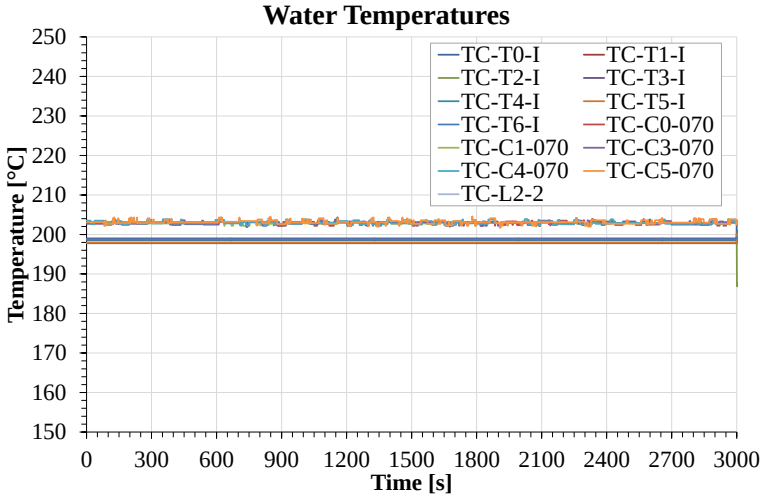

Fig. 5-44 – Water Temperatures at the inlet and outlet of the SGBT during the MY-Test4

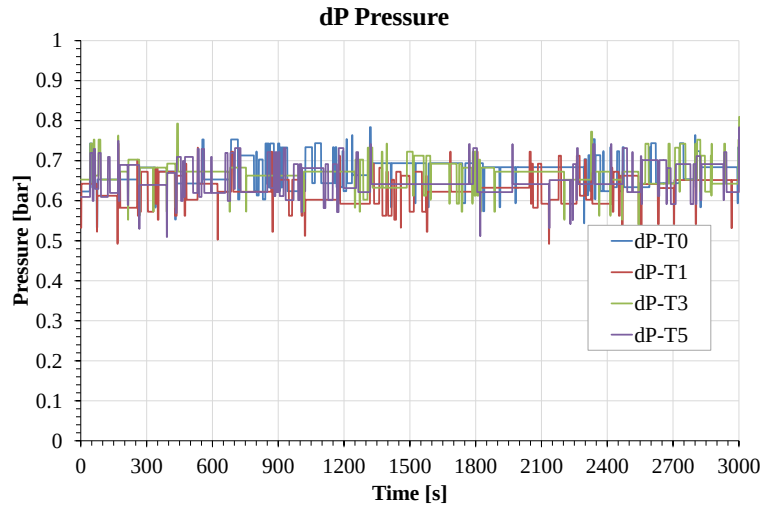

Fig. 5-45 – Pressure drops along the bayonet tubes during the MY-Test4

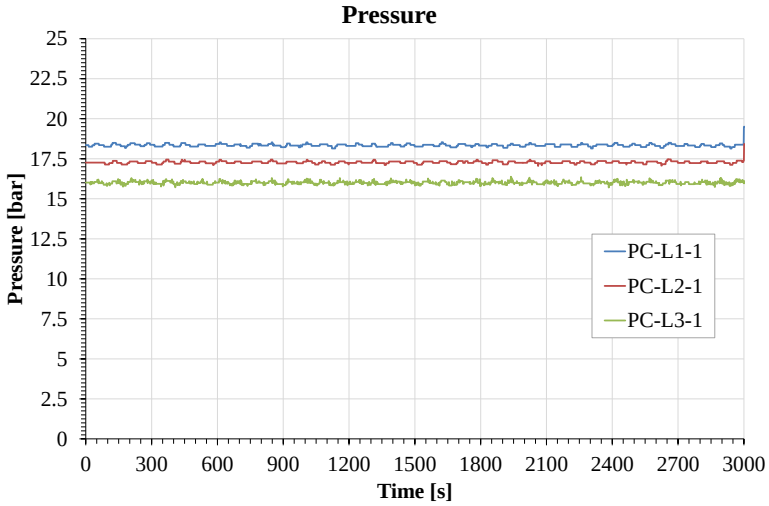

Fig. 5-46 – Pressure along the secondary loop during the MY-Test4

5.2.7 MY-TEST5

The MY-Test5 is the first test in which the parameters of the feedwater are changed in order to evaluate the influence of the secondary loop transients on the entire system. In particular, for this test the water inlet temperature has been increased from the 198°C of the Test Reference to 218°C. Accordingly with the increase of the temperature, the working pressure along the loop has been set to a higher value (23 bar), in order to assure at the inlet sections of the BTs liquid water with few degrees of sub-cooling. The argon flow rate and the water flow rate are maintained the same as the Test Reference, while the power of the FPS has been set at 35 kW in order to maintain a LBE SG inlet temperature of ~235°C. The pressure of the helium line in the AISI316L powder gap has been maintained at 8.0 bar. The test was ended after 1 h of steady-state.

The LBE mass flow rate reached during this test is about 30 kg/s, as reported in Fig. 5-47. Fig. 5-48, Fig. 5-49 and Fig. 5-50 show the temperature in the primary loop at the inlet and outlet of the FPS and the SG, and inside the pool respectively. The LBE temperature at the FPS inlet is about 229°C, while the outlet temperature is ~238°C. The LBE temperature at the SG inlet is ~236°C, with a temperature decrease along the fitting volume and riser of about 2°C. The power removed by HERO during this test, applying the thermal balance equation, is about 25 kW, with a LBE temperature at the outlet section of ~230°C. The low power removed by HERO in these conditions is due to the small temperature difference between the fluids of the primary and the secondary loop. This affects also the axial thermal stratification in the pool which is less pronounced, passing from a temperature of 234°C to 229°C between 5000 mm and 6000 mm.

The parameters monitored in the secondary loop are reported in Fig. 5-51, Fig. 5-52, Fig. 5-53 and Fig. 5-54. The water flow rates in the seven BTs have the same trends already seen in the previous tests. (see Fig. 5-51), while the water inlet and outlet temperature (see Fig. 5-52) are about 219°C, showing also for this test the saturation conditions at the BTs outlet. As already highlighted for the Test Reference the low water outlet temperature of TC-T1-I reported in Fig. 5-52 is due to a malfunction of its acquisition channel of the DACS and it is not related to the instrument. The pressure drops (see Fig. 5-53) in the BTs are about 0.15 bar, due to the low power removed and thus the small steam mass fraction produced. Finally, Fig. 5-54 shows the pressure along the water loop, passing from ~26 bar upstream the heater to ~23 bar at the steam outlet section.

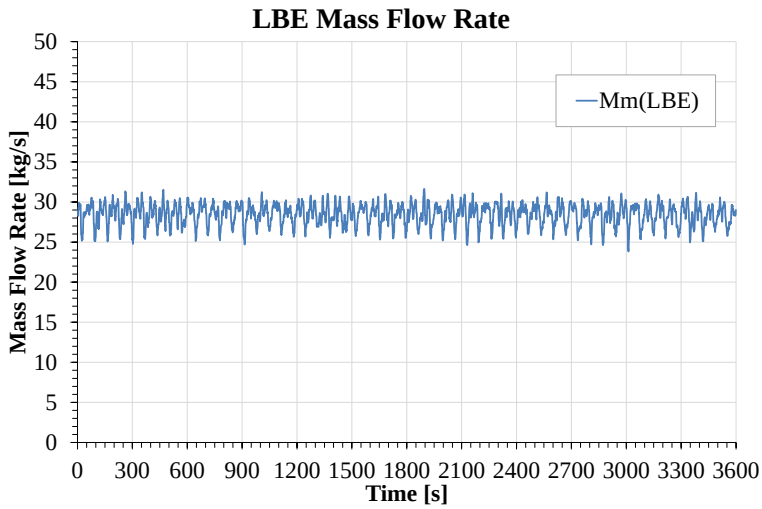

Fig. 5-47 – LBE Mass Flow Rate measured by VFM during the MY-Test5

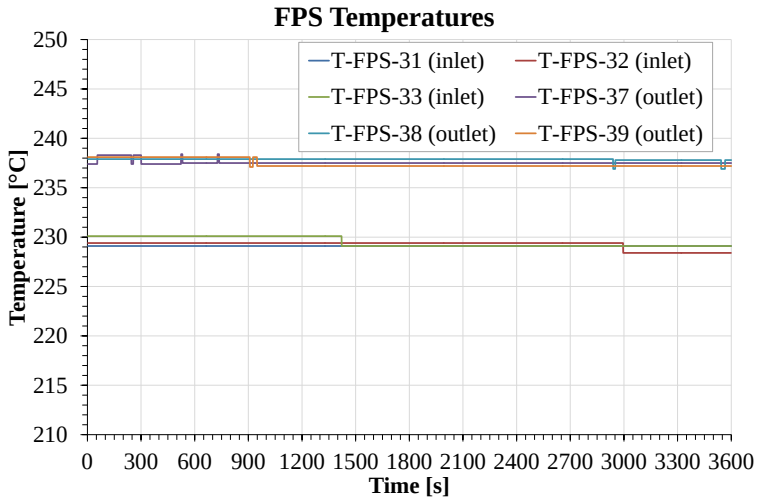

Fig. 5-48 – Inlet and Outlet Temperatures along the FPS during the MY-Test5

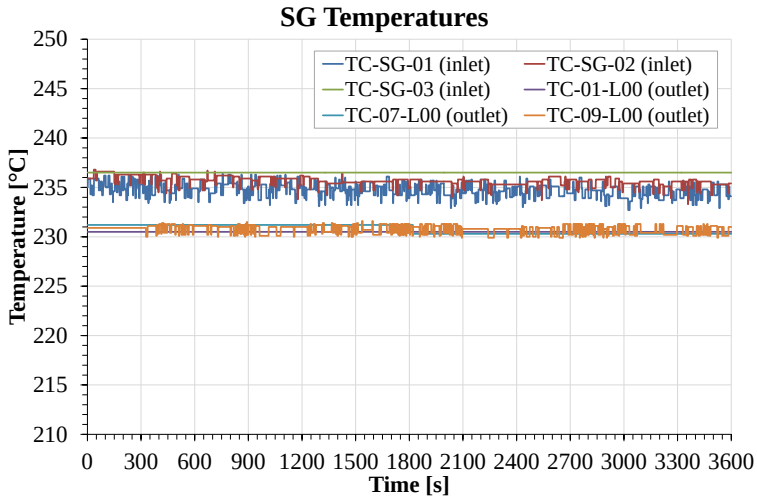

Fig. 5-49 – Inlet and Outlet Temperature along the SGBT Shell Side during the MY-Test5

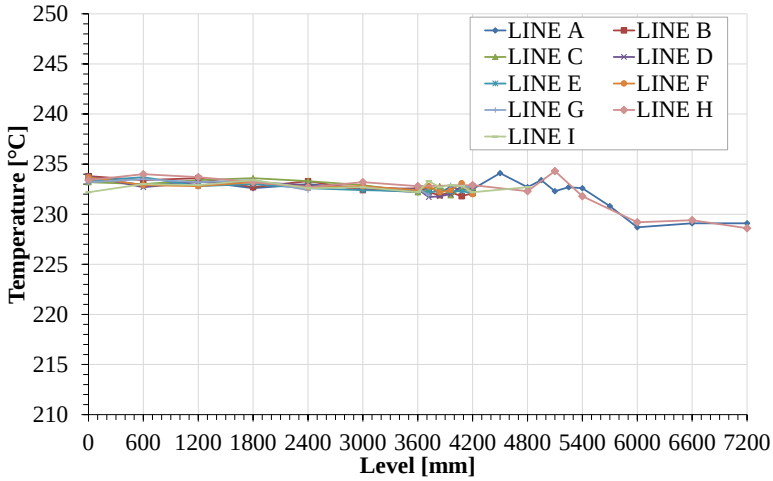

Fig. 5-50 – Axial profile of the temperature inside the S100 vessel during the MY-Test5

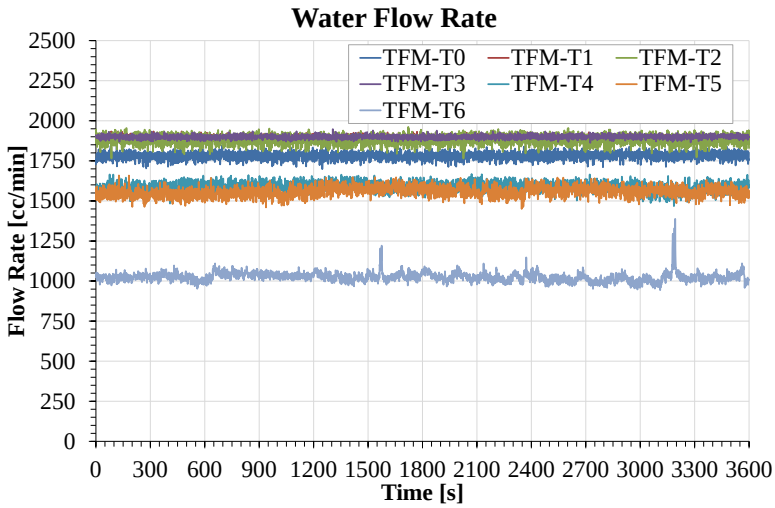

Fig. 5-51 – Water Mass Flow Rate measured by turbine flow meters during the MY-Test5

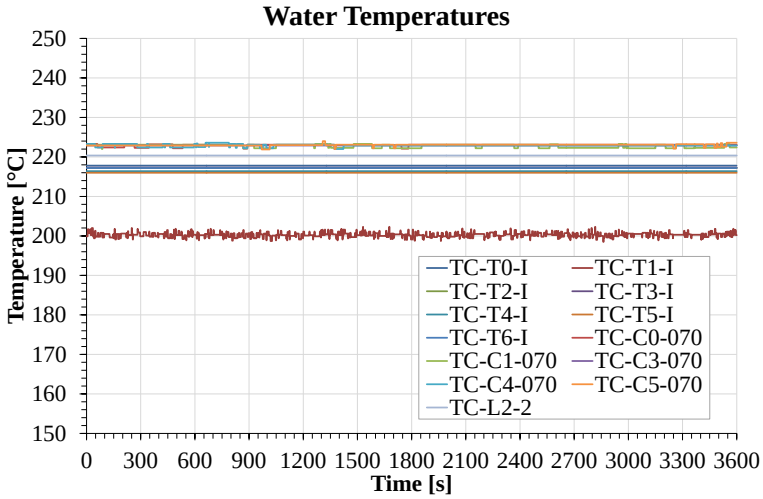

Fig. 5-52 – Water Temperatures at the inlet and outlet of the SGBT during the MY-Test5

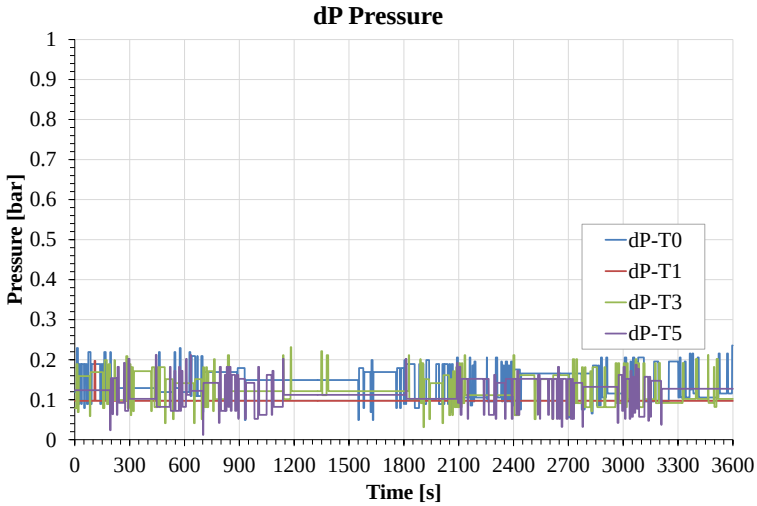

Fig. 5-53 – Pressure drops along the bayonet tubes during the MY-Test5

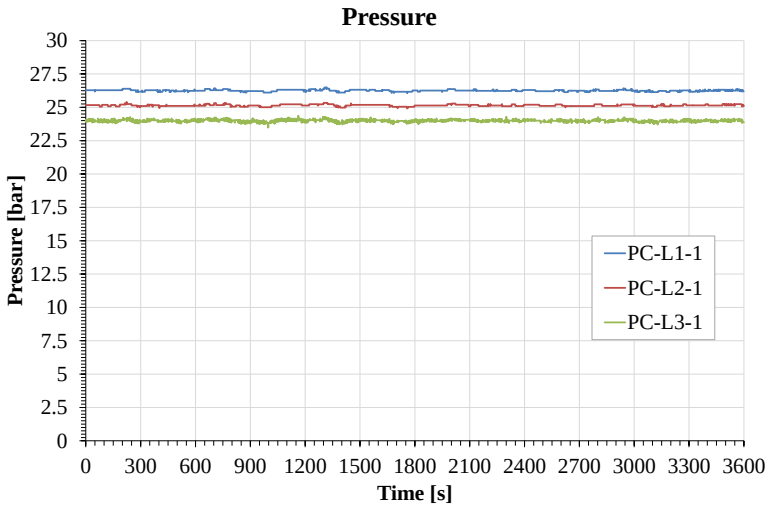

Fig. 5-54 – Pressure along the secondary loop during the MY-Test5

5.2.8 MY-TEST6

In the MY-Test6 the water inlet temperature has been reduced from the 198°C of the Test Reference to 178°C, while the other parameters (FPS power, argon flow rate and water conditions) are set as the Test Reference. The pressure of the helium line in the AISI316L powder gap has been maintained at 7.5 bar. The test was ended after 1 h of steady-state.

The LBE mass flow rate reached during this test is about 30 kg/s, as reported in Fig. 5-55. Fig. 5-56 reports the inlet and outlet temperature in the FPS, corresponding to 219°C and 239°C with a ΔT of about 20°C, Concerning the SG (see Fig. 5-57), in the LBE side the inlet temperature reached is ~236°C (~3°C lower than the FPS outlet) and the outlet temperature is ~220°C. The calculated power removed by HERO during the test is about 75 kW. The axial thermal stratification in the pool (see Fig. 5-58) occurs between 5000 mm and 6000 mm with a temperature range comprised between ~234°C and ~219°C.

Concerning the secondary loop, the water flow rate in the seven BTs is reported in Fig. 5-59, which shows also for this test a lower flow rate in Tube 6. The temperature at the inlet section of the BTs is maintained constant by the heater at about 178°C, while the outlet temperature is ~202°C (Fig. 5-60), corresponding to the T_{sat} at 16 bar.

Finally, the pressure drops along the BTs (see Fig. 5-61) are about 0.5 bar, lower than the pressure drops of the Test Reference, due to the higher water sub-cooling at the BTs inlet with the consequent lower steam mass fraction produced. The pressure along the entire water loop is reported in Fig. 5-62.

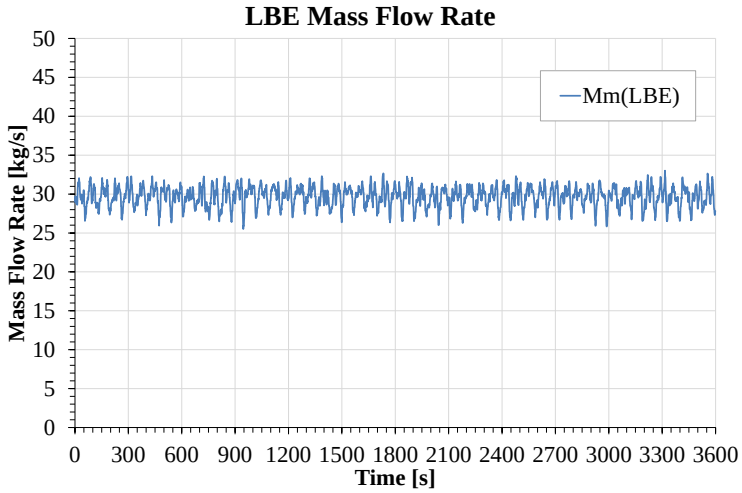

Fig. 5-55 – LBE Mass Flow Rate measured by VFM during the MY-Test6

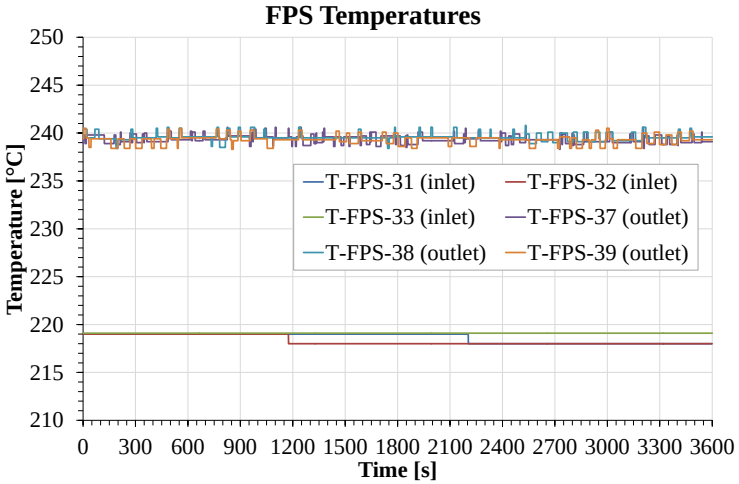

Fig. 5-56 – Inlet and Outlet Temperatures along the FPS during the MY-Test6

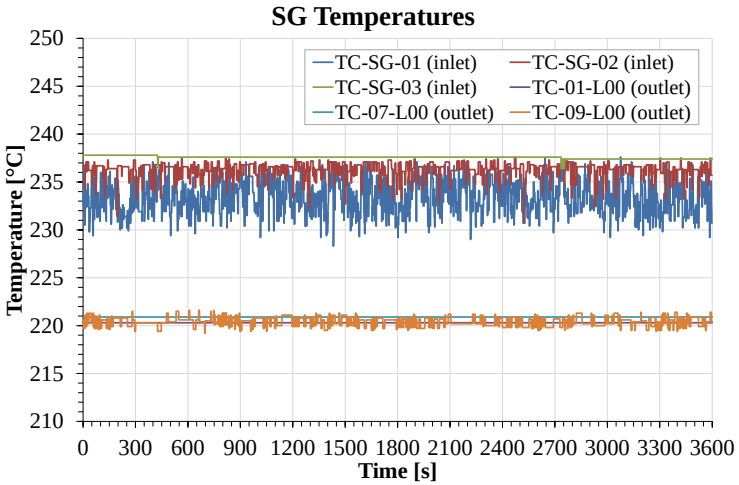

Fig. 5-57 – Inlet and Outlet Temperature along the SGBT Shell Side during the MY-Test6

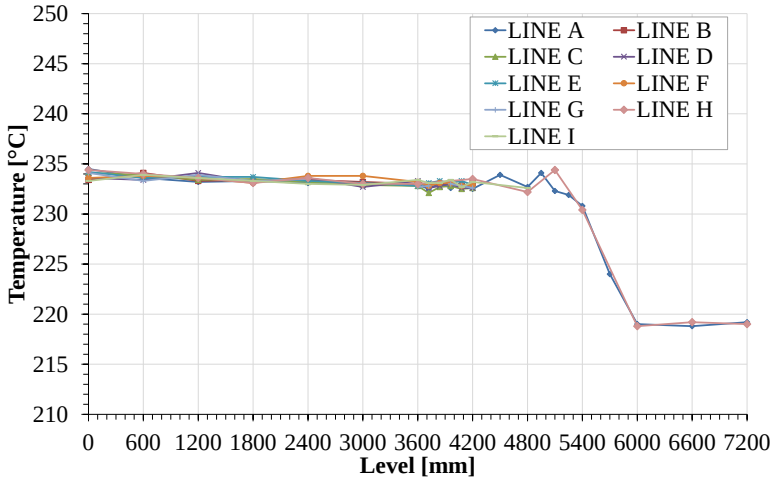

Fig. 5-58 – Axial profile of the temperature inside the S100 vessel during the MY-Test6

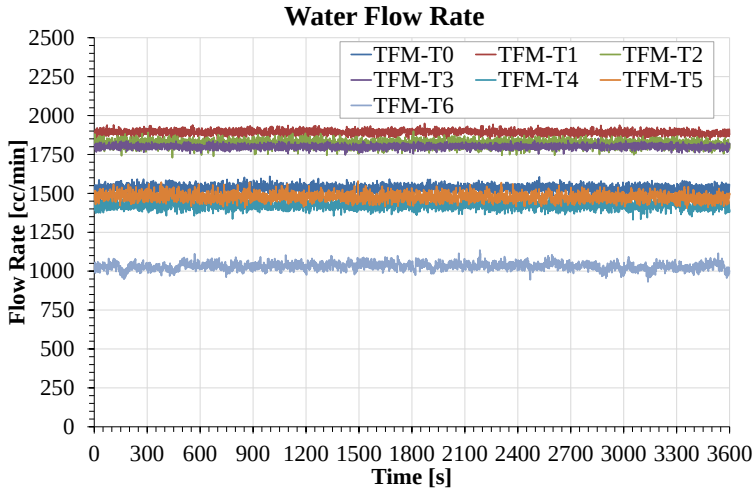

Fig. 5-59 – Water Mass Flow Rate measured by turbine flow meters during the MY-Test6

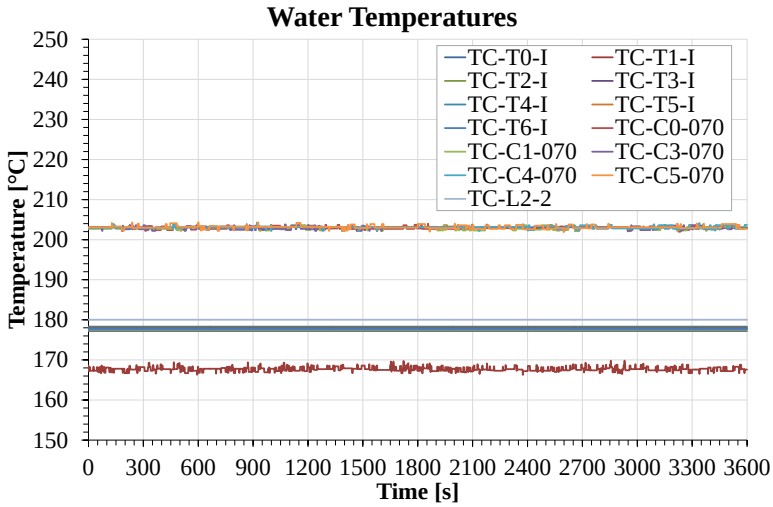

Fig. 5-60 – Water Temperatures at the inlet and outlet of the SGBT during the MY-Test6

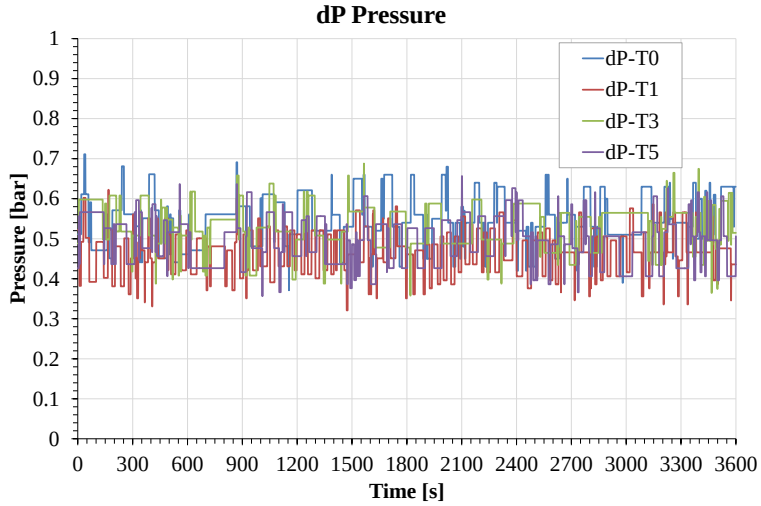

Fig. 5-61 – Pressure drops along the bayonet tubes during the MY-Test6

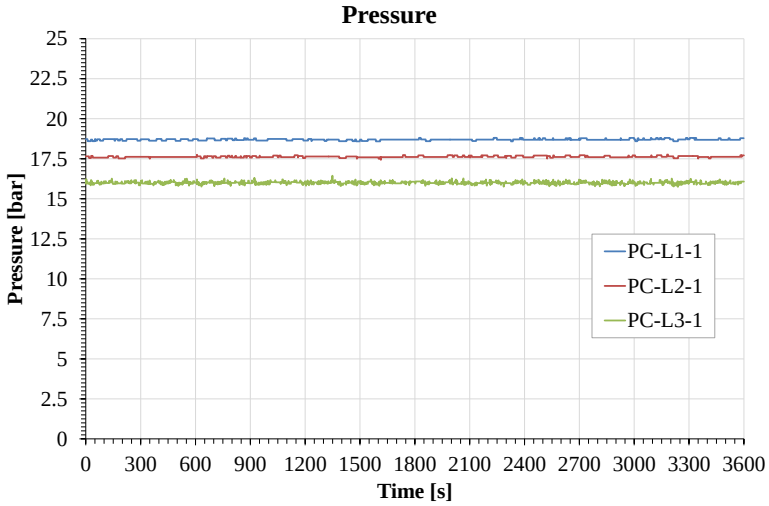

Fig. 5-62 – Pressure along the secondary loop during the MY-Test6

5.2.9 MY-TEST7

In the MY-Test7 the volumetric pump of the secondary loop is managed in order to increase the water mass flow rate from 0.160 kg/s of the Test Reference to 0.210 kg/s. During the test, all the other parameters are set as the Test Reference. The pressure of the helium line in the AISI316L powder gap has been maintained at 8.0 bar. The test was ended after 1 h of steady-state. The LBE mass flow rate reached during this test is about 30 kg/s, as reported in Fig. 5-63, with an argon flow rate set to 1 Nl/s.

Fig. 5-64, Fig. 5-65 and Fig. 5-66 show the temperature trends in the primary loop along the FPS, the SG and inside the pool respectively. In particular, the LBE temperature at the FPS inlet is ~220°C, while the LBE temperature achieved at the outlet section of the FPS in

this test is about 241°C, with a subsequent temperature decrease along the fitting volume and riser up to the SG inlet of about 3°C (T inlet SG ~238°C). The power removed by HERO, applying the thermal balance equation, is about 75 kW, with a LBE temperature at the outlet section of ~222°C. The stratification in the pool (see Fig. 5-66) occurs between 5000 mm and 6000 mm with a temperature range comprised between ~235°C and ~220°C.

The parameters monitored in the secondary loop are reported in Fig. 5-67, Fig. 5-68, Fig. 5-69, Fig. 5-70 and Fig. 69 shows the water flow rate in the seven BTs: it is possible to notice that also in the case with a higher water flow rate, the water flow is uniformly distributed among the tubes, except for the Tube 6, where the flow rate is still lower of about 50% respect to the other BTs.

Fig. 5-68 reports the BTs inlet and outlet temperatures, which are close to the saturation temperature of ~202°C. As already highlighted for the Test Reference and Test #5, the TC-T1-I temperature is affected by an error due to a malfunction of its acquisition channel of the DACS.

The pressure drops (see Fig. 5-69) in the BTs are about 1.25 bar, higher than the 0.8 bar of Test Reference, due to the higher water mass flow rate. For the same reason, also the pressure drops along the water loop are higher than the other tests (see Fig. 5-70), passing from ~22 bar upstream the heater to ~16 bar at the steam outlet section.

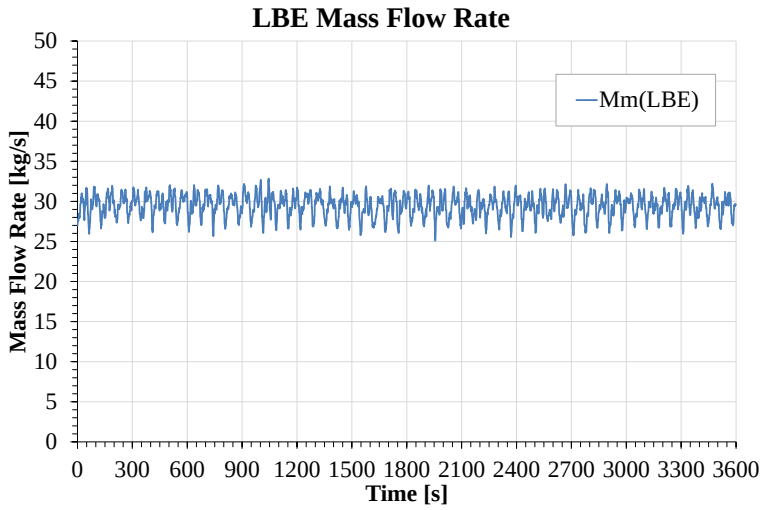

Fig. 5-63 – LBE Mass Flow Rate measured by VFM during the MY-Test7

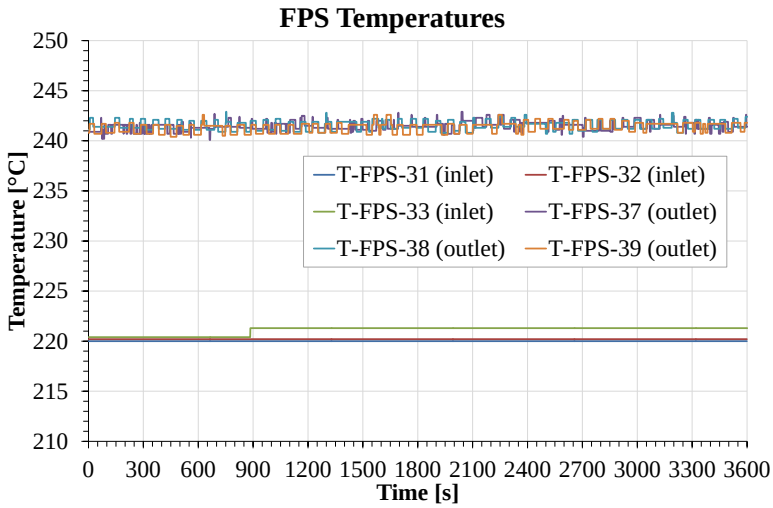

Fig. 5-64 – Inlet and Outlet Temperatures along the FPS during the MY-Test7

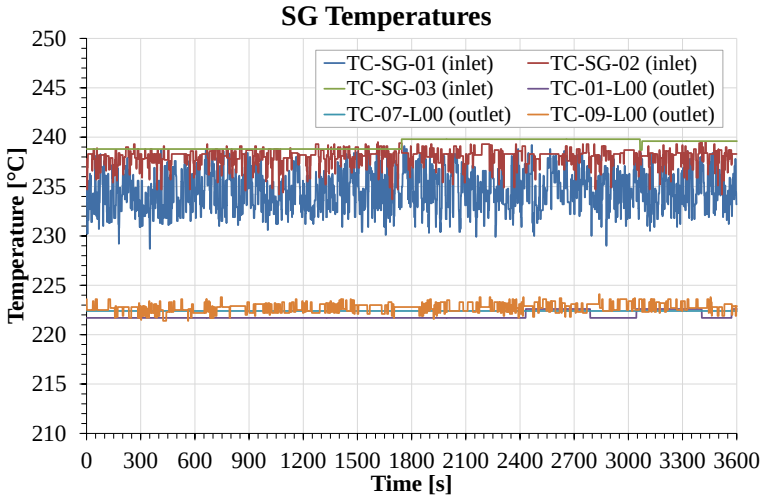

Fig. 5-65 – Inlet and Outlet Temperature along the SGBT Shell Side during the MY-Test7

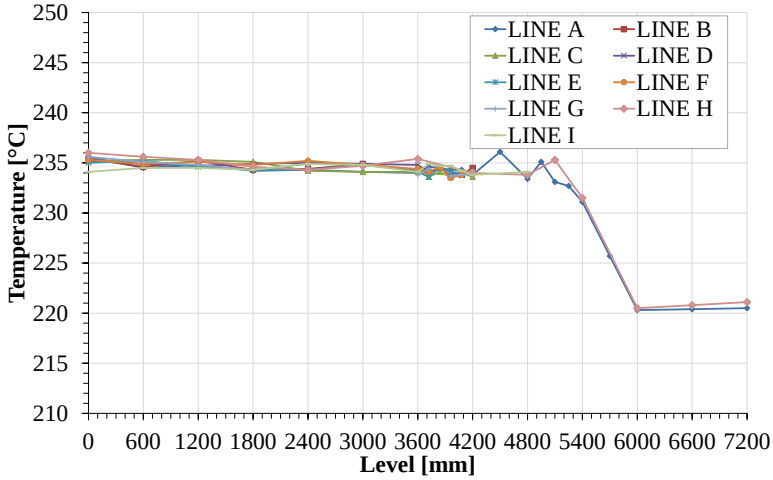

Fig. 5-66 – Axial profile of the temperature inside the S100 vessel during the MY-Test7

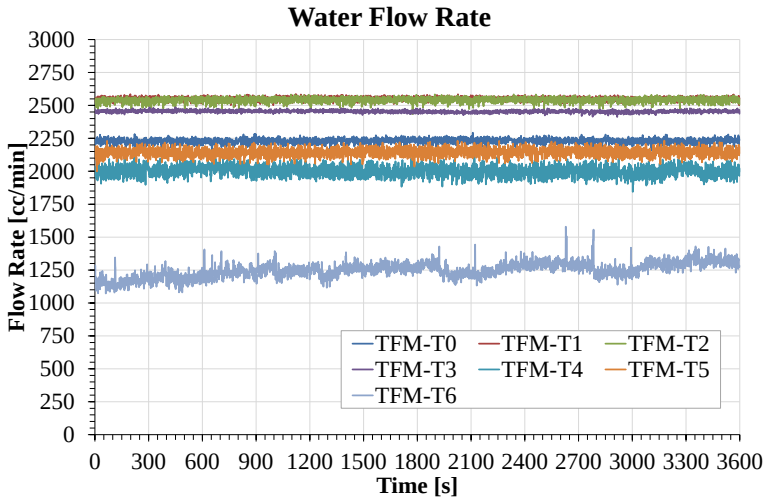

Fig. 5-67 – Water Mass Flow Rate measured by turbine flow meters during the MY-Test7

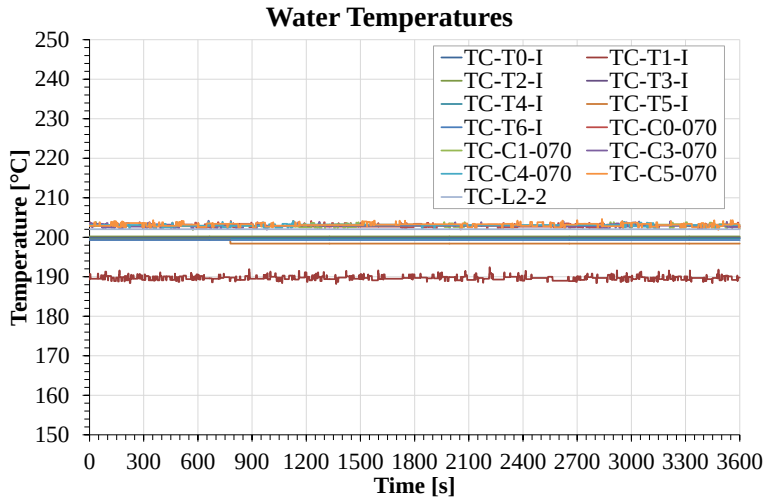

Fig. 5-68 – Water Temperatures at the inlet and outlet of the SGBT during the MY-Test7

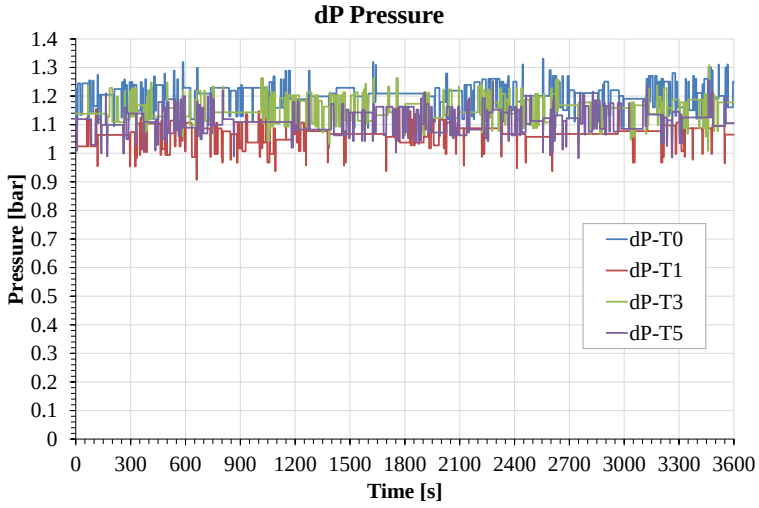

Fig. 5-69 – Pressure drops along the bayonet tubes during the MY-Test7

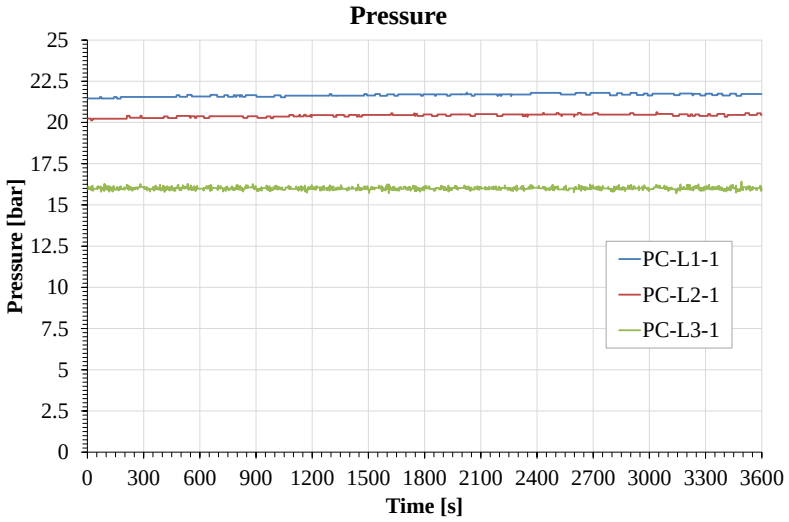

Fig. 5-70 – Pressure along the secondary loop during the MY-Test7

5.2.10 MY-TEST8

In the MY-Test8 the volumetric pump of the secondary loop is managed in order to reduce the water mass flow rate from 0.160 kg/s of the Test Reference to 0.120 kg/s. During the test, all the other parameters are set as the Test Reference. The pressure of the helium line in the AISI316L powder gap has been maintained at 8.0 bar. The test was ended after 1 h of steady-state.

The LBE mass flow rate reached during this test is about 30 kg/s, as reported in Fig. 5-71. Fig. 5-72 reports the inlet and outlet temperature in the FPS, corresponding to 221°C and 241°C respectively with a ΔT of about 20°C, Concerning the SG (see Fig. 5-73), in the LBE side the inlet temperature reached is ~237°C (~4°C lower than the FPS outlet) and the outlet temperature is ~222°C. The calculated power removed by HERO during the test is about 80 kW. The axial thermal stratification in the pool (see Fig. 5-74) occurs between 5000 mm and 6000 mm with a temperature range comprised between ~235°C and ~220°C.

In the secondary loop, the water flow rate in the seven BTs is reported in Fig. 5-75, which shows good stability and distribution also at low water mass flow rate. As in the previous tests, the water flow rate in Tube 6 is still lower of about 50% respect to the other BTs. Fig. 5-76 reports the BTs inlet and outlet temperatures, which are close to the saturation temperature of ~202°C. The pressure drops (see Fig. 5-77) in the BTs are about 0.5 bar, lower than the 0.8 bar of Test Reference, due to the lower water mass flow rate. For the same reason, also the pressure drops along the water loop are lower than the other tests (see Fig. 5-78).

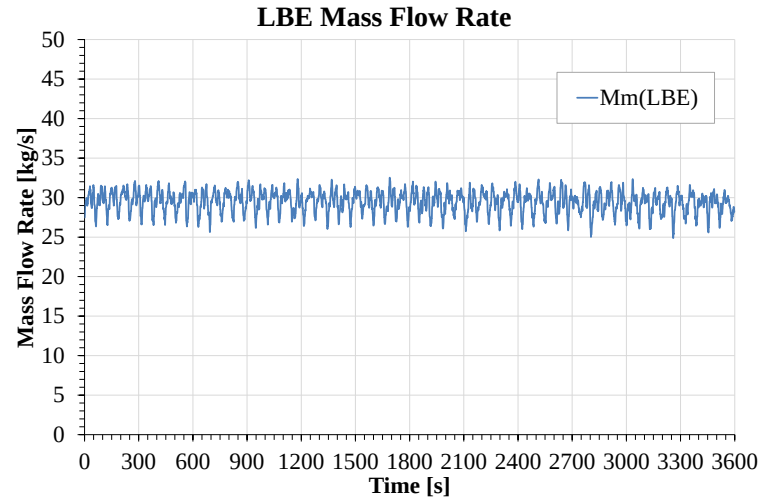

Fig. 5-71 – LBE Mass Flow Rate measured by VFM during the MY-Test8

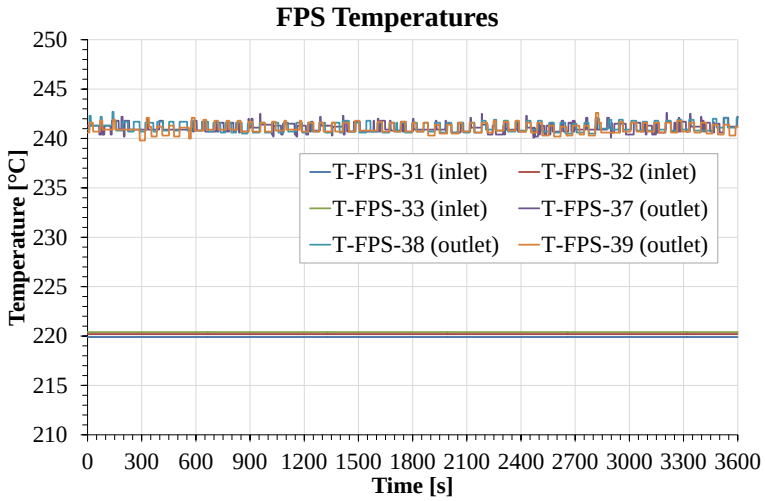

Fig. 5-72 – Inlet and Outlet Temperatures along the FPS during the MY-Test8

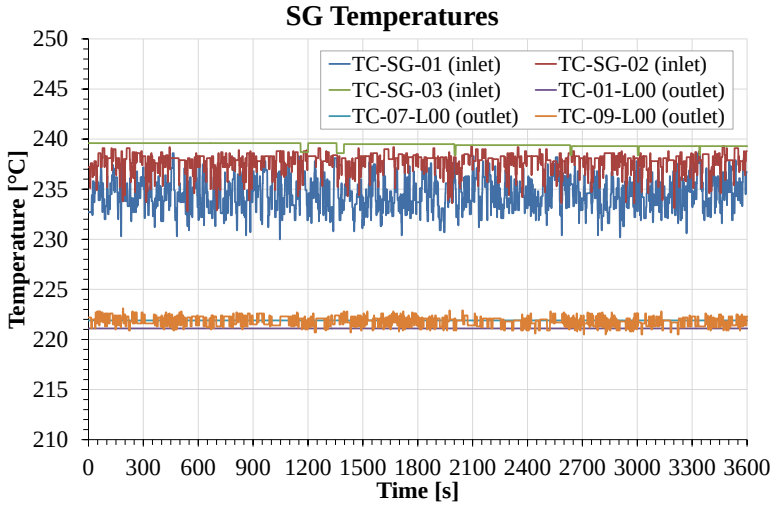

Fig. 5-73 – Inlet and Outlet Temperature along the SGBT Shell Side during the MY-Test8

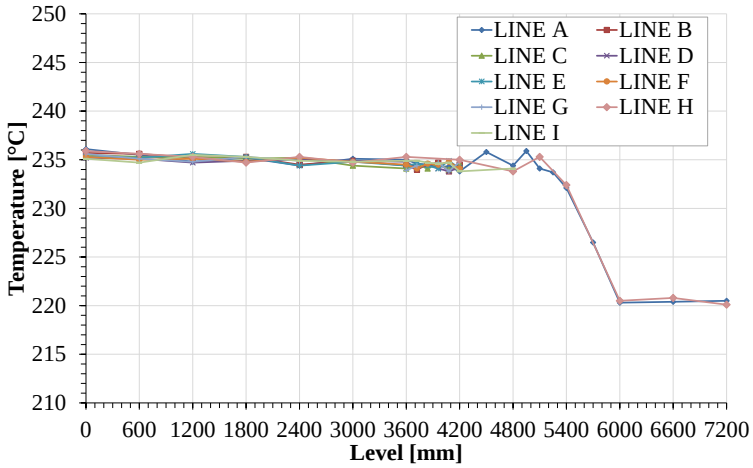

Fig. 5-74 – Axial profile of the temperature inside the S100 vessel during the MY-Test8

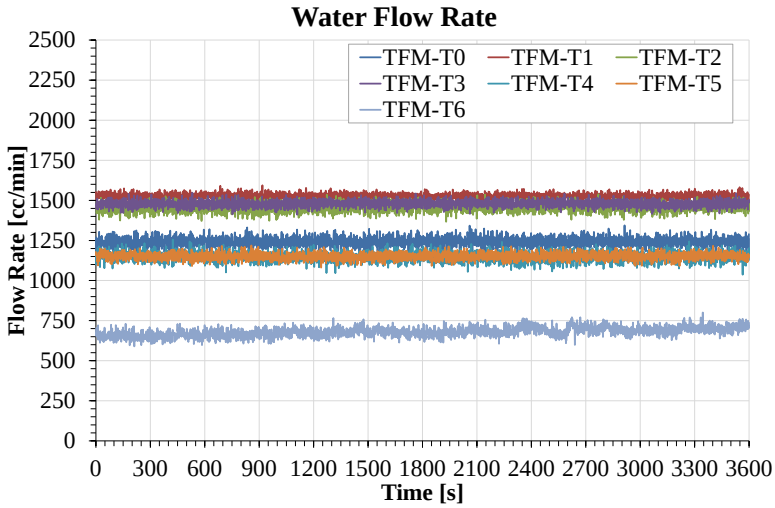

Fig. 5-75 – Water Mass Flow Rate measured by turbine flow meters during the MY-Test8

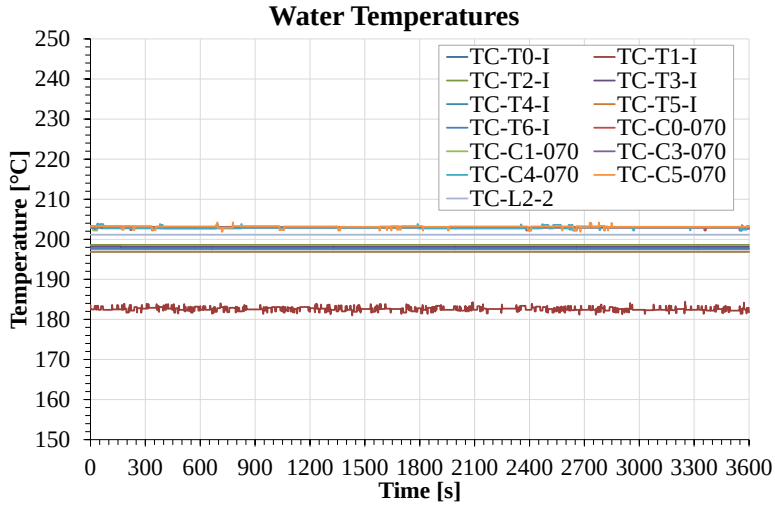

Fig. 5-76 – Water Temperatures at the inlet and outlet of the SGBT during the MY-Test8

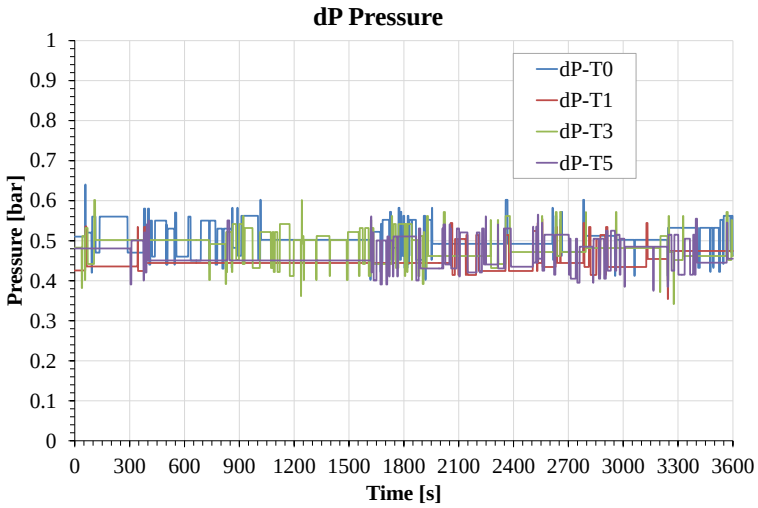

Fig. 5-77 – Pressure drops along the bayonet tubes during the MY-Test8

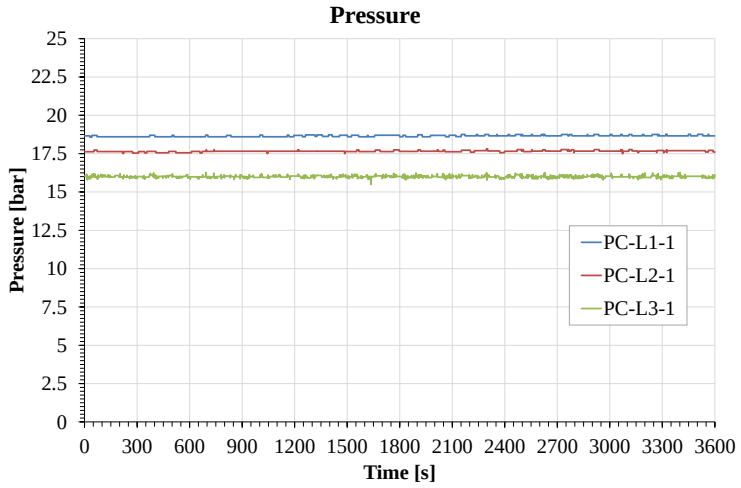

Fig. 5-78 – Pressure along the secondary loop during the MY-Test8

6 SYSTEM THERMAL-HYDRAULIC CODE BENCHMARK ACTIVITY

6.1 FRAMEWORK OF THE ACTIVITY

The present section describes numerical activities of Sapienza University of Rome in the Benchmark exercise intended for SYS-TH codes and CFD/SYS-TH codes validation based on experimental tests performed at ENEA Brasimone R.C. on the NACIE-UP facility. The Benchmark exercise is set in the framework of the WP4 and WP5 of the EU H2020 SESAME project. In particular, WP4 provided the necessary experimental reference data, where WP5 has dealt with the development and validation on integral system simulation approaches comprising improvement and validation of existing SYS-TH codes and development, improvement and validation of multi-scale approaches in which SYS-TH codes coupled to CFD codes.

A dedicated task (5.4) of the WP5 aims to execute a numerical benchmark among the well-known SYS-TH codes RELAP5, ATHLET and CATHARE, in order to evaluate their capabilities to reproduce the main thermal-hydraulic phenomena occurring in the LBE pool-type facility NACIE-UP [39]. The proposed activity contributes to the validation of these codes for HLM reactors, through the comparison among the different approaches adopted by the benchmark participants (UniRoma1, UniPi, ENEA, GRS) and by comparing the numerical results with the data that are available from the experiments with the NACIE-UP facility. For these purposes, the three fundamental tests have been proposed as a reference for the numerical exercise, reproducing different transients of power and/or gas lift transition.

6.2 SCOPE OF THE ACTIVITY

The following section reports about the "NAtural CIrculation Experiment UPgrade" (NACIE-UP), an experimental loop-type facility located at the ENEA Brasimone R.C., resulting from an upgrade of the pre-existent loop NACIE. It consists in a rectangular loop cooled by LBE and its purpose is to provide experimental support for the development of technologies based on cooling by liquid metals used in the design and safety assessment of GEN IV/ADS reactors. In particular, the scopes in which the research field is involved, applies to:

- assessment of thermal properties and fluid-dynamics of HLMs;
- characterization of natural circulation flow regime with HLMs;
- characterization of heat transfer in HLM-cooled systems, in particular in rod bundle assemblies and heat exchangers;
- evaluate the effectiveness of a GEC in a HML loop;
- characterization of components, prototypes and instrumentation;
- simulation of several operational and accident transients;
- validation of calculation codes (CFD) and qualification/ validation of SYS-TH codes

The Sapienza University of Rome activity in the NACIE-UP Benchmark is the assessment of fluid dynamic behaviour in heavy liquid metal systems through RELAP5-3D® ver. 4.3.4 system thermal-hydraulic code. In particular the validation is carried out through a series of experimental tests for the evaluation of the code capability to simulate a two-phase system with liquid LBE and gas, both for steady-state conditions and during transients from natural circulation to gas-enhanced circulation and vice-versa.

6.3 THE NACIE-UP FACILITY

The NACIE-UP loop [40] consists of a primary side in which the LBE flows and a secondary side filled with water at 16 bar and thermally coupled with the primary loop through the heat exchanger (the water flows in the shell side of the heat exchanger). A P&ID of the facility is reported in Fig. 6-1. The primary side (see Fig. 6-2) is a rectangular loop consisting of two vertical pipes, working as riser and downcomer, of 2 ½" and about 8 m long, and two horizontal pipes (O.D. 2 ½") 2.4 m long. All the piping is realized in stainless steel AISI 316L. At the end of the riser an expansion tank is connected and it is partially filled with argon as cover gas in order to avoid oxidation and to accommodate the thermal expansion of LBE, while a prototypical wire-spaced FPS is installed in the bottom. The total mass of LBE stored is about 2000 kg. On the other side, a Heat Exchanger (HX) is placed in the upper part of the downcomer. The difference in height between the centre of the heating section and the centre of the heat exchanger is about 5.5 m and is essential for the natural circulation regime. Furthermore, an argon gas injection system is placed in the middle of the riser and which provides the driving force to sustain forced convection in the loop. The entire loop is coated with an insulation material of about 10 cm thickness in order to minimize the heat losses in the external environment.

The facility includes:

- the primary side, with 2 ½" piping, consisting of two vertical pipes, two horizontal pipes and an expansion tank (Fig. 6-2);
- a new FPS (Fig. 6-3), composed of 19 electrically heated pins arranged in a hexagonal geometry, with an active length of 600 mm, for a maximum power of 235 kW;
- a Shell and Tube type HX operating in cross-flow regime with the LBE flowing in the pipe side and the water flowing in the shell side. It is divided in two sections, operating at low power (5-50 kW) and high power (50-250 kW), respectively. It is placed in the higher part of the downcomer;
- an argon injection device, to perform GEC regime. The system for the injection of gas inside the riser is made of a 12.70 mm (1/2 inch) O.D pipe, 6135 mm long, inserted from the 2 ½" coupling flange in the upper part of the expansion tank through a Swagelok tube fitting;
- a thermal flow meter, located in the lower leg, for LBE mass flow rate measurements;
- 3 bubble tubes to measure pressure drops across the main components and pipes;
- a differential pressure transducer (1mbar accuracy);
- a thermal flow meter, located in the lower leg, for LBE mass flow rate measurements;
- several bulk thermocouples to monitor the temperature inside the FPS and along the flow path in the loop;
- the secondary side, filled with water at 16 bar, connected to the HX, shell side. It includes a pump, a pre-heater, an air-cooler, by-pass and isolation valves, and a pressurizer with cover gas;
- an ancillary gas system, to ensure a proper cover gas in the expansion tank, and to provide gas-lift enhanced circulation;
- A LBE draining section, with ½" pipes, isolation valves and a storage tank.

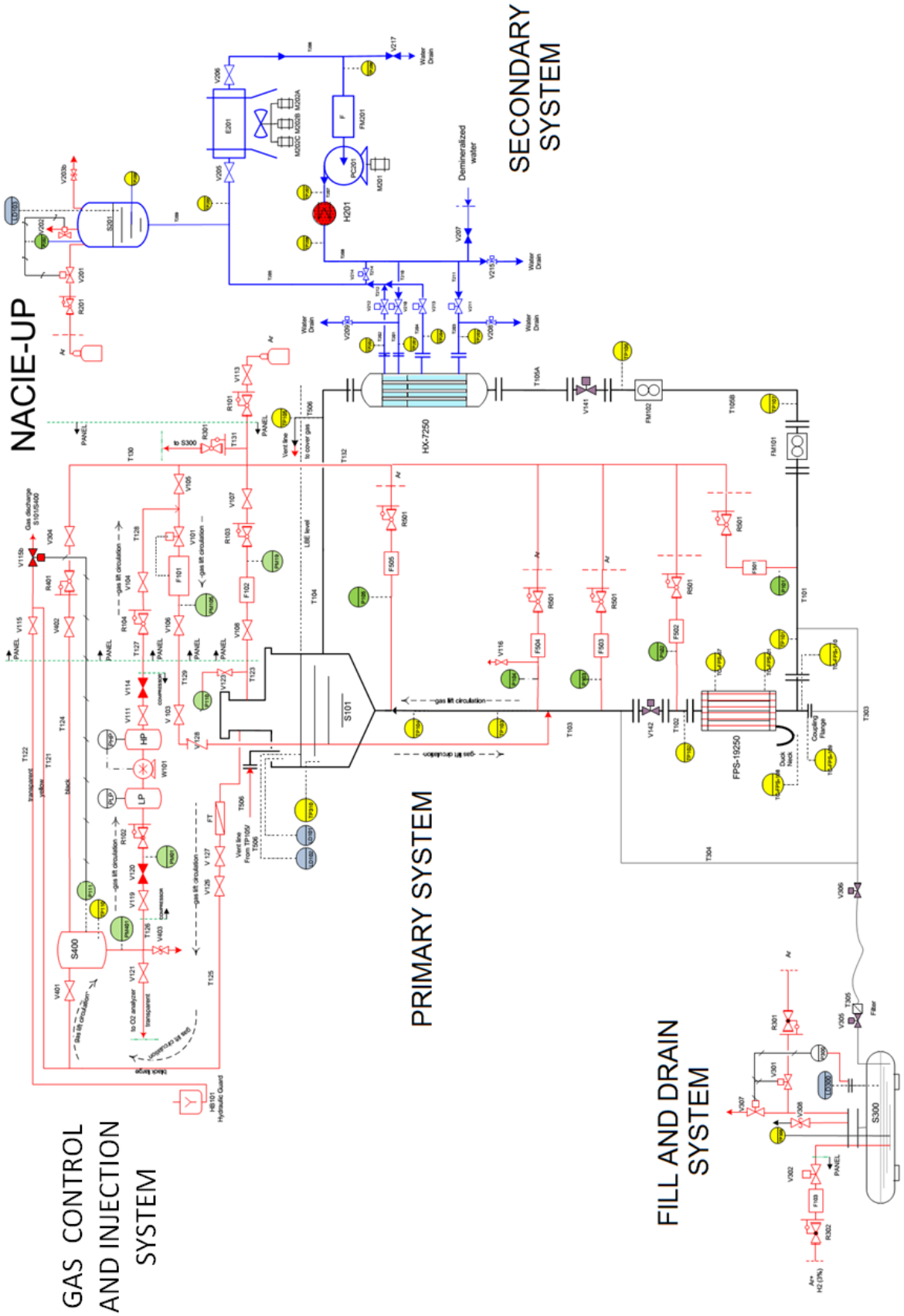

Fig. 6-1 – NACIE-UP P&ID

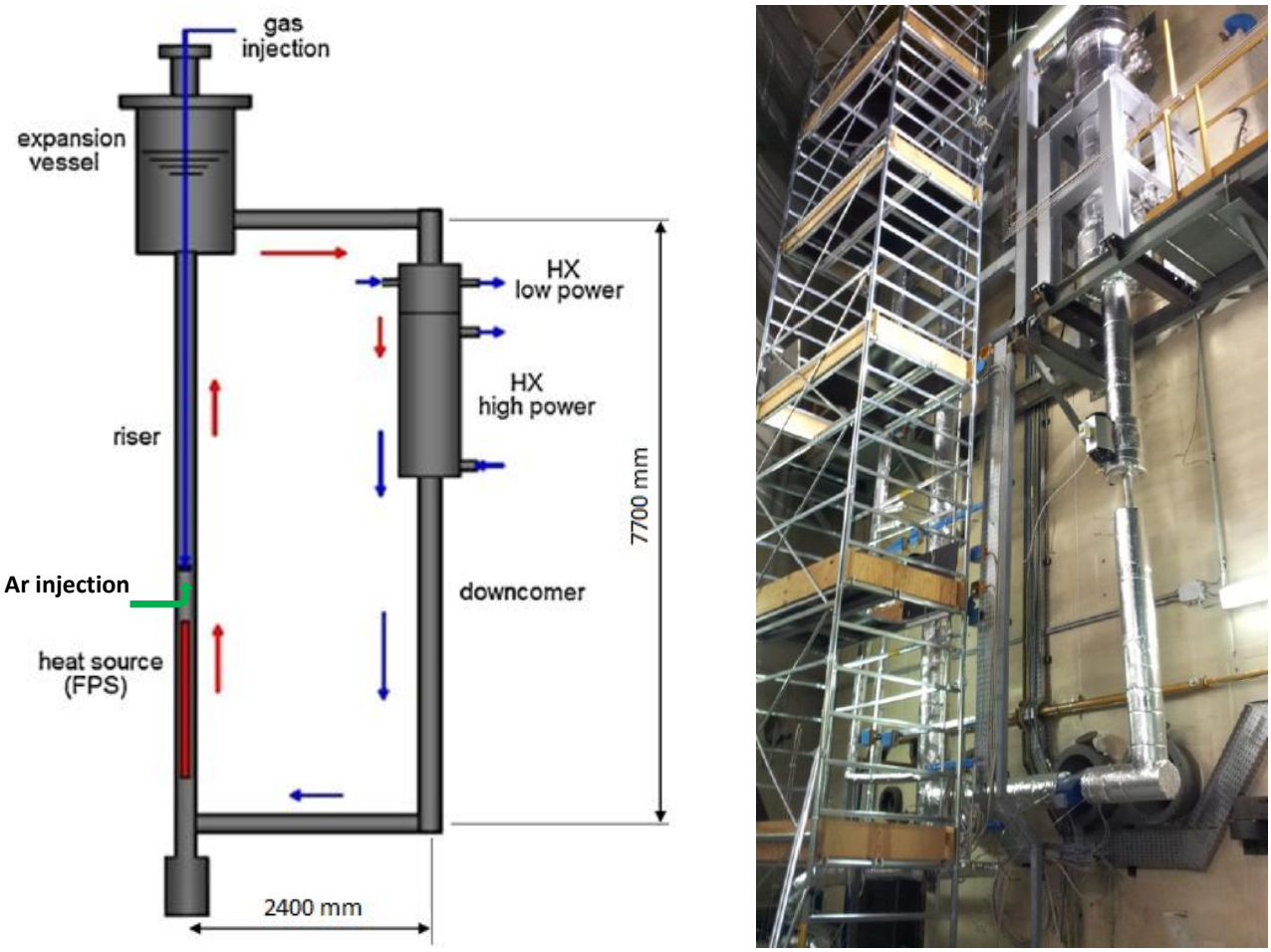

Fig. 6-2 – NACIE-UP facility layout

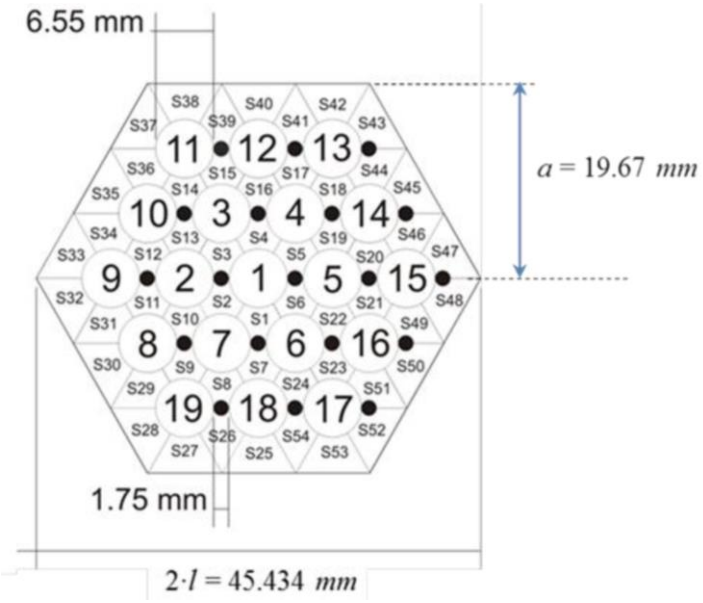

Fig. 6-3 – Fuel Pin Simulator geometry

6.4 STH CODE SIMULATIONS AND RESULTS

A 1-D model has been realized by the SYS-TH code RELAP5-3D® ver. 4.3.4 in the framework of the NACIE-UP Benchmark exercise, in order to evaluate the capability of the code to reproduce the thermal-hydraulic behaviour of the system during the three reference tests. The following paragraphs present a description of the RELAP5-3D® model realized, specifying the pressure drops models, the correlations for the heat transfer and the material properties adopted for the calculations.

6.4.1 Modelling of the hydrodynamic components

The nodalization consists of a one-dimensional model with several pipes and junctions connected each other in such a way to build an accurate simulation of the different parts of the loop. The entire system is composed of 185 hydrodynamic volumes, 183 junctions and 186 heat structures. The volumes have a mesh range between 0.09 m and 0.18 m in order to achieve a sufficiently detailed model.

Fig. 6-4 shows a schematic view of the entire nodalization which is composed of the following components:

- PIPE 001 represents the FPS, where the part represented in red is the active length composed by 19 pins, while the yellow part is the not-active region.
- PIPE 003 is the outlet pipe of the fuel pin bundle simulator;
- PIPE 005 is the riser;
- PIPE 103 and PIPE 007 are the large part and the closer part of the expansion tank, respectively;
- PIPE 011 simulates the primary side of the HX;
- PIPE 203 represents the secondary side of the low power HX;
- PIPE 208 represents the secondary side of the high power HX;
- PIPE 013 simulates the downcomer;
- PIPE 009 and PIPE 015 are the two horizontal legs.

The TMDPVOL 101 and TMDPJUN 102 provide the argon injection in the middle of the riser, while the TMDPVOL 105 on the top of the expansion tank represents the outlet of the gas. Concerning the secondary side of the heat exchanger, it is divided in two part: the low power HX and the high power HX. The low power section has a time dependent volume 201, which imposes the temperature and pressure of the water, while the time

dependent junction 202 fixes the water flow requested; the time dependent volume 205 represents the outlet of the water. At the same way, for the high power section, the time dependent volume 206 imposes the temperature and pressure of the water, the time dependent junction 207 fixes the water flow rate; the time dependent volume 210 represents the outlet of the water.

The division in volumes of the loop has been carried out in order to consider the correct position of the bubble tubes and the thermocouples located along the loop and the bulk thermocouples in the FPS sub-channels located at z= 38, 300, 562 mm along the active length of the rod bundle.

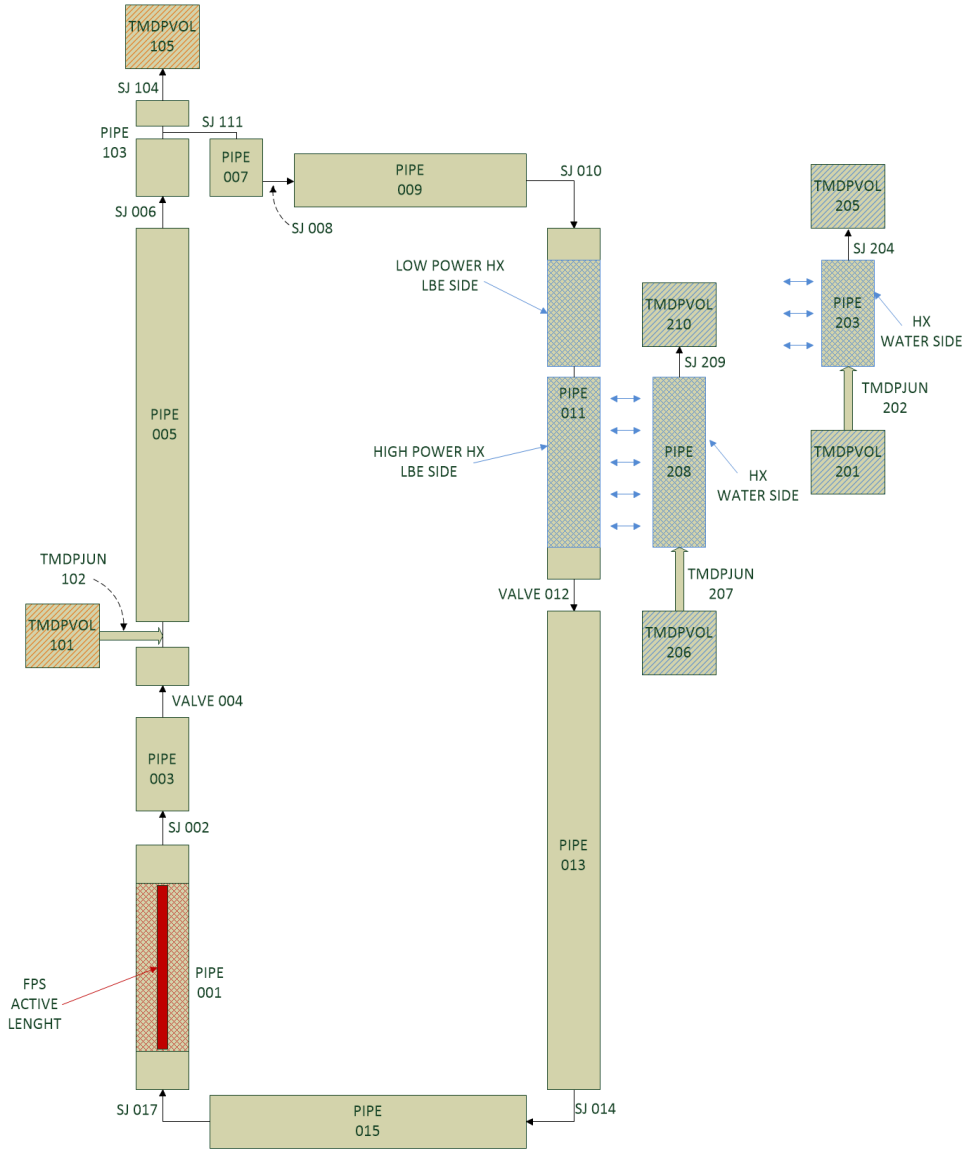

Fig. 6-4 – View of the RELAP5-3D nodalization

The singular pressure drops along the circuit are introduced for changes of directions and sudden area changes inside the expansion tank, HX and FPS inlet-outlet sections [41]. The evaluation of the K resistance coefficient for the FPS grid has been made using the Rehme correlation [5]. The friction factor for the wire-wrapped rod bundle has been evaluated with the detailed Cheng and Todreas correlation [42]:

- For laminar region $$f = \frac{C_{fL}}{Re}$$
- For turbulent region $$f = \frac{C_{fT}}{Re^{0.18}}$$
- For transition region: $$f = \left(\frac{C_{fL}}{Re}\right)(1-\psi)^{1/3} + \left(\frac{C_{fT}}{Re^{0.18}}\right)\psi^{1/3}$$

where:

$$C_{fL} = D_{eb}\left(\sum_{i=1}^{3}(N_i A_i/A_b)(D_{ei}/D_{eb})(D_{ei}/C_{fiL})\right)^{-1}$$

$$C_{fT} = D_{eb}\left(\sum_{i=1}^{3}(N_i A_i/A_b)(D_{ei}/D_{eb})^{0.0989}(D_{ei}/C_{fiT})^{0.54945}\right)^{-1.82}$$

$$Re_L = 300\left(10^{1.7(P/D-1.0)}\right)$$

$$Re_T = 10000\left(10^{0.7(P/D-1.0)}\right)$$

$$\psi = log(Re/Re_L)/log(Re_T/Re_L)$$

All the correlations for the other terms depend on geometrical parameters and they are reported in [42]. RELAP5-3D has the possibility to insert only two correlations, one for laminar zone (Re ≤ 2200) and one for turbulent (Re ≥ 3000):

$$\lambda_L = \frac{64}{Re\Phi_s} \quad for\ 0 \le Re \le 2200$$

$$\frac{1}{\sqrt{\lambda_T}} = -2log_{10}\left\{\frac{\varepsilon}{3.7D} + \frac{2.51}{Re}\left[1.14 - 2log_{10}\left(\frac{\varepsilon}{D} + \frac{21.25}{Re^{0.9}}\right)\right]\right\} \quad for\ 3000 \le Re$$

where Φ_s is a shape factor for noncircular flow channels and ε is the roughness [43].
The difference is the transition zone: in R5-3D a linear interpolation from the laminar friction evaluated with Re=2200 and the turbulent friction with Re=3000 is imposed:

$$\lambda_{L,T} = \left(3.75 - \frac{8250}{Re}\right)\left(\lambda_{T,3000} - \lambda_{L,2200}\right) + \lambda_{L,2200}$$

The differences between the detailed Cheng and Todreas correlations and the implemented friction factor are presented in Fig. 6-5.

For the friction loss coefficient evaluation of the piping, the default correlations of RELAP5-3D© have been used [43].

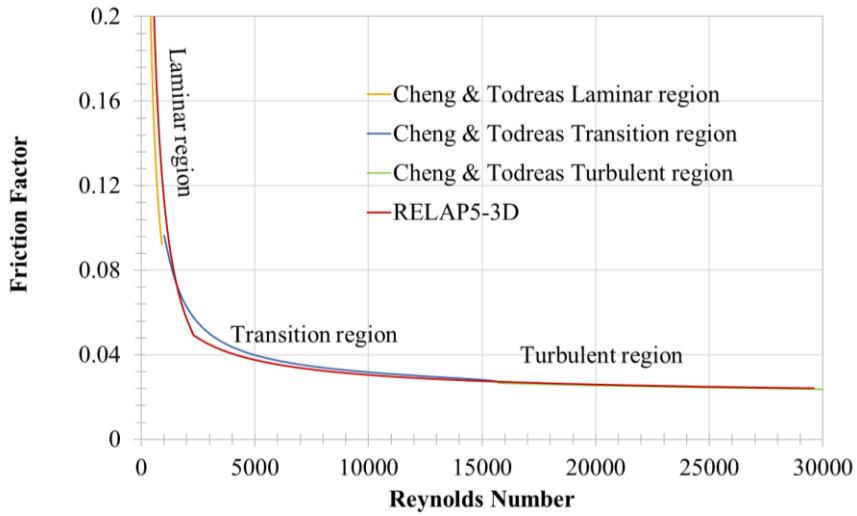

Fig. 6-5 – Friction factor implemented in R5-3D model

6.4.2 Modelling of the thermal coupling

Concerning the heat structures, a thermal coupling has been simulated:

- Between the active length of the FPS and the LBE in the primary side (HS001);
- Between the LBE of the primary side and the water in the secondary system (HS002);
- Between the primary system and the external environment.

The 19 pins of the FPS and the seven pipes of the HX have been simulated with a single equivalent heat structure respectively. All the differences of thickness in the insulation due to the flanges have been considered in the heat structures nodalization.

For the rod bundle of the FPS, the correlation for vertical bundles with in-line rods has been used, in case of parallel flow only (Geometry 110). The heat transfer correlation used for liquid metals in a rod bundle is (Kazimi and Carelli, 1976) [45]:

$$Nu = 4.0 + 0.33(P/D)^{3.8}(Pe/100)^{0.86} + 0.16(P/D)^{5}$$

where P/D is the pitch-to-diameter ratio of the rods and Pe is the Peclet number.

For the tube bundle of the HX, the correlation for vertical bundles with in-line rods has been used, for the particular case of parallel flow only (Geometry 110). The heat transfer correlations depending on the flow regime are:

- For natural convection (Churchill-Chu) [43]

$$Nu_L = \left\{ 0.825 + \frac{0.387(Ra_L)^{\frac{1}{6}}}{\left[1 + \left(\frac{0.492}{Pr}\right)^{\frac{9}{16}}\right]^{\frac{8}{27}}} \right\}^2$$

where:

- Ra_L is the Rayleigh number = Gr_l*Pr;
- $Gr_L = \frac{\rho^2 g\beta(T_w - T_b)L^3}{\mu^2}$

- For forced turbulent convection (Dittus-Boelter-Inayatov) [43]:

$$Nu = CRe^{0.8}Pr^n$$

where:

- n=0.4 for heating and 0.3 for cooling;
- C is a turbulent flow multiplier developed by Inayatov and it is implemented instead of the Mc Adams coefficient (0.023); for a bundle with in-line tubes and an equilateral triangle pitch, C becomes:

$$C = 0.023\left(\frac{P}{D}\right)$$

where P is the pitch and D is the tube diameter.

For the heat transfer through the pipes of the loop, the standard convective boundary type (Geometry 1) has been used. The correlation adopted for Lead-Bismuth Eutectic is [45]:

$$Nu = 5 + 0.025\,Pe^{0.8}$$

where Pe is the Peclet number.

For the evaluation of the heat losses along the loop, the following assumptions on external conditions have been considered:

- Air external temperature: 12°C;
- Air heat transfer coefficient 8 W/(m²K), value approximely estimated on the basis of a previous thermal characterization of the facility.

The entire loop has been coated with a layer of mineral wool as follows:

- 100 mm thickness along the FPS, riser, expansion vessel, heat exchanger and the two horizontal legs;
- 80 mm along the downcomer and the vertical pipe between the upper horizontal leg and the HX inlet.

The properties of the materials used to characterize the heat structures are reported in the following tables. In particular, Tab. 6-1 reports the properties of the steel powder AISI 316L+Helium at 5 bar inside the gap of the heat exchanger while Tab. 6-2 reports the properties of mineral wool used for thermal insulation. Concerning the piping, the thermal conductivity for the AISI 316L stainless steel is defined by this set of equations [46]:

$$k = \begin{cases} 7.58 + 0.0189T & for\ 300 \leq T \leq 1671\ K \\ 610.9393 - 0.342176T & for\ 1671 \leq T \leq 1727\ K \\ 20 & for\ T \geq 1727\ K \end{cases}$$

The equations for the stainless steel specific heat capacity are [46]:

$$C_p = \begin{cases} 326 - 0.242T + 3.71T^{0.719} & for\ 300 \leq T < 1671\ K \\ 691.98 & for\ T \geq 1671\ K \end{cases}$$

Tab. 6-1 – Steel powder AISI 316L+Helium at 5 bar thermal properties

Temperature [K]	Thermal Conductivity [W/(m*K)]	Heat Capacity [J/(m³*K)]]
273.15	3.2545	2.06E+06
473.15	3.2905	2.06E+06
573.15	3.3193	2.17E+06
673.15	3.4112	2.25E+06
873.15	3.4377	2.30E+06
1023.15	3.5025	2.33E+06

Tab. 6-2 – Thermal insulation by mineral wool thermal properties

Temperature [K]	Thermal Cond. [W/(m*K)]	Heat Capacity [J/(m³*K)]]
273.15	0.035	1.34E+05
473.15	0.043	1.34E+05
573.15	0.062	1.34E+05
673.15	0.074	1.34E+05

6.4.3 Blind Simulations

In the first phase of the benchmark, the blind simulations have been performed on the basis of detailed specifications proposed [47]. The assessment consists of the simulation of three well-defined test cases on the NACIE-UP facility representative of operative or accidental transient events, significant to HLM nuclear systems:

- Fundamental Test-1: Gas Flow Transition;
- Fundamental Test-2: Power Transition;
- Fundamental Test-3: Protected Loss of Flow Accident (PLOFA) scenario.

The boundary conditions designed for each test are summarized in Tab. 6-3.
During the numerical analysis, a specified number of parameters (flow rate, pressure, temperatures in the loop and in the bundle) is selected on the basis of their relevance for the thermal-hydraulic characterization of the facility. The same parameters have been acquired during the experimental campaign and used for the post-test analysis phase. The thermal-hydraulic parameters requested by the output specification [39] are summarized in Tab. 6-4 (from [48]), while the measurement points of such quantities are reported in Fig. 6-6 (from [48]).

Tab. 6-3 – Designed boundary conditions for NACIE-UP experiments

Parameter	Test 1	Test 2	Test 3
Power transition	no	yes	yes
Power [kW]	50	From 100 to 50	From 100 to 10
Gas transition	yes	no	yes
Gas lift [Nl/min]	From 20 to 10	18	From 20 to 0
H2O flow rate transition	no	no	yes
Water flow rate (high power HX) [m³/h]	10	10	From 10 to 6.6
Water T_{av} [°C]	170	170	170

Tab. 6-4 – Parameters for the SYS-TH codes benchmark exercise

Parameter	Loop position	Variable name
LBE mass flow rate	Entire Loop	LBE-MFR
LBE Temperatures inside the primary loop	FPS inlet	Tin-FPS
	FPS outlet	Tout-FPS
	HX inlet	TP105
	HX outlet	TP106
	Expansion vessel	TP310
	FPS Section A (z=38 mm)	Tlbe-A
	FPS Section B (z=300 mm)	Tlbe-B
	FPS Section C (z=562 mm)	Tlbe-C
Water temperature	HX secondary side outlet	TP204
Pressures inside the primary loop	Lower horizontal pipe	P101
	Downstream the FPS	P102
	Upstream the gas injection nozzle	P103
	Downstream the gas injection nozzle	P104

6.4.3.1 Test-1: Gas flow transition

The first test aims at evaluating the behaviour of the system when a reduction of the primary coolant mas flow rate occurs, due to a variation of the argon flow rate injected. The electrical power supplied by the FPS is set at 50 kW, uniformly distributed among the 19 pins and it is maintained constant during the whole duration of the test. The circuit is filled by LBE up to the second level sensor of the expansion tank (180 mm from the nozzle of the riser) and the argon cover gas is pressurized at 1.4 bar. The gas injection device supplies an initial argon flow rate of 20 Nl/min. Concerning the secondary loop, the low power section of the heat exchanger is maintained empty while the higher power section is fed by water at 170°C and 16 bar with a volumetric flow rate of 10 m^3/h.

The test starts after that the steady-state conditions are reached in the primary and secondary loop, with a permanence for one hour at the working conditions described above. After one hour, the gas injection device is managed by reducing the argon flow rate from 20 Nl/min to 10 Nl/min with a time ramp of 10 seconds (Fig. 6-7). After this transition, a new steady-state condition is achieved and maintained for 30 minutes.

During the simulation of Test 1, after an initial period of 10 minutes, the steady-state condition is reached and kept up to 60 min, with a LBE mass flow rate of ~4.9 kg/s (see Fig.

6-8). After the gas flow rate reduction, a new steady state is immediately obtained after a sudden transition, with a new LBE mass flow rate of ~4 kg/s, lower than the previous one, according with the lower gas contribution.

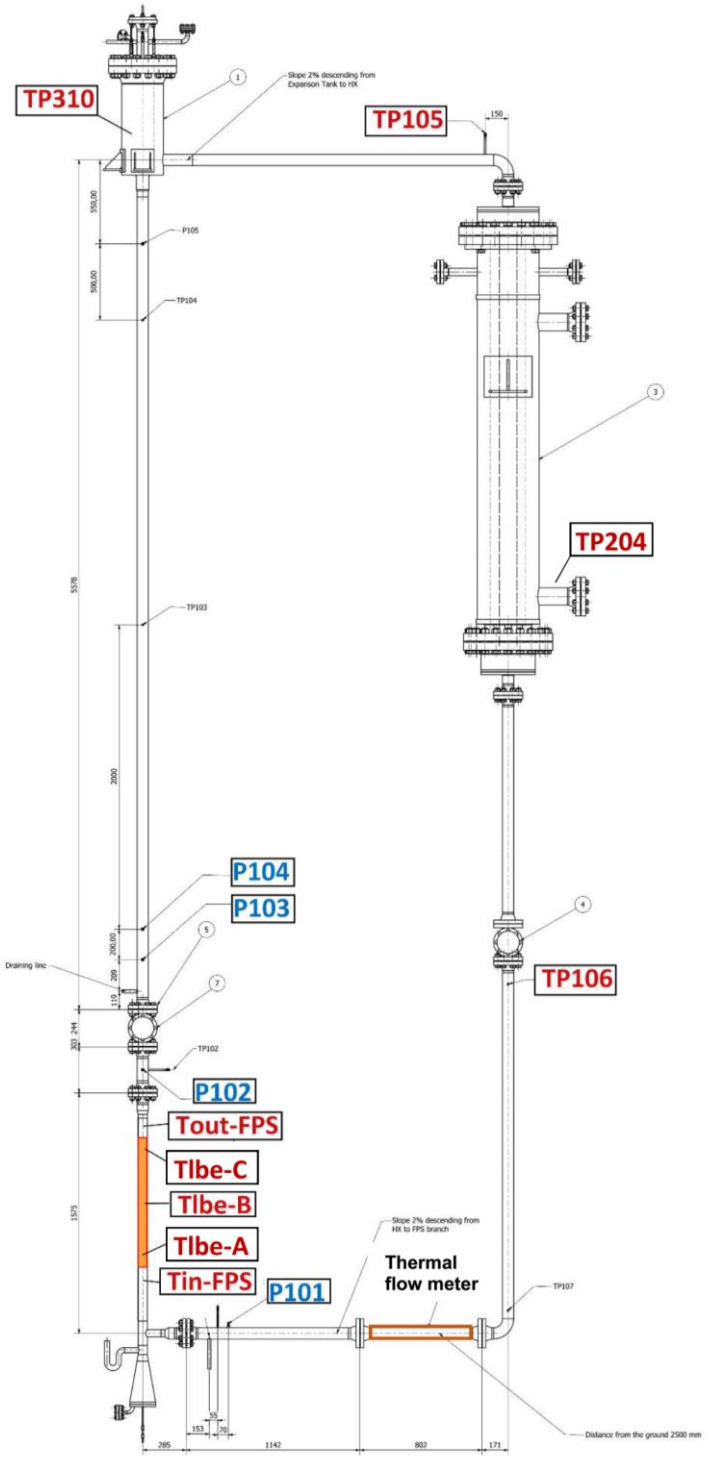

Fig. 6-6 – Measurement points of the simulated quantities (from [48])

The FPS temperatures are reported in Fig. 6-9 and Fig. 6-10. In particular, Fig. 6-9 shows the temperatures at the inlet and outlet sections of the FPS and at three different sections at 38 mm, 300 mm and 562 mm, respectively, assuming as 0 mm the beginning of the active length. The figure highlights the temperature increase from the inlet to the outlet of the bundle active length, accordingly with the heating of the LBE flowing through the FPS. It is possible to notice the temperature peaks in correspondence of the gas flow rate reduction which causes a lower velocity of the LBE and its further heating. After the peaks, the following steady state is characterised by temperatures higher than the previous ones. This phenomenon is emphasized passing from the inlet to the outlet sections of the FPS due to the higher temperatures reached. Fig. 6-10 reports the LBE temperature along the active length before and after the gas flow rate reduction, highlighting the higher temperature field achieved after the transient.

Fig. 6-11 reports the LBE temperature at the HX. Before the transient, the temperatures at the inlet and outlet sections are ~282°C and ~214°C, respectively, with a ΔT of about 68°C, while after the transient, the ΔT inlet/outlet increases (ΔT~85°C), since the inlet temperature is ~296°C and the outlet temperature decreases to 211°C, accordingly with the reduction of the mass flow rate of the primary coolant.

The water temperatures at the inlet ad outlet section of the HX are reported in Fig. 6-12. It can be noticed the temporal reduction of the temperatures during and immediately after the gas transient, with a greater oscillation at the outlet nozzle. The temperature reached in the outlet section is ~174°C.

The pressure along the loop are reported in Fig. 6-13, which shows the values at four different positions: lower horizontal pipe (upstream the FPS), downstream the FPS, upstream the gas injection nozzle and downstream the gas injection nozzle. The higher pressure drop is calculated across the FPS, resulting in a ΔP of about 200 kPa.

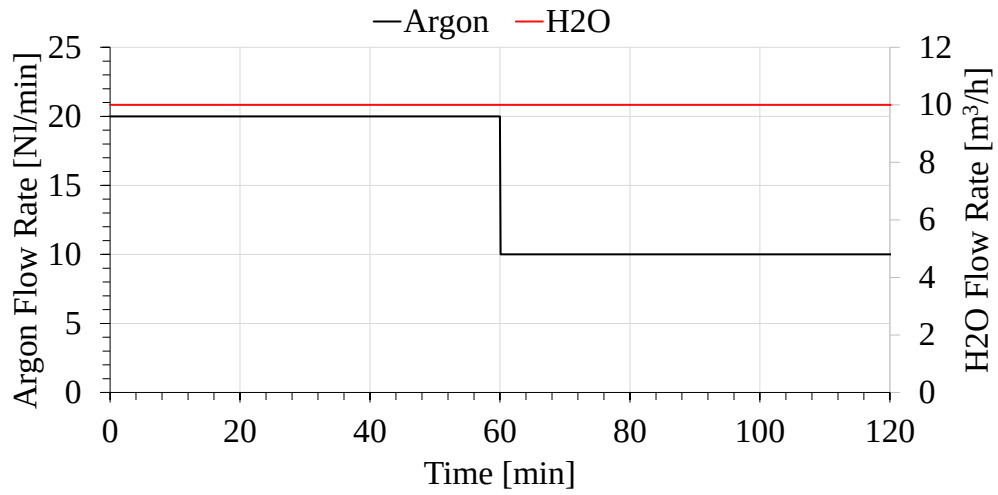

Fig. 6-7 – Test 1, R5-3D boundary conditions

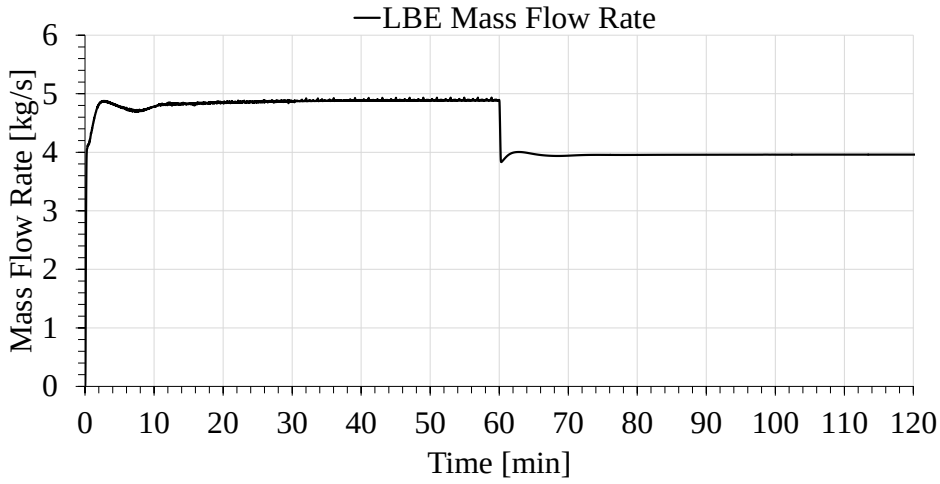

Fig. 6-8 – Test 1, LBE mass flow rate

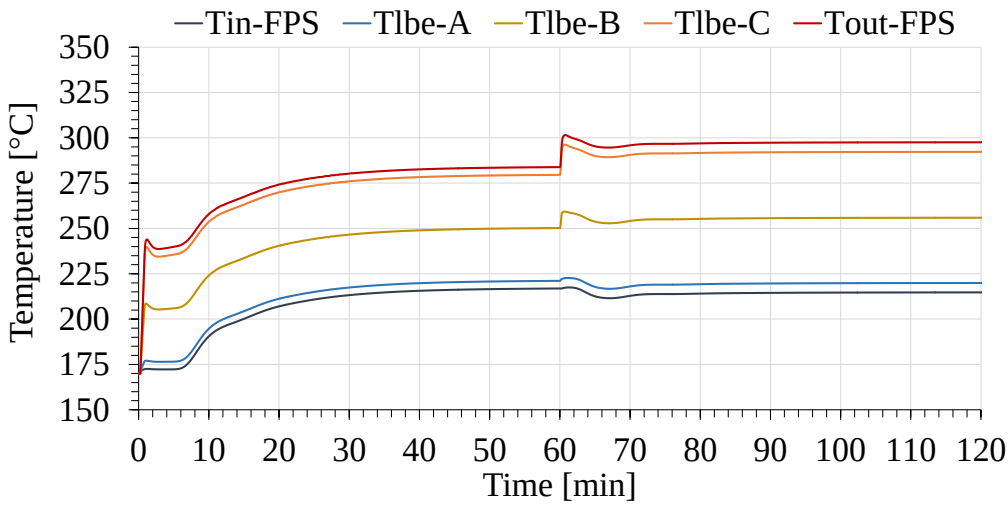

Fig. 6-9 – Test 1, LBE temperature at FPS inlet/outlet and sections A:38 mm, B:300 mm, C:562 mm

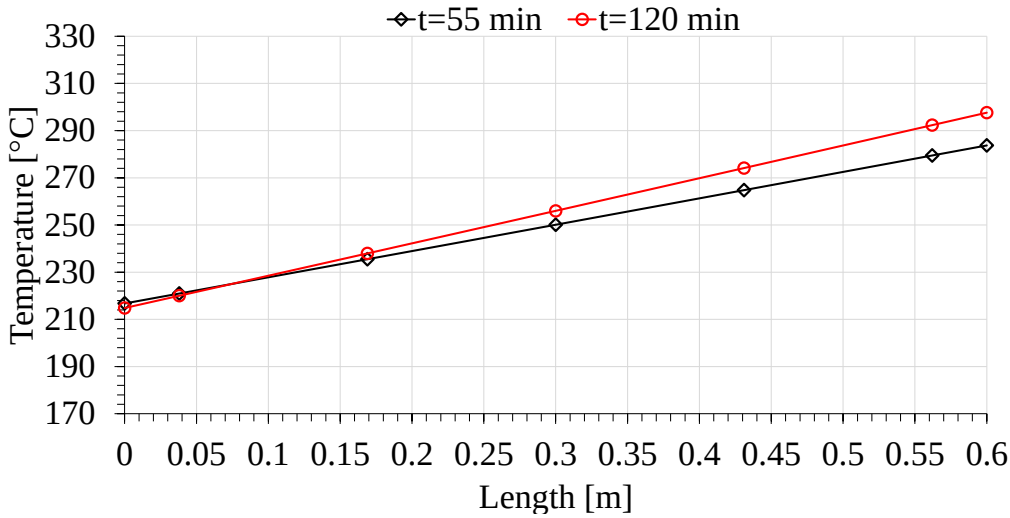

Fig. 6-10 – Test 1, FPS temperature trend along the active length before and after the transient

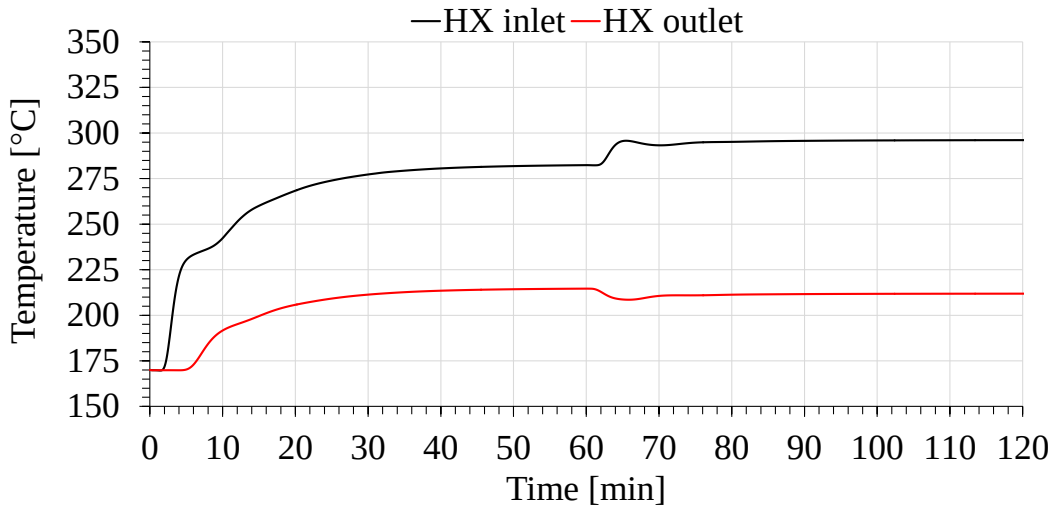

Fig. 6-11 – Test 1, LBE temperature at the HX inlet and outlet sections

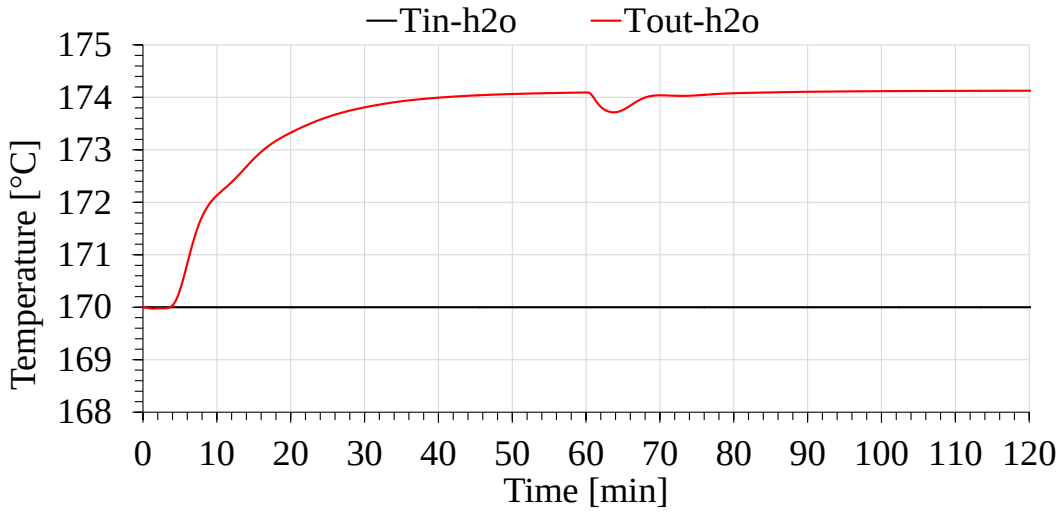

Fig. 6-12 – Test 1, H2O temperature at the HX inlet and outlet sections

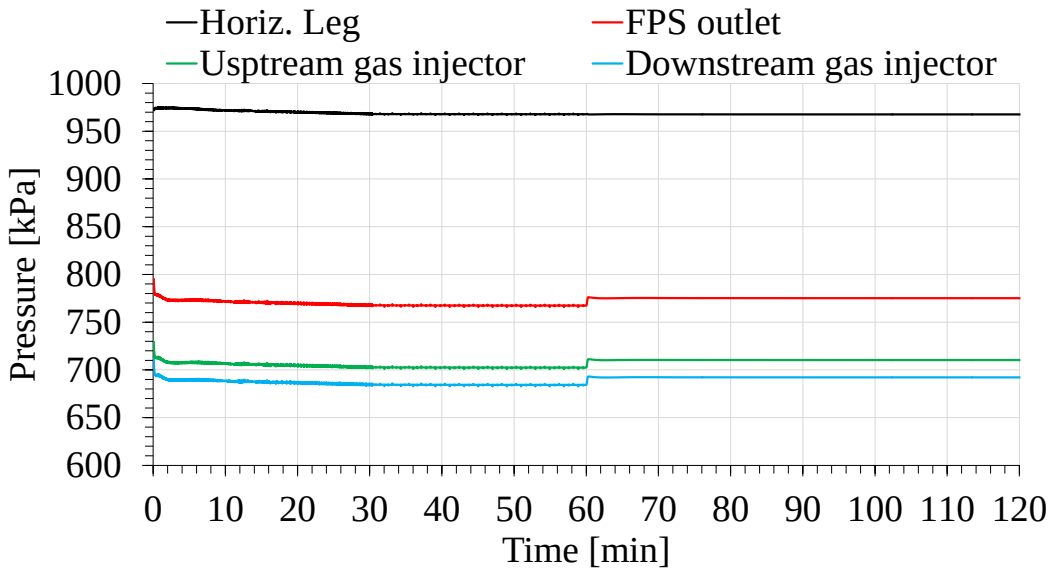

Fig. 6-13 – Test 1, pressure along the primary loop

6.4.3.2 Test-2: Power transition

The second test consists of a power transition transient, switching from an initial FPS power of 100 kW to 50 kW. As seen for Test-1, the primary side is filled up to the second level sensor of the expansion tank and the argon gas above is pressurized at 1.4 bar. The gas flow rate injected is maintained constant to a value of 18 Nl/min during the entire duration of the test. The secondary side of the high power section of the heat exchanger is fed by water at 170°C and 16 bar with a volumetric mass flow rate of 10 m^3/h, while the low power section is empty and disabled. The test starts after the achievement of the steady-state conditions; after one hour, the transient is carried reducing the FPS power from 100 kW to 50 kW with a power decreasing rate of 1 kW/s, for a total time of 50 seconds (Fig. 6-14). A second steady state is achieved after the transient and it is maintained for an additional time of 30 minutes.

Fig. 6-15 shows the LBE mass flow rate: the value computed by the code reaches the maximum at ~5.3 kg/s before the power transient, then it decreases to 4.7 kg/s in 2-3 minutes after the transition, reaching the final value of 4.6 kg/s when the new steady-state conditions are reached.

LBE temperatures inside the primary circuit are reported in Fig. 6-16 and Fig. 6-17 for the FPS and Fig. 6-18 for the HX. In particular, the temperatures across the FPS are subjected to a sudden decrease due to the reduction of the power supplied to the system. As occurred in Test 1, the phenomenon is emphasized passing from the inlet to the outlet

sections of the FPS. After the transient, the temperatures achieve a second steady-state condition with a temperature range lower than the first one. The effects of the transient are also visible in Fig. 6-17 which reports the LBE temperature along the active length (inlet/outlet sections and three intermediate sections) before and after the power reduction, highlighting the lower temperatures achieved after the transient.

A similar behaviour can be found in the LBE side of the HX (Fig. 6-18), where the LBE inlet temperature decreases from ~379°C to ~288°C when the transient occurs, with the consequent decrease of the outlet temperature from ~253°C to ~214°C and the reduction of the ΔT from 126°C to 74°C. It can be noticed that the temperatures inside the HX start to decrease with a delay of 3-4 minutes respect to the beginning of the power reduction and with a smoothed ramp, due to the thermal inertia of the system. Concerning the secondary side (Fig. 6-19), the water temperature is also characterised by a decrease of few degrees from ~178°C to ~174°C according to the power reduction.

The pressure trends calculated along the loop are reported in Fig. 6-20, which shows trends and values similar to Test 1.

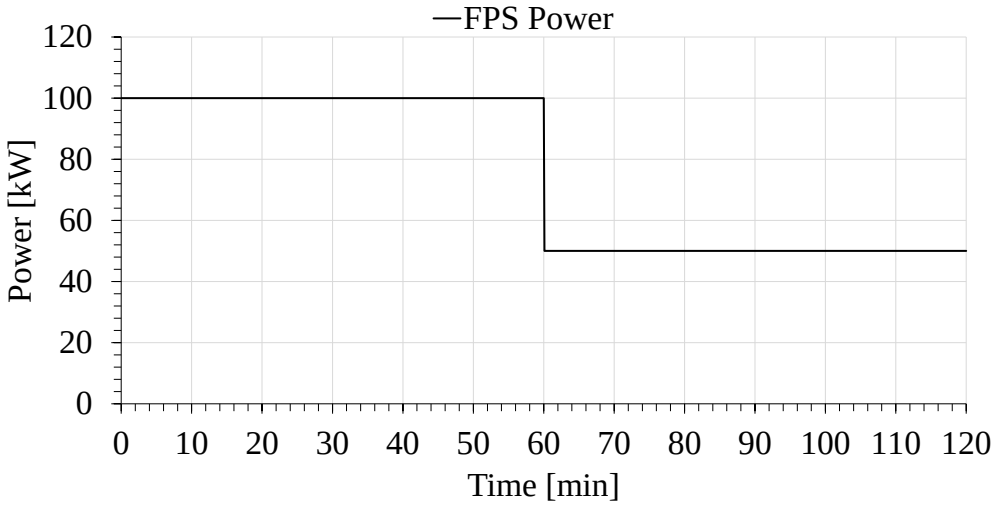

Fig. 6-14 – Test 2, R5-3D boundary conditions

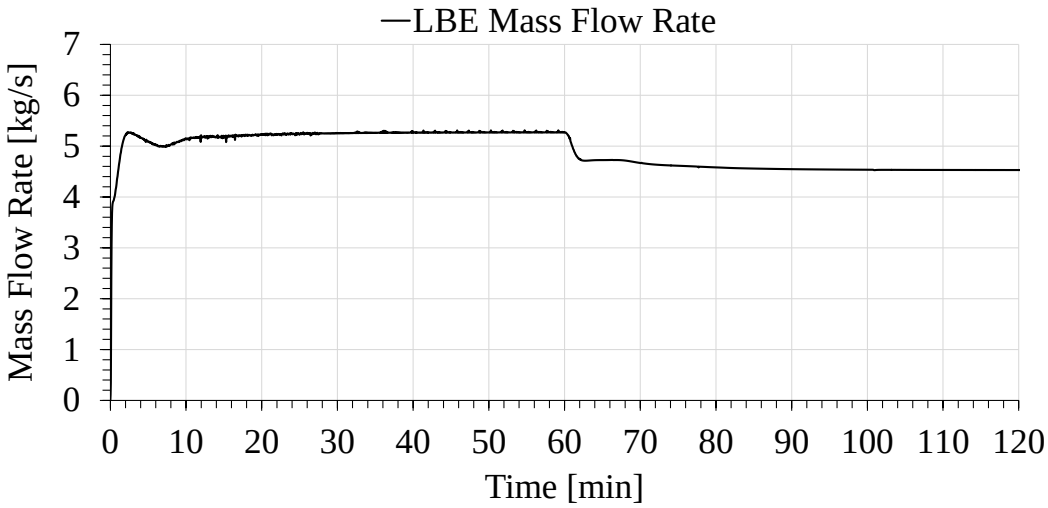

Fig. 6-15 – Test 2, LBE mass flow rate

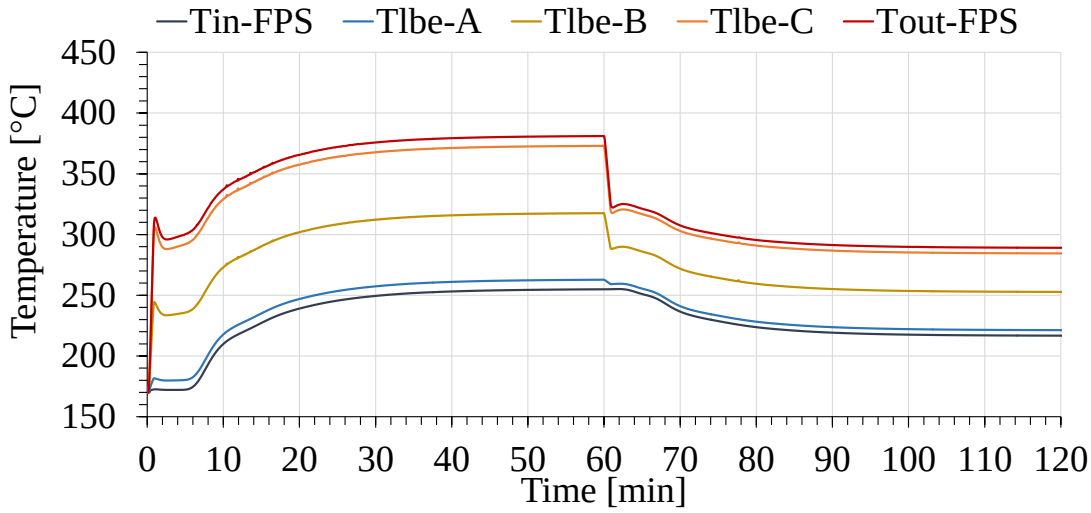

Fig. 6-16 – Test 2, LBE temperature at FPS inlet/outlet and sections A:38 mm, B:300 mm, C:562 mm

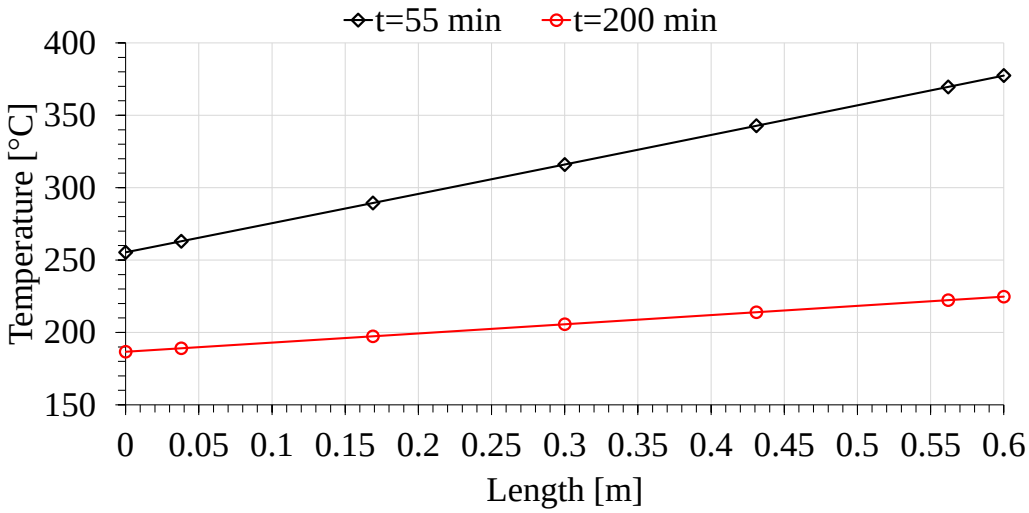

Fig. 6-17 – Test 2, FPS temperature trend along the active length before and after the transient

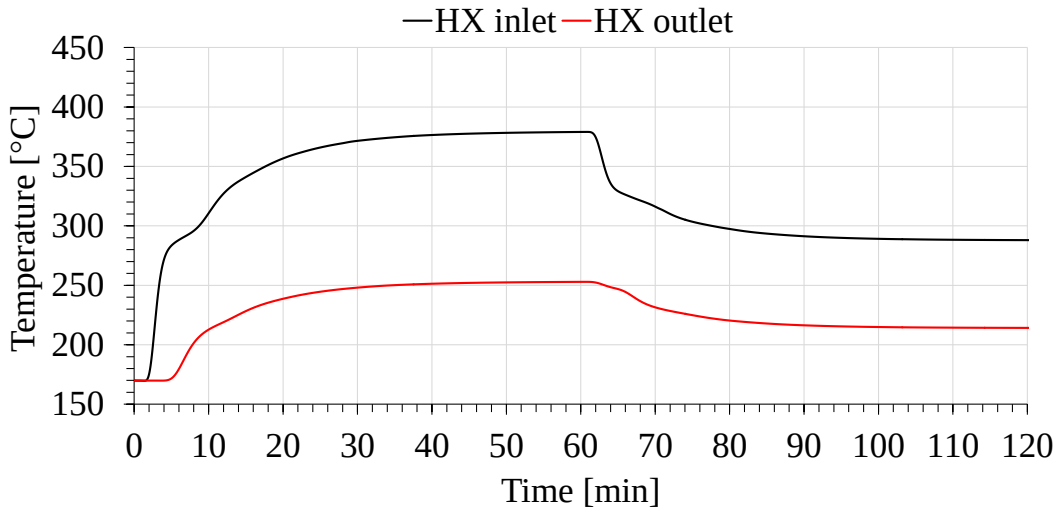

Fig. 6-18 – Test 2, LBE temperature at the HX inlet and outlet sections

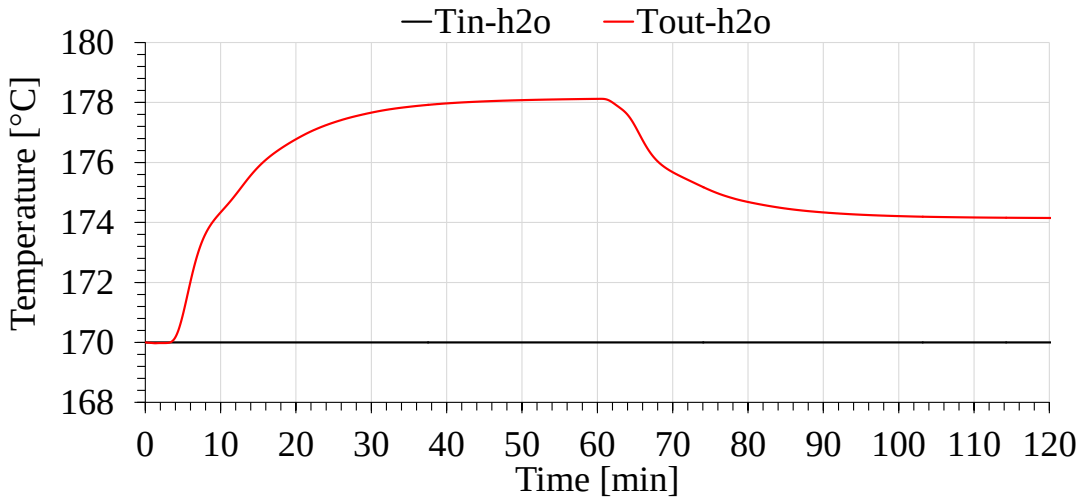

Fig. 6-19 – Test 2, H2O temperature at the HX inlet and outlet sections

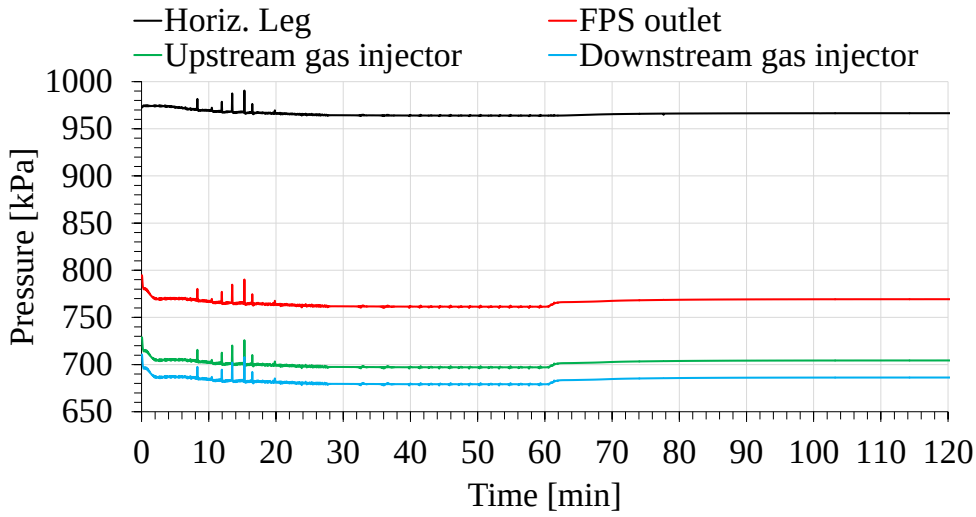

Fig. 6-20 – Test 2, pressure along the primary loop

6.4.3.3 Test-3: Protected Loss of Flow Accident (PLOFA)

The last test aims at reproducing a PLOFA scenario, starting from a steady-state with high FPS power and high mass flow rate in GEC regime and performing a transition to low power with low mass flow rate in NC regime. During the transition, the power level is decreased before switching off the gas injection device in order to avoid too high temperature peaks at the pins clads. The primary loop is filled up to the second level sensor of the expansion tank and the cover gas is maintained at 1.4 bar, while the secondary side of the heat exchanger (the higher power section only) is fed by water at 170°C and 16 bar. The beginning of the test is characterised by a total power supplied of 100 kW, an argon gas rate of 20 Nl/min and a water flow rate of 10 m^3/h. After one hour, the power is subjected to a sudden decrease from 100 kW to 10 kW in a time lapse of 10 seconds (power decreasing rate of 10 kW/s). When the power transition is completed, the argon injection device is switched off passing from 20 Nl/min to 0 Nl/s in 10 seconds. After the transition in the primary loop, the water flow rate is reduced from 10 m^3/h to 6.6 m^3/h in 10 seconds. After the transition, a new steady-state condition is achieved and maintained for about 30 minutes.

The LBE mass flow rate is reported in Fig. 6-22 which identifies two steady states before and after the transient: the first one characterised by a LBE mass flow rate of 5.4 kg/s, while the second one with a mass flow rate of about 1.6 kg/s.

The temperature trends in the FPS are shown in Fig. 6-23 and Fig. 6-24. The transient is characterised by a relevant decrease of the temperature, especially in the upper zone of the active length, due to the final low fraction of power supplied. Fig. 6-24 also highlights the lower temperature field after the PLOFA occurrence, once that the steady-state conditions are reached. Thanks to the power control, no temperature peaks are present during the simulation.

Fig. 6-25 and Fig. 6-26 report the LBE and the water temperatures inside the HX at the inlet and outlet sections. At the inlet, the temperature passes from 375°C to 219°C when the transient occurs, while at the outlet it decreases from 253°C to 176°C, with a significant reduction of ΔT from 128°C to 43°C. As occurred for Test 1 and Test 2, the temperatures transient inside the HX starts with a delay of 3-4 minutes respect to the beginning of the transient, due to the thermal inertia of the system. Concerning the secondary loop, the transition is characterised by temperatures peaks which are evident near the outlet nozzle of the HX, where the maximum of ~180°C is achieved. The water outlet temperature in the

first steady state is about 179°C, while after the transient the value tends to decrease near the 170°C.

Finally, Fig. 6-27 shows the pressure along the primary loop. As occurred in the previous tests, the higher pressure drop is calculated across the FPS, with a ΔP of about 205 kPa. In this case is also possible to notice a reduction of ΔP after the transient, reaching the final value of 180 kPa, due to the significant reduction of LBE mass flow rate.

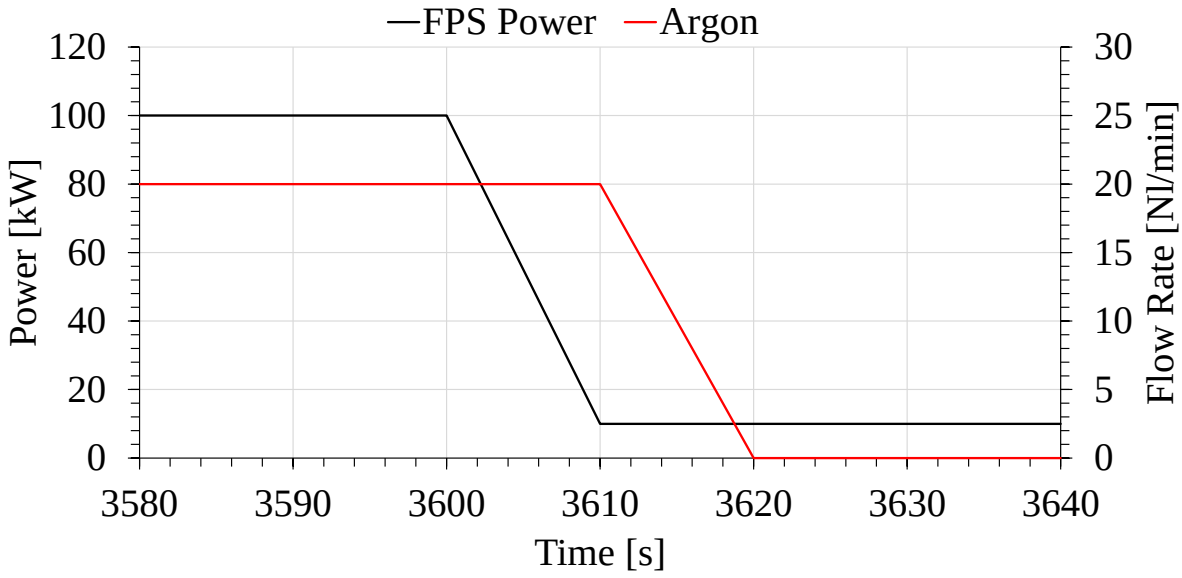

Fig. 6-21 – Test 3, R5-3D boundary conditions

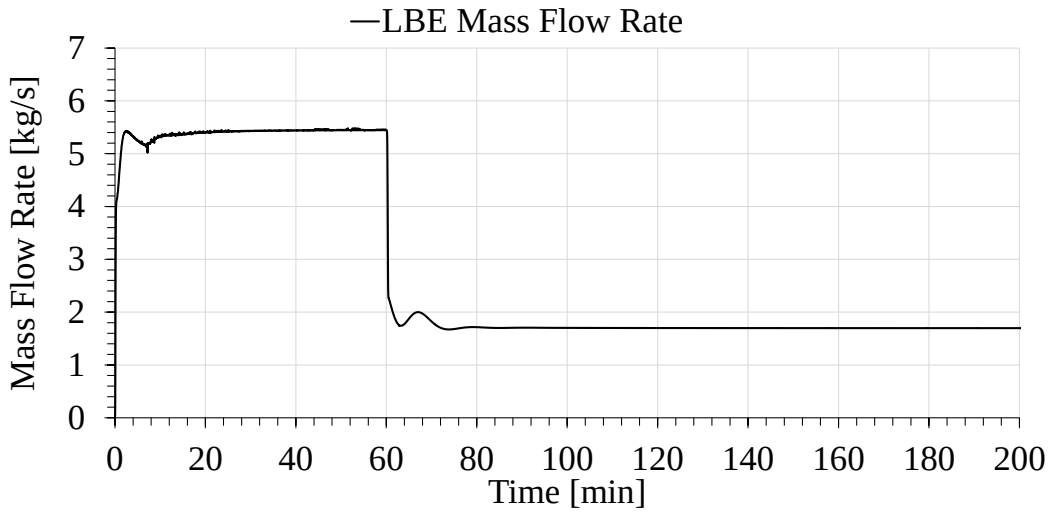

Fig. 6-22 – Test 3, LBE mass flow rate

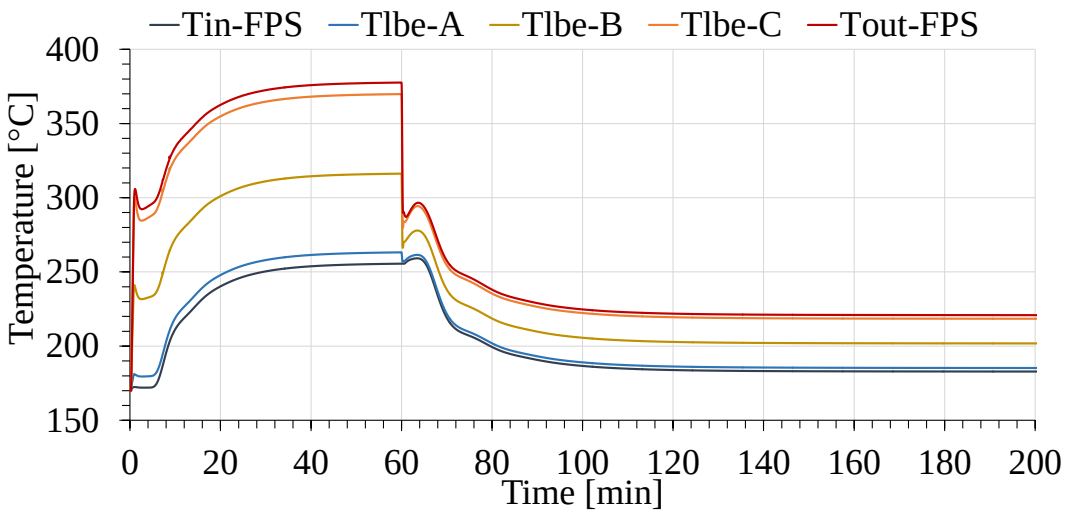

Fig. 6-23 – Test 3, LBE temperature at FPS inlet/outlet and sections A:38 mm, B:300 mm, C:562 mm

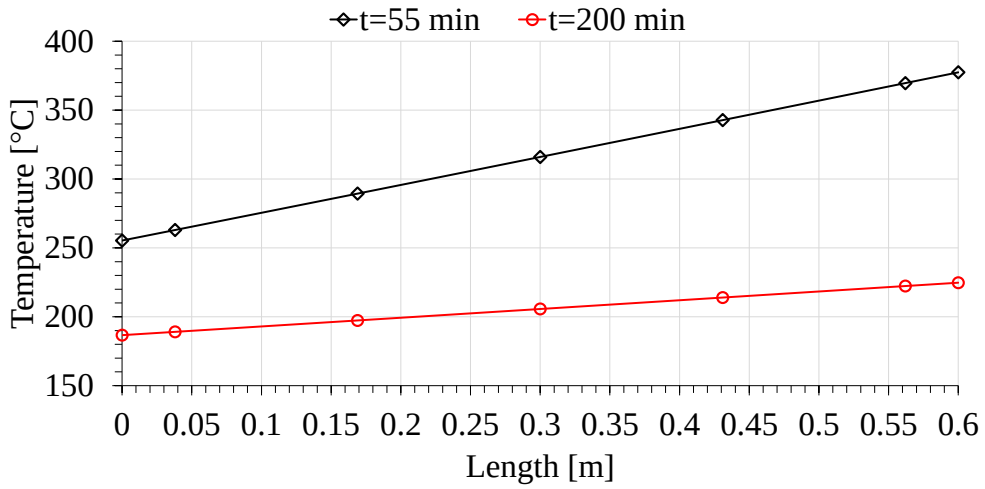

Fig. 6-24 – Test 3, FPS temperature trend along the active length before and after the transient

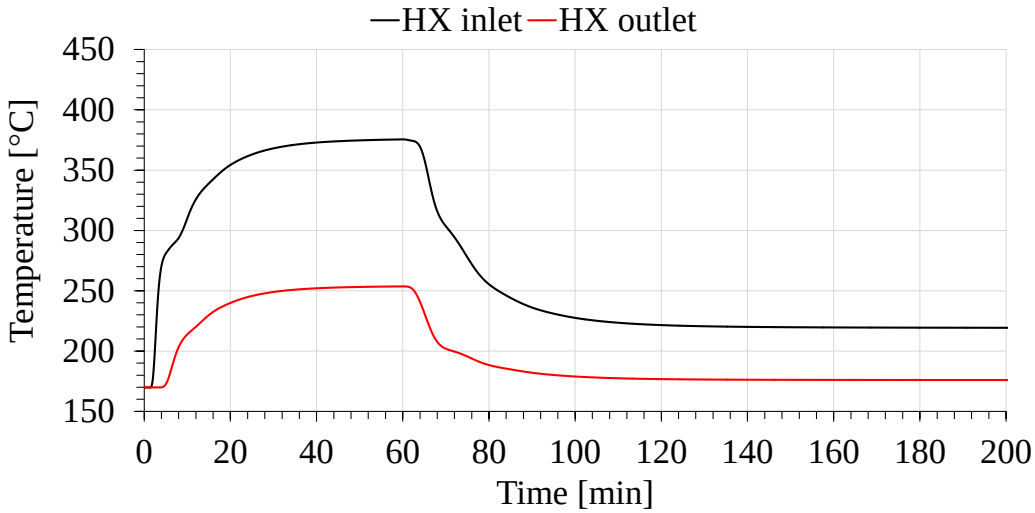

Fig. 6-25 – Test 3, LBE temperature at the HX inlet and outlet sections

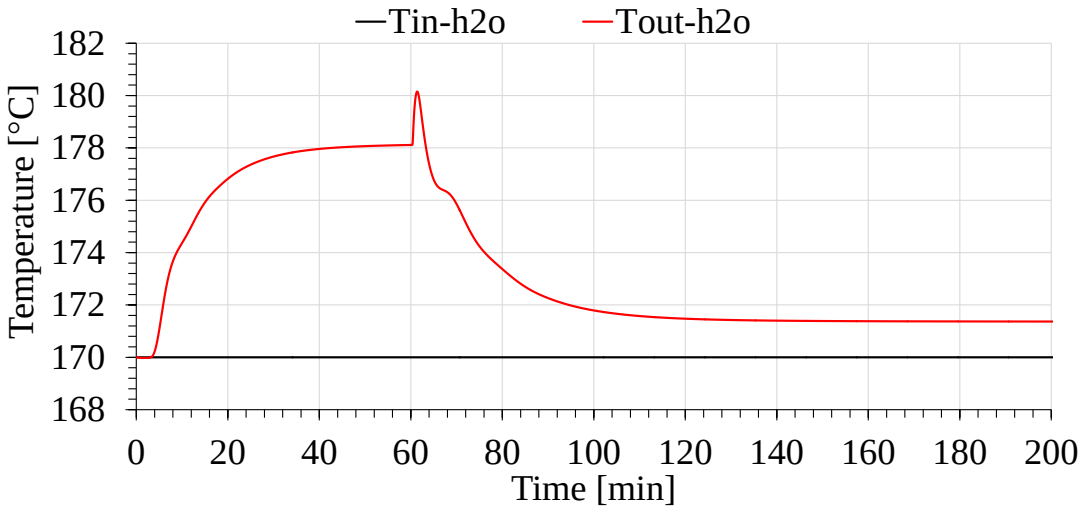

Fig. 6-26 – Test 3, H2O temperature at the HX inlet and outlet sections

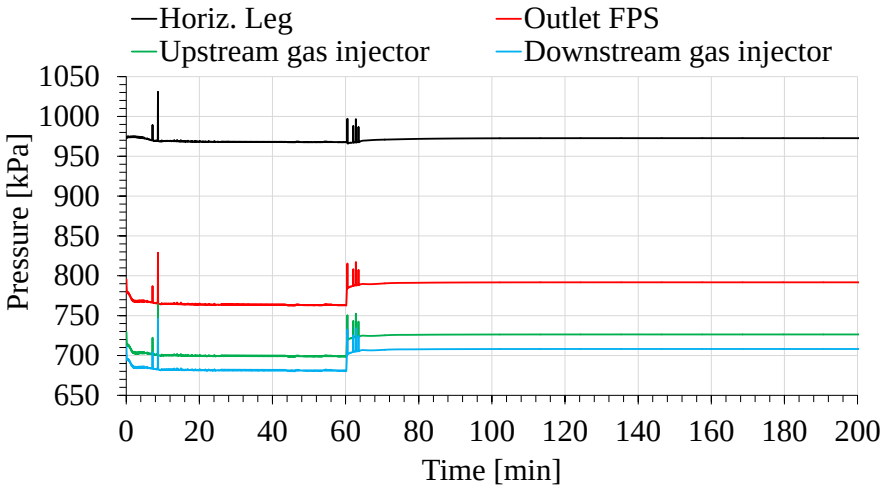

Fig. 6-27 – Test 3, pressure along the primary loop

6.4.4 Post-Test Simulations

In the second phase of the benchmark, the experimental data collected during the experimental campaign [49] have been delivered to the participants, allowing to improve and to calibrate the models on the basis of the final layout of the facility and assuming the real boundary conditions reached during the tests.

The preliminary comparison of the outcomes from the blind simulations with the experimental data has highlighted that the numerical model requires some adjustments for the post-test analysis. The up-dating aims at improving the hydraulic and thermal features of the model, reproducing as well as possible the system behaviour, as well as to adjust the boundary conditions assumed in the input deck, in order to take into account

the real boundary conditions reached during the experiments. In fact, several differences have been found between the designed boundary conditions, already presented in Tab. 6-3, and the experimental boundary conditions reported in Tab. 6-5, which have a relevant influence on the final results.

In the following paragraph, the up-dated model used to carry out the post-test simulations is presented and the numerical results are compared against the available experimental data. The comparison among the numerical model performed by all the participants of the benchmark is reported in [50].

Tab. 6-5 – Experimental boundary conditions of NACIE-UP tests

Parameter	Test 1	Test 2	Test 3
Power transition	no	yes	yes
Power [kW]	50	From 100 to 50	From 100 to 10
Gas transition	yes	no	yes
Gas lift [Nl/min]	From 20 to 10	18	From 20 to 0
H2O flow rate transition	no	no	~~yes~~ no
Water flow rate (high power HX) [m³/h]	10	~~10~~ 6.6	~~From 10 to 6.6~~ 10
Water T_{av} [°C]	170 (oscillations)	170 (oscillations)	170 (oscillations)

6.4.4.1 Model improvements

The thermal-hydraulic model reported in Section 6.4 has been updated on the basis of the comparison between the blind simulations results and the experimental data achieved during the tests. In particular, the following modifications have been implemented in the model:

- re-calibration of the singular pressure drops inside the expansion tank and along the loop;

- an additional heat structure (HS 051) has been added on the lower part of the loop in order to consider the power supplied by the thermal flow meter;
- an additional heat structure (HS 052) has been added upstream the FPS active region to simulate the power released to the LBE before the active length (~7%).

The updated model of the NACIE-UP loop used in the post-test analysis is reported in Fig. 6-28.

During the Post-Test activity, a sensitivity analysis has been carried out in order to evaluate the influence of the AISI 316L thermal conductivity on the thermal-hydraulic performances of the heat exchanger. The steel powder thermal conductivity is a function of the temperature and it is influenced by different factors, i.e. the grain size and growth, powder compaction, thermal cycling. Starting from the experimental correlations reported in [51], two cases have been considered:

- CASE A $C = 2 * 10^{-6} * T^2 + 0.0013 * T + 0.3601$
- CASE B $C = 7 * 10^{-7} * T^2 + (13 * 10^{-4}) * T + 0.2426$

and several simulations have been realized, considering the trends presented in Fig. 5.1. The results reported in the following figures are referred to the simulations of the three tests, with the implementation of the correlation of CASE E, which is close to the correlation obtained in the post test activity described in [50] and reported in the graph as CASE F.

Furthermore, during the post-test analysis, the real test conditions have been taken into account and assumed as Boundary Conditions (BCs) for the R5-3D simulations, as explained in the following paragraphs.

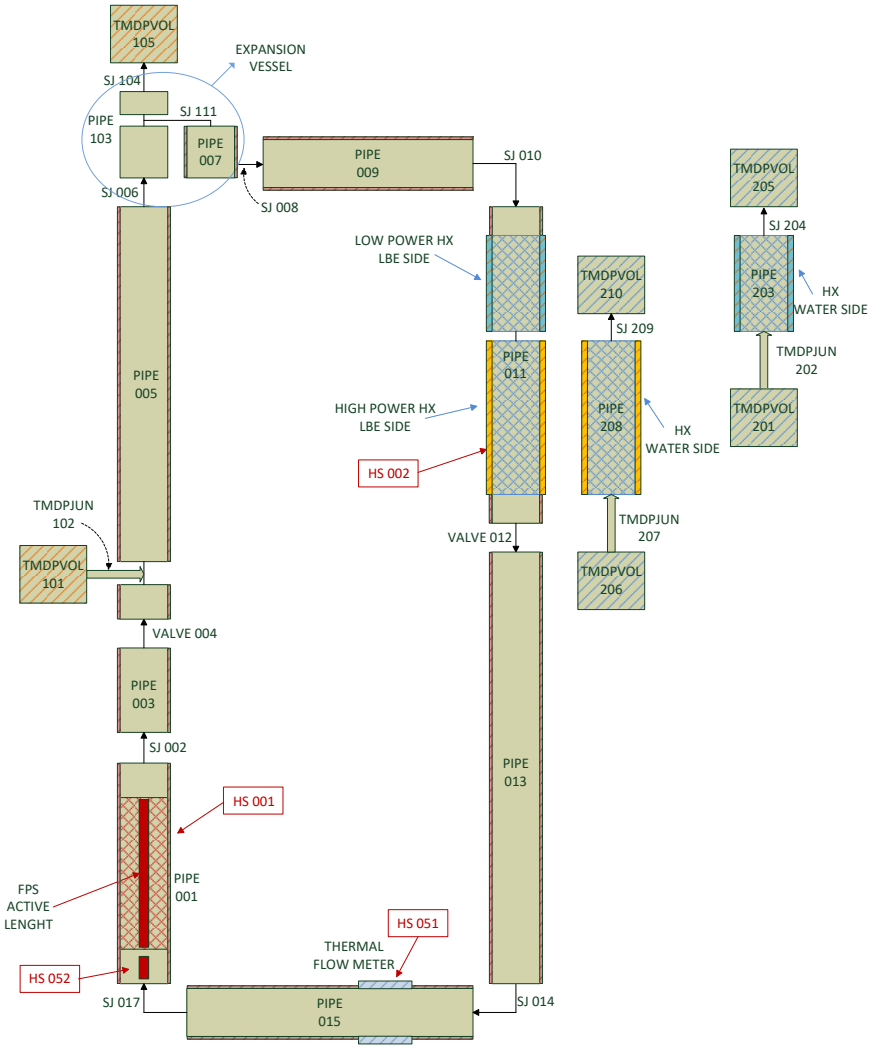

Fig. 6-28 – Up-dated model of the NACIE-UP loop

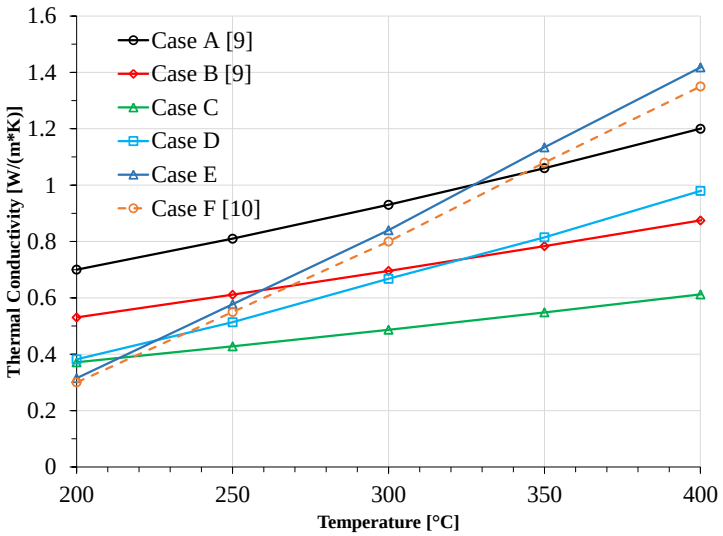

Fig. 6-29 – Stainless Steel Powder Thermal Conductivity

6.4.4.2 Test-1: Gas flow transition

The Fundamental Test 1 consists of a gas transition transient with the power of the Fuel Pin Simulator maintained constant at about 50 kW. The power trends of the FPS and the thermal flow meter are reported in Fig. 6-30, which shows as the BC assumed in the RELAP5-3D input data (red line in Fig. 6-30) reproduce truthfully the experimental trends. Fig. 6-31 shows the transition of the argon flow rate, which passes from the initial value of ~20 Nl/s (~$6x10^{-4}$ kg/s) to 10 Nl/s (~$3x10^{-4}$ kg/s) after the transient. The same figure also reports the water temperature at the inlet section of the heat exchanger. It is possible to notice as the water temperature suffers of slight oscillations when the transient occurs, which have been taken into account in the simulations. During the test, the water flow rate is set constant at 10 m^3/h.

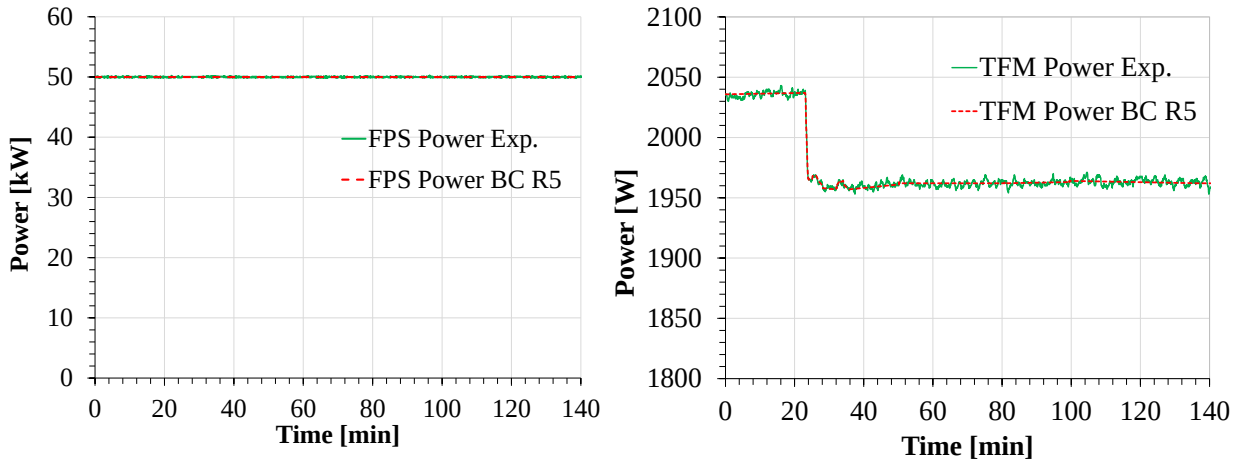

Fig. 6-30 – Power supplied by the Fuel Pin Simulator (left) and the Thermal Flow Meter (right) during the Test 1, experimental vs R5-3D

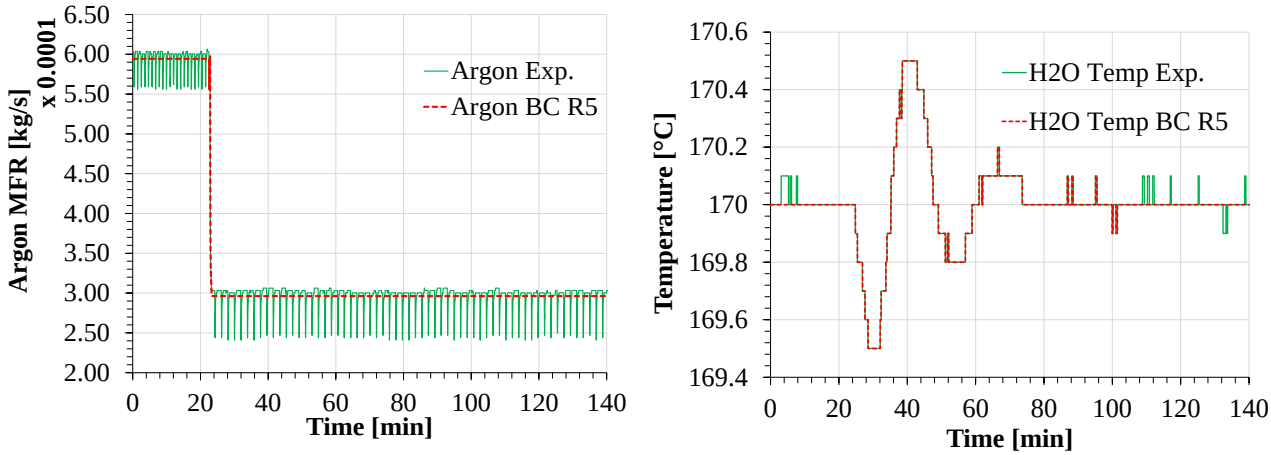

Fig. 6-31 – Argon Mass Flow Rate (left) and HX water inlet temperature (right) during Test 1, experimental vs R5-3D

The following graphs shows the numerical results, compared with the experimental data. In particular, the LBE mass flow rate is reported in Fig. 6-32, which shows a good agreement between the mass flow rate computed and the experimental data, both before and after the transient.

Concerning the temperatures, Fig. 6-33 and Fig. 6-34 report the LBE temperatures at the inlet and outlet sections of the FPS and HX respectively. From the comparison, it is possible to notice that the transient trends are well reproduced by the code. The temperatures achieved in the simulations are close to the experimental data with a maximum discrepancy of ~3°C. Finally, Fig. 6-35 reports the water temperatures at the inlet and outlet sections of the HX, showing that the transient trend is well reproduced. It can be noticed that the water outlet temperature is ~1°C higher than the experimental value. Considering the experimental data and applying the thermal balance equation in the HX, it is possible to see that there is an unbalance of thermal power between the LBE and water side. In particular, in Test 1 the power removed by water results ~40 kW, instead of 50 kW measured in the LBE side. This discrepancy could be due to the experimental uncertainty in the water mass flow rate and/or in the temperature measurements. Concerning the temperatures, the thermocouples typically have an error of ±1/±1.5°C which can affect significantly the measure, especially in this case in which the water delta T is small (~4°C in Test 1).

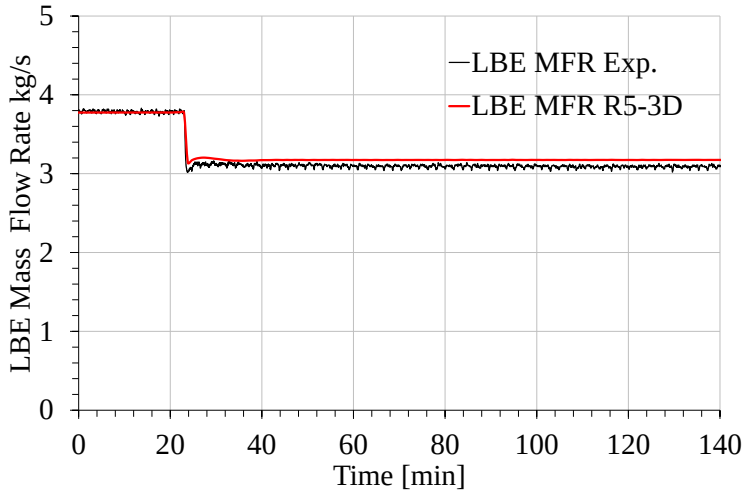

Fig. 6-32 – Test1, LBE Mass Flow Rate, experimental vs R5-3D

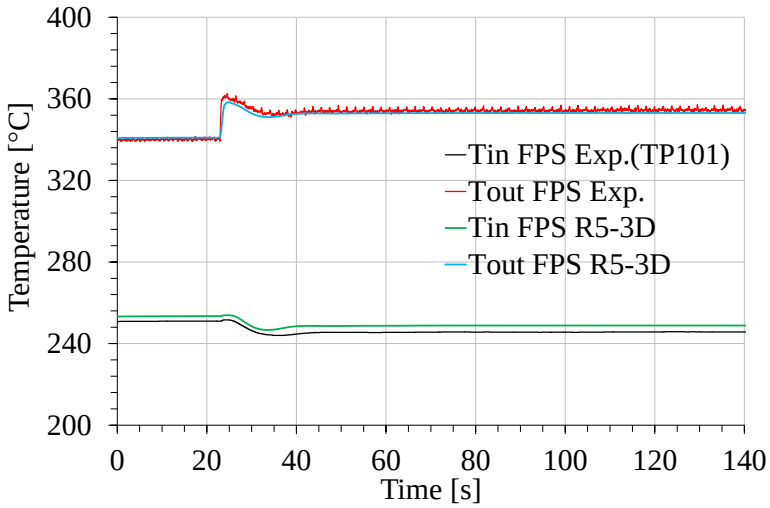

Fig. 6-33 – Test1, LBE temperatures at FPS inlet-outlet sections, experimental vs R5-3D

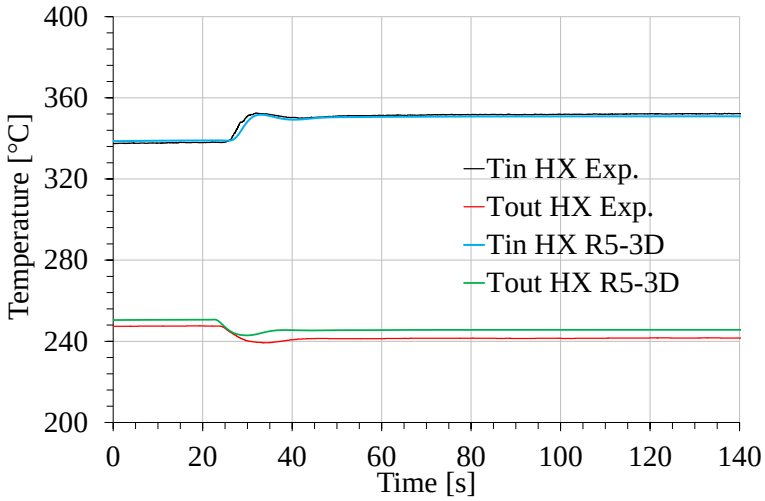

Fig. 6-34 – Test1, LBE temperatures at HX inlet-outlet sections, experimental vs R5-3D

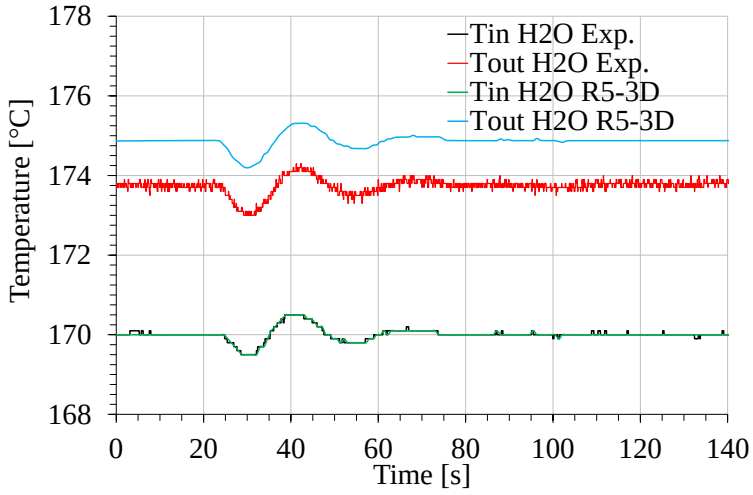

Fig. 6-35 – Test1, H2O temperatures at HX inlet-outlet sections, experimental vs R5-3D

6.4.4.3 Test-2: Power transition

The Fundamental Test 2 consists of a power transition transient, with the FPS power reduced from the initial value of ~100 kW to the final value of ~50 kW. The power trends of the FPS and the thermal flow meter have been reproduced and assumed as boundary conditions in the simulation, as reported in Fig. 6-36. During the test, the argon flow rate is maintained constant (see Fig. 6-37) at about 18 Nl/s (~5.35x10^{-4} kg/s), while the water mass flow rate is set constant at ~6.6 m^3/h. Also for this test, the HX feedwater temperature presents an instability when the transient occurs, which has been reproduced in the simulation (Fig. 6-37).

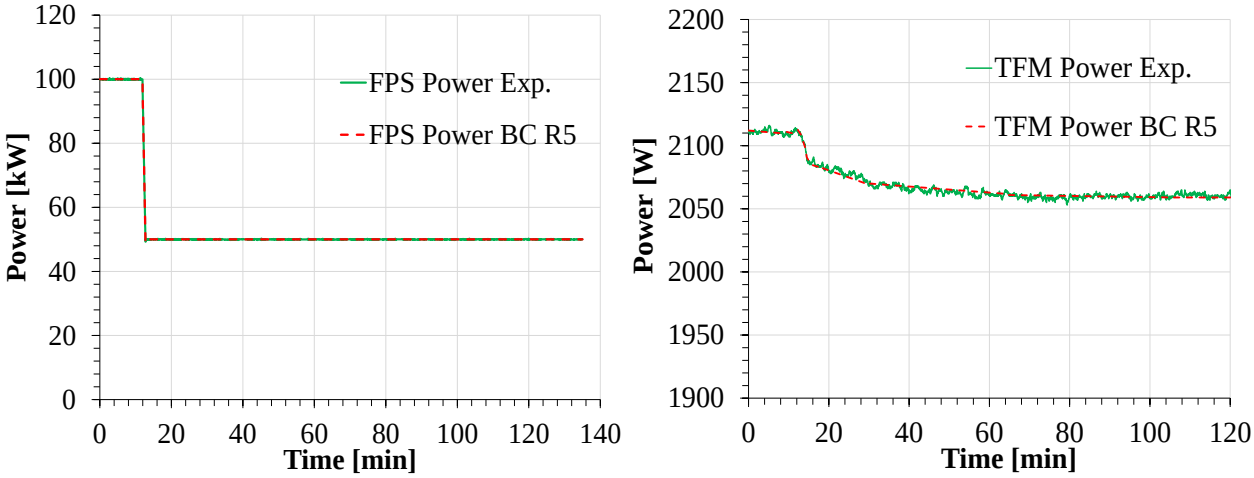

Fig. 6-36 – Power supplied by the Fuel Pin Simulator (left) and the Thermal Flow Meter (right) during the Test 2, experimental vs R5-3D

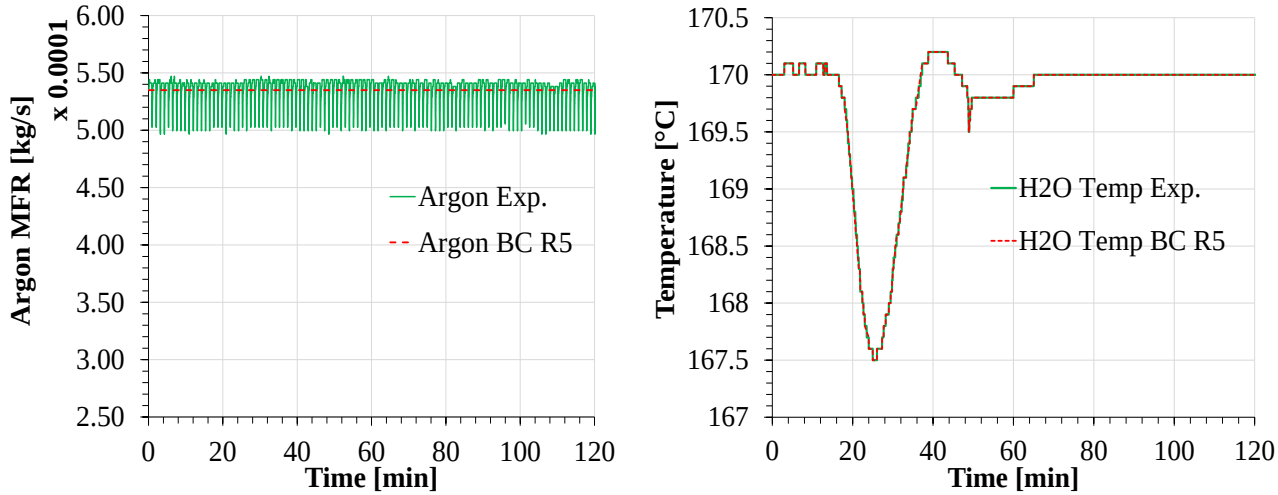

Fig. 6-37 – Argon Mass Flow Rate (left) and HX water inlet temperature (right) during Test 2, experimental vs R5-3D

Here below the results of the simulation of the Fundamental Test 2 are presented and compared with the experimental data. The LBE mass flow rate is reported in Fig. 6-38: before the transient, the mass flow rate computed by the code is about 4.2 kg/s, a value about 5% higher than the experimental one (~4.0 kg/s). During the transition, the mass flow calculated follows with a good agreement with the experimental data, overlapping the final value achieved when the steady-state is reached.

The temperatures in the primary loop are reported in Fig. 6-39 and Fig. 6-40 for the FPS and HX respectively. The comparison shows as the phenomena involved in the system during the experiment are well reproduced by the code, with the temperature transient trends which follow with a good agreement the experimental trends. Before the transient, the temperatures obtained from the simulations at the FPS outlet and HX inlet are very close to the experimental data, while the temperatures calculated at the FPS inlet and HX outlet are higher than the values reached during the experiments, due to the overestimation of the water mass flow rate. After the transient, all the temperatures are well captured by the code. Fig. 6-41 reports the water temperatures at the inlet and outlet sections of the HX. The water transient is well reproduced, while the outlet temperature calculated is ~2°C higher than the experimental value before the transient and ~1°C higher after the transient. The application of the thermal balance equation to the experimental data in the LBE and water side of the HX shows that the thermal power is not balanced. As reported in Test 1, the reason for this discrepancy could be found in the measurement's uncertainties of water mass flow rate or temperatures.

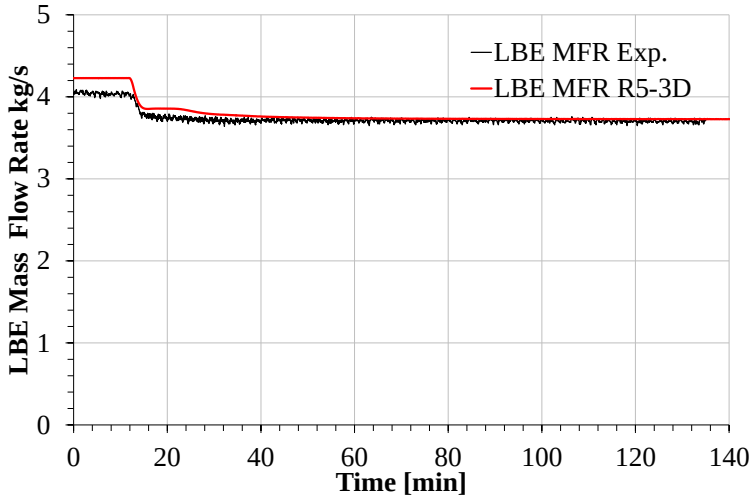

Fig. 6-38 – Test 2, LBE Mass Flow Rate, experimental vs R5-3D

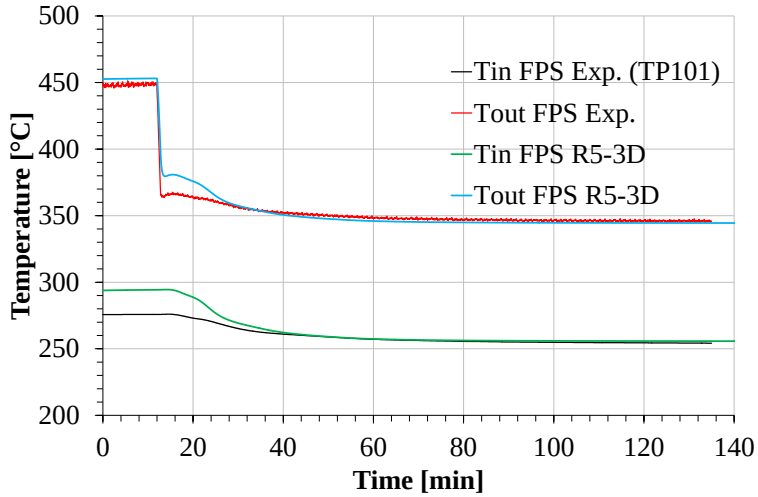

Fig. 6-39 – Test2, LBE temperatures at FPS inlet-outlet sections, experimental vs R5-3D

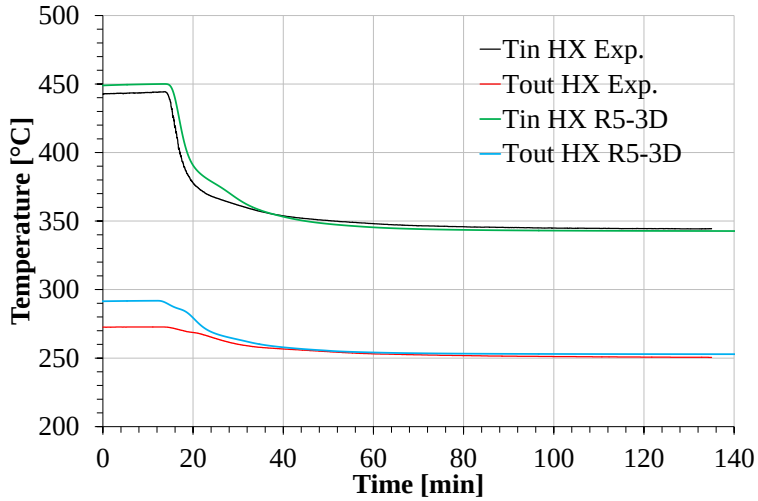

Fig. 6-40 – Test2, LBE temperatures at HX inlet-outlet sections, experimental vs R5-3D

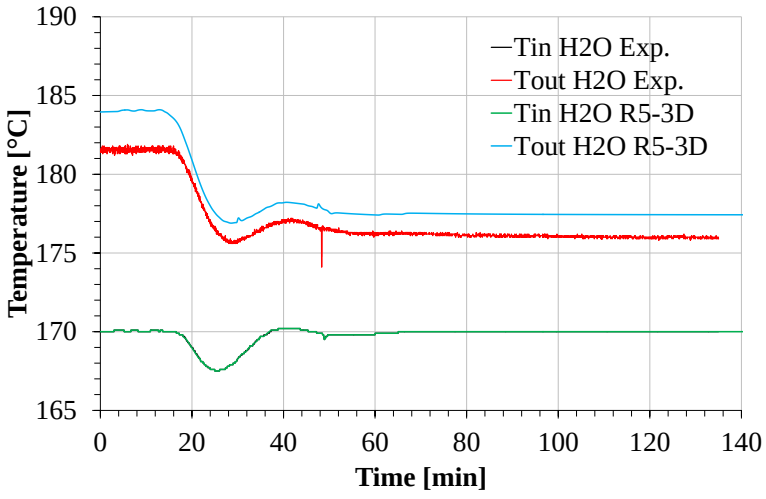

Fig. 6-41 – Test2, H2O temperatures at HX inlet-outlet sections, experimental vs R5-3D

6.4.4.4 Test-3: Protected Loss of Flow Accident (PLOFA)

The third fundamental test aims to reproduce a transient similar to a PLOFA, consisting of a power and argon mass flow rate transition in the primary loop, passing from a high power steady-state condition (FPS power ~100 kW) to a low power condition (FPS power ~10 kW), and with the argon flow rate reduced from 20 Nl/s to 0 Nl/s. The water mass flow rate of the secondary loop is set to 10 m^3/h. The boundary conditions assumed for the simulation of the test are reported in Fig. 6-42 and Fig. 6-43.

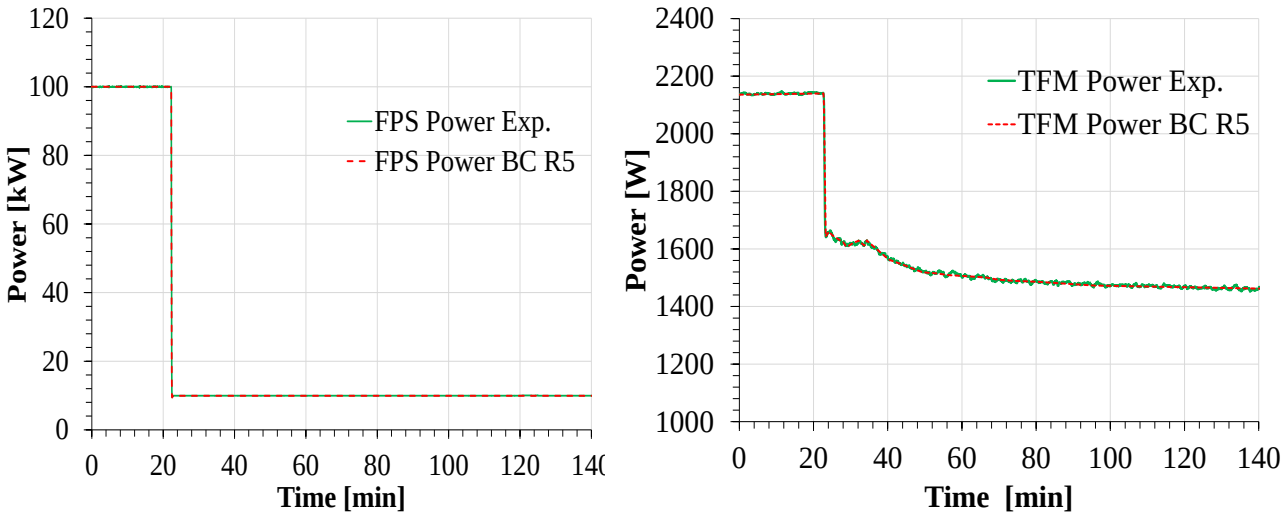

Fig. 6-42 – Power supplied by the Fuel Pin Simulator (left) and the Thermal Flow Meter (right) during the Test 3, experimental vs R5-3D

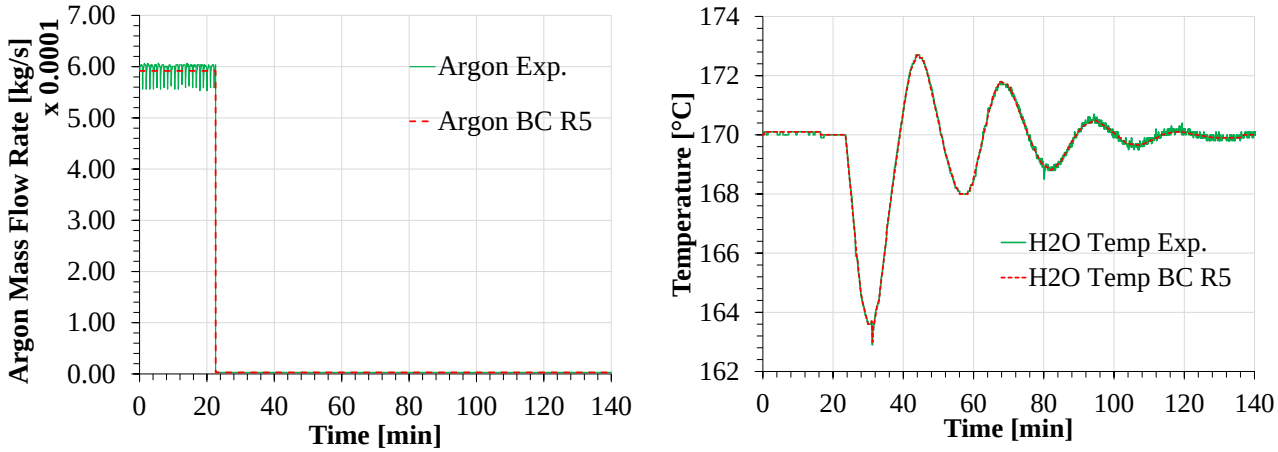

Fig. 6-43 – Argon Mass Flow Rate (left) and HX water inlet temperature (right) during Test 3, experimental vs R5-3D

Fig. 6-44 shows the LBE mass flow rate measured by the thermal mass flow meter and the mass flow rate obtained by R5-3D. The comparison shows a good agreement between the

two sets of values, with a good reproduction of the mass flow rate trend during the transient and during the two steady states achieved before and after the transition.

Concerning the primary loop, Fig. 6-45 and Fig. 6-46 report the LBE temperatures for the FPS and HX respectively. As already seen in the previous two tests, the comparison shows as the code is capable to reproduce in a reliable way the transient trends occurred during the experiment. Also for this test, the temperature range obtained from the simulations is comparable with the temperatures reached during the experiments. A slight overestimation of the HX outlet and FPS inlet can be noticed before the transient, due to the higher LBE mass flow rate computed. In the secondary loop, Fig. 6-47 reports the water temperatures at the inlet and outlet sections of the HX, showing that the temperature oscillations during the transient are well reproduced. As occurred in Test 1 and Test 2, there is a small discrepancy of ~0.5/~1°C between the numerical and experimental values, for the reasons already presented in the previous paragraphs.

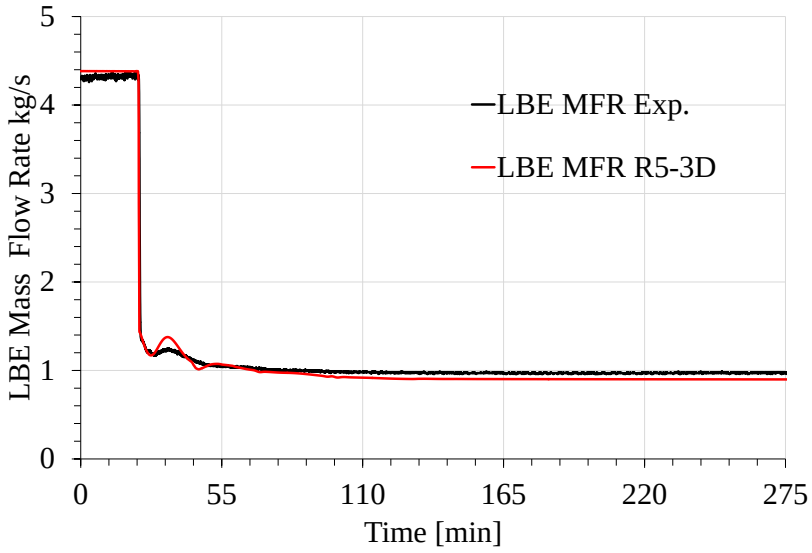

Fig. 6-44 – Test 3, LBE Mass Flow Rate, experimental vs R5-3D

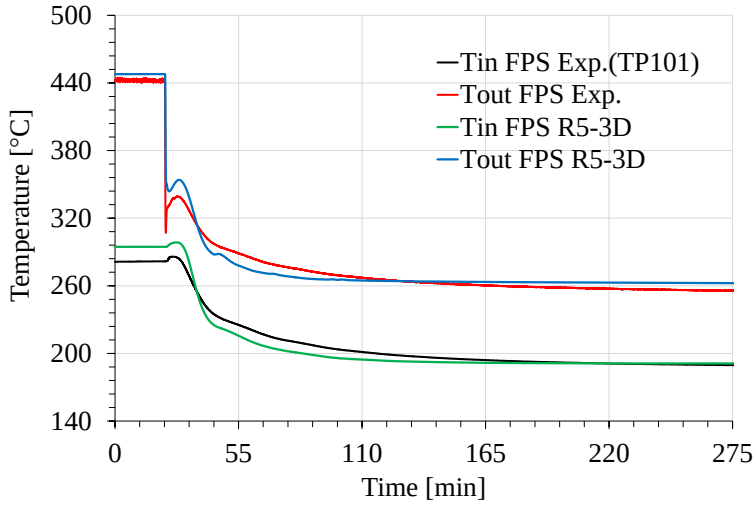

Fig. 6-45 – Test3, LBE temperatures at FPS inlet-outlet sections, experimental vs R5-3D

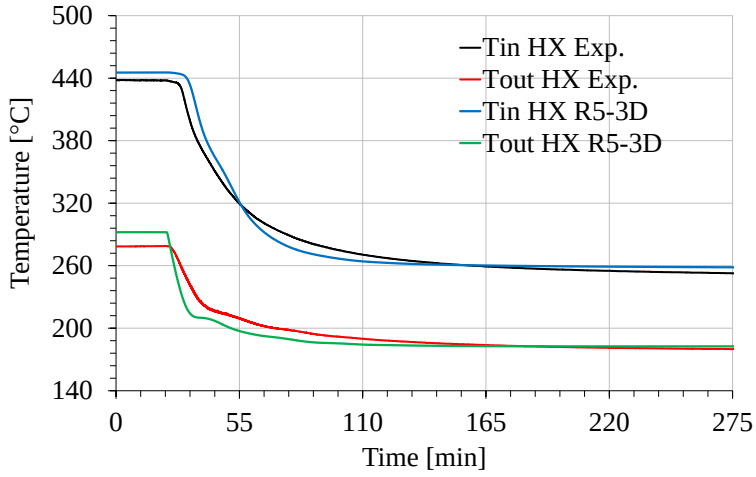

Fig. 6-46 – Test3, LBE temperatures at HX inlet-outlet sections, experimental vs R5-3D

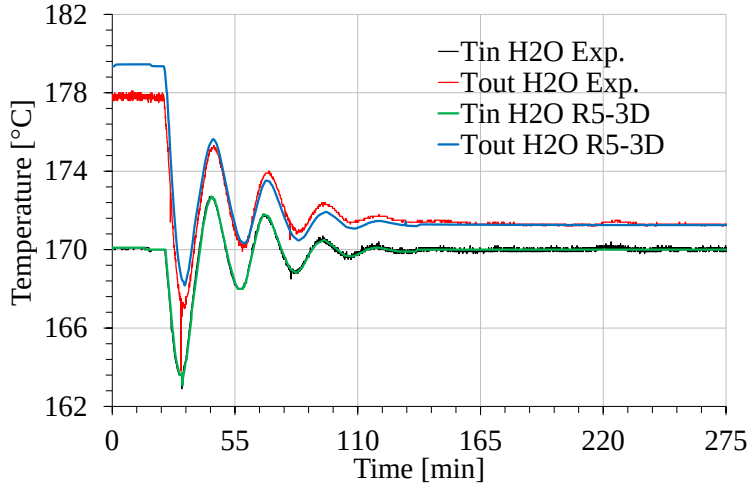

Fig. 6-47 – Test3, H2O temperatures at HX inlet-outlet sections, experimental vs R5-3D

(Page intentionally left blank)

7 FINAL SUMMARY AND CONCLUSIONS

7.1 FINAL SUMMARY

The present work has been realized thanks to the collaboration between the DIAEE of Sapienza University of Rome and ENEA and it aims at supporting the development of the LFRs - GEN IV reactors by means of experimental and numerical analysis of prototypical heavy liquid metal facilities. The activity is part of the research program of two EU projects: the H2020 SESAME project, which supports the development of the most relevant European liquid metal cooled reactors and H2020 MYRTE project, which supports the development of the MYRRHA research rector.

For two of the most important reactors under development in EU, ALFRED (LFR) and MYRRHA (ADS), a new configuration of the steam generator has been proposed, consisting of a tube bundle with double-wall bayonet tubes. The single-tube consists of four concentric tubes: starting from the inner one (slave tube), the water flows down and then it enters in an annular region (between the first and second tubes), flowing upward. In this zone the fluid starts its vaporization due to the heat exchange with the primary coolant (lead or LBE) which flows in counter-current along the shell side of the SG. The direct contact of the primary coolant with the second tube is avoided thanks to an additional tube (Third tube) which creates with the Second Tube an annular gap filled by stainless steel powder and inert gas in overpressure (~8-10 bar). This solution improves the plant safety, reducing the possibility of water-lead/LBE interaction, and allowing an easier control of eventual leakages from the coolant by pressurizing the separation region with inert gas.

In this framework, two experimental campaigns have been set-up and performed, involving the CIRCE facility at ENEA Brasimone R.C.. The experiments allowed to achieve important feedback on the HLM thermal-hydraulics, reproducing in relevant scale the operative conditions of LFRs, acquiring engineering and safety feedbacks for designer and high quality data for code validation/model development. Furthermore, a numerical benchmark activity has been performed on the LBE-cooled NACIE-UP experimental facility, developed and built in the ENEA Brasimone R.C., with the objective to validate the code RELAP5-3D© for the assessment of the thermal-hydraulic behaviour of the heavy liquid metals, in order to apply it for the simulation of the next LFRs - GEN IV reactors.

At the end of the doctoral activity, the following main goals have been achieved:

- set-up of the experimental facility CIRCE and implementation of the HERO test section;
- preliminary numerical analysis by RELAP5-3D© v. 4.3.4 code for the start-up procedure definition and thermal-hydraulic characterization of the HERO steam generator;
- execution and analysis of an experimental campaign on CIRCE-HERO facility in the framework of HORIZON2020 SESAME European project, in support of the development of the ALFRED steam generator;
- execution and analysis of an experimental campaign on CIRCE-HERO facility in the framework of HORIZON2020 MYRTE European project, in support of the development of the primary heat exchanger of MYRRHA;
- participation at Benchmark numerical activity on NACIE-UP HLM experimental facility in the framework of HORIZON2020 SESAME European project.

7.1.1 Set up and pre-test analysis of the experimental facility CIRCE-HERO

The large LBE pool-type facility CIRCE, has been involved in several experimental tests in support to the development of the LFR technologies. In particular, a focus has been given to investigate about the steam generator double-wall bayonet tube proposed for the ALFRED reactor in the framework of the LEADER project. For this purpose, a dedicated test section named HERO, representing the ALFRED steam generator (mockup 1:1 in length), has been designed by ENEA. The HERO SGBT is composed of a hexagonal shroud containing 7 SGBTs of similar geometry to the ALFRED SG and it is designed to be installed inside the main vessel of the CIRCE pool facility. When the facility is in operation, the LBE contained inside the pool is heated in the FPS and it reaches the separator on the top of the test section passing through the riser. Then it flows down crossing the shell side of the tube bundle for six meters (as in the SG of ALFRED), leaving the component from the bottom. A secondary once-through loop has been realized and instrumented, and it has been connected to the HERO SGBT, feeding the steam generator with demineralizer water at 335°C and about 172 bar.

A preliminary test analysis has been carried out by RELAP5-3D© ver. 4.3.4 in order to investigate on the secondary system behaviour, defining a procedure for the start-up of the facility and providing information about the managing of the water mass flow rate and the electrical power supplied to the helical heater. The steps defined for the procedure allow the system to achieve the nominal working operations with smooth time trends both

for pressure and temperatures. The control parameters (water mass flow rate, pressure, heater thermal power) have been managed in order to avoid thermal and mechanical stresses to the HERO bundle, allowing the passage of the feeding water only when the conditions required at the SGBT inlet are reached.

A preliminary thermal-hydraulic characterization of the HERO steam generator (~172 bar) has been carried out using RELAP5-3D©, evaluating the system behaviour during the nominal operating conditions. A sensitivity analysis has been realized considering different LBE mass flow rates and two sets of values for the AISI316L powder thermal conductivity. The simulations show a LBE temperature difference of about 75°C and a power removed of ~420 kW for the case with higher thermal conductivity and nominal LBE mass flow rate (RUN #1), while a LBE temperature difference of ~71°C and a power removed by HERO of ~400 kW for case with the lower thermal conductivity (RUN #4), showing that the powder thermal conductivity influences significantly the thermal-hydraulic performances of the steam generator.

7.1.2 Experimental campaign on CIRCE-HERO within H2020 SESAME

A high-pressure (172 bar) secondary loop experimental campaign has been realized in CIRCE-HERO in the framework of the HORIZON2020 SESAME European project. The test matrix is composed of three experimental transient tests aiming at reproducing PLOFA scenarios. The tests realized allow to evaluate the thermal-hydraulic performance of an LBE pool-type facility when an accidental scenario occurs, and to achieve experimental data relevant for the ALFRED SG and code validations.

The three transient tests start from the same steady-state conditions, characterized by ~0.33 kg/s of sub-cooled water entering into the 7 tubes of SGBT mock-up at about 172 bar and 335°C, and exiting in superheated steam condition at about 400°C. The LBE, flowing in the shell side of the SGBT with a mass flow rate of ~ 37 kg/s, is cooled from about 480°C to ~400°C. The transient tests investigated PLOFA scenarios, discerned on the basis of different transient reduction of power supplied by FPS, liquid metal gas lift (GEC) and feedwater mass flow rate. More specifically, in SE-Test#1 power decreased following the decay heat curve, gas lift was set to 0 kg/s and feedwater to 30% mass flow rate (simulating DHR system) in 2 s. The SE-Test#2 differs from the first one only for the feedwater reduction to 0% in about 2 s (without DHR). The SE-Test#3 simulated the power

decay curve, DHR (feedwater to 30% in 2 s) and reactor pump flywheel by a gas lift reduction based on a defined table.
During the tests, it has been possible to monitor the main thermal hydraulic parameters (temperatures, flow rates, pressures) for both primary and secondary systems, before and after the transient. The FPS power, the argon injection and the feedwater have been operated in order to reproduce as well as possible the features of the accidental scenario. The results show that in nominal operating conditions, the SG is capable to produce high temperature superheated steam. During the transients, despite the loss of the forced circulation regime of the coolant in the primary loop, the power transient leads to a sudden decrease of the LBE and pin clad temperatures along the FPS, avoiding dangerous peaks in the active region. The most severe condition has been achieved in SE-Test#2, in which the full loss of the heat sink leads to a temporal increase of the temperatures along the active length of the FPS, as long as the thermal heat losses from the main vessel balance the power supplied by the FPS. In SE-Test#1 and SE-Test#3, the overall reduction of the temperatures in the primary loop shows that, after the transients, the power removed by HERO acting as DHR system is higher than the power supplied by the FPS, leading the entire system to a safe long-term cooling condition.

7.1.3 Experimental campaign on CIRCE-HERO within H2020 MYRTE

A low-pressure (16 bar) secondary loop experimental campaign has been performed on CIRCE-HERO in the framework of the HORIZON2020 MYRTE European project. A test matrix consisting of nine low-pressure experimental tests in steady-state conditions has been performed. The tests realized allowed to evaluate the thermal-hydraulic performance of the HERO SG in working conditions relevant for the MYRRHA PHX.

During the steady-state tests, it has been possible to evaluate the supplied power to the FPS aiming at balancing the power removed by the SG and the heat losses to the environment, maintaining the LBE SG inlet temperature as close as possible to the target values foreseen for each test. The argon injection has been regulated in order to achieve the GEC and the stationary conditions of the LBE mass flow rate in each test have been successfully achieved. In the same way, the main components of the secondary loop (i.e. volumetric pump, helical heater, regulation valves) have been managed in order to maintain the water conditions designed for each test. A reference test has been set assuming an LBE inlet temperature of 235°C, a mass flow rate of 30 kg/s and water injection in the HERO SGBT at 198°C and 16 bar, with a total mass flow rate ~0.17 kg/s. An

experimental sensitivity analysis for each of these parameters has been performed in order to see the influence of their variations on the results.
The experimental sensitivity showed a similar general behaviour for Test Reference, Test #3, Test #4, Test #6, Test #7 and Test #8, characterized by a power removed by HERO in the range of 70-80 kW. The higher value of power removed by HERO has been achieved in Test #1 (~125 kW) characterised by the higher LBE SG inlet temperature, while the lower power has been achieved in Test #2 (~20 kW) characterised by the lower LBE SG inlet temperature, highlighting that the parameters which mostly influence the thermal-hydraulic performances of the system are the feedwater temperature and the temperature field inside the LBE pool. A low power removed is also achieved in Test #5 (~25 kW), where the HERO water inlet temperature has been increased from 198°C to 218°C, reducing in such a way the temperature difference between the LBE and the water, and consequently reducing the overall performances of the steam generator. About the pressure drops in the bayonet tubes, Test Reference, Test #3, Test #4, Test #6 and Test #8 present a similar behaviour with a ΔP between the inlet and outlet section of the BTs comprised between 0.5 bar and 0.8 bar. Test #1 and Test #2 show the higher pressure drops (1.4 bar and 1.15 bar, respectively): in the first case it is due to the higher power removed (higher LBE temperatures) which caused the higher steam mass fraction produced, in the second case it is due to the higher water mass flow rate. The opposite situation can be found in Test #2 (ΔP ~0.1 bar) and Test #5 (ΔP ~0.15 bar), due to the lower steam mass fraction produced, caused by the lower power removed for the Test #2, and by the higher overall pressure (23 bar) for the Test #5.

7.1.4 Benchmark numerical activity for RELAP5-3D© validation

In the framework of the HORIZON-2020 SESAME European Project, a numerical simulation activity has been carried out by the DIAEE of Sapienza University of Rome, aiming at supporting the validation process of the system thermal-hydraulic code RELAP5-3D© for heavy liquid metal reactors, in particular for the LBE. For this purpose, a numerical model of the loop-type facility NACIE-UP has been developed and used in a post-test analysis for the simulation of three experimental tests characterized by three different transients (power transient, gas flow rate transient and PLOFA scenario), comparing the numerical results obtained with the experimental data available from the experimental campaign.

The results of the simulations presented show that the RELAP5-3D© hydrodynamic model matches in a reliable way the experimental behaviour, with a good agreement between the LBE mass flow rate computed by the code and the mass flow rate measured by the thermal flow meter. The transient trends for the three tests are well captured by the code and the main phenomena have been well reproduced.

Concerning the thermal model, the temperature trends of LBE and water obtained by the code are very similar to the experimental ones, both for steady-state and transient conditions. An unbalance in the measured power removed by water from the LBE side produces a limited shift in the calculated outlet water temperature with respect to the experimental data. This discrepancy could be explained by the experimental uncertainty in the water mass flow rate and/or in the temperature measurements. An influence to such discrepancies can be also found in the set-up of the numerical model and, in particular, in the assumptions about the stainless steel powder thermal conductivity. For this reason, a sensitivity analysis on this parameter has been carried out, which led to a good reproduction of the experimental temperature trends, reducing in a relevant way the discrepancy between the computed and experimental temperatures ranges.

7.2 CONCLUSIONS AND FUTURE PLANS

The experimental data collected during the campaigns on CIRCE-HERO have provided relevant support on the knowledge and the experience in terms of design and operation of HLM pool facilities, such as CIRCE. During the experiments, the main components (i.e. FPS and SG) have been tested in a relevant scale for LFRs, as well as the main pool thermal-hydraulic phenomena have been reproduced and analysed. The activity has been finalized with the publication of Journal Papers and Conference Papers as reported in ANNEX 2. The thermal-hydraulic characterization of the system realized during the performed experimental campaigns has provided experimental data suitable for the comparison against the numerical simulations, allowing to carry out the improvement and refinement of the numerical model for the SYS-TH code validation activities. The experimental results presented in this document have been used during the code development and validation activities to perform post-test analyses for SYS-TH codes [52][53][54] and coupled calculation with SYS-TH/CFD codes [52][55].
Concerning the benchmark activity, the post-test analysis highlighted that RELAP5-3D© code is capable to predict in a reliable way both operational and accidental transients

reproduced by NACIE-UP and it represents a promising numerical tool for the simulation of the main thermal-hydraulic phenomena occurring in LBE-cooled loop-type facilities.
The next steps foresee the refurbishment of the CIRCE facility. The HERO test section will be substituted with a new one in which the gas injection system will be replaced by an axial centrifugal pump designed ad-hoc for heavy liquid metals. The 7 tube SG will be also replaced with a new one consisting of a helical tube bundle SG. This new configuration will support one of the last up-dated solutions of the ALFRED SG. The experimental activities will be supported by thermal-hydraulic numerical analyses by SYS-TH codes to continue the development and validation process of software tools for their application for LFRs - GEN IV nuclear reactors.

(Page intentionally left blank)

REFERENCES

[1] USDOE & GIF, 2002. A Technology Roadmap for Generation-IV Nuclear Energy Systems, GIF-002–00.

[2] USDOE & GIF, 2014. Technology Roadmap Update for Generation IV Nuclear Energy Systems.

[3] Cinotti, L., Smith, C., F., Artioli, C., Grasso, G., Corsini, G., 2010. Lead-Cooled Fast Reactor (LFR) Design: Safety, Neutronics, Thermal Hydraulics, Structural Mechanics, Fuel, Core, and Plant Design, Handbook of Nuclear Engineering, DOI 10.1007/978-0-387-98149-9_23.

[4] The Generation IV International Forum, 2018. GIF R&D Outlook for Generation IV Nuclear Energy Systems: 2018 Update.

[5] OECD/NEA Nuclear Science Committee, 2015. Handbook on Lead-bismuth Eutectic Alloy and Lead Properties, Materials Compatibility, Thermal-hydraulics and Technologies. https://www.oecd-nea.org/science/pubs/2015/7268-leadbismuth-2015.pdf.

[6] MYRRHA Team, 2011, MYRRHA Technical Description, SCK-CEN report.

[7] Alemberti, A., Frignani, M., Villabruna, G., Agostini, P., Grasso, G., Tarantino, M., Turcu, I., Constantin, M.. Diaconu, D., Di Gabriele, F., Witzanyová, N., Kryková, M., 2015. ALFRED and the lead technology research infrastructure, Proceedings of European Research Reactor Conference (RRFM) 2015.

[8] Frignani, M., Alemberti, A., Villabruna, G., Grasso, G., Tarantino, M., Constantin M., Turcu I., Valeca, S., Di Gabriele, F., Romanello. V., 2015. FALCON advancements towards the implementation of the ALFRED Project, IAEA-CN245-485.

[9] Agostini, P., et al., 2014. HLM-cooled Nuclear Systems Status and Prospective of Development, LR-P-R-105.

[10] IAEA Nuclear Energy Series,.2018. Experimental facilities in support of liquid metal cooled fast neutron systems, No. NP-T-1.15.

[11] Stieglitz, R., Knebel, J., Fazio, C., Müller, G. Konys, J., 2006, Heavy liquid metal thecnologies development in KALLA, Proceedings of ICAPP '06 Reno, NV USA, June 4-8, 2006.

[12] Grishchenko, D., Jeltsov, M., Kööp, K., Karbojian, A., Villanueva, W., Kudinov, P., 2015. The TALL-3D facility design and commissioning tests for validation of coupled STH and CFD codes, Nucl. Eng. Des., 290(2015)144–153, http://dx.doi.org/10.1016/j.nucengdes.2014.11.045.

[13] Van Tichelen, K., Mirelli, F., Greco, M., Viviani, G., 2015. E-SCAPE: A scale facility for liquid-metal, pool-type reactor thermalhydraulic investigations, Nucl. Eng. Des., 290 (2015) 65–77, http://dx.doi.org/10.1016/j.nucengdes.2014.11.011.

[14] Kennedy, G., Van Tichelen, K., Doolaard, H., 2015. Experimental investigation of the pressure loss characteristics of the full-scale MYRRHA fuel bundle in the COMPLOT LBE facility, NURETH-16, Chicago, IL, August 30-September 4, 2015.

[15] Del Giacco, M.; Weisenburger, A.; Mueller, G. Fretting corrosion of steels for lead alloys cooled ADS. Journal of Nuclear Materials, 450(2014) pp.225-236.

[16] Wu, Y., 2016. CLEAR-S: an integrated non-nuclear test facility for China lead-based research reactor, International Journal of Energy Research 2016; 40:1951–1956, DOI: 10.1002/er.3569.

[17] Wu, Y., 2016. Design and R&D Progress of China Lead-Based Reactor for ADS Research Facility, Engineering 2 (2016) 124–131, http://dx.doi.org/10.1016/J.ENG.2016.01.023.

[18] Lorusso P., Pesetti A., Tarantino M., 2019, ALFRED Steam Generator Assessment: design and pre-test analysis of HERO experiment, Proceedings of the 2018 26th International Conference on Nuclear Engineering, July 22-26, 2018, London, England, ICONE26-81824, doi: 10.1115/ICONE26-81824.

[19] Pesetti, A., Tarantino, M., Gaggini, P., Polazzi, G., Forgione, N., 2017. Commissioning of CIRCE Facility for SGTR Experimental Investigation for HLMRS and Pre-Test Analysis by SIMMER-IV Code, International Conference on Nuclear Engineering, paper ICONE25-67419, Shanghai, China, DOI: 10.1115/ICONE2567419.

[20] Rozzia, D., Pesetti, A., Del Nevo, A., Tarantino, M., Forgione, N., 2017. Hero test section for experimental investigation of steam generator bayonet tube of ALFRED. International Conference on Nuclear Engineering, Proceedings, ICONE, 5 doi: 10.1115/ICONE2567422.

[21] Pesetti., A., et al., ENEA CIRCE-HERO test facility: geometry and instrumentation description, ENEA report CI-I-R-343, June 2018.

[22] Tarantino, M., Martelli, D., Barone, G., Di Piazza, I., Forgione, N., 2015. Mixed convection and stratification phenomena in a heavy liquid metal pool. Nucl. Eng. Des. 286, 261–277. https://doi.org/10.1016/j.nucengdes.2015.02.012.

[23] Narcisi V., Giannetti F., Del Nevo A., Tarantino M., Caruso G., Pre-test analysis of accidental transients for ALFRED SGBT mock-up characterization. Nucl. Eng. Des., vol. 333, pp. 181-195. https://doi.org/10.1016/j.nucengdes.2018.04.015

[24] Narcisi, V., Giannetti, F., Tarantino, M., Martelli, D., Caruso, G., 2017, Pool temperature stratification analysis in CIRCE-ICE facility with RELAP5-3D© model and comparison with experimental tests. Journal of Physics: Conference Series, 923 (1), art. no. 012006, DOI: 10.1088/1742-6596/923/1/012006

[25] Ambrosini W., Azzati M., Benamati G., Bertacci G., Cinotti L., Forgione N., Oriolo F., Scaddozzo G. Tarantino M., 2004, Testing and qualification of CIRCE instrumentation based on bubble tubes, Journal of Nuclear Materials 335 (2004) 293–298, doi:10.1016/j.jnucmat.2004.07.030

[26] Lorusso P., Del Nevo A., Tarantino M., Hamidouche T., Castelliti D., Rozzia D., Narcisi V., Giannetti F., Caruso G., 2019, D5.8 CIRCE-HERO Blind Simulations, D5.8, deliverable SESAME, May, 28, 2019.

[27] Rozzia, D., Forgione, N., Fasano, G., Tarantino, M., Del Nevo, A., Alemberti, A., 2015. "Experimental Investigation on Powder Conductivity for the Application to Double Wall Bayonet Tube Bundle Steam Generator", 24th NENE Conference, (2015).

[28] ENEA internal report on characterization of AISI316L powder and helium thermal conductivity in NACIE facility experiments.

[29] SESAME Project, EURATOM H2020, Grant Agreement N. 654935, April 2015.

[30] Frignani, M, Alemberti, A., Villabruna, G, Adinolfi, R., Tarantino, M., Grasso, G., Pizzuto, A., Turcu, I., Valeca, S., 2017. ALFRED: A Strategic Vision for LFR Deployment. ANS Winter Meeting 2017, Washington, D.C., October 29-November 2, 2017.

[31] P. Lorusso, D4.4 CIRCE-HERO PLOFA Experiment, D4.4, SESAME report, January, 22, 2019.

[32] Lorusso P., Pesetti A., Tarantino M., Narcisi V., Giannetti F., Forgione N., Del Nevo A., 2019, Experimental Analysis Of Stationary And Transient Scenarios Of ALFRED Steam Generator Bayonet Tube In CIRCE-HERO Facility, Nuclear Engineering and Design 352 (2019) 110169, https://doi.org/10.1016/j.nucengdes.2019.110169.

[33] Lorusso P., Pesetti A., Tarantino M., Narcisi V., 2019, Protected Loss Of Flow Accident Simulation In Circe-Hero Facility: Experimental Test And System Code Assessment, Proceedings of the 2019 27th International Conference on Nuclear Engineering, May 19-24, 2019, Tsukuba, Ibaraki, Japan, ICONE27-2269.

[34] MYRTE Project, EURATOM H2020, 2015, Grant Agreement N. 662186.

[35] De Bruyn D., Fernandez R. Baeten P., 2018, The Belgian MYRRHA ADS Programme. Part 2: Recent developments in the reactor primary system, 2018 International Congress on Advances in Nuclear Power Plants (ICAPP'18), Charlotte (North Carolina, USA), paper 23801, 1074-1079.

[36] Lorusso, P., CIRCE Experimental Report, D3.2, MYRTE report, October, 31, 2018.

[37] Lorusso P., Pesetti A., Tarantino M., 2019, Double Wall Bayonet Tube Steam Generator Investigation In HERO Experimental Campaign, Proceedings of the 2019 27th International Conference on Nuclear Engineering, May 19-24, 2019, Tsukuba, Ibaraki, Japan, ICONE27-2208.

[38] Lorusso P., Pesetti A., Barone G., Castelliti D., Caruso G., Forgione N., Giannetti F., Martelli D., Rozzia D., Van Tichelen K., Tarantino M., 2019, MYRRHA primary heat exchanger experimental simulations on CIRCE-HERO, Nuclear Engineering and Design 353C (2019) 110270, https://doi.org/10.1016/j.nucengdes.2019.110270.

[39] Forgione N., Angelucci M., Martelli D., Ambrosini W., Di Piazza I., 2017, Proposal for a Numerical Benchmark on thermal-hydraulics for heavy liquid metal cooled system, rev.1, Task 5.4 SESAME.

[40] Di Piazza, I., Angelucci, M., Marinari, R., Tarantino, M., Forgione, N., Heat transfer on HLM cooled wire-spaced fuel pin bundle simulatorin the NACIE-UP facility, Nuclear Engineering and Design 300 (2016) 256–267, http://dx.doi.org/10.1016/j.nucengdes.2016.02.008.

[41] Idelchik I. E., "Handbook of hydraulic Resistance", 3rd edition, Jaico Publishing House, 2003.

[42] S.K.Chen et al., "Evaluation of existing correlations for the prediction of pressure drop in wire-wrapped hexagonal array pin bundles", Nuclear Engineering and Design 267 (109-131), 2014.

[43] The RELAP5-3D Code Development Team, "RELAP5-3D© Code Manual Vol. IV: Models and Correlations", INEEL-EXT-98-00834.

[44] The RELAP5-3D Code Development Team, "RELAP5-3D© Input Data Requirements", INEEL-EXT-98-00834-V2AppA

[45] C. B. Davis A. S. Shieh, "Overview of the Use of ATHENA for Thermal-Hydraulic Analysis of Systems with Lead-Bismuth Coolant", 8th International Conference on Nuclear Engineering, INEEL/CON-2000-00127

[46] The RELAP5-3D Code Development Team, "RELAP5-3D© Code Manual Vol. I: Code Structure, System Models and Solution Methods", INEEL-EXT-98-00834.

[47] Forgione N., Angelucci M., Barone G., Polidori M., Cervone A., Di Piazza I., Giannetti F., Lorusso P., Hollands T., Papukchiev A., 2018, Blind simulations of NACIE-UP experimental tests by STH codes, Proceedings of the 2018 26th International Conference on Nuclear Engineering, July 22-26, 2018, London, England, ICONE26-81434, doi:10.1115/ICONE26-81434.

[48] Forgione N., Angelucci M., Barone G., Caruso G., Hollands T., Polidori M., Cervone A., 2017, D5.18 – NACIE-UP blind simulations, Task 5.4 SESAME.

[49] Di Piazza, I., Angelucci, M., Marinari, R., Tarantino, M., Martelli, D., 2019. Thermo-fluid dynamic transients in the NACIE-UP facility, Nuclear Engineering and Design 352 (2019) 110182, https://doi.org/10.1016/j.nucengdes.2019.110182.

[50] Forgione, N., Martelli, D., Barone, G., Giannetti, F., Lorusso, P., Hollands, T., Papukchiev, A., Polidori, M., Cervone, A., Di Piazza, I., 2019, Post-test simulations for the NACIE-UP benchmark by STH codes, Nuclear Engineering and Design 353 (2019) 110279, https://doi.org/10.1016/j.nucengdes.2019.110279.

[51] Rozzia, D., Fasano, G., Di Piazza, I., Tarantino, M., 2015. "Experimental investigation on powder conductivity for the application to double wall heat exchanger (NACIE-UP)", Nuclear Engineering and Design 283 (2015) 100–113, 2014, https://doi.org/10.1016/j.nucengdes.2014.06.037.

[52] Del Nevo, A., Lorusso, P., Tarantino, M., Zwijsen, K., Breijder, P.A., Hamidouche, T., Castelliti, D., Rozzia, D., Narcisi, V., Giannetti, F., Caruso, G., D5.11 CIRCE-HERO simulation validation summary report, D5.11, SESAME report, May, 30, 2019.

[53] Narcisi, V., Giannetti, F., Del Nevo, A., Tarantino, M., Caruso, G., 2019. Post-test simulation of a PLOFA transient test in the CIRCE-HERO facility, Nuclear Engineering and Design 355 (2019) 110321, https://doi.org/10.1016/j.nucengdes.2019.110321.

[54] Castelliti, D., Hamidouche, T., Lorusso, P., Tarantino, M., 2019. H2020 MYRTE CIRCE-HERO experimental campaign post-test activity and code validation, 18th

International Topical Meeting on Nuclear Reactor Thermal Hydraulics (NURETH-18), Portland, Oregon, August 18-23, 2019.

[55] Galleni, F., Barone, G., Martelli, D., Pucciarelli, A., Lorusso, P., Tarantino, M., Forgione, N., 2019. Simulation of operational conditions of HX-HERO in the CIRCE facility with CFD/STH coupled codes, Submitted to Nuclear Engineering and Design.

ANNEX 1 – CIRCE-HERO Instrumentation List

LBE SIDE										
#	**ID**	**Instrument Location**			**Measurement**					**Data File**
		SYS	**Zone**	**Elev./ Pos.**	**Variable**	**Unit**	**MST Range**			
							Min	**Max**	**Er.**	
1	DP Ven	S100	DP of Venturi Flow Meter	Between inlet and throat taps of Venturi flow meter	Pressure	[mbar]	0 bar(g)	0.4 bar(g)	±0.1%	LBE-Side_Pressure.txt
2	PC-LH	Helium Line	Pressure of the Helium Line	----	Pressure	[bar]	0	25	±0.5%	LBE-Side_Pressure.txt
3	PE007	S100	Pressure of BT inside the CIRCE Cover Gas	----	Pressure	[mbar]	0 bar(g)	1 bar(g)	±0.1%	LBE-Side_Pressure.txt
4	PE003	S100	Pressure of BT in the Fitting Volume	α = ~160° 170 mm from FV bottom	Pressure	[mbar]	0 bar(g)	5 bar(g)	±0.1%	LBE-Side_Pressure.txt
5	PE004	S100	Pressure of BT at the inlet of the RISER	170 mm from FV bottom	Pressure	[mbar]	0 bar(g)	5 bar(g)	±0.1%	LBE-Side_Pressure.txt
6	PE005	S100	Pressure of BT at the outlet of the RISER	42 mm above separator bottom	Pressure	[mbar]	0 bar(g)	2 bar(g)	±0.1%	LBE-Side_Pressure.txt
7	FE400	Argon Injection Line	Gas Lift - Argon Flow Rate	Downstream Ar tank	Flow Rate	Nl/s	0.2	10	±(0.1% +0.5%Read)	LBE-Side_Flow_Rate.txt
8	Mm(LBE)	S100	LBE mass flow rate (measured)		Mass Flow Rate	kg/s	----	----	----	LBE-Side_Flow_Rate.txt
9	LE001	S100	LBE Level Probe inside the Separator	800 mm from the bottom (50 mm from top)	Level		----	----	----	LBE-Side_Levels.txt
10	LE002	S100	LBE Level Probe inside the Separator	310 mm from the bottom	Level		----	----	----	LBE-Side_Levels.txt

11	DC-kW	Supply System	FPS electrical power supplied	----	Power	kW	----	----	Transmitter: ±(0.1%+0.5%) V: ±0.1%	LBE-Side_Power.txt
12	T-FPS-01	S100 - Fuel Pin Simulator	Subchannel temperature among Pin 1-2-7	20 mm upstream Middle Spacer Grid Section 1	Temperature	°C	0	600	±1.5/±2°C	LBE-Side_FPS_Temp.txt
13	T-FPS-02	S100 - Fuel Pin Simulator	Subchannel temperature among Pin 7-17-18	20 mm upstream Middle Spacer Grid Section 1	Temperature	°C	0	600	±1.5/±2°C	LBE-Side_FPS_Temp.txt
14	T-FPS-03	S100 - Fuel Pin Simulator	Subchannel temperature among Pin 17-33-34	20 mm upstream Middle Spacer Grid Section 1	Temperature	°C	0	600	±1.5/±2°C	LBE-Side_FPS_Temp.txt
15	T-FPS-04	S100 - Fuel Pin Simulator	Wall temperature Pin 1	20 mm upstream Middle Spacer Grid Section 1	Temperature	°C	0	600	±1.5/±2°C	LBE-Side_FPS_Temp.txt
16	T-FPS-05	S100 - Fuel Pin Simulator	Wall temperature Pin 7	20 mm upstream Middle Spacer Grid Section 1	Temperature	°C	0	600	±1.5/±2°C	LBE-Side_FPS_Temp.txt
17	T-FPS-08	S100 - Fuel Pin Simulator	Wall temperature Pin 34	20 mm upstream Middle Spacer Grid Section 1	Temperature	°C	0	600	±1.5/±2°C	LBE-Side_FPS_Temp.txt
18	T-FPS-10	S100 - Fuel Pin Simulator	Wall temperature Pin 1	Middle Spacer Grid bottom Section 2	Temperature	°C	0	600	±1.5/±2°C	LBE-Side_FPS_Temp.txt
19	T-FPS-14	S100 - Fuel Pin Simulator	Wall temperature Pin 33	Middle Spacer Grid bottom Section 2	Temperature	°C	0	600	±1.5/±2°C	LBE-Side_FPS_Temp.txt
20	T-FPS-16	S100 - Fuel Pin Simulator	Wall temperature Pin 1	60 mm upstream Upper Spacer Grid Section 3	Temperature	°C	0	600	±1.5/±2°C	LBE-Side_FPS_Temp.txt
21	T-FPS-18	S100 - Fuel Pin Simulator	Wall temperature Pin 18	60 mm upstream Upper Spacer Grid Section 3	Temperature	°C	0	600	±1.5/±2°C	LBE-Side_FPS_Temp.txt

22	T-FPS-19	S100 - Fuel Pin Simulator	Wall temperature Pin 17	60 mm upstream Upper Spacer Grid Section 3	Temperature	°C	0	600	±1.5/±2°C	LBE-Side_FPS_Temp.txt
23	T-FPS-20	S100 - Fuel Pin Simulator	Wall temperature Pin 33	60 mm upstream Upper Spacer Grid Section 3	Temperature	°C	0	600	±1.5/±2°C	LBE-Side_FPS_Temp.txt
24	T-FPS-21	S100 - Fuel Pin Simulator	Subchannel temperature among Pin 17-33-34	60 mm upstream Upper Spacer Grid Section 3	Temperature	°C	0	600	±1.5/±2°C	LBE-Side_FPS_Temp.txt
25	T-FPS-22	S100 - Fuel Pin Simulator	Wall temperature Pin 34	60 mm upstream Upper Spacer Grid Section 3	Temperature	°C	0	600	±1.5/±2°C	LBE-Side_FPS_Temp.txt
26	T-FPS-23	S100 - Fuel Pin Simulator	Subchannel temperature among Pin 7-17-18	60 mm upstream Upper Spacer Grid Section 3	Temperature	°C	0	600	±1.5/±2°C	LBE-Side_FPS_Temp.txt
27	T-FPS-24	S100 - Fuel Pin Simulator	Subchannel temperature among Pin 1-2-7	60 mm upstream Upper Spacer Grid Section 3	Temperature	°C	0	600	±1.5/±2°C	LBE-Side_FPS_Temp.txt
28	T-FPS-25	S100 - Fuel Pin Simulator	Subchannel temperature among Pin 18-34-35	Through Middle Spacer Grid	Temperature	°C	0	600	±1.5/±2°C	LBE-Side_FPS_Temp.txt
29	T-FPS-26	S100 - Fuel Pin Simulator	Subchannel temperature among Pin 18-34-35	Through Upper Spacer Grid	Temperature	°C	0	600	±1.5/±2°C	LBE-Side_FPS_Temp.txt
30	T-FPS-27	S100 - Fuel Pin Simulator	Subchannel temperature among Pin 18-34-35	Through Lower Spacer Grid	Temperature	°C	0	600	±1.5/±2°C	LBE-Side_FPS_Temp.txt
29	T-FPS-28	S100 - Fuel Pin Simulator	Subchannel temperature among Pin 17-33-34	60 mm downstream Lower Spacer Grid Section 4	Temperature	°C	0	600	±1.5/±2°C	LBE-Side_FPS_Temp.txt
32	T-FPS-29	S100 - Fuel Pin Simulator	Subchannel temperature among Pin 7-17-18	60 mm downstream Lower Spacer Grid Section 4	Temperature	°C	0	600	±1.5/±2°C	LBE-Side_FPS_Temp.txt
33	T-FPS-30	S100 - Fuel Pin Simulator	Subchannel temperature among Pin 1-2-7	60 mm downstream Lower Spacer Grid Section 4	Temperature	°C	0	600	±1.5/±2°C	LBE-Side_FPS_Temp.txt

34	T-FPS-31	S100 - Fuel Pin Simulator	LBE temperature at FPS inlet	Aligned to bubble tube connections of Lower Spacer Grid at 120° to T-FPS-32 and T-FPS-33	Temperature	°C	0	600	±1.5/±2°C	LBE-Side_FPS_Temp.txt
35	T-FPS-32	S100 - Fuel Pin Simulator	LBE temperature at FPS inlet	At 120° to T-FPS-31 and T-FPS-33	Temperature	°C	0	600	±1.5/±2°C	LBE-Side_FPS_Temp.txt
36	T-FPS-33	S100 - Fuel Pin Simulator	LBE temperature at FPS inlet	At 120° to T-FPS-31 and T-FPS-32	Temperature	°C	0	600	±1.5/±2°C	LBE-Side_FPS_Temp.txt
37	T-FPS-34	S100 - Fuel Pin Simulator	LBE temperature at FPS outlet	Aligned to T-FPS-31 penetration at 120° to T-FPS-35 and T-FPS-36	Temperature	°C	0	600	±1.5/±2°C	LBE-Side_FPS_Temp.txt
38	T-FPS-35	S100 - Fuel Pin Simulator	LBE temperature at FPS outlet	Aligned to T-FPS-32 penetration at 120° to T-FPS-34 and T-FPS-36	Temperature	°C	0	600	±1.5/±2°C	LBE-Side_FPS_Temp.txt
39	T-FPS-36	S100 - Fuel Pin Simulator	LBE temperature at FPS outlet	Aligned to T-FPS-33 penetration at 120° to T-FPS-34 and T-FPS-35	Temperature	°C	0	600	±1.5/±2°C	LBE-Side_FPS_Temp.txt
40	T-FPS-37	S100 - Fuel Pin Simulator	LBE temperature at FPS outlet windows	Top windows of FPS hexagonal shroud	Temperature	°C	0	600	±1.5/±2°C	LBE-Side_FPS_Temp.txt
41	T-FPS-38	S100 - Fuel Pin Simulator	LBE temperature at FPS outlet windows	Top windows of FPS hexagonal shroud	Temperature	°C	0	600	±1.5/±2°C	LBE-Side_FPS_Temp.txt
42	T-FPS-39	S100 - Fuel Pin Simulator	LBE temperature at FPS outlet windows	Top windows of FPS hexagonal shroud	Temperature	°C	0	600	±1.5/±2°C	LBE-Side_FPS_Temp.txt
43	T-FV-01	S100 - Fitting Volume	Fitting volume outer surface temperature	180° from segment between dead volume and riser centres	Temperature	°C	0	600	±1.5/±2°C	LBE-Side_FV_Temp.txt

44	T-FV-02	S100 - Fitting Volume	Fitting volume outer surface temperature	-290° from segment between dead volume and riser centres	Temperature	°C	0	600	±1.5/±2°C	LBE-Side_FV_Temp.txt
45	T-FV-03	S100 - Fitting Volume	Fitting volume outer surface temperature	-340° from segment between dead volume and riser centres	Temperature	°C	0	600	±1.5/±2°C	LBE-Side_FV_Temp.txt
46	T-FV-04	S100 - Fitting Volume	Fitting volume outer surface temperature	-20° from segment between dead volume and riser centres	Temperature	°C	0	600	±1.5/±2°C	LBE-Side_FV_Temp.txt
47	T-FV-05	S100 - Fitting Volume	Fitting volume outer surface temperature	-70° from segment between dead volume and riser centres	Temperature	°C	0	600	±1.5/±2°C	LBE-Side_FV_Temp.txt
48	T-MS-001	S100 - Mixing & Stratification	Supported by rod at separator, SG side A	0mm	Temperature	°C	0	600	±1.5/±2°C	LBE-Side_M&S_Temp.txt
49	T-MS-002	S100 - Mixing & Stratification	Supported by rod at separator, SG side B	0mm	Temperature	°C	0	600	±1.5/±2°C	LBE-Side_M&S_Temp.txt
50	T-MS-003	S100 - Mixing & Stratification	Supported by rod at separator, SG side C	0mm	Temperature	°C	0	600	±1.5/±2°C	LBE-Side_M&S_Temp.txt
51	T-MS-004	S100 - Mixing & Stratification	Supported by rod at separator, SG side D	0mm	Temperature	°C	0	600	±1.5/±2°C	LBE-Side_M&S_Temp.txt
52	T-MS-005	S100 - Mixing & Stratification	Supported by rod at separator, SG side E	0mm	Temperature	°C	0	600	±1.5/±2°C	LBE-Side_M&S_Temp.txt
53	T-MS-006	S100 - Mixing & Stratification	Supported by rod at dead volume, SG side F	0mm	Temperature	°C	0	600	±1.5/±2°C	LBE-Side_M&S_Temp.txt
54	T-MS-007	S100 - Mixing & Stratification	Supported by rod at dead volume, SG side G	0mm	Temperature	°C	0	600	±1.5/±2°C	LBE-Side_M&S_Temp.txt
55	T-MS-008	S100 - Mixing & Stratification	Along Argon line I	0mm	Temperature	°C	0	600	±1.5/±2°C	LBE-Side_M&S_Temp.txt

56	T-MS-009	S100 - Mixing & Stratification	Supported by rod at dead volume, opposite the rod at separator SG side H	0mm	Temperature	°C	0	600	±1.5/±2°C	LBE-Side_M&S_Temp.txt
57	T-MS-010	S100 - Mixing & Stratification	Supported by rod at separator, SG side A	-600 mm	Temperature	°C	0	600	±1.5/±2°C	LBE-Side_M&S_Temp.txt
58	T-MS-011	S100 - Mixing & Stratification	Supported by rod at separator, SG side B	-600 mm	Temperature	°C	0	600	±1.5/±2°C	LBE-Side_M&S_Temp.txt
59	T-MS-012	S100 - Mixing & Stratification	Supported by rod at separator, SG side C	-600 mm	Temperature	°C	0	600	±1.5/±2°C	LBE-Side_M&S_Temp.txt
60	T-MS-013	S100 - Mixing & Stratification	Supported by rod at separator, SG side D	-600 mm	Temperature	°C	0	600	±1.5/±2°C	LBE-Side_M&S_Temp.txt
61	T-MS-014	S100 - Mixing & Stratification	Supported by rod at separator, SG side E	-600 mm	Temperature	°C	0	600	±1.5/±2°C	LBE-Side_M&S_Temp.txt
62	T-MS-015	S100 - Mixing & Stratification	Supported by rod at dead volume, SG side F	-600 mm	Temperature	°C	0	600	±1.5/±2°C	LBE-Side_M&S_Temp.txt
63	T-MS-016	S100 - Mixing & Stratification	Supported by rod at dead volume, SG side G	-600 mm	Temperature	°C	0	600	±1.5/±2°C	LBE-Side_M&S_Temp.txt
64	T-MS-017	S100 - Mixing & Stratification	Along Argon line I	-600 mm	Temperature	°C	0	600	±1.5/±2°C	LBE-Side_M&S_Temp.txt
65	T-MS-018	S100 - Mixing & Stratification	Supported by rod at dead volume, opposite the rod at separator SG side H	-600 mm	Temperature	°C	0	600	±1.5/±2°C	LBE-Side_M&S_Temp.txt
66	T-MS-019	S100 - Mixing & Stratification	Supported by rod at separator, SG side A	-1200 mm	Temperature	°C	0	600	±1.5/±2°C	LBE-Side_M&S_Temp.txt
67	T-MS-020	S100 - Mixing &	Supported by rod at separator, SG side B	-1200 mm	Temperature	°C	0	600	±1.5/±2°C	LBE-Side_M&S_Temp.txt

		Stratification								
68	T-MS-021	S100 - Mixing & Stratification	Supported by rod at separator, SG side C	-1200 mm	Temperature	°C	0	600	±1.5/±2°C	LBE-Side_M&S_Temp.txt
69	T-MS-022	S100 - Mixing & Stratification	Supported by rod at separator, SG side D	-1200 mm	Temperature	°C	0	600	±1.5/±2°C	LBE-Side_M&S_Temp.txt
70	T-MS-023	S100 - Mixing & Stratification	Supported by rod at separator, SG side E	-1200 mm	Temperature	°C	0	600	±1.5/±2°C	LBE-Side_M&S_Temp.txt
71	T-MS-024	S100 - Mixing & Stratification	Supported by rod at dead volume, SG side F	-1200 mm	Temperature	°C	0	600	±1.5/±2°C	LBE-Side_M&S_Temp.txt
72	T-MS-025	S100 - Mixing & Stratification	Supported by rod at dead volume, SG side G	-1200 mm	Temperature	°C	0	600	±1.5/±2°C	LBE-Side_M&S_Temp.txt
73	T-MS-026	S100 - Mixing & Stratification	Along Argon line I	-1200 mm	Temperature	°C	0	600	±1.5/±2°C	LBE-Side_M&S_Temp.txt
74	T-MS-027	S100 - Mixing & Stratification	Supported by rod at dead volume, opposite the rod at separator SG side H	-1200 mm	Temperature	°C	0	600	±1.5/±2°C	LBE-Side_M&S_Temp.txt
75	T-MS-028	S100 - Mixing & Stratification	Supported by rod at separator, SG side A	-1800 mm	Temperature	°C	0	600	±1.5/±2°C	LBE-Side_M&S_Temp.txt
76	T-MS-029	S100 - Mixing & Stratification	Supported by rod at separator, SG side B	-1800 mm	Temperature	°C	0	600	±1.5/±2°C	LBE-Side_M&S_Temp.txt
77	T-MS-030	S100 - Mixing & Stratification	Supported by rod at separator, SG side C	-1800 mm	Temperature	°C	0	600	±1.5/±2°C	LBE-Side_M&S_Temp.txt
78	T-MS-031	S100 - Mixing & Stratification	Supported by rod at separator, SG side D	-1800 mm	Temperature	°C	0	600	±1.5/±2°C	LBE-Side_M&S_Temp.txt
79	T-MS-	S100 -	Supported by rod at	-1800 mm	Temperature	°C	0	600	±1.5/±2°C	LBE-Side_M&S_Temp.txt

	032	Mixing & Stratification	separator, SG side E							
80	T-MS-033	S100 - Mixing & Stratification	Supported by rod at dead volume, SG side F	-1800 mm	Temperature	°C	0	600	±1.5/±2°C	LBE-Side_M&S_Temp.txt
81	T-MS-034	S100 - Mixing & Stratification	Supported by rod at dead volume, SG side G	-1800 mm	Temperature	°C	0	600	±1.5/±2°C	LBE-Side_M&S_Temp.txt
82	T-MS-035	S100 - Mixing & Stratification	Along Argon line I	-1800 mm	Temperature	°C	0	600	±1.5/±2°C	LBE-Side_M&S_Temp.txt
83	T-MS-036	S100 - Mixing & Stratification	Supported by rod at dead volume, opposite the rod at separator SG side H	-1800 mm	Temperature	°C	0	600	±1.5/±2°C	LBE-Side_M&S_Temp.txt
84	T-MS-037	S100 - Mixing & Stratification	Supported by rod at separator, SG side A	-2400 mm	Temperature	°C	0	600	±1.5/±2°C	LBE-Side_M&S_Temp.txt
85	T-MS-038	S100 - Mixing & Stratification	Supported by rod at separator, SG side B	-2400 mm	Temperature	°C	0	600	±1.5/±2°C	LBE-Side_M&S_Temp.txt
86	T-MS-039	S100 - Mixing & Stratification	Supported by rod at separator, SG side C	-2400 mm	Temperature	°C	0	600	±1.5/±2°C	LBE-Side_M&S_Temp.txt
87	T-MS-040	S100 - Mixing & Stratification	Supported by rod at separator, SG side D	-2400 mm	Temperature	°C	0	600	±1.5/±2°C	LBE-Side_M&S_Temp.txt
88	T-MS-041	S100 - Mixing & Stratification	Supported by rod at separator, SG side E	-2400 mm	Temperature	°C	0	600	±1.5/±2°C	LBE-Side_M&S_Temp.txt
89	T-MS-042	S100 - Mixing & Stratification	Supported by rod at dead volume, SG side F	-2400 mm	Temperature	°C	0	600	±1.5/±2°C	LBE-Side_M&S_Temp.txt
90	T-MS-043	S100 - Mixing & Stratification	Supported by rod at dead volume, SG side G	-2400 mm	Temperature	°C	0	600	±1.5/±2°C	LBE-Side_M&S_Temp.txt

91	T-MS-044	S100 - Mixing & Stratification	Along Argon line I	-2400 mm	Temperature	°C	0	600	±1.5/±2°C	LBE-Side_M&S_Temp.txt
92	T-MS-045	S100 - Mixing & Stratification	Supported by rod at dead volume, opposite the rod at separator SG side H	-2400 mm	Temperature	°C	0	600	±1.5/±2°C	LBE-Side_M&S_Temp.txt
93	T-MS-046	S100 - Mixing & Stratification	Supported by rod at separator, SG side A	-3000 mm	Temperature	°C	0	600	±1.5/±2°C	LBE-Side_M&S_Temp.txt
94	T-MS-047	S100 - Mixing & Stratification	Supported by rod at separator, SG side B	-3000 mm	Temperature	°C	0	600	±1.5/±2°C	LBE-Side_M&S_Temp.txt
95	T-MS-048	S100 - Mixing & Stratification	Supported by rod at separator, SG side C	-3000 mm	Temperature	°C	0	600	±1.5/±2°C	LBE-Side_M&S_Temp.txt
96	T-MS-049	S100 - Mixing & Stratification	Supported by rod at separator, SG side D	-3000 mm	Temperature	°C	0	600	±1.5/±2°C	LBE-Side_M&S_Temp.txt
97	T-MS-050	S100 - Mixing & Stratification	Supported by rod at separator, SG side E	-3000 mm	Temperature	°C	0	600	±1.5/±2°C	LBE-Side_M&S_Temp.txt
98	T-MS-051	S100 - Mixing & Stratification	Supported by rod at dead volume, SG side F	-3000 mm	Temperature	°C	0	600	±1.5/±2°C	LBE-Side_M&S_Temp.txt
99	T-MS-052	S100 - Mixing & Stratification	Supported by rod at dead volume, SG side G	-3000 mm	Temperature	°C	0	600	±1.5/±2°C	LBE-Side_M&S_Temp.txt
100	T-MS-053	S100 - Mixing & Stratification	Along Argon line I	-3000 mm	Temperature	°C	0	600	±1.5/±2°C	LBE-Side_M&S_Temp.txt
101	T-MS-054	S100 - Mixing & Stratification	Supported by rod at dead volume, opposite the rod at separator SG side H	-3000 mm	Temperature	°C	0	600	±1.5/±2°C	LBE-Side_M&S_Temp.txt
102	T-MS-055	S100 - Mixing &	Supported by rod at separator, SG side A	-3600 mm	Temperature	°C	0	600	±1.5/±2°C	LBE-Side_M&S_Temp.txt

		Stratification								
103	T-MS-056	S100 - Mixing & Stratification	Supported by rod at separator, SG side B	-3600 mm	Temperature	°C	0	600	±1.5/±2°C	LBE-Side_M&S_Temp.txt
104	T-MS-057	S100 - Mixing & Stratification	Supported by rod at separator, SG side C	-3600 mm	Temperature	°C	0	600	±1.5/±2°C	LBE-Side_M&S_Temp.txt
105	T-MS-058	S100 - Mixing & Stratification	Supported by rod at separator, SG side D	-3600 mm	Temperature	°C	0	600	±1.5/±2°C	LBE-Side_M&S_Temp.txt
106	T-MS-059	S100 - Mixing & Stratification	Supported by rod at separator, SG side E	-3600 mm	Temperature	°C	0	600	±1.5/±2°C	LBE-Side_M&S_Temp.txt
107	T-MS-060	S100 - Mixing & Stratification	Supported by rod at dead volume, SG side F	-3600 mm	Temperature	°C	0	600	±1.5/±2°C	LBE-Side_M&S_Temp.txt
108	T-MS-061	S100 - Mixing & Stratification	Supported by rod at dead volume, SG side G	-3600 mm	Temperature	°C	0	600	±1.5/±2°C	LBE-Side_M&S_Temp.txt
109	T-MS-062	S100 - Mixing & Stratification	Along Argon line I	-3600 mm	Temperature	°C	0	600	±1.5/±2°C	LBE-Side_M&S_Temp.txt
110	T-MS-063	S100 - Mixing & Stratification	Supported by rod at dead volume, opposite the rod at separator SG side H	-3600 mm	Temperature	°C	0	600	±1.5/±2°C	LBE-Side_M&S_Temp.txt
111	T-MS-064	S100 - Mixing & Stratification	Supported by rod at separator, SG side A	-3720 mm	Temperature	°C	0	600	±1.5/±2°C	LBE-Side_M&S_Temp.txt
112	T-MS-065	S100 - Mixing & Stratification	Supported by rod at separator, SG side B	-3720 mm	Temperature	°C	0	600	±1.5/±2°C	LBE-Side_M&S_Temp.txt
113	T-MS-066	S100 - Mixing & Stratification	Supported by rod at separator, SG side C	-3720 mm	Temperature	°C	0	600	±1.5/±2°C	LBE-Side_M&S_Temp.txt
114	T-MS-	S100 -	Supported by rod at	-3720 mm	Temperature	°C	0	600	±1.5/±2°C	LBE-Side_M&S_Temp.txt

	067	Mixing & Stratification	separator, SG side D							
115	T-MS-068	S100 - Mixing & Stratification	Supported by rod at separator, SG side E	-3720 mm	Temperature	°C	0	600	±1.5/±2°C	LBE-Side_M&S_Temp.txt
116	T-MS-069	S100 - Mixing & Stratification	Supported by rod at dead volume, SG side F	-3720 mm	Temperature	°C	0	600	±1.5/±2°C	LBE-Side_M&S_Temp.txt
117	T-MS-070	S100 - Mixing & Stratification	Supported by rod at dead volume, SG side G	-3720 mm	Temperature	°C	0	600	±1.5/±2°C	LBE-Side_M&S_Temp.txt
118	T-MS-071	S100 - Mixing & Stratification	Along Argon line I	-3720 mm	Temperature	°C	0	600	±1.5/±2°C	LBE-Side_M&S_Temp.txt
119	T-MS-072	S100 - Mixing & Stratification	Supported by rod at separator, SG side A	-3840 mm	Temperature	°C	0	600	±1.5/±2°C	LBE-Side_M&S_Temp.txt
120	T-MS-073	S100 - Mixing & Stratification	Supported by rod at separator, SG side B	-3840 mm	Temperature	°C	0	600	±1.5/±2°C	LBE-Side_M&S_Temp.txt
121	T-MS-074	S100 - Mixing & Stratification	Supported by rod at separator, SG side C	-3840 mm	Temperature	°C	0	600	±1.5/±2°C	LBE-Side_M&S_Temp.txt
122	T-MS-075	S100 - Mixing & Stratification	Supported by rod at separator, SG side D	-3840 mm	Temperature	°C	0	600	±1.5/±2°C	LBE-Side_M&S_Temp.txt
123	T-MS-076	S100 - Mixing & Stratification	Supported by rod at separator, SG side E	-3840 mm	Temperature	°C	0	600	±1.5/±2°C	LBE-Side_M&S_Temp.txt
124	T-MS-077	S100 - Mixing & Stratification	Supported by rod at dead volume, SG side F	-3840 mm	Temperature	°C	0	600	±1.5/±2°C	LBE-Side_M&S_Temp.txt
125	T-MS-078	S100 - Mixing & Stratification	Supported by rod at dead volume, SG side G	-3840 mm	Temperature	°C	0	600	±1.5/±2°C	LBE-Side_M&S_Temp.txt
126	T-MS-079	S100 - Mixing &	Along Argon line I	-3840 mm	Temperature	°C	0	600	±1.5/±2°C	LBE-Side_M&S_Temp.txt

		Stratification								
127	T-MS-080	S100 - Mixing & Stratification	Supported by rod at separator, SG side A	-3960 mm	Temperature	°C	0	600	±1.5/±2°C	LBE-Side_M&S_Temp.txt
128	T-MS-081	S100 - Mixing & Stratification	Supported by rod at separator, SG side B	-3960 mm	Temperature	°C	0	600	±1.5/±2°C	LBE-Side_M&S_Temp.txt
129	T-MS-082	S100 - Mixing & Stratification	Supported by rod at separator, SG side C	-3960 mm	Temperature	°C	0	600	±1.5/±2°C	LBE-Side_M&S_Temp.txt
130	T-MS-083	S100 - Mixing & Stratification	Supported by rod at separator, SG side D	-3960 mm	Temperature	°C	0	600	±1.5/±2°C	LBE-Side_M&S_Temp.txt
131	T-MS-084	S100 - Mixing & Stratification	Supported by rod at separator, SG side E	-3960 mm	Temperature	°C	0	600	±1.5/±2°C	LBE-Side_M&S_Temp.txt
132	T-MS-085	S100 - Mixing & Stratification	Supported by rod at dead volume, SG side F	-3960 mm	Temperature	°C	0	600	±1.5/±2°C	LBE-Side_M&S_Temp.txt
133	T-MS-086	S100 - Mixing & Stratification	Supported by rod at dead volume, SG side G	-3960 mm	Temperature	°C	0	600	±1.5/±2°C	LBE-Side_M&S_Temp.txt
134	T-MS-087	S100 - Mixing & Stratification	Along Argon line I	-3960 mm	Temperature	°C	0	600	±1.5/±2°C	LBE-Side_M&S_Temp.txt
135	T-MS-088	S100 - Mixing & Stratification	Supported by rod at separator, SG side A	-4080 mm	Temperature	°C	0	600	±1.5/±2°C	LBE-Side_M&S_Temp.txt
136	T-MS-089	S100 - Mixing & Stratification	Supported by rod at separator, SG side B	-4080 mm	Temperature	°C	0	600	±1.5/±2°C	LBE-Side_M&S_Temp.txt
137	T-MS-090	S100 - Mixing & Stratification	Supported by rod at separator, SG side C	-4080 mm	Temperature	°C	0	600	±1.5/±2°C	LBE-Side_M&S_Temp.txt
138	T-MS-091	S100 - Mixing &	Supported by rod at separator, SG side D	-4080 mm	Temperature	°C	0	600	±1.5/±2°C	LBE-Side_M&S_Temp.txt

		Stratification								
139	T-MS-092	S100 - Mixing & Stratification	Supported by rod at separator, SG side E	-4080 mm	Temperature	°C	0	600	±1.5/±2°C	LBE-Side_M&S_Temp.txt
140	T-MS-093	S100 - Mixing & Stratification	Supported by rod at dead volume, SG side F	-4080 mm	Temperature	°C	0	600	±1.5/±2°C	LBE-Side_M&S_Temp.txt
141	T-MS-094	S100 - Mixing & Stratification	Supported by rod at dead volume, SG side G	-4080 mm	Temperature	°C	0	600	±1.5/±2°C	LBE-Side_M&S_Temp.txt
142	T-MS-095	S100 - Mixing & Stratification	Along Argon line I	-4080 mm	Temperature	°C	0	600	±1.5/±2°C	LBE-Side_M&S_Temp.txt
143	T-MS-096	S100 - Mixing & Stratification	Supported by rod at separator, SG side A	-4200 mm	Temperature	°C	0	600	±1.5/±2°C	LBE-Side_M&S_Temp.txt
144	T-MS-097	S100 - Mixing & Stratification	Supported by rod at separator, SG side B	-4200 mm	Temperature	°C	0	600	±1.5/±2°C	LBE-Side_M&S_Temp.txt
145	T-MS-098	S100 - Mixing & Stratification	Supported by rod at separator, SG side C	-4200 mm	Temperature	°C	0	600	±1.5/±2°C	LBE-Side_M&S_Temp.txt
146	T-MS-099	S100 - Mixing & Stratification	Supported by rod at separator, SG side D	-4200 mm	Temperature	°C	0	600	±1.5/±2°C	LBE-Side_M&S_Temp.txt
147	T-MS-100	S100 - Mixing & Stratification	Supported by rod at separator, SG side E	-4200 mm	Temperature	°C	0	600	±1.5/±2°C	LBE-Side_M&S_Temp.txt
148	T-MS-101	S100 - Mixing & Stratification	Supported by rod at dead volume, SG side F	-4200 mm	Temperature	°C	0	600	±1.5/±2°C	LBE-Side_M&S_Temp.txt
149	T-MS-102	S100 - Mixing & Stratification	Supported by rod at dead volume, SG side G	-4200 mm	Temperature	°C	0	600	±1.5/±2°C	LBE-Side_M&S_Temp.txt
150	T-MS-103	S100 - Mixing &	Along Argon line I	-4200 mm	Temperature	°C	0	600	±1.5/±2°C	LBE-Side_M&S_Temp.txt

		Stratification								
151	T-MS-104	S100 - Mixing & Stratification	Supported by rod at dead volume, opposite the rod at separator SG side H	-4200 mm	Temperature	°C	0	600	±1.5/±2°C	LBE-Side_M&S_Temp.txt
152	T-MS-120	S100 - Mixing & Stratification	Supported by rod at separator, SG side A	-4500 mm	Temperature	°C	0	600	±1.5/±2°C	LBE-Side_M&S_Temp.txt
153	T-MS-105	S100 - Mixing & Stratification	Supported by rod at dead volume, opposite the rod at separator SG side H	-4800 mm	Temperature	°C	0	600	±1.5/±2°C	LBE-Side_M&S_Temp.txt
154	T-MS-106	S100 - Mixing & Stratification	Supported by rod at separator, SG side A	-4800 mm	Temperature	°C	0	600	±1.5/±2°C	LBE-Side_M&S_Temp.txt
155	T-MS-107	S100 - Mixing & Stratification	Along Argon line I	-4800 mm	Temperature	°C	0	600	±1.5/±2°C	LBE-Side_M&S_Temp.txt
156	T-MS-121	S100 - Mixing & Stratification	Supported by rod at separator, SG side A	-4950 mm	Temperature	°C	0	600	±1.5/±2°C	LBE-Side_M&S_Temp.txt
157	T-MS-111	S100 - Mixing & Stratification	Supported by rod at separator, SG side A	-5100 mm	Temperature	°C	0	600	±1.5/±2°C	LBE-Side_M&S_Temp.txt
158	T-MS-122	S100 - Mixing & Stratification	Supported by rod at dead volume, opposite the rod at separator SG side H	-5100 mm	Temperature	°C	0	600	±1.5/±2°C	LBE-Side_M&S_Temp.txt
159	T-MS-114	S100 - Mixing & Stratification	Supported by rod at separator, SG side A	-5250 mm	Temperature	°C	0	600	±1.5/±2°C	LBE-Side_M&S_Temp.txt
160	T-MS-108	S100 - Mixing & Stratification	Along Argon line (TC slow) I	-5400 mm	Temperature	°C	0	600	±1.5/±2°C	LBE-Side_M&S_Temp.txt
161	T-MS-109	S100 - Mixing &	Supported by rod at separator, SG side A	-5400 mm	Temperature	°C	0	600	±1.5/±2°C	LBE-Side_M&S_Temp.txt

		Stratification								
162	T-MS-110	S100 - Mixing & Stratification	Supported by rod at dead volume, opposite the rod at separator SG side H	-5400 mm	Temperature	°C	0	600	±1.5/±2°C	LBE-Side_M&S_Temp.txt
163	T-MS-117	S100 - Mixing & Stratification	Supported by rod at separator, SG side A	-5700 mm	Temperature	°C	0	600	±1.5/±2°C	LBE-Side_M&S_Temp.txt
164	T-MS-112	S100 - Mixing & Stratification	Supported by rod at separator, SG side A	-6000 mm	Temperature	°C	0	600	±1.5/±2°C	LBE-Side_M&S_Temp.txt
165	T-MS-113	S100 - Mixing & Stratification	Supported by rod at dead volume, opposite the rod at separator SG side H	-6000 mm	Temperature	°C	0	600	±1.5/±2°C	LBE-Side_M&S_Temp.txt
166	T-MS-115	S100 - Mixing & Stratification	Supported by rod at separator, SG side A	-6600 mm	Temperature	°C	0	600	±1.5/±2°C	LBE-Side_M&S_Temp.txt
167	T-MS-116	S100 - Mixing & Stratification	Supported by rod at dead volume, opposite the rod at separator SG side H	-6600 mm	Temperature	°C	0	600	±1.5/±2°C	LBE-Side_M&S_Temp.txt
168	T-MS-118	S100 - Mixing & Stratification	Supported by rod at separator, SG side A	-7200 mm	Temperature	°C	0	600	±1.5/±2°C	LBE-Side_M&S_Temp.txt
169	T-MS-119	S100 - Mixing & Stratification	Supported by rod at dead volume, opposite the rod at separator SG side H	-7200 mm	Temperature	°C	0	600	±1.5/±2°C	LBE-Side_M&S_Temp.txt
170	T-RIB-04	S100 - Riser Bottom	Upstream gas injector Dead volume side	LBE inlet riser temperature (Riser bottom)	Temperature	°C	0	600	±1.5/±2°C	LBE-Side_Riser_Temp.txt
171	T-RIB-05	S100 - Riser Bottom	Upstream gas injector Outer side	LBE inlet riser temperature (Riser bottom)	Temperature	°C	0	600	±1.5/±2°C	LBE-Side_Riser_Temp.txt

172	T-RIB-06	S100 - Riser Bottom	Upstream gas injector Heat exchanger side	LBE inlet riser temperature (Riser bottom)	Temperature	°C	0	600	±1.5/±2°C	LBE-Side_Riser_Temp.txt
173	T-RIT-01	S100 - Riser Top	Dead volume side	LBE outlet riser temperature Top, 42 mm above separator	Temperature	°C	0	600	±1.5/±2°C	LBE-Side_Riser_Temp.txt
174	T-RIB-02	S100 - Riser Top	Outer side	LBE outlet riser temperature Top, 42 mm above separator	Temperature	°C	0	600	±1.5/±2°C	LBE-Side_Riser_Temp.txt
175	T-RIB-03	S100 - Riser Top	Heat exchanger side	LBE outlet riser temperature Top, 42 mm above separator	Temperature	°C	0	600	±1.5/±2°C	LBE-Side_Riser_Temp.txt
176	T-TS-07	S100 - Cover Gas	Cover Gas	----	Temperature	°C	0	600	±1.5/±2°C	LBE-Side_Cover_Gas_Temp.txt
177	TC-01-L00	S100 - Steam Generator	LBE subchannel 1 centre (pipes 1, 2 and 0), OUTLET	0.0 mm	Temperature	°C	0	600	±1.5/±2°C	LBE-Side_SG_Temp.txt
178	TC-07-L00	S100 - Steam Generator	LBE subchannel 7 centre (pipes 1, 2 and wall), OUTLET	0.0 mm	Temperature	°C	0	600	±1.5/±2°C	LBE-Side_SG_Temp.txt
179	TC-09-L00	S100 - Steam Generator	LBE subchannel 9 centre (pipes 3, 4 and wall), OUTLET	0.0 mm	Temperature	°C	0	600	±1.5/±2°C	LBE-Side_SG_Temp.txt
180	TC-01-L15	S100 - Steam Generator	LBE subchannel 1 centre (pipes 1, 2 and 0)	1500 mm	Temperature	°C	0	600	±1.5/±2°C	LBE-Side_SG_Temp.txt
181	TC-07-L15	S100 - Steam Generator	LBE subchannel 7 centre (pipes 1, 2 and wall)	1500 mm	Temperature	°C	0	600	±1.5/±2°C	LBE-Side_SG_Temp.txt
182	TC-09-L15	S100 - Steam Generator	LBE subchannel 9 centre (pipes 3, 4 and wall)	1500 mm	Temperature	°C	0	600	±1.5/±2°C	LBE-Side_SG_Temp.txt
183	TC-11-L15	S100 - Steam Generator	LBE subchannel 11 centre (pipes 5, 6 and wall)	1500 mm	Temperature	°C	0	600	±1.5/±2°C	LBE-Side_SG_Temp.txt
184	TC-07-L30	S100 - Steam	LBE subchannel 7 centre (pipes 1, 2 and	3000 mm	Temperature	°C	0	600	±1.5/±2°C	LBE-Side_SG_Temp.txt

		Generator	wall)							
185	TC-09-L30	S100 - Steam Generator	LBE subchannel 9 centre (pipes 3, 4 and wall)	3000 mm	Temperature	°C	0	600	±1.5/±2°C	LBE-Side_SG_Temp.txt
186	TC-11-L30	S100 - Steam Generator	LBE subchannel 11 centre (pipes 5, 6 and wall)	3000 mm	Temperature	°C	0	600	±1.5/±2°C	LBE-Side_SG_Temp.txt
187	TC-01-L42	S100 - Steam Generator	LBE subchannel 1 centre (pipes 1, 2 and 0)	4200 mm	Temperature	°C	0	600	±1.5/±2°C	LBE-Side_SG_Temp.txt
188	TC-09-L42	S100 - Steam Generator	LBE subchannel 9 centre (pipes 3, 4 and wall)	4200 mm	Temperature	°C	0	600	±1.5/±2°C	LBE-Side_SG_Temp.txt
189	TC-11-L42	S100 - Steam Generator	LBE subchannel 11 centre (pipes 5, 6 and wall)	4200 mm	Temperature	°C	0	600	±1.5/±2°C	LBE-Side_SG_Temp.txt
190	TC-SG-01	S100 - Steam Generator	LBE inlet temperature (slot on riser side)	Inlet Steam Generator middle hight of LBE inlet slot at 120° inside the separator	Temperature	°C	0	600	±1.5/±2°C	LBE-Side_SG_Temp.txt
191	TC-SG-02	S100 - Steam Generator	LBE inlet temperature (slot on dead volume side)	Inlet Steam Generator middle hight of LBE inlet slot at 120° inside the separator	Temperature	°C	0	600	±1.5/±2°C	LBE-Side_SG_Temp.txt
192	TC-SG-03	S100 - Steam Generator	LBE inlet temperature (slot on outer side)	Inlet Steam Generator middle hight of LBE inlet slot at 120° inside the separator	Temperature	°C	0	600	±1.5/±2°C	LBE-Side_SG_Temp.txt
193	TC-W0-L10	S100 - Wall Steam Generator	tube 0 - LBE side, outer wall temperature	1500 mm / 0°	Temperature	°C	0	600	±1.5/±2°C	LBE-Side_WallSG_Temp.txt
194	TC-W0-L11	S100 - Wall Steam Generator	tube 0 - LBE side, outer wall temperature	1500 mm / 120°	Temperature	°C	0	600	±1.5/±2°C	LBE-Side_WallSG_Temp.txt
195	TC-W0-L12	S100 - Wall Steam	tube 0 - LBE side, outer wall	1500 mm / 240°	Temperature	°C	0	600	±1.5/±2°C	LBE-Side_WallSG_Temp.txt

		Generator	temperature							
196	TC-W0-L30	S100 - Wall Steam Generator	tube 0 - LBE side, outer wall temperature	3000 mm / 0°	Temperature	°C	0	600	±1.5/±2°C	LBE-Side_WallSG_Temp.txt
197	TC-W0-L31	S100 - Wall Steam Generator	tube 0 - LBE side, outer wall temperature	3000 mm / 120°	Temperature	°C	0	600	±1.5/±2°C	LBE-Side_WallSG_Temp.txt
198	TC-W0-L40	S100 - Wall Steam Generator	tube 0 - LBE side, outer wall temperature	4200 mm / 0°	Temperature	°C	0	600	±1.5/±2°C	LBE-Side_WallSG_Temp.txt
199	TC-W0-L41	S100 - Wall Steam Generator	tube 0 - LBE side, outer wall temperature	4200 mm / 120°	Temperature	°C	0	600	±1.5/±2°C	LBE-Side_WallSG_Temp.txt
200	TC-W0-L42	S100 - Wall Steam Generator	tube 0 - LBE side, outer wall temperature	4200 mm / 240°	Temperature	°C	0	600	±1.5/±2°C	LBE-Side_WallSG_Temp.txt
201	TC-W1-L11	S100 - Wall Steam Generator	tube 1 - LBE side, outer wall temperature	1500 mm / 120°	Temperature	°C	0	600	±1.5/±2°C	LBE-Side_WallSG_Temp.txt
202	TC-W1-L31	S100 - Wall Steam Generator	tube 1 - LBE side, outer wall temperature	3000 mm / 120°	Temperature	°C	0	600	±1.5/±2°C	LBE-Side_WallSG_Temp.txt
203	TC-W1-L41	S100 - Wall Steam Generator	tube 1 - LBE side, outer wall temperature	4200 mm / 120°	Temperature	°C	0	600	±1.5/±2°C	LBE-Side_WallSG_Temp.txt
204	TC-W2-L12	S100 - Wall Steam Generator	tube 2 - LBE side, outer wall temperature	1500 mm / 240°	Temperature	°C	0	600	±1.5/±2°C	LBE-Side_WallSG_Temp.txt
205	TC-W2-L32	S100 - Wall Steam Generator	tube 2 - LBE side, outer wall temperature	3000 mm / 240°	Temperature	°C	0	600	±1.5/±2°C	LBE-Side_WallSG_Temp.txt
206	TC-W2-L42	S100 - Wall Steam Generator	tube 2 - LBE side, outer wall temperature	4200 mm / 240°	Temperature	°C	0	600	±1.5/±2°C	LBE-Side_WallSG_Temp.txt
207	TE-102	S100 - External	External side of the Vessel	S100 Coupling Flange	Temperature	°C	0	600	±1.5/±2°C	LBE-Side_Ext_Vessel_Temp.txt

		Vessel								
208	TE-103	S100 - External Vessel	External side of the Vessel	S100 Coupling Flange	Temperature	°C	0	600	±1.5/±2°C	LBE-Side_Ext_Vessel_Temp.txt
209	TE-104	S100 - External Vessel	External side of the Vessel	S100 Coupling Flange	Temperature	°C	0	600	±1.5/±2°C	LBE-Side_Ext_Vessel_Temp.txt
210	TE-110	S100 - External Vessel	External side of the Vessel	-2065 mm	Temperature	°C	0	600	±1.5/±2°C	LBE-Side_Ext_Vessel_Temp.txt
211	TE-111	S100 - External Vessel	External side of the Vessel	-1650 mm	Temperature	°C	0	600	±1.5/±2°C	LBE-Side_Ext_Vessel_Temp.txt
212	TE-112	S100 - External Vessel	External side of the Vessel	-1235 mm	Temperature	°C	0	600	±1.5/±2°C	LBE-Side_Ext_Vessel_Temp.txt
213	TE-113	S100 - External Vessel	External side of the Vessel	-820 mm	Temperature	°C	0	600	±1.5/±2°C	LBE-Side_Ext_Vessel_Temp.txt
214	TE-114	S100 - External Vessel	External side of the Vessel	-405 mm	Temperature	°C	0	600	±1.5/±2°C	LBE-Side_Ext_Vessel_Temp.txt
215	TE-115	S100 - External Vessel	External side of the Vessel	-4010 mm	Temperature	°C	0	600	±1.5/±2°C	LBE-Side_Ext_Vessel_Temp.txt
216	TE-116	S100 - External Vessel	External side of the Vessel	-3315 mm	Temperature	°C	0	600	±1.5/±2°C	LBE-Side_Ext_Vessel_Temp.txt
217	TE-117	S100 - External Vessel	External side of the Vessel	-2620 mm	Temperature	°C	0	600	±1.5/±2°C	LBE-Side_Ext_Vessel_Temp.txt
218	TE-118	S100 - External Vessel	External side of the Vessel	-6070 mm	Temperature	°C	0	600	±1.5/±2°C	LBE-Side_Ext_Vessel_Temp.txt
219	TE-119	S100 - External	External side of the Vessel	-5405 mm	Temperature	°C	0	600	±1.5/±2°C	LBE-Side_Ext_Vessel_Temp.txt

		Vessel								
220	TE-120	S100 - External Vessel	External side of the Vessel	-4709 mm	Temperature	°C	0	600	±1.5/±2°C	LBE-Side_Ext_Vessel_Temp.txt
221	TE-121	S100 - External Vessel	External side of the Vessel	-7380 mm	Temperature	°C	0	600	±1.5/±2°C	LBE-Side_Ext_Vessel_Temp.txt
222	TE-122	S100 - External Vessel	External side of the Vessel	-6760 mm	Temperature	°C	0	600	±1.5/±2°C	LBE-Side_Ext_Vessel_Temp.txt
223	TE-123	S100 - External Vessel	External side of the Vessel	Bottom Part of the Vessel	Temperature	°C	0	600	±1.5/±2°C	LBE-Side_Ext_Vessel_Temp.txt
224	TE-124	S100 - External Vessel	External side of the Vessel	Bottom Part of the Vessel	Temperature	°C	0	600	±1.5/±2°C	LBE-Side_Ext_Vessel_Temp.txt
WATER SIDE										
1	dp-T0	Secondary Side	DP of the orifice on Tube 0		Pressure	[bar]	0	20	±0.5%	Water-Side_Pressure.txt
2	dp-T1	Secondary Side	DP of the orifice on Tube 1		Pressure	[bar]	0	20	±0.5%	Water-Side_Pressure.txt
3	dp-T3	Secondary Side	DP of the orifice on Tube 3		Pressure	[bar]	0	20	±0.5%	Water-Side_Pressure.txt
4	dp-T5	Secondary Side	DP of the orifice on Tube 5		Pressure	[bar]	0	20	±0.5%	Water-Side_Pressure.txt
5	PC-L1-1	Secondary Side	Pressure upstream the HEATER		Pressure	[bar]	0	200	±0.1%	Water-Side_Pressure.txt
6	PC-L2-1	Secondary Side	Pressure downstream the HEATER		Pressure	[bar]	0	200	±0.1%	Water-Side_Pressure.txt
7	PC-L3-1	Secondary Side	Pressure upstream the valve V-3		Pressure	[bar]	0	200	±0.1%	Water-Side_Pressure.txt
8	PC-L3-2	Secondary Side	Pressure downstream the valve V-3		Pressure	[mbar]	0 bar	200 bar	±0.1%	Water-Side_Pressure.txt
9	PC-M	Secondary Side	Pressure inside the MANIFOLD		Pressure	[bar]	0	200	±0.1%	Water-Side_Pressure.txt

10	PC-T0-I	Secondary Side	Pressure at the inlet of Tube 0		Pressure	[bar]	0	200	±0.1%	Water-Side_Pressure.txt
11	PC-T1-I	Secondary Side	Pressure at the inlet of Tube 1		Pressure	[bar]	0	200	±0.1%	Water-Side_Pressure.txt
12	PC-T3-I	Secondary Side	Pressure at the inlet of Tube 3		Pressure	[bar]	0	200	±0.1%	Water-Side_Pressure.txt
13	PC-T5-I	Secondary Side	Pressure at the inlet of Tube 5		Pressure	[bar]	0	200	±0.1%	Water-Side_Pressure.txt
3	dp-T3	Secondary Side	DP of the orifice on Tube 3		Pressure	[bar]	0	20	±0.5%	Water-Side_Pressure.txt
4	dp-T5	Secondary Side	DP of the orifice on Tube 5		Pressure	[bar]	0	20	±0.5%	Water-Side_Pressure.txt
5	PC-L1-1	Secondary Side	Pressure upstream the HEATER		Pressure	[bar]	0	200	±0.1%	Water-Side_Pressure.txt
6	PC-L2-1	Secondary Side	Pressure downstream the HEATER		Pressure	[bar]	0	200	±0.1%	Water-Side_Pressure.txt
14	PSH kW	Secondary Side	HEATER electrical power supplied		Power	[kW]	----	----	----	Water-Side_Power_Heater.txt
15	Pump %	Secondary Side					----	----	----	Water-Side_Flow_Rate.txt
15	TFM-0	Secondary Side	Flow Rate of the Turbine Flow Meter on Tube 0		Flow Rate	cc/min	400	4500	Linearity ±1.0% Repeatibility ±0.25% Transmitter accuracy ±0.02%	Water-Side_Flow_Rate.txt
16	TFM-1	Secondary Side	Flow Rate of the Turbine Flow Meter on Tube 1		Flow Rate	cc/min	400	4500	Linearity ±1.0% Repeatibility ±0.25% Transmitter accuracy ±0.02%	Water-Side_Flow_Rate.txt
17	TFM-2	Secondary Side	Flow Rate of the Turbine Flow Meter on Tube 2		Flow Rate	cc/min	400	4500	Linearity ±1.0% Repeatibility ±0.25% Transmitter accuracy ±0.02%	Water-Side_Flow_Rate.txt

18	TFM-3	Secondary Side	Flow Rate of the Turbine Flow Meter on Tube 3		Flow Rate	cc/min	400	4500	Linearity ±1.0% Repeatibility ±0.25% Transmitter accuracy ±0.02%	Water-Side_Flow_Rate.txt
19	TFM-4	Secondary Side	Flow Rate of the Turbine Flow Meter on Tube 4		Flow Rate	cc/min	400	4500	Linearity ±1.0% Repeatibility ±0.25% Transmitter accuracy ±0.02%	Water-Side_Flow_Rate.txt
20	TFM-5	Secondary Side	Flow Rate of the Turbine Flow Meter on Tube 5		Flow Rate	cc/min	400	4500	Linearity ±1.0% Repeatibility ±0.25% Transmitter accuracy ±0.02%	Water-Side_Flow_Rate.txt
21	TFM-6	Secondary Side	Flow Rate of the Turbine Flow Meter on Tube 6		Flow Rate	cc/min	400	4500	Linearity ±1.0% Repeatibility ±0.25% Transmitter accuracy ±0.02%	Water-Side_Flow_Rate.txt
22	TC-C0-O05	Secondary Side	tube 0 - H2O side, annulus centre temperature	500 mm	Temperature	°C	0	600	±1.5/±2°C	Water-Side_Temp.txt
23	TC-C0-O15	Secondary Side	tube 0 - H2O side, annulus centre temperature	1500 mm	Temperature	°C	0	600	±1.5/±2°C	Water-Side_Temp.txt
24	TC-C0-O42	Secondary Side	tube 0 - H2O side, annulus centre temperature	4200 mm	Temperature	°C	0	600	±1.5/±2°C	Water-Side_Temp.txt
25	TC-C0-O60	Secondary Side	tube 0 - H2O side, annulus centre temperature	6000 mm	Temperature	°C	0	600	±1.5/±2°C	Water-Side_Temp.txt
26	TC-C0-O70	Secondary Side	tube 0 - H2O side, annulus centre, outlet	7065 mm	Temperature	°C	0	600	±1.5/±2°C	Water-Side_Temp.txt

			temperature							
27	TC-C1-O70	Secondary Side	tube 1 - H2O side, annulus centre, outlet temperature	7016 mm	Temperature	°C	0	600	±1.5/±2°C	Water-Side_Temp.txt
28	TC-C3-O70	Secondary Side	tube 3 - H2O side, annulus centre, outlet temperature	7016 mm	Temperature	°C	0	600	±1.5/±2°C	Water-Side_Temp.txt
29	TC-C4-O70	Secondary Side	tube 4 - H2O side, annulus centre, outlet temperature	7016 mm	Temperature	°C	0	600	±1.5/±2°C	Water-Side_Temp.txt
30	TC-C5-O70	Secondary Side	tube 5 - H2O side, annulus centre, outlet temperature	7016 mm	Temperature	°C	0	600	±1.5/±2°C	Water-Side_Temp.txt
31	TC-L2-2	Secondary Side	Hot feed water temperature	Upstream MANIFOLD	Temperature	°C	0	600	±1.5/±2°C	Water-Side_Temp.txt
32	TC-L3-1	Secondary Side	Steam line temperature, downstream DWBTs	Upper part of the tube	Temperature	°C	0	600	±1.5/±2°C	Water-Side_Temp.txt
33	TC-L3-2	Secondary Side	Steam line temperature, downstream DWBTs	Central part of the tube	Temperature	°C	0	600	±1.5/±2°C	Water-Side_Temp.txt
34	TC-L3-3	Secondary Side	Steam line temperature, downstream DWBTs	Bottom part of the tube (condensation feedback)	Temperature	°C	0	600	±1.5/±2°C	Water-Side_Temp.txt
35	TC-L3-4	Secondary Side	Steam line temperature, downstream V3	Downstream bypass connection	Temperature	°C	0	600	±1.5/±2°C	Water-Side_Temp.txt
36	TC-M-1	Secondary Side	MANIFOLD inner temperature	Top position	Temperature	°C	0	600	±1.5/±2°C	Water-Side_Temp.txt
37	TC-M-2	Secondary Side	MANIFOLD inner temperature	Middle position	Temperature	°C	0	600	±1.5/±2°C	Water-Side_Temp.txt
38	TC-T0-I	Secondary Side	Hot feed water inlet temperature in tube 0	Upstream DWBT 0	Temperature	°C	0	600	±1.5/±2°C	Water-Side_Temp.txt
39	TC-T1-I	Secondary Side	Hot feed water inlet temperature in tube 1	Upstream DWBT 1	Temperature	°C	0	600	±1.5/±2°C	Water-Side_Temp.txt
40	TC-T2-I	Secondary	Hot feed water inlet	Upstream DWBT 2	Temperature	°C	0	600	±1.5/±2°C	Water-Side_Temp.txt

		Side	temperature in tube 2							
41	TC-T3-I	Secondary Side	Hot feed water inlet temperature in tube 3	Upstream DWBT 3	Temperature	°C	0	600	±1.5/±2°C	Water-Side_Temp.txt
42	TC-T4-I	Secondary Side	Hot feed water inlet temperature in tube 4	Upstream DWBT 4	Temperature	°C	0	600	±1.5/±2°C	Water-Side_Temp.txt
43	TC-T5-I	Secondary Side	Hot feed water inlet temperature in tube 5	Upstream DWBT 5	Temperature	°C	0	600	±1.5/±2°C	Water-Side_Temp.txt
44	TC-T6-I	Secondary Side	Hot feed water inlet temperature in tube 6	Upstream DWBT 6	Temperature	°C	0	600	±1.5/±2°C	Water-Side_Temp.txt
45	V1	Secondary Side	Valve V1 Control	Upstream HERO SGBT	Temperature	°C	----	----	----	Water-Side_Valve.txt
46	V2-%	Secondary Side	Valve V2 Control	Bypass Line	Temperature	°C	----	----	----	Water-Side_Valve.txt
47	V3-%	Secondary Side	Valve V3 Control	Downstream HERO SGBT	Temperature	°C	----	----	----	Water-Side_Valve.txt

ANNEX 2 – Publications

Journal and Conference Publications

Lorusso P., Bassini S., Del Nevo A., Di Piazza I., Giannetti F., Tarantino M., Utili M., 2018, GEN-IV LFR development: Status & perspectives, Progress in Nuclear Energy 105 (2018) 318–331, https://doi.org/10.1016/j.pnucene.2018.02.005.

Lorusso P., Pesetti A., Tarantino M., 2018, ALFRED Steam Generator Assessment: design and pre-test analysis of HERO experiment, Proceedings of the 2018 26th International Conference on Nuclear Engineering, July 22-26, 2018, London, England, ICONE26-81824, doi: 10.1115/ICONE26-81824.

Forgione N., Angelucci M., Barone G., Polidori M., Cervone A., Di Piazza I., Giannetti F., Lorusso P., Hollands T., Papukchiev A., 2018, Blind simulations of NACIE-UP experimental tests by STH codes, Proceedings of the 2018 26th International Conference on Nuclear Engineering, July 22-26, 2018, London, England, ICONE26-81434, doi:10.1115/ICONE26-81434.

Narcisi V., Lorusso P., Giannetti F., Alfonsi A., Caruso G., 2019, Uncertainty Quantification method for RELAP5-3D© using RAVEN and application on NACIE experiments, Annals of Nuclear Energy 127 (2019) 419–432, https://doi.org/10.1016/j.anucene.2018.12.034.

Tarantino M., Di Piazza I., Martelli D., Rozzia D., Marinari R., Pesetti A., Lorusso P., 2019, Design of Experimental Liquid Metal Facilities, Thermal Hydraulics Aspects of Liquid Metal Cooled Nuclear Reactors, pp.83-105, January 2019, DOI: 10.1016/B978-0-08-101980-1.00012-0.

Lorusso P., Pesetti A., Tarantino M., Narcisi V., Giannetti F., Forgione N., Del Nevo A., 2019, Experimental Analysis Of Stationary And Transient Scenarios Of ALFRED Steam Generator Bayonet Tube In CIRCE-HERO Facility, Nuclear Engineering and Design 352 (2019) 110169, https://doi.org/10.1016/j.nucengdes.2019.110169.

Lorusso P., Pesetti A., Tarantino M., 2019, Double Wall Bayonet Tube Steam Generator Investigation In HERO Experimental Campaign, Proceedings of the 2019 27th International Conference on Nuclear Engineering, May 19-24, 2019, Tsukuba, Ibaraki, Japan, ICONE27-2208.

Lorusso P., Pesetti A., Tarantino M., Narcisi V., 2019, Protected Loss Of Flow Accident Simulation In Circe-Hero Facility: Experimental Test And System Code Assessment, Proceedings of the 2019 27th International Conference on Nuclear Engineering, May 19-24, 2019, Tsukuba, Ibaraki, Japan, ICONE27-2269.

Lorusso P., Pesetti A., Barone G., Castelliti D., Caruso G., Forgione N., Giannetti F., Martelli D., Rozzia D., Van Tichelen K., Tarantino M., 2019, MYRRHA primary heat exchanger experimental simulations on CIRCE-HERO, Nuclear Engineering and Design 353 (2019) 110270, https://doi.org/10.1016/j.nucengdes.2019.110270.

Forgione N., Martelli D., Barone G., Giannetti F., Lorusso P., Hollands T., Papukchiev A., Polidori M., Cervone A., Di Piazza I., Post-test simulations for the NACIE-UP benchmark by STH codes, Nuclear Engineering and Design 353 (2019) 110279, https://doi.org/10.1016/j.nucengdes.2019.110279

Castelliti, D., Hamidouche, T., Lorusso, P., Tarantino, M., 2019. H2020 MYRTE CIRCE-HERO experimental campaign post-test activity and code validation, 18th International Topical Meeting on Nuclear Reactor Thermal Hydraulics (NURETH-18), Portland, Oregon, August 18-23, 2019.

Galleni, F., Barone, G., Martelli, D., Pucciarelli, A., Lorusso, P., Tarantino, M., Forgione, N., 2019. Simulation of operational conditions of HX-HERO in the CIRCE facility with CFD/STH coupled codes, Submitted to Nuclear Engineering and Design.

Breijder P.A., Stempniewicz M.M., Narcisi, V., Lorusso, P., Giannetti, F., Caruso, G., Alcaro F., Roelofs, F., Tarantino, M., 2019, Analysis Of Argon-Enhanced Circulation In CIRCE-HERO with RELAP5-3D and SPECTRA codes, Submitted to Nuclear Engineering and Design.

Deliverable in H2020 SESAME & MYRTE

P. Lorusso, CIRCE Experimental Report, D3.2, H2020 MYRTE report, October, 31, 2018.

G. Caruso, P. Lorusso, F. Giannetti, D5.19 NACIE-UP RELAP5/RELAP5-3D simulations, D5.19, H2020 SESAME report, December, 31, 2018.

P. Lorusso, D4.4 CIRCE-HERO PLOFA Experiment, D4.4, H2020 SESAME report, January, 22, 2019.

N. Forgione, D. Martelli, G. Barone, F. Giannetti, P. Lorusso, G. Caruso, T. Hollands, A. Papukchiev, M. Polidori, A. Cervone, I. Di Piazza, D5.22 - NACIE_UP simulation validation: summary report, D5.22, H2020 SESAME report, March, 29, 2019.

V. Narcisi, P. Lorusso, F. Giannetti, G. Caruso, D. Martelli, M. Tarantino, A. Del Nevo, CIRCE-HERO RELAP5/ CFD simulations, D5.9, H2020 SESAME report, May, 24, 2019.

P. Lorusso, A. Del Nevo, M. Tarantino, Hamidouche, D. Castelliti, D. Rozzia, V. Narcisi, F. Giannetti, G. Caruso, D5.8 CIRCE-HERO Blind Simulations, D5.8, H2020 SESAME report, May, 28, 2019.

A. Del Nevo, P. Lorusso, M. Tarantino, K. Zwijsen, P.A. Breijder, Hamidouche, D. Castelliti, D. Rozzia, V. Narcisi, F. Giannetti, G. Caruso, D5.11 CIRCE-HERO simulation validation summary report, D5.11, H2020 SESAME report, May, 30, 2019.